

Peripheral blood mononuclear cell-secretome attenuates fibrotic effects in wound healing and scar formation.

Doctoral thesis at the Medical University of Vienna
for obtaining the academic degree

Doctor of Philosophy

Submitted by

Dr. med.univ. Vera Vorstandlechner

Supervisor:

Univ.Prof. Dr. Hendrik Jan Ankersmit

FFG Projekt „APOSEC“

Wiener Wirtschaftsförderung "APOSEC to clinic"

Department of Thoracic Surgery

Waehringer Guertel 18-20, 1090 Vienna, Austria

Vienna, August 2023

Declaration

The experiments conducted to accomplish this thesis were carried out at the Department of Thoracic Surgery and the Department of Dermatology at the Medical University of Vienna under the supervision of Hendrik Jan Ankersmit and Michael Mildner. The project was financed by the Aposcience AG and peer reviewed third party funding as described in the manuscripts' sections "Funding". Peripheral blood mononuclear cell secretome was produced by the Austrian Red Cross Blood Transfusion Service for Upper Austria, Linz according to GMP-requirements. Interpretation of results, writing and experimental design leading to the publication underlying this thesis were accomplished under the supervision of Michael Mildner and Hendrik Jan Ankersmit.

Table of contents

Declaration	ii
Table of contents	iii
List of figures	vi
List of tables	vi
Abstract	vii
Abstract (German)	viii
Publications arising from this thesis	ix
Abbreviations	x
Acknowledgements	xii
1. Introduction	1
1.1. Research in context: Establishing PBMCsec in regenerative medicine	1
1.2. Research in context: Skin scarring	9
1.3. Human skin	11
1.3.1. Epidermis	11
1.3.2. Dermis	12
1.3.3. Adipose tissue and subcutis	13
1.4. Wound healing	13
1.4.1. Acute response – “the second burn”	13
1.4.2. Inflammation and new tissue formation	15
1.4.3. Dermal remodeling	15
1.4.4. Considerations of differences of human and mouse wound healing	16
1.5. Skin scarring and tissue fibrosis	18

1.5.1.	Fibrosis	18
1.5.2.	Cells involved in fibrotic processes.....	18
1.5.3.	Signaling in fibrosis	24
1.5.4.	Extracellular matrix components and their role in fibrosis	29
1.6.	Human skin scarring: translational aspects	42
1.6.1.	Stem cell-based therapies.....	42
1.6.2.	Conditioned medium and cell-free therapies.....	43
1.7.	Aims of the thesis	46
2.	Results.....	47
2.1.	Chapter 1: Deciphering the functional heterogeneity of skin fibroblasts using single-cell RNA sequencing	47
2.2.	Chapter 2: The serine proteases dipeptidyl-peptidase 4 and urokinase are key molecules in human and mouse scar formation.....	48
2.3.	Chapter 3: The secretome of irradiated peripheral mononuclear cells attenuates hypertrophic skin scarring.....	49
3.	Discussion.....	50
3.1.	General discussion	50
3.2.	Conclusions and future prospects.....	60
4.	Materials and Methods	62
4.1.	Skin and scar samples.....	62
4.2.	Mouse scar models.....	62
4.3.	Mouse wound and scar treatments	63
4.4.	Cell isolation and generation of single-cell suspension for single-cell RNA sequencing	63
4.5.	Generation of single-cell gel-bead in emulsions (GEMs) and library preparation.....	64

4.6. Cell–gene matrix preparation and downstream analysis	64
References	66
Appendix	80

List of figures

Figure 1: The GMP-according preparation of PBMCsec.

Figure 2: Mechanisms of action of secretomes in regenerative processes.

Figure 3: Stages of wound repair.

Figure 4: Therapeutic secretomes and their components. Secretomes from various MSCs and their components.

Figure 5 Graphic summary: The characterization of functional heterogeneity of human skin fibroblasts.

Figure 6 Graphic summary: The serine proteases dipeptidyl-peptidase 4 and urokinase are key molecules in human and mouse scar formation.

Figure 7 Graphic summary: The anti-fibrotic mechanisms of PBMCsec in scars.

List of tables

Table 1: Pre-clinical and clinical *in vivo* studies of PBMCsec.

Abstract

Hypertrophic scars pose a significant medical problem and a substantial global disease burden, and effective therapeutic options are insufficient. This thesis aimed to thoroughly explore mechanisms of healthy skin and skin scarring, in an attempt to discover new agents to effectively treat hypertrophic scars.

First, we attempted to investigate the diversity of fibroblast subsets in human skin and their role in extracellular matrix (ECM) assembly. Using single-cell RNA sequencing, we identified six distinct fibroblast clusters, challenging the traditional classification of papillary and reticular fibroblasts. Dipeptidyl-peptidase 4 (DPP4)-expressing fibroblasts were found to be the main producers of ECM components in human skin, suggesting their potential as targets for anti-fibrotic therapies.

The second study focused on understanding the mechanisms underlying hypertrophic scar formation. Through single-cell analysis of human scars and maturing scars in mice, we found a group of serine proteases, including DPP4 and urokinase (*PLAU*), as potential key players in scar formation. Inhibiting these proteases showed anti-fibrotic activity and improved scar quality in mice.

Finally, we investigated the effects of secreted factors from peripheral blood mononuclear cells (PBMCsec) on skin scarring using single-cell analysis. Topical and intradermal application of PBMCsec affected the expression of genes involved in pro-fibrotic processes and tissue remodeling, prevented TGF β -mediated myofibroblast differentiation and attenuated exaggerated elastin expression through non-canonical signaling inhibition. PBMCsec may have potential as a therapy for skin fibrosis, with elastin identified as a shared key player of their antifibrotic action.

Taken together, we present a comprehensive overview of the gene expression profiles in healthy skin and hypertrophic scars. Additionally, we identify two potential novel targets for therapeutic agents, DPP4 and Urokinase. Moreover, the detailed investigation of PBMCsec provides a promising new therapeutic approach for the treatment of hypertrophic scars.

Abstract (German)

Narben und hypertrophe Narben nach Operationen, Verletzungen und Unfällen stellen weltweit ein signifikantes Gesundheitsproblem dar. Schmerzen, Jucken und Einschränkung der Beweglichkeit durch Narben können die Lebensqualität entscheidend reduzieren. Wirksame Therapien sind kaum verfügbar, und die genauen Prozesse und Genexpressionsmuster in (hypertrophem) Narbengewebe sind unzureichend beschrieben. In den drei Studien dieser Dissertation werden daher die zellulären Mechanismen von hypertrophen Narben völlig neu beleuchtet, und potenzielle neue Wirkstoffe zur Therapie von Narben untersucht.

In der ersten Studie wird die genetische Landschaft, das Transkriptom, gesunder Haut mit besonderem Fokus auf Fibroblasten-Populationen genau untersucht, um eine Ausgangsbasis für den Vergleich mit Narbengewebe zu schaffen. Es wurde eine neue, auf funktionellen Kriterien beruhende Einteilung der verschiedenen FB-Cluster etabliert, sowie ein Dipeptidyl-peptidase 4 (DPP4) -exprimierender Cluster beschrieben, der für den Großteil der Produktion von extrazellulärer Matrix (ECM) verantwortlich ist.

Die zweite Studie verglich nun die Transkriptome von gesunder Haut mit jenem von hypertrophen Narben, und identifizierte eine Gruppe von Serinproteasen, unter anderem DPP4 und Urokinase, als potenzielle neue Angriffspunkte von Therapeutika für verbesserte Narbenbildung. Die Hemmung von DPP4 und Urokinase verhinderte die Differenzierung von fibrogenen Myofibroblasten, und reduzierte die übermäßige Ausschüttung von ECM.

Zu guter Letzt wurde, auf Basis der beiden vorhergehenden Studien, die Wirkung der sezernierten Faktoren -das Sekretom- aus bestrahlten peripheren Leukozyten (PBMCsec) auf Narbenbildung untersucht. PBMCsec bewirkte ebenfalls eine Hemmung der Myofibroblasten-Differenzierung und geringere Ausschüttung von ECM. Zudem übte PBMCsec über eine Hemmung des Abbaus und der Reduktion der übermäßigen Ausschüttung von Elastin, sowie durch Interaktion mit dem fibrogenen TGF β eine Hemmung auf hypertrophe Narbenbildung aus.

Zusammenfassend präsentieren wir in dieser Arbeit einerseits eine Basis der Genexpression in gesunder Haut und hypertrophen Narben, sowie mit DPP4 und Urokinase zwei potenzielle neue Angriffspunkte bzw. Wirkstoffe. Andererseits bietet die genaue Untersuchung von PBMCsec eine vielversprechende neue Option für die Therapie hypertropher Narbenbildung.

Publications arising from this thesis

Vorstandlechner, V., Laggner, M., Kalinina, P., Haslik, W., Radtke, C., Shaw, L., Lichtenberger, B. M., Tschachler, E., Ankersmit, H. J., & Mildner, M. (2020). Deciphering the functional heterogeneity of skin fibroblasts using single-cell RNA sequencing. *FASEB journal : official publication of the Federation of American Societies for Experimental Biology*, 34(3), 3677–3692. <https://doi-org.ez.srv.meduniwien.ac.at/10.1096/fj.201902001RR>

Vorstandlechner, V., Laggner, M., Copic, D., Klas, K., Direder, M., Chen, Y., Golabi, B., Haslik, W., Radtke, C., Tschachler, E., Hötzenecker, K., Ankersmit, H. J., & Mildner, M. (2021). The serine proteases dipeptidyl-peptidase 4 and urokinase are key molecules in human and mouse scar formation. *Nature communications*, 12(1), 6242. <https://doi-org.ez.srv.meduniwien.ac.at/10.1038/s41467-021-26495-2>

Vorstandlechner, V., Copic, D., Klas, K., Direder, M., Golabi, B., Radtke, C., Ankersmit, H. J., & Mildner, M. (2023). The Secretome of Irradiated Peripheral Mononuclear Cells Attenuates Hypertrophic Skin Scarring. *Pharmaceutics*, 15(4), 1065. <https://doi-org.ez.srv.meduniwien.ac.at/10.3390/pharmaceutics15041065>

Abbreviations

ADAMTS	a disintegrin and metalloproteinase with thrombospondin motifs
AMI	acute myocardial infarction
CCNs	centralized coordination network
CCR	chemokine receptors
CD	cluster of differentiation
CM	Conditioned medium
COMP	Cartilage oligomeric matrix protein
CTGF	platelet derived growth factor connective tissue growth factor, Connective tissue growth factor
DAMPs	danger associated molecular patterns
DPP4	dipeptidyl-peptidase 4
DWAT	dermal white adipose tissue
ECM	extracellular matrix
EDA	extra domain A
EMT	endothelial to mesenchymal transition
FBs	fibroblasts
FGF	fibroblast growth factor
FN	Fibronectin
GMP	good manufacturing practice
GSK	glycogen synthase kinase
IFN γ	interferon gamma
IGF	insulin-like growth factor
IGFBP	insulin-like growth-factor binding protein
IL	interleukin
iPSCs	induced pluripotent stem cells
JNK	Jun kinase
KC(s)	keratinocyte(s)
LCs	Langerhans cells
LOX	Lysyl oxidases
MMP	matrix metalloproteinase
MSCs	mesenchymal stem cells
myoFBs	myofibroblasts
NE	Neutrophil elastase
NET	Neutrophil extracellular trap
NF κ B	nuclear factor kappa b
PAI	plasminogen activator inhibitor
PBMCs	peripheral blood mononuclear cells
PBMCsec	irradiated peripheral blood mononuclear cell secretome
PDGF	Platelet-derived growth factor
ROS	reactive oxygen species
scRNAseq	single cell transcriptome sequencing
sFRPs	secreted frizzled-related proteins
SPARCs	secreted protein acidic and rich in cysteine
SWAT	subcutaneous white adipose tissue
TGF β (1)	transforming growth factor beta (1)

TIMPs	tissue inhibitors of MMPs
TNF α	Tumor necrosis factor alpha
VEGF	vascular endothelial growth factor
α SMA	alpha-Smooth muscle actin

Acknowledgements

I hereby deeply thank my doctoral supervisors Prof. Hendrik Jan Ankersmit and Prof. Michael Mildner. Their continuous intellectual, organizational, moral, emotional, scientific, and financial support has enabled this extensive project.

I thank all colleagues, from the Ankersmit-Mildner Collaboration laboratory, particularly Dragan Copic, Martin Direder and Katharina Klas, for their experimental help and support, and for the good times and friendship found during the work on these studies.

We thank the HPH and the CRISCAR Familienstiftung for their belief in this private public partnership to augment basic and translational clinical research.

My special thanks go to my husband Stefan Spalt, who has loyally, continuously supported me, believed in me, and strengthened me for all those years working on this thesis. I also would like to thank my family, particularly my parents Elisabeth and Peter Vorstandlechner, who so lovingly set the basis for all my scientific endeavors.

1. Introduction

1.1. Research in context: Establishing PBMCsec in regenerative medicine

This thesis comprises a trilogy of studies, ultimately elucidating the effect of the secretome of irradiated peripheral blood mononuclear cells (PBMCsec) on skin and scar formation. The use of PBMCsec for tissue regeneration has been established in a scientific journey over almost fifteen years in the research group of Ankersmit et al., and was developed upon the basis of centuries of research of initial cell therapies, stem cells, conditioned medium, the secretome of viable cells, and lastly, resulted in the development of PBMCsec. The extensive scientific process of the development of PBMCsec for application in regenerative medicine laid the foundation for the pertinent thesis and is thus discussed here in closer detail.

The idea of therapies based upon cell transplantation was studied long ago and was already proposed in the nineteenth century. Paul Niehans, a Swiss physician, performed subcutaneous application of xenogeneic cell suspensions derived from the endocrine glands, heart, kidney, liver, bone marrow, intestinal mucosa, and reticulo-endothelial system into the corresponding organ, to restore the respective tissues' function (1). Among his prominent patients of the so-called "Frischzellentherapie" were Winston Churchill, Pope Pius XII, Agha Kahn, and Charles de Gaulle (1). During the late 20th and early 21st century, a new interest for the idea of applying stem cells for restoring or engineering pathological tissue to re-establish physiological function was re-introduced, and the idea stem cell-based regeneration emerged (1).

In various in vivo animal experimental models, transplantation of autologous or allogeneic stem cells showed promising results to regenerate diseased tissue. E.g., Scorsin, Menasché et al. demonstrated that intracardial injection of skeletal myoblasts and fetal cardiomyocytes are effective for improving postinfarction left ventricular function (2). Subsequently, Kocher et al. demonstrated that human bone-marrow-derived angioblasts prevent cardiomyocyte apoptosis, enable neovascularization of ischemic myocardium, reduce remodeling, and improve cardiac function in rats (3). Similarly, Orlic et al transplanted adult bone marrow cells after myocardial infarcts in mice, and found improved ventricular function (4, 5).

Not only in cardiac regeneration, but also in wound healing and tissue engineering, the use of stem cells demonstrated promising results in pioneering works (6). In an early human trial application, Strauer et al. applied human autologous stem cells intracoronary after acute myocardial infarction (AMI) to regenerate infarcted myocardium (7). Bartsch, Strauer et al. later also applied autologous mononuclear bone marrow stem cells in patients with peripheral arterial disease (the TAM-PAD study), and showed significant better pain-free walking distance of the transplanted patients (8). Multiple subsequent animal trials continued to show promising results in tissue regeneration upon stem cell application (9). However, initial clinical trials, such as the randomized controlled trial TOPCARE-AMI, did not show significant left ventricular function improvement after intracoronary application of autologous progenitor cells (10).

Further mechanistical studies found that mesenchymal stem cells engraft and differentiate into cardiomyocytes, and also stimulate the proliferation and differentiation of endogenous cardiac stem cells (11). Moreover, allogeneic MSCs stimulate the proliferation of endothelial progenitor cells (12). However, others reported that only very few of transplanted stem cells embed in the heart, are thus not sufficiently biologically relevant, and do not sufficiently explain the observed pro-regenerative effects (1, 13). Wollert et al suggested already in 2005, that the factors secreted from the cells, i.e., the secretome, not the stem cells themselves, are causing the observed positive effects in tissue regeneration (14). Confirming their speculation, Gneocchi *et al.* in 2005 were among the first to show that paracrine factors released from mesenchymal stem cells not only prevent further damage, but are able to promote tissue regeneration (15).

Interestingly, a much earlier work by Holzinger et al. in 1994 first proposed that not only stem cells, but also other autologous cells exert pro-regenerative action. Non-healing skin ulcers were treated topically with autologous activated mononuclear cells, and the ulcers resolved significantly faster after application of these activated cells (16). Putting the pieces of the puzzle together, Ankersmit hypothesized that not necessarily the secretome of stem cell is required for pro-regenerative effects, but that also the secretome of other, more easily available cell types, e.g., peripheral blood mononuclear cells (PBMCs), suffices.

Thus, in 2009, Ankersmit et al. first demonstrated that the infusion of apoptotic PBMC suspension in a rat AMI model attenuated inflammation, led to enhanced homing of regenerative c-kit⁺ cells, and salvaged infarcted myocardium *in vivo* (17). In the same publication, experimental data indicated that the secretome of irradiated PBMCs induced upregulation of cytoprotective components (MMP9, VEGF, IL-8) *in vitro*. This experimental finding suggested already in 2007-2008 that the secretome of stressed PBMC, and not the cells themselves, caused the regenerative effects described after AMI (17). In a subsequent study, Lichtenauer et al. showed that the intramyocardial injection of stressed PBMC suspension also improved experimental AMI in a rodent model. Interestingly, the ratio of elastin to collagen in the resulting AMI scar tissue was increased (18). The ultimate confirmation that the secretome of stressed PBMCs is responsible for the salvaging of hypoxic myocardium after experimental AMI was published in 2011. Here, Lichtenauer et al. showed conclusively that only one intravenous application of stressed PBMCsec prevented myocardial remodeling and improved left ventricular function in a rodent and porcine AMI model (19).

Subsequently, the pro-regenerative effects of irradiated apoptotic PBMCs were studied in various models of tissue damage. To assess its efficacy in wound healing, Mildner et al. topically applied the (non-irradiated) PBMC secretome in cutaneous wound in mice, and showed that it accelerated wound closure, enhanced angiogenesis, and induced cell migration (20). Similarly, Hacker et al. applied PBMCsec in porcine burn wounds, which resulted in increased epidermal thickness, higher number of rete ridges, and more advanced epidermal differentiation than control, as well significantly more angiogenesis (21). Pavo et al. investigated endomyocardial application of secretome of apoptotic PBMCsec on chronic post-myocardial infarction left ventricular insufficiency in pigs, and again, PBMCsec significantly reduced the extent of infarcted tissue and led to a higher cardiac index and myocardial function (22). Altmann showed that PBMCsec attenuates neurological damage in rats with focal ischemia (23), and Haider demonstrated that PBMCsec ameliorates the outcome after spinal cord injury in rats (24).

In a first attempt to characterize the mechanisms of action of PBMCsec, Beer et al. closer analyzed the gene expression patterns of PBMCs upon irradiation (25). Ionizing radiation induced the release of oxidized phosphatidylcholines, microparticles, and exosomes. The most abundantly regulated pathways

in PBMCs after irradiation were associated with in pro-angiogenic and regenerative genes, as well as the generation of oxidized phospholipids with known pro-angiogenic and inflammation-modulating properties. Further in vitro assays demonstrated that the protein and exosome fraction of the secretome enhanced cell mobility, however, secreted lipids and microparticles alone did not exert these effects, but only the combined secretome (25). In a further step to characterize all beneficial properties of PBMCsec, Kasiri et al. confirmed that PBMCsec possesses intrinsic antimicrobial activity, inhibiting bacterial growth from gram-positive as well as gram-negative bacteria. Expression of antimicrobial peptides, e.g. angiogenin, cathelicidins, and calprotectin, were increased in the secretome, and again irradiated PBMCs again showed stronger antimicrobial activity than that from non-irradiated PBMCs (26). Further research by Wagner et al. revealed the separate roles of the components of PBMCsec, and closer elucidated the role of extracellular vesicles, proteins, lipids, and miRNA present in PBMCsec. Irradiation significantly increased the number and size of extracellular vesicles released from PBMCs; however, this study demonstrated that compared to individual PBMCsec subfractions, only the full secretome with all subfractions unfolds the regenerative potential (27).

Further unraveling the composition and activity of PBMCsec, Simader et al. closely investigated the modes of cell death after PBMC irradiation, and the contribution of the different cell subpopulations (CD4⁺ and CD8⁺ T cells, B cells, monocytes, and natural killer cells) to PBMCsec. Similar to Wagner et al., they found that not only all subfractions are needed for the full regenerative potential, but also that interactions of the cellular subsets are important for the generation of a pro-angiogenic secretome (28). They also described that γ -irradiated PBMCs revealed distinct morphological changes, indicating not only apoptotic, but also necroptotic cell death. Blocking apoptosis did not inhibit on the pro-angiogenic activity of the secretome, however, blocking necroptosis in stressed PBMCs impaired the pro-angiogenic effect (28).

To prepare PBMCsec for further clinical application, the development of PBMCsec-production according to good manufacturing practice-guidelines (GMP) was established, encountering numerous challenges along the way (29). A viral safety protocol was prepared, and an ethylene blue-assisted viral reduction protocol, lyophilization and gamma irradiation in combination was shown to provide sufficient viral safety of GMP-PBMCsec (*Figure 1*) (30, 31). Aortic ring sprouting, tube formation assays, protein and cytokine

profiling were established as potency assays to confirm comparable efficacy of the various batches of GMP-PBMCsec (31). These assays demonstrated that PBMCsec displays continuous, equivalent potency between batches, and that batch effects are negligible (31). Lastly, toxicity testing in rats and pigs confirmed the safety of PBMCsec and showed no major toxicities or signs of local intolerance at levels above the intended total human dose (32) When comparing experimentally prepared PBMCsec to GMP-according PBMCsec, Beer et al. did not find significant differences in their regenerative effects (25). Having conquered all these steps, a Phase I study for the topical application of PBMCsec in cutaneous wounds of healthy male volunteers was initiated. In the phase I study, autologous PBMCsec was used, thus a viral clearance protocol was not yet necessary. The application of PBMCsec on wounds was demonstrated to be safe, and no adverse events occurred; however, wound healing was not improved by PBMCsec (33, 34).

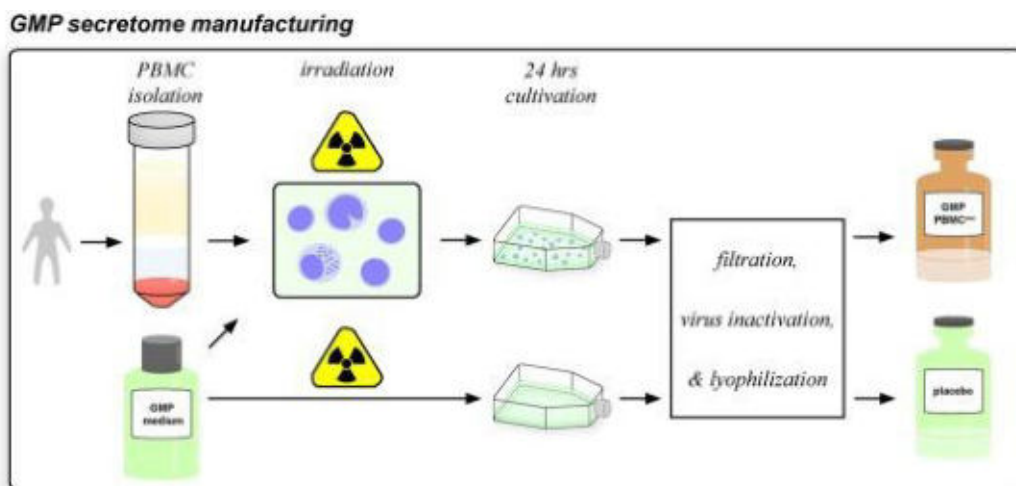


Figure 1: The GMP-according preparation of PBMCsec. PBMCs are isolated from leucocyte concentrations after blood donations from healthy donors. PBMCs are subsequently irradiated with 60Gy, and cultivated at a concentration of 25Mio cells/ml for 24h. Cells are removed, the secretome is filtrated, treated with virus inactivation, and lyophilized. Analogically, the placebo for clinical studies is prepared by irradiation, filtration, viral clearance and lyophilization of the medium alone (31).

After the successful completion of the Phase I study, further pre-clinical evaluation of the possible applications of PBMCsec continued. In a rodent epigastric flap model, Hacker et al. demonstrated that

PBMCsec enhanced tissue survival, angiogenesis and clinical parameters highlighting a potential use for support in reconstructive surgeries (35). Laggner et al. further evaluated the anti-inflammatory properties, and showed that PBMCsec is able to reduce activation of mast cells and basophils, and thereby laying a promising basis for further studies on the potential use of PBMCsec for treating allergy (36). Explaining the salvaging effects of PBMCsec after tissue damage and reperfusion, Klas et al. found that PBMCsec attenuated neutrophil extracellular trap (NET)-formation by inhibiting the activation arginine deiminase 4 (PAD4). NETs usually form an important defense mechanism for the clearance of infections; however, increased NET formation has been shown to abolish tissue-regeneration after injury. Thus, PBMCsec provides a promising new therapeutic option for conditions resulting from exaggerated NET formation (37). In further preparation for intravenous use of PBMCsec, Copic et al. explored the possible effects of PBMCsec on vascular endothelial cells and PBMCs, and discovered that PBMCsec not only again exerts angiogenic effects, but also possesses a potent anti-proteolytic and barrier-protective effect properties on human blood components (38). An overview of all pre-clinical and clinical *in vivo* studies investigating PBMCsec is given in Table 1.

Species	Experimental model	Effects on disease	Application	PBMCsec source	References	Year
Rat	AMI	Reduced infarct size, improved functional parameters	i.v.	syngen	(39)	2009
Rat	AMI		i.v.	syngen	(19)	2011
Rat	AMI		i.v.	syngen	(18)	2011
Pig	AMI		i.v.	syngen	(40)	2012
Mice	experimental autoimmune myocarditis	Resolution of acute inflammation	i.p.	syngen	(41)	2013
Mice	Dermal wound	Improved wound healing	Topical	syngen	(20)	2013
Pig	Chronic HF	Improved functional parameters	i.m.	syngen	(42)	2014
Rat	Stroke	Reduced infarct size, improved neurological parameters	i.v.	Syngen/human GMP viral cleared	(23)	2014

Rat	Spinal cord injury	Reduced trauma size, improved neurological parameters	i.p.	Human GMP viral cleared	(24)	2015
Pig	AMI	Reduced infarct size, improved functional parameters	i.v.	Syngen GMP viral cleared	(25)	2015
Pig	Burn wound	Improved wound healing	Topical	Human	(21)	2016
Human	Phase I Dermal wound	Safety and tolerability (ClinicalTrials.gov NCT02284360)	Topical	Human GMP autologous	(34)	2017
Mouse	Dermal wound (diabetic mice)	Improved wound healing	Topical	Human GMP viral cleared	(27)	2018
Mouse	Flap model	Improved flap perfusion,	Topical	Human GMP viral cleared	(35)	2020
Mouse	Contact hypersensitivity	alleviated tissue inflammation, reduced DC maturation, antigen uptake, lipopolysaccharides-induced cytokine secretion	Topical	Human GMP viral cleared	(43)	2020
Mouse	Ear swelling model	reduced activation of mast cells and basophils	Topical	Human GMP viral cleared	(36)	2022
Mouse	Scar model	Reduced fibrosis, attenuated myoFB-differentiation	Topical + intradermal	Human GMP viral cleared	(44)	2023
Human	Phase II Dermal foot ulcer	Efficacy in wound healing (EudraCT 2018-001653-27, ClinicalTrials.gov NCT04277598)	Topical	Human pooled GMP viral cleared, sterilized	(30)	2023

Table 1: Pre-clinical and clinical in vivo models of PBMcsec. Modified and updated after Beer et al 2016. syngen =same species, autologous =same patient; Human GMP viral cleared = from pooled donors.

During the extensive preclinical investigations, a plethora of modes of action (MOA) of PBMcsec in regeneration was defined. In summary, topical PBMcsec enhances reepithelialization by enhancing keratinocyte proliferation and migration (20, 21). After local injection or intravenous application, PBMcsec prevents NETosis (37), inhibits mast cell and basophile degranulation (36) as well as dendritic cell proliferation, maturation and cytokine release (43), and balances macrophage polarization (45). In

the various regenerative processes, PBMCsec promotes angiogenesis (20, 27, 35, 46, 47), enhances neuronal sprouting and neurogenesis (23, 24), and modulates the cytokine milieu, tackling pro-inflammatory cytokines TNF α and IL-6, and enhancing the anti-inflammatory response (39, 48). The MOAs are summarized in Figure 2: *Mechanisms of action of secretomes in regenerative processes*.

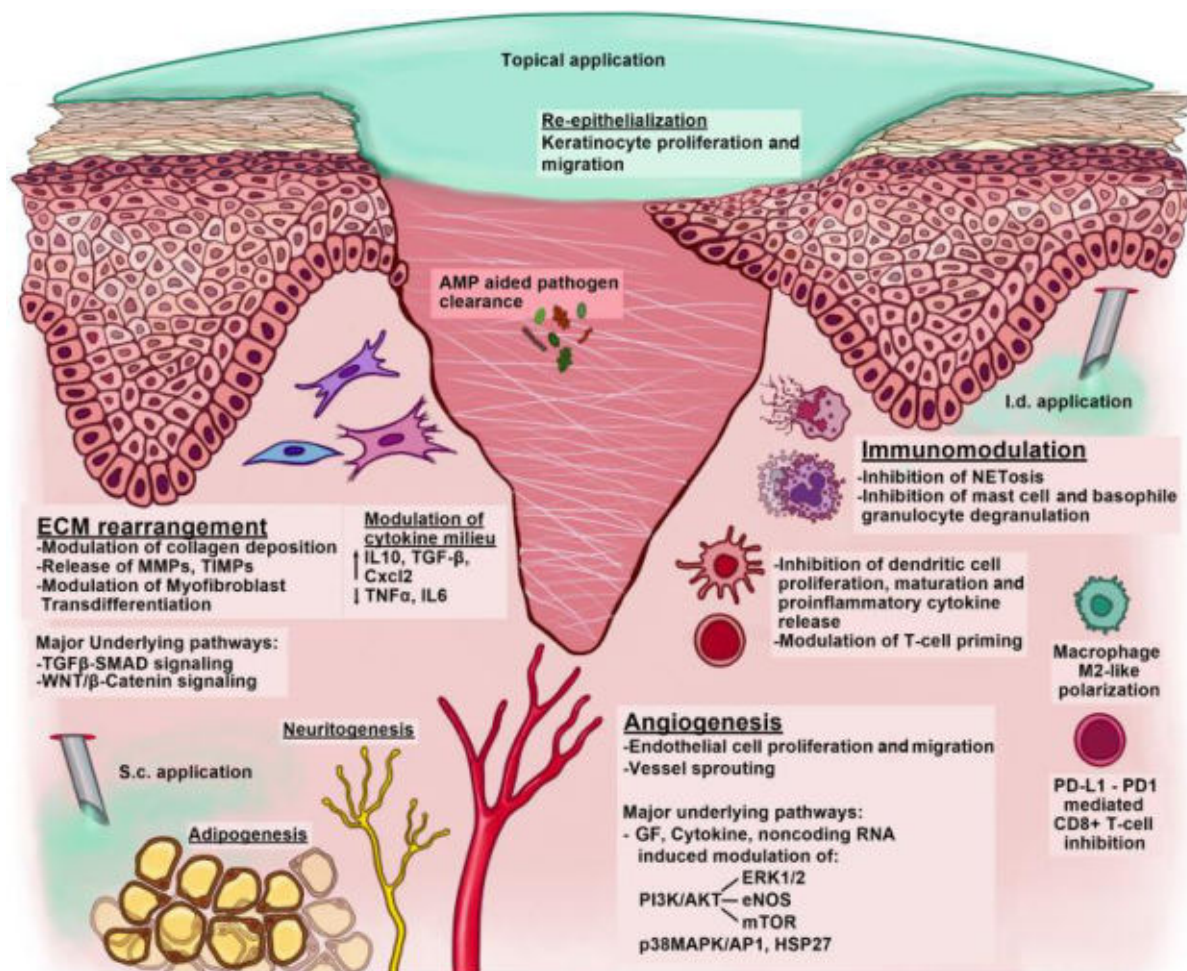


Figure 2: Mechanisms of action of secretomes in regenerative processes. Illustration of typical secretome administration routes, significant mechanisms of action, and associated signaling pathways supporting the improvement of therapeutic secretomes applied topically, intradermally, or subcutaneously in relation to wound healing. PBMCsec affects ECM arrangement, cytokine secretion, mechanisms in reepithelialization, immunomodulation, macrophage polarization, and adipogenesis, neuritogenesis, and angiogenesis (49). Use of graphic permitted according to CC BY 4.0 license.

Following these extensive pre-clinical approaches, a clinical phase-II (“MARSYAS II”) study was launched, investigating the efficacy of PBMCsec in wound healing of chronic diabetic foot ulcers (30). (ClinicalTrials.gov Identifier: NCT04277598). The MARSYAS II main study is a multicenter, randomized, double-blind, placebo-controlled, parallel group, dose-ranging phase II study to investigate the safety and

clinical efficacy of PBMCsec compared with placebo in patients with diabetic foot ulcer (30). After a safety lead-in period, the main study includes 120 eligible patients, who receive PBMCsec three times per week during the 4-week active treatment period. This clinical study is currently ongoing, expected to be completed in August 2023, and results are expected within the next year.

1.2. Research in context: Skin scarring

Scars, keloids, and hypertrophic scarring represent a multifaceted medical issue and impose a substantial global disease burden (50, 51)., an estimated 100 million individuals are affected by scars annually in western countries, comprising 4 million burn scars around and 11 million keloid scars (50). The treatment of skin scarring in the USA is associated with an estimated annual market value of 12 billion dollars, with an additional 25 billion dollars expended on wound treatment in general in 2015 (52).

Pathological hypertrophic scars or keloids arising from scars can lead to both aesthetic concerns and notable functional impairment for the patient, resulting in pain, pruritus, and a diminished quality of life (53, 54). In the context of burn wounds, the reported prevalence of pathological scarring ranges from 30% to 90%, with a higher incidence observed in the black population (55). Keloids or hypertrophic scars are characterized by excessive tissue contraction and an abundance of extracellular matrix compared to that of normal skin (55).

For the prevention or treatment of (hypertrophic) scars, often used therapies include topical silicone application, compression or massage therapy, laser ablation, surgery, and intralesional injection of triamcinolone (TAC), corticosteroids, or 5-Fluorouracil (5-FU) (55, 56). Nevertheless, a significant number of these therapeutic modalities lack substantial evidence of their efficacy and safety, and the precise mechanisms of action for these treatments remain unclear (57, 58).

Continuing the long journey of the development of PBMCsec and its extensive mechanistic and pre-clinical investigation, the author of this thesis wondered whether PBMCsec not only has potential in acute damage (e.g., cutaneous wound healing), but also in the setting of chronic tissue dysfunction of skin scarring and fibrosis. In their porcine burn model, Hacker et al. investigated the quality of the resulting scar tissue after PBMCsec-treated burn injuries. They found that PBMCsec contributes to better scar quality, higher elasticity, and less scar stiffness (21). However, the exact mechanisms and the

applicability of PBMCsec in already present, mature scars were hitherto not investigated. As wound healing, skin scarring and fibrosis are such complex and evolutionary conserved processes, almost all cell types present in skin are involved in their regulation. Thus, the recently available technology of single cell transcriptome sequencing (scRNAseq) was established and laid the basis for deciphering the interaction of PBMCsec with the various cell types in the skin. This thesis will thus thoroughly discuss the skin, wound healing and scarring as the foundation for elucidating the regenerative processes supported by PBMCsec in skin scarring.

1.3. Human skin

1.3.1. Epidermis

As the outermost layer of the skin, the epidermis constitutes the border between the body and the environment. Even though it is not the largest organ of the body (59), the skin is crucial in maintaining fluid and temperature homeostasis, and protection of organs against pathogens, ultraviolet light, and other harmful impact (60, 61). The epidermis consists of a multi-layer epithelium of keratinocytes (KCs), and comprises associated structures such as hair follicles, sweat glands and sebaceous glands (61). KCs are critical actors in maintaining skin homeostasis, and their differentiation commencing with mitosis of the basal stem cells and terminating with shedding as corneocytes, is a tightly controlled process (62, 63).

Proliferating basal KCs from the *Stratum basale*, marked by the expression of collagen 17 and Ki67 (63), move upwards through the *Stratum spinosum* and *Stratum granulosum*, accumulating KC-specific proteins, mainly pro-filaggrin, and ultimately undergo cornification and shed from the *Stratum corneum* (62). The differentiation process is controlled by a calcium gradient, increasing from the *Stratum basale* to the *Stratum granulosum*, and the decreasing towards the *Stratum corneum* (62). While lower KCs highly express dimerizing keratin 5 (*KRT5*) and 14 (*KRT14*), KCs of the spinous and granular layer contain more keratin 1 and 10 (63).

Aside from its barrier function, the epidermis plays a critical role in skin repair in wound healing and dermal remodeling. Interfollicular and hair follicle stem cells facilitate re-epithelialization after skin wounding (64), and KCs interact with dermal fibroblasts (FBs) by secreting growth factors or instructing FBs to secrete growth factors (65). On the basal edge of the epidermis, melanocytes provide protection against UV-radiation, and specialized key immune cells, the Langerhans cells (LCs), act as tissue-resident macrophages as well as antigen-presenting cells of the epidermis (66).

1.3.2. Dermis

Beneath the epidermis, the fibrous dermis supports the epidermis, provides nutrition, strength, and elasticity, and contains innervation for pain, vibration, and touch sensation of the skin (67, 68). It consists predominantly of extracellular matrix (ECM), and its key cells are FBs (69, 70).

The dermis is classically categorized into the upper papillary and the lower reticular dermis, with a correlating FB classification into papillary and reticular FBs. Papillary FBs are described as smaller and spindle shaped, show less alpha-Smooth muscle actin (α SMA) expression, synthesize more proteoglycans, but less collagen, and show a high proliferation *in vitro* (70-72). Reticular FBs have a more flattened appearance, contain more α SMA, proliferate slower and secrete more transforming growth factor beta 1 (TGF β 1) than papillary FBs (70, 71). FBs are responsible for secretion, organization, and breakdown of ECM, mainly collagen and elastic fibers. In healthy papillary dermis, smaller diameter collagen fibers are interspersed with elastic fibers, while in reticular dermis, less dense, but larger diameter collagen fibers are loosely interwoven with branching elastic fibers, consisting of fibrillin-rich microfibrils and microfibrils with an elastin core (67). Fibrillar Collagen I, the most abundant ECM component of the dermis, is secreted as pro-collagen molecules. After proteolytic splitting of the propeptides, triple-helical collagen containing short telopeptides on both ends molecules are formed. Subsequently, these triple helices assemble into highly ordered, aggregated collagen fibrils (73).

Elastin is an insoluble polymer of soluble precursor tropoelastin and is the main component of elastic fibers in matrix tissue, providing elastic recoil and resilience in connective tissues. Elastin also plays a role in regulating activity of TGF β 1, in cell adhesion, cell migration, and participates in cell signaling (74, 75). Another key ECM component is fibronectin, which forms a bridge between cell surface receptors (e.g., integrins) and compounds such as collagen, proteoglycans, and other focal adhesion molecules, and helps to assemble fibrillin-1 into a structured network (75). In both elastic and non-elastic extracellular matrices, fibrillins serve as the microfibril core, interact closely with tropoelastin, and act as a scaffold for elastogenesis in elastic tissues. (67, 75).

Fibulins play a role in the development of elastic fibers and are closely linked to elastic fibers, basement membranes, and other ECM components. Tenascins are glycoproteins mediating both inflammatory and

fibrotic processes to enable effective tissue repair. Cartilage oligomeric matrix protein (COMP) or thrombospondin-5 is primarily present in the cartilage, but high levels of COMP are also present in fibrotic scars and systemic sclerosis of the skin (67, 75).

The dermis further contains a variety of other celltypes: endothelial cells, pericytes and smooth muscle cells forming blood vessels, lymphatic endothelial cells, dendritic cells, mast cells, macrophages, and T-cells. Pericytes not only stabilize blood vessels and control capillary flow, but play a key role in wound healing and scarring, as they can acquire a fibrotic phenotype (76). Dendritic cells, macrophages, mast cells, and T-cells regulate immune response and are involved in a plethora of skin pathologies e.g. psoriasis, atopic dermatitis, contact sensitivity and allergic reactions (68). Moreover, they are considered as major drivers of skin scarring and fibrosis by facilitating prolonged inflammation after skin wounding (68).

1.3.3. Adipose tissue and subcutis

The subcutis, is a layer of adipose tissue located beneath the reticular dermis. The skin contains two adipose tissue types: the dermal white adipose tissue (DWAT) which surrounds hair follicles in humans, and a deeper layer of subcutaneous white adipose tissue (SWAT). DWAT adipocytes play a crucial role in maintaining dermal homeostasis by controlling hair folliculogenesis and promoting wound healing through paracrine signaling (77). The growth and shrinkage of DWAT adipocytes are cyclically regulated by hair-derived Wnt signaling. Furthermore, dermal adipogenesis is activated in response to bacterial skin infection, which triggers the secretion of antimicrobial peptides and serves as an innate immune defense mechanism (77).

1.4. Wound healing

1.4.1. Acute response – “the second burn”

Immediately after tissue damage, coagulation cascades, inflammatory pathways and immune response are activated to prevent blood and fluid loss, infection, and to remove dead tissue (78, 79). After formation of a platelet and, later, a fibrin clog, neutrophils are first recruited to the wound by complement activation. Two to three days later, they are followed by monocytes, which then differentiate into macrophages clear up cell debris, and secrete cytokines, coordinating the further inflammatory response (78, 79) (*Figure 3*).

The immediate response to the initial trauma is coordinated by numerous “danger-sensing molecules” (Danger associated molecular patterns, i.e. DAMPs) of plasmatic defense cascades (e.g., acute phase reaction, coagulation cascade, kallikrein-kinin system, complement system) (80, 81). Serum levels of DAMPs e.g., high mobility group box 1 (HMGB1), extracellular cold-inducible RNA-binding protein (eCIRP), and H3 correspond with increased with disease severity (68).

Upon tissue injury, the coagulation cascade and kallikrein-kinin system are activated to seal off damaged and leaky sub-endothelial structures. The immune system recognizes tissue damage via DAMPs, especially the complement system, with its trigger molecules C1q, C3b, and mannose-binding lectine (80). DAMPS are produced upon activation by exogenous (microorganisms) or from endogenous triggers (injured and apoptotic cells), the complement cascade detects DAMPs and transmits the danger signal to the cellular defense, resulting a specific cellular signaling and an effective immune response to ultimately eliminate exogenous and endogenous danger (80). DAMPs further fuel pro-inflammatory cytokine and chemokine production by macrophages and other immune cells, leading to abundant neutrophil infiltration into the tissue. Activated neutrophils produce reactive oxygen species (ROS), inducible nitric oxide synthase (iNOS), and NETs which contain noxious molecules, further fueling tissue inflammation and injury in sepsis (81). In burn injuries, the “zone of coagulation” represents the core burn area of the primary injury (82). The adjunct “zone of stasis“ is characterized by decreased tissue perfusion, which is potentially salvageable. However, acute inflammation and additional damage such as prolonged hypotension, infection, or oedema can result in complete tissue loss (82).

Upon extensive tissue injury, such as polytrauma or burns, an additional trauma (“second hit”) such as extensive surgical procedures, anesthesiological interventions (“iatrogenic load”), or additional stress (e.g., hypoxia, hypothermia, microbiological invasion), the danger response may aggravate. This second hit response is characterized by an uncontrolled and excessive release of pro-inflammatory cytokines, chemokines, neuromodulators, heat shock proteins, and oxygen radicals, which is clinically reflected in the Systemic inflammatory response syndrome (SIRS) or sepsis (80).

1.4.2. Inflammation and new tissue formation

After 2-10 days, keratinocytes, stimulated by hepatocyte growth factor (HGF), fibroblast growth factor 7 and 10 (FGF7/10) and transforming growth factor α , begin to migrate over the granulation tissue. Next, angiogenesis, stimulated by vascular endothelial growth factor A (VEGFA) and fibroblast growth factor 2 (FGF2 or bFGF), begins. Subsequently, FBs are attracted to the wound edge, partially differentiate into myofibroblasts, and begin deposition of ECM (78, 79).

Except during the embryonic stages, when an inflammatory or thrombotic response is not yet possible, tissue damage is always associated with inflammation (83). Tissue damage with subsequent cell death leads to inflammation, and vice versa, a process which was named “necroinflammation”, and inflammation is present both in tissue regeneration and fibrotic processes. However, inflammation is not mandatory for tissue regeneration and does not necessarily result in fibrosis (83), and the mechanisms causing fibrosis are comparable under sterile and non-sterile conditions (83, 84). Necrotic cells or damaged tissues release inflammatory stimuli derived from the nucleus, from the mitochondria, from the cytosol or from the extracellular matrix. These include factors like High mobility group box 1 protein (*HMGB1*), DNA, RNA, histones, N-formyl peptides, mitochondrial DNA, ATP, heat shock proteins, S100 proteins, hyaluronan, biglycan, versican and heparan sulphate. These factors are often summarized under the term “danger associated molecular patterns”, or DAMPs, and are recognized by the corresponding receptors, the “pattern recognition receptors” (PRR) (83, 84). PRRs include Toll like receptors, NOD-like receptors, retinoic acid inducible gene-like receptors and C-type lectin receptors. Some of the DAMPs are also called alarmins and possess the ability to promptly recruit monocytes and granulocytes by directly binding to chemokine receptors. Typical alarmins are interleukins IL-1, IL-33, TSLP, defensins, cathelicidins, among others (83). Bacterial infections trigger a strong and acute proinflammatory Th-1 response to clear pathogens, while other tissue destruction requires tissue repair and fibrosis to preserve organ function. Several cytokines, e.g. IL25, IL-33 and TSLP promote a Th-2 immune response, contributing to fibrosis (83, 84)

1.4.3. Dermal remodeling

After initial tissue formation, the third stage of wound repair -dermal remodeling- begins 2-3 weeks after the injury and persists 1-2 years (78). After healing, a matrix made largely of collagen and other ECM,

as well as few cells remain. The majority of the endothelial cells, macrophages, and myofibroblasts undergo apoptosis or leave the wound (70, 78). In the early remodeling phase, reticular FBs and hypodermal cells populate the wound dermis (85). They produce thick, collagen III fibers in parallel organization typical for fibrosis (70, 78). In later stages of remodeling, papillary FBs invade the wound, and the immature matrix of collagen III is partially replaced by mature, well-organized collagen I, a process mediated by matrix-metalloproteases derived from FBs, macrophages, and endothelial cells (78, 86).

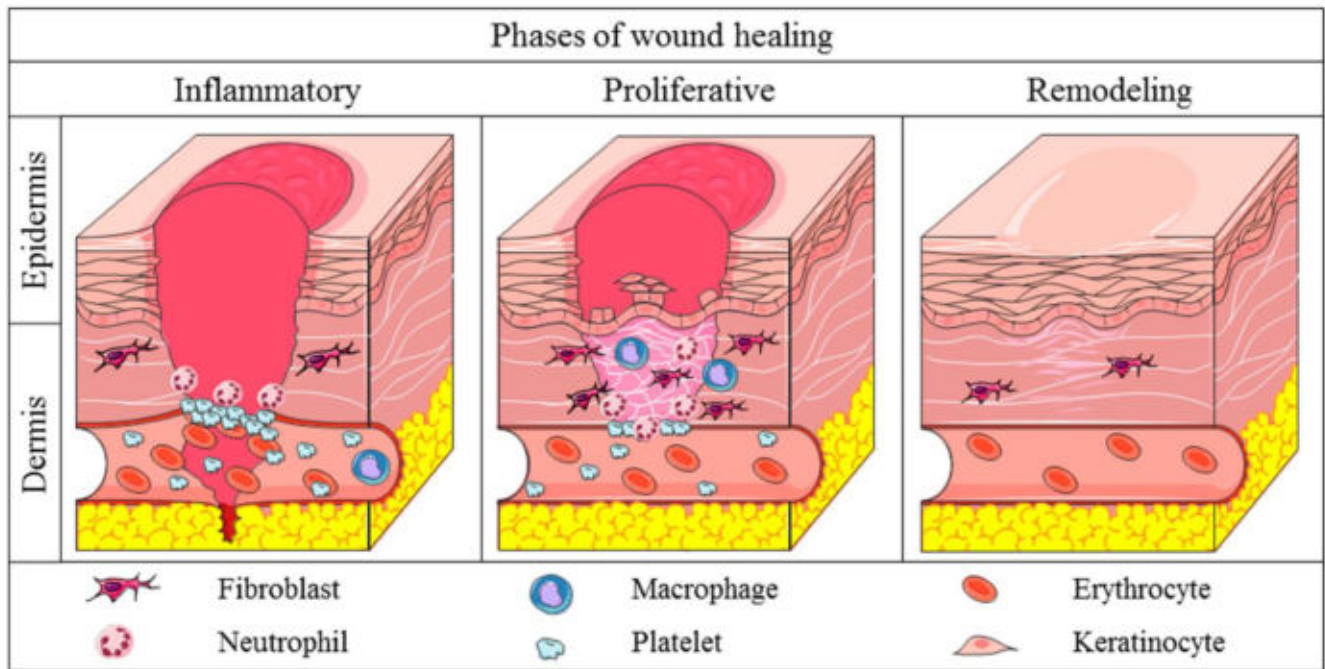


Figure 3: Stages of wound repair (87). During the inflammatory phase, hemostasis of wounded area and acute inflammation is achieved by secretion of growth factors and cytokines, and subsequently by migration of leukocytes in the area. During the proliferative phase, the migration and proliferation of the keratinocytes, fibroblasts, endothelial cells, and leukocytes is increased, and the synthesis of ECM, angiogenesis and re-epithelialization mechanisms are increased. During Remodeling, collagen III is substituted for collagen I, matrix metalloproteinase (MMP) activity is enhanced, provisional endothelial cells, fibroblasts, and myofibroblasts undergo apoptosis (87). Use of graphic permitted according to CC BY 4.0 license.

1.4.4. Considerations of differences of human and mouse wound healing

When studying wound healing and skin scarring, differences between human and mouse skin must be considered. Mouse and human have the same layers of cells in epidermis and dermis but differ in thickness (88). Human epidermis is thicker, with more cell layers (5-10) and is connected with the underlying tissue, while mouse epidermis is thinner (2-3 epidermal cell layers), and only loosely connected with the subcutaneous fascia, whereas human skin is tightly interwoven with subcutaneous

fat (88, 89). In mouse skin, the subcutaneous *Panniculus carnosus*, virtually absent in human skin, a thin layer of muscular tissue, greatly contributes to wound healing. Excisional wounds in mouse heal up to 90% via contraction of the *Panniculus carnosus*, while human wounds heal predominantly by the formation of granulation tissue and reepithelialization (88, 89).

Other differences between mouse and human skin are evident in hematoxylin and eosin (H&E) or Elastica van Giessen- (EvG) stainings. In human skin, epidermal Rete ridges intersect dermal papillae with the epidermis, while they are absent in mouse skin (90). The presence of hair follicles in human is strongly dependent on the location, but mainly sparse, while they are present with high density in mice, and eccrine sweat glands are present in humans, but absent in mice (88). Despite named differences, mouse and human wound healing occurs very similar in terms of the main phases of wound healing, homeostasis, inflammation, and remodeling (78, 79, 88), and if these disparities are considered in the experimental setup, mouse models for wound healing are still suitable to translate the results to human applications (88). Upon injury, healing and full scar maturation takes up to 80 days in mice and rats, while human skin takes up to two years to fully remodel (91).

1.5. Skin scarring and tissue fibrosis

1.5.1. Fibrosis

Fibrosis is defined as any process where functional mesenchymal or parenchymal tissue is replaced with fibrillar, collagen-rich ECM (92). Fibrosis is a necessary and fast physiological reaction to tissue damage in several organs, e.g. to provide stability to the heart muscle after myocardial infarction, reduce pressure on an overloaded kidney, or stabilize lung tissue or skin after injury (92). However, excessive, uncontrolled fibrosis leads to impaired organ function, and in its final stages to pain and impaired life quality, e.g. in Dupuytren's contracture (93), keloids or hypertrophic skin scarring (94), scleroderma, corneal fibrosis (95), or life-threatening diseases e.g. cardiac, renal, pulmonary, or hepatic fibrosis (96).

1.5.2. Cells involved in fibrotic processes

Fibroblasts

FBs are the main cells within connective tissue, they are responsible for synthesizing and organizing matrix protein, including collagens, nidogens, elastin, laminins, fibronectin, tenascin, and glycoproteins. They are heterogeneous in their origins, molecular markers, and functions, particularly during pathological remodeling of organ tissue (97). They are present in de facto every tissue and every organ of the body (97, 98). FBs are responsible for producing and remodeling the ECM of tissues, which provides structural support and regulates cellular behavior. In the skin, fibroblasts contribute to wound healing and skin aging by secreting collagen and elastin fibers. In the lung, fibroblasts play a role in the development of fibrosis by depositing ECM proteins in response to injury. In the liver, fibroblasts (also called hepatic stellate cells) are involved in liver fibrosis, where they produce and secrete excessive amounts of ECM proteins (95). In bone, FBs (also called osteoblasts) are responsible for bone formation and remodeling. Fibroblasts are a diverse group of cells with varying functions and phenotypes, which can change in response to environmental cues (95).

Morphologically, FBs are elongated, spindle-shaped cells, in culture, they adhere substrates and migrate over these substrates. However, they can vary considerably in phenotypic expressions and may exhibit a variety of shapes and sizes in culture (98). They have multiple embryonic origins: while dermal FBs in the dorsal region arise developmentally from the dermomyotome. FBs in the scalp and facial skin

originate from the neural crest (98). Dermal FBs in other body sites arise from an undifferentiated mesenchyme during fetal development. Fetal dermal fibroblasts are physiologically distinct from their adult descendants, and are, in contrast to adult FBs, able to fully regenerate skin without scarring (99-101).

In the skin, FBs are traditionally characterized as papillary and reticular FBs. The upper layer beneath the dermal papillae, contains papillary FBs, the deeper dermis the reticular FBs. The cell density is increased in the papillary dermis, and the thickness of the ECM is increased in the reticular dermis (72). In addition, the expression and secretion of several matrix constituents differ in both the layers. Decorin and collagen XVI are found in the papillary dermis, whereas versican is associated with the reticular dermis (72). However, the traditional skin FB classification was rethought during the last years. scRNAseq studies, including our study in Chapter 1, indicate that FB populations are not limited exclusively to either reticular or papillary layer. We suppose that these attributions are rather a result of the cell isolation process from the skin, as the FBs were harvested from a respective depth of skin layer to study the populations (102, 103). Moreover, different skin subpopulations are found depending on the body site. E.g. Tabib et al. found a specific dipeptidyl-peptidase 4 (*DPP4*) cluster in skin from the upper extremity, while these were not found in other datasets from e.g. abdominal skin (98, 102, 103). However, across datasets, some human skin FB populations are conserved, and when comparing datasets of several authors, three major FB populations, A-C, with 10 major subtypes can be distinguished (104). According to Ascension et al., they are characterized by (A) *ELN, MMP2, QPCT, SFRP2*, (B) *APOE, C7, CYBG and IGFBP7* and C) *DKK3, SFRP1, TNMD, TNN* (104).

A major challenge in investigating FBs is the lack of reliable cell markers. FBs are isolated from skin by consecutive negative selection of immune cells (CD45+, LIN+), endothelial and lymphatic cells (CD31+), erythrocytes (CD235ab+), mesenchymal stem cells (MSCs; CD106+), dead cells (DAPI+), (99). A proposed pan-FB marker is vimentin, and alleged papillary markers are *CD26, NTN1, PDPN*, and reticular fibroblast markers are *ACTA2, PPAR γ , CNN1, COL11A1* (99). The characterization of FB populations and their markers in the skin was traditionally difficult, as majority of previous studies have investigated their functions in vitro. Isolation and culturing of cells strongly affects phenotype and function

of FBs (105). Others used mechanical separation to isolate FB populations, e.g. a dermatome to separate papillary and reticular dermis to characterize the major FB population in each dermal layer by the expression levels of Thy-1 cell surface antigen (*THY1*) and fibroblast activation protein-alpha (*FAP*) (99).

Myofibroblasts

The hallmark cells of all fibrotic pathologies are myofibroblasts (myoFBs), which are mostly FBs that differentiate into myoFBs, or 'activated FBs', upon TGF β 1-signaling (95). The processes regulating the activation of FBs, the characteristics of myoFBs and their consequences are similar in all fibrotic organ pathologies. Thus, it was suggested that myoFB-activation represents a primitive reaction of the body to facilitate immediate tissue repair (95). MyoFBs are marked by their expression of thick bundles ("stress fibers") of α SMA (*ACTA2*) (95), which significantly increases their contractility (106, 107). Smooth muscle cells also express α SMA and are contractile, but myoFBs do not express their smooth muscle cell markers, e.g. myosin heavy chains, h-caldesmon, and smoothelin (108). Aside from tissue-resident differentiation of FBs to myoFBs, there are several other known sources of myoFBs: epithelial cells during epithelial-mesenchymal transition (EMT) and endothelial cells in endothelial to mesenchymal transition (EnMT) (109), pericytes (110), and fibrocytes (111). Fibrocytes are peripheral cells expressing FB specific markers as well as hematopoietic stem cell markers CD34, and the leukocyte antigen CD45. They migrate into damaged tissue and differentiate into myoFBs (112). However, to differentiate into α SMA-expressing mature myoFBs, three steps are necessary: 1) mechanical stress caused by changes to the ECM including an increase in matrix stiffness, 2) the presence of the ED-A splice variant of cellular fibronectin, and 3) the presence of active TGF β 1 (108).

Aside from TGF β 1, several other cytokines and factors were described to directly activate or enhance activation of myoFBs. connective tissue growth factor (*CTGF*) is a well-studied myofibroblast-inducing factor (113), but only acts synergistically with TGF β 1, and does not replace its action (114). Platelet-derived growth factor (PDGF) alone does not induce myoFBs, inhibition thereof was suggested as potential antifibrotic strategy (115).

Upon their activation, myoFBs secrete significantly more ECM, predominantly collagen I and III, but also fibronectin, elastin, fibulin and fibrillin, than quiescent FBs (108). After successful acute tissue repair,

myoFBs physiologically undergo apoptosis or become de-activated (95). However, in case of prolonged inflammation (108), oxidative stress (116), infection (117) or mechanical strain (118), myoFBs persist, and their contractile activity, together with ECM synthesis and degradation, leads to connective tissue remodeling, followed by irreversible and long contractures (119).

Fibrocytes

Fibrocytes are FB-like cells derived from bone marrow mesenchymal and hematopoietic cells (111, 120). Circulating leukocytes infiltrate tissue injured in vivo and gradually acquire the fibrocyte phenotype (CD34⁺CD45⁺VIM⁺), produce collagen, and express α SMA (121). The induction of fibrocyte recruitment is mediated by chemokine receptors CCR2, CCR5, CCR7, CXCR4, CXCR6, growth factor PDGF-BB and Thymic stromal lymphopoietin (*TSLP*) (83). Other cytokines involved in fibrocyte activation are TGF β 1, endothelin-1, IL13, and GM-CSF (83). Moreover, fibroblasts secrete lumican to promote fibrocyte differentiation (122). In contrast, Th1-associated cytokines IL2, transforming growth factor (TNF α), interferon gamma (IFN γ) and IL12 inhibit the activation of fibrocytes (83). Fibrocytes were found to significantly contribute to a plethora of fibrotic pathologies, including pulmonary fibrosis, skin wounds, and kidney fibrosis (123-126).

Pericytes, smooth muscle cells and endothelial cells

Pericytes are mesenchymal cells ensheathing blood vessels. They are involved in development, stabilization, and remodeling of vasculature in homeostasis and during angiogenesis (127, 128). In response to injury, pericytes can detach from the vasculature and differentiate into α SMA-expressing myoFBs. Stimulation with TGF β 1, PDGF, IL1 or activation of toll-like receptors was found to contribute to pericyte-myofibroblast transition (83, 127). Pericytes were described as myofibroblast-precursors and contributors to collagen-deposition and subsequent fibrosis in the kidney, spinal cord, skin, and skeletal muscle (110, 127, 129, 130).

Immune cells

Immune cells substantially regulate fibrosis by controlling the initial and pathologically prolonged inflammatory response to tissue damage. Neutrophils, the first to enter the site of tissue damage, are

innate immune phagocytes that are able to secrete web-like chromatin structures, neutrophil extracellular traps (NETs) (131). NETs protect against infection, particularly by large pathogens, and are associated with a growing number of immune-mediated pathologies (131). NET-mediated tissue damage is believed to promote age-related organ fibrosis (132).

After neutrophils clear pathogens and debris in the early response, they undergo apoptosis. Subsequently, macrophages invade, and clear these apoptotic neutrophils (133). Macrophages are the hallmark cells regulating the immune response following tissue damage. They either invade the tissue as monocytes that differentiate into macrophages, mediated by cytokines like IL-4, IL-10, IFN- γ , IL-13, bacterial products like lipopolysaccharides, or proliferate from tissue-resident embryonic-derived macrophages (133, 134). Macrophages of the early inflammation phase exert phagocytosis, and predominantly display the M1 protein expression pattern and function, which is induced by Th1 cytokines. They effectively kill bacteria and release pro-inflammatory cytokines, such as IL1 β , IL-12, and TNF α (133). Thus, macrophages contribute to wound healing during the inflammatory phase by exerting pro-inflammatory activity via secretion of inflammatory cytokines and growth factors, antigen-presentation and phagocytosis (134). Later during tissue repair, M2-macrophages dominate the macrophage population, releasing anti-inflammatory factors IL10, insulin-like growth factor (IGF), PDGF and TGF β 1, and promote repair and regeneration (133, 134). Later in wound healing, macrophages stimulate keratinocytes, fibroblasts and endothelial cells to enable reepithelialization, ECM formation, and neovascularization during proliferation (134). Macrophages can influence the structure of the ECM in the various phases of wound healing by secreting both of degrading enzymes and ECM components (134). Thus, macrophages directly and indirectly stimulate proliferation of connective, endothelial and epithelial tissue during the proliferative phase. Depletion of macrophages in the early stage of wound healing significantly impairs granulation and epithelialization, but results in minimized scar formation (135).

After minor tissue damage, T-cells play only a minute role in tissue repair and remodeling. However, in major tissue damage or prolonged wound healing or infection, T-cells are activated and participate in tissue repair (134, 136). Macrophages and T-cells communicate via cytokines and co-stimulators, and macrophages facilitate T-cell expansion and differentiation to Th1 and Th2 -cells (134). T-cell activation

results in more complex and prolonged wound healing, resulting in necrosis, increased fibrosis, ulcer or granuloma formation (134).

Type 2/Th2-immune response is mediated by interleukins IL4, IL5, IL9 and IL13 from T-helper 2 cells, mast cells, basophils and type 2 innate lymphoid cells, and is mainly found in allergic inflammation or as response to parasites (137). When type-2 mechanisms become exuberant, they contribute to development of fibrosis, however, blockage of type 2 immunity might result in even more harmful type 1 rebound (137)

Keratinocytes

FBs and KCs were demonstrated to closely interact and influence each other during wound healing and scar formation in a double-paracrine signaling mode (65). Immediately after wounding, KCs secrete pro-inflammatory IL-1, which induces the expression of IL-1-responsive genes e.g., keratinocyte growth factor (KGF), IL-6, epithelial growth factor (EGF) endothelin-1 in FBs. These factors induce KC proliferation and -differentiation, and in later phases of wound healing, shift the cytokine secretion from the early IL-1 response towards a later TGF β 1-response. Another factor, TGF α , is primarily expressed in KCs and has an autocrine effect on KCs in wound healing. Expression of TGF α is upregulated in keratinocytes after skin injury. In the early phase response to wounding, nuclear factor kappa b (NF κ B)-activity in FBs is higher, partially suppressing TGF β -signaling, and is later decreased (65).

During wound healing, KCs undergo the process of epithelial-to-mesenchymal transition (EMT). This term describes a process during which otherwise sessile epithelial cells undergo phenotypic changes, lose cell-cell adhesion and apical-basal polarity, and acquire mesenchymal characteristics to enable cell migration. Factors such as fibroblast growth factor (FGF), hepatocyte growth factor (HGF), EGF and TGF β , among others, were found to facilitate EMT (138). EMT enables KCs to migrate across the wound and restore the epidermis (138). Lack of reepithelialization by KCs in wounds has dramatic effects on subsequent scarring. If wounds are reepithelialized after 2-3 weeks, 22% of the wound sites become fibrotic. If reepithelialization occurs later than 21 days, the rate of fibrotic areas increases to 78% (139).

1.5.3. Signaling in fibrosis

TGFβ1

TGFβ1 constitutes the main driver and central linchpin of all fibrotic processes. It activates several precursor cells to myoFBs, suppresses inflammation and epithelial overgrowth, and shows a plethora of pleiotropic effects on various cell types during wound healing (96, 140). TGFβ1 is secreted together with its latency-associated peptide, and has to be activated to its biological active state, a process that is facilitated by a range of agents including cathepsins, plasmin, calpain, thrombospondin, MMPs and integrins (96, 127). TGFβ1 exerts its activity via several canonical and non-canonical signaling pathways. If a TGFβ ligand binds to the heteromeric TGF-beta I/II receptor, canonical signaling occurs via phosphorylation of Smad2/3, formation of complexes with Smad4 and translocation into the nucleus, with subsequent positive or negative regulation of transcription via binding sites, enhancers or promoters (108, 141). Canonical signaling is tightly controlled via a negative feedback loop by the inhibitors Smad 6 and Smad 7 (142). Non-canonical, or Smad-independent TGFβ signaling occurs via Jun kinase (JNK), p38, MAPK, NFκB, PI3K-Akt-mTOR, and Raf-MEK1/2-ERK1/2, or Rho/Rho-associated kinase (141). In fibrosis and wound healing, the most important target genes include *PAI1*, *COL1A1*, *CCN2*, and *ACTA2*. TGFβ coordinates all phases of wound healing and scar formation by regulating keratinocyte migration, angiogenesis, conversion of fibroblasts to myofibroblasts, and stimulation of ECM production (140, 141). TGFβ1 knockout mice (TGF-β1^{-/-}) exhibit an autoimmune-like inflammatory response that leads to their death at around 3-4 weeks of age (143). On the other hand, immunodeficient TGF-β1^{-/-} Scid^{-/-} mice showed a major delay in wound healing even at the later stages of healing (143). Also TGFβ-2 receptor knockout mice showed defective wound contraction, enhanced re-epithelialization, but also reduced dermal scarring (143). Due to its wide-spread actions, directly targeting TGFβ1-signaling to tackle scar formation failed in clinical trials (140, 141).

Growth factors

Aside from TGFβ, several other growth factors critically regulate wound healing, scar formation and fibrosis. EGF, PDGF, FGF, vascular endothelial growth factor (VEGF), platelet derived growth factor

connective tissue growth factor (CTGF), the interleukin (IL) and tumor necrosis factor-alpha family are critically involved in these processes (144). FGF contains a family of growth factors. FGF-7, or keratinocyte growth factor-1 (KGF-1), and its homologue FGF-10, or KGF-2, are both expressed in acute wounds. They stimulate proliferation, migration and re-epithelialization. Moreover, they facilitate transcription of factors involved in the detoxification of reactive oxygen species (ROS) (144). PDGF is released from degranulating platelets and is crucially involved in all phases of wound healing by stimulation, facilitation of mitogenicity and attraction of neutrophils, macrophages, FBs, and SMCs. Moreover, PDGF induces angiogenesis and is involved in blood vessel maturation (144).

The most important inducer of angiogenesis during wound healing, however, is VEGF-A by promoting migration and proliferation of endothelial cells (144). Increased VEGF-signaling was found in hypertrophic scars and in keloids. VEGF acts directly by stimulating FB migration, proliferation and collagen expression, and indirectly via recruitment of inflammatory cells, and by stimulating protein production, adhesion molecules and mediator production in endothelial cells (145). Vice versa, TGF β , EGF, KGF and PDGF can increase the release of VEGF (144).

EGF and other member of the EGF group, e.g., heparin binding EGF, transforming growth factor-alpha (TGF- α), epiregulin, amphiregulin, betacellulin, epigen, neuregulins (*NRG1*, *NRG2*, *NRG3*, *NRG4*, *NRG5*, and *NRG6*), are released by platelets, macrophages, and fibroblasts. EGF plays the most important role in reepithelialization by increasing KC proliferation and cell migration in acute wounds (144). Activation of EGF-pathways are increased in human burn hypertrophic scars, and EGF also controls the ECM-equilibrium by regulating the MMP-system. However, animal experiment results are contradicting, and the exact role of EGF in the advanced stage of hypertrophic scars is still unclear (146).

Connective tissue growth factor (CTGF) is a multifunctional heparin binding glycoprotein that affects important cellular functions. It is synthesized by FBs and stimulates proliferation and chemotaxis of FBs. CTGF expression is increased after injury and is involved in granulation tissue formation, reepithelialization, and matrix formation and remodeling (144). These effects are not executed by CTGF alone, but synergistic with specific growth factors or through direct interaction with ECM or cell-surface molecules. CTGF is significantly enriched in most fibrotic conditions and its expression also markedly

increased in hypertrophic scars and keloids (144). It is well-known for its roles in ECM production and tissue remodeling. CTGF synergizes the effects of TGF β -signaling and is thus considered a TGF β -downstream modulator in FBs (145, 146).

Angiogenesis

Vasculogenesis is the generation of new blood vessels *de novo*, while angiogenesis describes the formation of new blood vessels from preexisting vessels (147). Angiogenesis is initiated by several cytokines, most notably VEGF, FGF-2, PDGF, and members of the TGF β family, as well other factors such as cardiac ankyrin repeat protein (*CARP*) (148). Angiogenesis begins in the proliferative phase several days after wounding, and angiogenic capillaries begin to sprout into the fibrin/fibronectin wound clot (149). In the granulation tissue, they arrange into a microvascular network, and subsequently, collagen content in the granulation tissue increases, resulting in scar tissue. After full wound closure, the density of blood vessels diminishes during the remodeling phase (149). Endothelial cells, angiogenic cytokines, such as FGF, VEGF, TGF β , angiopoietin, mast cell tryptase, and the ECM environment tightly interact in the angiogenic process. Endothelial cell ECM receptors, especially $\alpha\beta 3$, an integrin receptor binding to fibrin and fibronectin, essentially affect all morphogenetic changes in blood vessels during wound repair (149). Additionally, $\alpha\beta 3$ is expressed on the tips of angiogenic capillary sprouts invading the wound clot, and inhibition of $\alpha\beta 3$ prevents formation of granulation tissue (149). The wound ECM was shown to affect angiogenesis partially by affecting the expression of integrin receptors (148, 149). Wound angiogenesis also appears to be modulated by endothelial cell interaction within the specific three-dimensional ECM setting in the wound area (148, 149). Blocking VEGF signaling via antibody treatment showed an approximately 50% reduction in peak wound vascularity in adult skin wounds, and thus treated wounds also showed a significant reduction in wound scar width. More recent studies have suggested an association of robust capillary growth with the development of keloids and demonstrated that hypertrophic scar formation is associated with higher levels of angiogenesis (148).

Wnt and β -Catenin

Wnt/ β catenin signaling is involved in a vast number of processes, including embryonic development, homeostasis, and self-renewal in adult tissues. An increasing number of studies suggests that Wnt/beta-

catenin is linked with fibrotic processes (150). Wnt proteins are lipid-modified glycoproteins that function through three known pathways, the canonical one of which is Wnt/ β -catenin signaling pathway. Wnt proteins transmit their signal across the plasma membrane through interacting with the Fzd (“Frizzled”) receptor family and members of LRP5/6 (150). Without activation of the Wnt receptor, cytoplasmic β -catenin is phosphorylated by axin, adenomatous polyposis coli protein (*APC*), and glycogen synthase kinase (*GSK*)-3 β , and degraded by the proteasome. However, if activated by a Wnt protein binding to a receptor, β -catenin is dephosphorylated and accumulates in the cytoplasm and enters the nucleus. It then binds to T cell factor Lymphoid enhancer-binding factor to stimulate the transcription of Wnt target genes, including fibrosis-related gene expression, such as fibronectin, matrix metalloproteinase-7 (*MMP*-7), plasminogen activator inhibitor-1 (*PAI*-1), connective tissue growth factor, twist and snail (150, 151). Activation of Wnt/ β -catenin signaling is upregulated in liver, skin, lung, kidney, and cardiac fibrosis, and Wnt was shown to be activated by TGF β 1 and enhance ECM production in ocular fibrosis, while Wnt inhibition suppresses the TGF β 1 inducing effects in ECM synthesis (95).

Wnt signaling is controlled by six known Wnt inhibitor families, Dickkopf proteins (*Dkks*), secreted frizzled-related proteins (*sFRPs*), Wnt-inhibitory factor (*WIF*-1), Wise/*SOST*, Cerberus, insulin-like growth-factor binding protein 4 (*IGFBP4*), Shisa, Wnt-activated inhibitory factor 1 (*Wai1/5T4*), adenomatous polyposis coli down-regulated 1 (*APCDD1*), and *TIK1* (152). In systemic sclerosis, *WIF*-1 and *sFRP* were downregulated, and mice overexpressing *Wnt10b* showed subcutaneous fat loss and dermal fibrosis, indicating an important role of Wnt signaling in fibrosis (150). The canonical Wnt/ β -catenin pathway is activated by *Wnt1*, and thereby also targets a plethora of genes, e.g. connective tissue growth factor (151). β -catenin/*CTNNB1* is an intracellular scaffold protein that interacts with numerous targets, including adhesion molecules, transmembrane-type mucins signaling regulators, and epigenetic or transcriptional regulators, and is involved in myoFB activation and organ fibrosis (75).

Dipeptidyl-peptidase 4 (DPP4)

Aside from above-mentioned well described signaling pathways involved in fibrosis, a new mediator, *DPP4*, was recently closer investigated for its involvement in fibrotic cell signaling. Rinkevich et al. demonstrated that *DPP4*-positive FBs represent a specific fibrogenic dermal lineage and that inhibition

of CD26/DPP4 enzymatic activity during wound healing results in diminished dermal scarring in mice (153).

DPP4 is a cell surface protease classified as a member of the S9 family of proline oligopeptidases, capable of cleaving n-terminal dipeptides adjacent to proline or alanine residues. DPP4 is found ubiquitously in various cell types, including blood cells, fibroblasts, mesothelial cells, epithelial cells, and endothelial cells. Moreover, DPP4 has been identified in numerous organs, such as the placenta, kidney, intestines, prostate, gallbladder, pancreas, and liver (154). DPP4 inactivates several biologically active peptides by removing the n-terminal dipeptide, cleaving a broad range of substrates, including chemokines and vasoactive peptides (155). Moreover, DPP4 also contains binding sites, such as adenosine deaminase e (ADA), that bind to components of the ECM, e.g. fibronectin (154). DPP4 tightly interacts with T-cells and regulates proliferation, activation, migration, inflammation and autoactivation. Moreover, it stimulates T-cell proliferation and promotes TH1 cells as well as proinflammatory factors such as IFN γ , IL-6 and tumor necrosis factor- α (154). In the early stages of wound healing, DPP4 inhibits the recruitment of macrophages, thereby disrupting the inflammatory response, and gradually slowing down the inhibition of macrophages during, leading to higher macrophage count in the wound, which subsequently results in increased fibrosis during wound healing (154, 156, 157).

In the treatment of diabetes mellitus, DPP4 inhibitors (gliptins) are in wide use for control of blood sugar levels (158). In several fibrotic pathologies, including cardiac, hepatic, renal, and dermal fibrosis, DPP4 activity was also found to be altered (159-163) and inhibition of DPP4 activity in animal models attenuated fibrosis(156, 157, 164-167).

Others also reported that inhibition of DPP4-activity tackled ECM secretion and TGF β -mediated pro-fibrotic effects, indicating a prominent role of DPP4 in wound healing and scar formation (168, 169). However, in contrast to mouse studies, reports on the expression and the properties of DPP4 in human skin are scarce and inconsistent (99, 102, 170-174). The expression of DPP4 in skin varies during development: while DPP4 was found in mouse papillary dermis during embryonic and early postnatal development, adult mice expressed DPP4 mainly in the reticular dermis (175, 176). DPP4 expression in FBs of both dermal layers of human skin was described by Tabib et al. (102) who also proposed the

existence of a new significant FB population that is defined by the co-expression of DPP4 and secreted frizzled related protein 2 (*SFRP2*) (177, 178). In contrast, Korosec et al. identified DPP4⁺ FBs mainly in the papillary dermis, but also in the reticular dermis (99).

1.5.4. Extracellular matrix components and their role in fibrosis

Collagen

In skin, as in the entire body, type I collagen is the predominant protein in humans. It interacts with cell surfaces, other extracellular matrix molecules, and growth and differentiation factors. Almost 50 molecules were shown to interact with type I collagen (179). Collagens are categorized into several groups, with 28 various types of collagens that were discovered. By far, the most common collagens are collagen type I through IV, with type I comprising over 90% of the collagen in the human body (180). Collagens type I, II, III and V are fibrillar collagens that typically contain a triple-helical domain and are up to 300 nm long, and assemble into highly ordered, long aggregates called fibrils (181). In skin, several different collagens are present, mainly collagen I and III, forming a so-called heterotypic collagen matrix (181). To form collagen fibrils, the cleavage of globular N- and C-propeptides from procollagen by the procollagen N- and C-proteinases is required as a first step (181). Several proteases, including Members of the tolloid family of zinc metalloproteinases, bone morphogenetic protein 1 (*BMP1*), mammalian tolloid and tolloid like 1 possess C-proteinase activity, and N-proteinase activity is provided by members of the for 'a disintegrin and metalloproteinase with thrombospondin motifs' (ADAMTS) family partake in this first proteolytic step (181). Specifically, ADAMTS2, ADAMTS3 and ADAMTS14 are thus tightly involved in collagen synthesis (181).

After tissue injury, FBs are stimulated by chemokines and growth factors, mainly TGF β , to secrete collagen. Upon activation of FB to myoFBs, they increase the production of collagen, and subsequently replace preliminary fibrin-fibronectin wound matrix by a more complex, stable ECM (182). The provisional ECM containing Collagen I and III is further degraded by matrix-MMPs during the remodeling phase, which in turn are regulated by tissue inhibitors of MMPs (TIMPs) (182). An imbalance of MMPs to TIMPs contributes to hypertrophic scar formation. In contrast to normal skin, hypertrophic scars contain more collagen fibers, and show a different ECM pattern compared to normal skin. In scar, fiber bundles that

are more parallel, thinner, flatter, and organized in a wavy whorl-like pattern (182). Proteoglycans affect the ECM structure during remodeling, leading to a looser architecture with larger interfibrillar spaces, which further contributes to the altered structure of the scar (182).

Elastin

Elastic fibers are present in arteries, lung, skin, ligaments, vocal chords, and elastic cartilage. They confer the properties of elastic recoil and resilience on all vertebrate elastic tissues, properties that are critical to the long-term function of these tissues (183). Only 2-3% of the skin are made of elastin, however, it critically contributes to its structure and function. In the skin, collagens and elastin tightly interact, limiting the stretchability of elastin fibers (182). Elastin derives from monomeric tropoelastin that polymerize to Covalent crosslinks further support the elastin fibers to distribute mechanic forces (182). Despite only one human gene present for tropoelastin (*ELN*), splicing variants can yield at least 13 known isoforms of tropoelastin that all vary in structure (184). During embryonic development, tropoelastin levels are transcriptionally controlled, and synthetization ceases upon completion of tissue formation. In later life, elastin production is not active, unless new tissue formation is required after injury or in pathologies (185). Other than its structural function, elastin pivots in cellular signaling. Tropoelastin mediates the adhesion of various celltypes, binds to protein and integrin receptors and activates signaling pathways (182, 185). In hypertrophic scars, FBs produce less elastin, and elastin levels decrease in the superficial and deep dermis (186), resulting in higher stiffness and impaired mobility (182). Elastin and TGF β tightly interact and significantly contribute to (hypertrophic) scar formation. Their interaction is complex: TGF β is well known to foster the expression and synthesis of elastin (187) and stabilize elastin mRNA (187, 188), which is believed to be caused by post-transcriptional control of elastin expression (187). Elastic fiber degradation can release elastin fragments named elastokines, exerting cytokine-like signaling properties (189), that mediate cell signaling via integrin and syndecan receptors, moreover, microfibrils store TGF β family growth factors for later release, in turn further promoting fibrosis (190).

Fibronectin

Fibronectin (*FN1*) is an abundant soluble constituent of plasma (300 µg/ml) and other body fluids and also part of the insoluble extracellular matrix. FN can be divided into two forms, soluble plasma FN and cellular FN. Plasma FN is synthesized predominantly in the liver by hepatocytes, and cellular FN is expressed by FBs and KCs (182, 191, 192). Fibronectin molecules are the product of a single gene, however, the protein can exist in multiple forms that are derived from alternative splicing of a single pre-mRNA that can produce as many as 20 variants in human fibronectin (191).

Fibronectin is usually present as a dimer composed of two nearly identical ~250 kDa subunits linked covalently near their C-termini by a pair of disulfide bonds. Each monomer consists of three types (FNI-III) of repeating units. FNI contains 12 type I repeats, two type II repeats and 15-17 type III repeats, which together account for approximately 90% of the FN sequence. Type I repeats are about 40 amino-acid residues long and have two disulfide bonds; type II repeats are approximately 60 amino acids in length and two intrachain disulfide bonds; and type III repeats contains 90 residues, but no disulfide bonds (191). FN contributes to cell adhesion and migration processes including embryogenesis, host defense, blood and can produce 20 different transcript variants (191). In wound healing, both plasma and tissue fibronectin are present (192). Upon stimulation by TGFβ, FBs migrate into the wound and facilitate the secretion of cellular FN to form granulation tissue. In early stages of wound healing, plasma fibronectin binds to platelets to form the fibrin clot. Subsequently, tissue fibronectin binds to integrins, collagens and fibrin, newly forming ECM. Additionally, the provisional FN matrix acts as storage for growth factors (192). In hypertrophic scars, FN content is increased (182). The fibronectin slicing variant of extra domain A (EDA) is upregulated in tissue repair, fibrosis, angiogenesis, and cell migration. EDA was found in granules of platelets and contributed to enhanced thrombosis (193). To enable the progression from inflammation to the repair phase, EDA is necessary in wound healing. Thus, cellular fibronectin-EDA contributes of the preliminary ECM and enables FB migration. It was found to enhance the TGFβ-mediated differentiation of FBs to myoFBs in hypertrophic scarring, and EDA-deficient mice were unable to generate αSMA (182). The fibronectin slicing variant of extra domain B (EDB) assists in regulating the fibronectin matrix assembly and regulation of fibronectin-dependent cell growth (182). Cellular and plasmatic fibronectin exert different functions during development: knockout of FN during development is lethal, and levels of cell-secreted fibronectin drop in aging animals (193). Surprisingly, preventing

secretion of cellular FN from FBs prevents scarring after AMI in mice, however, systemic ablation of plasma FN does not inhibit clot formation, nor impair skin wound healing (193).

Proteoglycans

Glycosylated proteins called proteoglycans consist of a core protein with one or more covalently attached glycosaminoglycan-chain(s) (194, 195). The Ser residue is usually bound in the sequence -Ser-Gly-X-Gly-, where X can be any amino acid residue but proline. The chains are long, linear carbohydrate polymers; under physiological conditions, they are negatively charged due to the high content of sulfate and uronic acid groups (194, 195).

Proteoglycans assist in the formation of a normal, healthy ECM to establish and maintain flexibility, strength, and appropriate environment for (skin) cells. Thus, proteoglycans are critically involved in the aggregation and organization of fibrous and elastic ECM components, and moreover affect the presence of growth factors in the skin, coordinating its turnover and regeneration (196). Proteoglycans can be grouped into types according to their size and their glycosaminoglycan chains. The major glycosaminoglycans are chondroitin sulfates/dermatan sulfates, sulfate/chondroitin sulfate proteoglycans, chondroitin sulfate proteoglycans and keratan sulfates. Moreover, based on their structure, location, and function, proteoglycans are sometimes classified into 4 groups: intracellular and extracellular proteoglycans, basement membrane, and cell-surface proteoglycans (196).

Chondroitin sulfates/dermatan sulfates include e.g. decorin (*DCN*) and biglycan (*BGN*), and the larger aggrecan (*ACAN*), the major proteoglycan in cartilage (194, 195). Members of the heparan sulfate/chondroitin sulfate proteoglycans are e.g. small testican (*SPOCK1/2/3*), and larger perlecan (*HSPG2*), betaglycan (*TGFBR3*, Transforming growth factor beta receptor III) and agrin (*AGRN*) (194, 195). Bikunin (*AMBIP*), neurocan (*NCAN*), versican (*VCAN*) and brevican (*BCAN*) are chondroitin sulfate proteoglycans, and fibromodulin (*FMOD*) and lumican (*LUM*) are members of the family of keratan sulfates. Decorin, biglycan, fibromodulin, lumican, ECM protein X (*ECMX*) and ECM protein 2 (*ECM2*) are considered members of the "small leucine-rich proteoglycan family" (SLRPs) (194, 195). Characteristic SLRPs have a core protein of 40–60 kDa with 10–12 leucine-rich repeat motifs (196). They

orchestrate ECM fibril organization, collagen fibril aggregation, and ECM assembly in physiological conditions (196).

Decorin (*DCN*) is the most important interstitial proteoglycan in human skin. It consists of a 36 kDa core protein with single chondroitin sulfate or dermatan sulfate chain (196, 197). Dermal decorin was found with minor expression in the epidermis, to a higher degree in the reticular dermis, but was not present in the papillary dermis (196, 197). Decorin binds to type I collagen-binding proteoglycans in human skin and is thus a critical regulator of fibrillar components (196, 197). In hypertrophic scarring, the levels of decorin and fibromodulin were significantly decreased, whereas biglycan was increased when compared with normal skin. In contrast, there was an enhanced expression of biglycan, fibromodulin, and lumican in the basement membrane and around basal epithelial cells in skin, but these proteoglycans were absent or weakly expressed in HTS (198).

When the versican-degrading protease ADAMTS5 is knocked out, myoFB-differentiation is enhanced, which leads to versican accumulation. This finding indicates that versican regulates wound healing, wound contraction and scarring (196). In scar tissue, aggrecan, another extracellular proteoglycan, was found, but not in normal skin (196, 199). Aggrecan was found to prevent the differentiation of FB progenitors into mature FBs by inhibiting the migration of cells into the wound. Thus, it was suggested as a target for future therapies to prevent scar formation (196, 199).

Other proteoglycans found associated with fibrosis is syndecan-1 (*SDC1*) and SLRPs are biglycan, lumican, decorin, dermapontin and fibromodulin. Biglycan and lumican are upregulated in fibrosis whereas both high and low levels of decorin were reported in tissue repair and fibrosis (197, 198).

Glycoproteins

Glycoproteins are proteins with covalently attached oligosaccharide chains to amino acid side-chains. These proteins are widely present in diverse tissues and include e.g. antibodies, molecules of the major histocompatibility complex (MHC), gonadotropins, ABO-blood antigens, structural ECM glycoproteins, and many more (200, 201). In the matrisome, thrombospondins, laminins, IGFbps, tenascins and fibulins are member of the glycoprotein family (202-206).

The thrombospondin protein family (*THSB1-4*) are highly evolutionary conserved glycoproteins that bind to and interact with various ECM components in a transient or long-term manner. They not only function as ECM components, cytokines, adaptor proteins, and chaperones, but also orchestrate collagen molecules and their structure, and also bind to several proteases and growth factors (202). They also interact with various cell-surface receptors and trigger signaling pathways and phenotypic changes (202). The specific thrombospondin signaling depends on the momentary context, but the pleiotropic mechanisms affect wound healing and angiogenesis, changes of the vasculature, connective tissue organization, and formation of synapses (202).

The members of the family of laminins (*LAMA1-5/LAMB1-4/LAMC1-3*) are glycoproteins in the epithelial basement membrane, and in the basement membrane surrounding fat, muscle and peripheral nerve cells (204, 207). The laminin molecules trimerize into large glycoproteins that contain three disulphide-bonded chains, and were the first ECM components that were described in the embryonic development (204, 207). In neuromuscular diseases, alterations of the laminin molecules and the number and localization of its homologues were found recently. Laminins mainly control the cell-matrix interaction, but affect numerous processes, including cell growth and migration, tumor growth and metastases, neurite outgrowth, nerve regeneration, wound repair, and graft survival (204, 207).

Insulin-like growth factors (IGFs) are essential growth-promoting peptides that act as both endocrine hormones and autocrine and paracrine growth factors. In the blood stream and in specific tissues, most IGF molecules are bound by one of the IGFBP family members, of which six distinct types exist. As the IGFBPs bind to IGF with equal or greater affinity as to the IGF1 receptor, they are thus in an important position to regulate IGF signaling globally and locally. Binding to IGFBP increases the half-life of circulating IGF and blocks its ability to bind to the insulin receptor (106). Furthermore, IGFBPs bind non-IGF ligands in the extracellular space, cell membrane, cytoplasm and nucleus, and thereby affect cell proliferation, survival, and migration in an IGF-independent manner. transcriptional mechanisms as well as by post-translational modifications and proteolysis regulate IGFBP activity (203). The IGFBPs are a family of homologous proteins that have co-developed with IGF and confer both functional and tissue specificity to the IGF regulatory system. IGFBPs are not simply carrier proteins for IGFs but are pivotal

in interactions with ligands and IGF receptors by influencing both the bioavailability and distribution of IGFs in the extracellular environment. In addition, IGFBPs appear to have intrinsic biological activity independent of IGFs (106).

Tenascins are a group of large multimeric ECM glycoproteins. They are transiently expressed after tissue injury, where they are predominantly found in the wound edge. In fibrotic processes, however, they were found to be consistently upregulated (208). They were found widely expressed in connective tissue of all vertebrates, and are classified into four tenascins termed tenascin-C, -R, -X and -W. Each tenascin has a specific expression pattern. Tenascins were described as anti-adhesive, adhesion-modulating, or even repelling ECM proteins despite exerting modest cell adhesion and not promoting cell spreading in comparison to many other ECM proteins (205). Tenascin-C and tenascin-R deficient mice display abnormalities in the nervous system and tenascin-C deficient mice, in addition, have regenerative deficiency. In tenascin-X deficient mice lacking tenascin, hyperelastic skin much like Ehlers Danlos patients was observed (205).

Tenascin-C supports FB migration within the preliminary fibrin-fibronectin matrices of early wound healing. Some parts of the tenascin-C molecule are critical for facilitating cell migration, however, other domains prevent FB migration (208). Tenascin-C is temporarily necessary to enable wound healing to attract FBs into the wound, but if tenascin-C fragments remain in the wound, they might cause exaggerated FB infiltration and thus contribute to fibrosis (208).

In systemic sclerosis, a complex disease with a pathogenic triad of autoimmunity, vasculopathy, and fibrosis of the skin and multiple internal organs, tenascin-C was one of the most highly up-regulated ECM proteins in skin and lung biopsies (208). Additionally, tenascin-C is responsible for prolonged FB activation, thereby driving progression of fibrosis (208).

Fibulins (*FBLN1/2/5/7*) are a family of glycoproteins, like laminins associated with basement membranes, but in contrast to laminins are secreted, and also affiliated with elastic fibers, and other ECM components (209). They are expressed widely across tissues and interact with many ECM constituents. The seven members of the family are characterized by the presence of two structural modules, a tandem repeat of epidermal growth factor-like modules and a unique C-terminal fibulin-type module. They act as mediators

for cellular processes and intermolecular bridges within the ECM to form supramolecular structures, and thus regulate tissue remodeling. These crucial functions of fibulins in a variety of biological processes were shown in in vitro systems, gene knockout mice, and human genetic disorders (209). Fibulins have an elongated multidomain structure that is dominated by numerous calcium-binding epidermal growth factor-like modules, and their isoforms vary considerably in size (50–200 kDa). The activities of fibulins involve the binding of integrin receptors, the regulation of cell proliferation and malignant transformation (210). TGF β stimulates fibulin 5 expression, and overexpression of fibulin 5 enhances basal and TGF β -mediated activation of p38 mitogen-activated protein kinase and Mitogen-activated protein kinase 3 (ERK1/ERK2). Moreover, overexpression of fibulins 5 and 3 increase FB DNA synthesis, thus affecting FB activation (209).

Matricellular proteins

Matricellular proteins form a group of ECM components that do not primarily form the ECM, but rather act as modulators of cell-matrix interactions. Members of the group include e.g. thrombospondins (*TSP1*, *TSP2*), tenascin-C, as already discussed above, secreted protein acidic and cysteine rich (*SPARC*), centralized coordination network (*CCNs*) protein family members, periostin, and osteopontin (*OPN*) (211). These molecules participate in a number of processes related to tissue repair, they can alter the course of wound healing, and lead to fibrosis (92, 212). The respective functions are highly dependent on the context, and the matricellular proteins exert either bind to cell surface receptors or directly to other ECM proteins to form a scaffold that can trigger extracellular signaling pathways, upregulating inflammatory cytokines and other growth factors (213). It was originally described that “classic” matricellular proteins were primarily anti- or de-adhesive (211). *SPARC* (secreted protein acidic and rich in cysteine; BM40, osteonectin), was one of the first described matricellular proteins. The *SPARC* family includes *SPARCs*, *SPARCL1*, *SMOCs*, *SPOCKs*, and follistatin-like protein-1 (*FSTL1*) (214). The *SPARC* family members affect a plethora of processes and regulate cytokine activity, inhibit cell adhesion and cell-cycle progression, regulate ECM assembly, deposition, and cell differentiation, and activate matrix metalloproteinases. In adults, *SPARC* proteins are only expressed during wound healing and remodeling (214).

The matricellular gene family of CCNs includes six cysteine-rich proteins, whose first three initials form the acronym of the CCN genes: CCN1 (*CYR61*), CCN2 (*CTGF*), CCN3 (*NOV*). Further members are CCN4 (*WISP1*), CCN5 (*WISP2*), and CCN6 (*WISP3*) (214). Each one of these genes consists of four characteristic domains: insulin-like growth factor-binding protein domain (IGFBP), Von Willebrand issue type C domain (VWC), thrombospondin kind-1 repeat module (TSR), and carboxy-terminal cysteine-knot (CT) motif (eleven) (214). CCNs are required for embryonic mesenchymal development, and postnatally are only active in pathologies, where they assist in collagen stability and ECM organization (214).

The protein family of small integrin-binding ligand N-linked glycoprotein (*SIBLINGs*) contains the Matrix extracellular phosphoglycoprotein (*MEPE*), dentin sialophosphoprotein (*DSPP*), osteopontin (*SPP1*, *OPN*), and bone sialoprotein (*IBSP*). Even these matricellular components partake mainly in mineralized tissue such as bones and teeth, they also affect and regulate response to injury, cellular proliferation/survival pathways, collagen fibrillogenesis, and MMPs activities (214).

17 proteins form the matrix-gla-family, with matrix Gla-protein (*MGP*) as its most reknown member. The respective gene products are involved in ECM cross-linking and cell migration, adhesion, and proliferation in epithelial and endothelial cells, FBs, osteoblasts, and myocytes. In the ECM, MPG is found in surrounding chondrocytes or endothelial cells, while POSTN is expressed in osteoblasts, mesangial, fibroblasts, mesenchymal, and vascular smooth muscle cells (214).

Integrins

A superfamily of cell adhesion receptors called integrins predominantly detects cell-surface ligands and ECM ligands (215). They are evolutionary very old and highly conserved adhesion receptors, mediating mechanical forces and signaling between cells and the surrounding ECM (216). They contain two subunits, α and β , forming a head and two legs that span and bi-directionally transmit signals through the plasma membrane(216). At least 18 α and eight β subunits are known in humans (215, 216). The mammalian integrins are classified into laminin-binding integrins ($\alpha1\beta1$, $\alpha2\beta1$, $\alpha3\beta1$, $\alpha6\beta1$, $\alpha7\beta1$, and $\alpha6\beta4$), collagen-binding integrins ($\alpha1\beta1$, $\alpha2\beta1$, $\alpha3\beta1$, $\alpha10\beta1$, and $\alpha11\beta1$), leukocyte integrins ($\alphaL\beta2$, $\alphaM\beta2$, $\alphaX\beta2$, and $\alphaD\beta2$), and RGD-recognizing integrins ($\alpha5\beta1$, $\alpha\nu\beta1$, $\alpha\nu\beta3$, $\alpha\nu\beta5$, $\alpha\nu\beta6$, $\alpha\nu\beta8$, and $\alpha11b\beta3$) (215).

Integrins produce an intracellular signal after binding an external ligand, and vice versa, signals from inside the cell can control their activity (215). Binding to ECM macromolecules induces activation, which increases the affinity of individual integrins for ECM ligands and induces clustering of integrins leading to immediate effects, up-regulation of lipid kinase activity and phosphorylation of protein substrate (215, 216). Upon activation, signals are transduced from ECM to the cytoplasm, resulting in outside-in signaling. However, affinity regulation plays a role in integrin priming can also result in inside-out signaling. This induces the lateral redistribution (clustering) which strengthens adhesion. Activated and clustered integrins can then transmit outside-in signaling which can alter cell migration, shape, growth and survival (216).

Integrins $\alpha 1\beta 1$, $\alpha 2\beta 1$, and $\alpha 11\beta 1$ bind to various collagens, including type I and III (91). However, as tight alpha helices of the collagen molecules do not allow adequate integrin binding, integrins have only limited binding properties under physiological conditions. Like many other extracellular matrix proteins mentioned above, integrins thus only actively interact with matrix during development, and during adulthood only upon the secretion and assembly of the provisional ECM after tissue damage (91).

Integrins tightly interact with TGF β and influence tissue regeneration and wound healing by binding to a specific sequence and thus releasing the latent TGF β - complex and all TGF β isoforms that are bound in the ECM, except for TGF $\beta 2$ (193). The TGF $\beta 2$ molecule does not contain these specific motifs, thus TGF $\beta 2$ is liberated from the matrix not by integrins, but rather upon mechanical stimulation (193). When experimentally administering antibodies targeting $\alpha v\beta 1$ -integrin, some cell lines are still able to access and release latent TGF β (193). This finding suggests that $\alpha v\beta 1$ is the main liberator of ECM-bound TGF β in fibrosis (193). The integrin $\alpha 11\beta 1$ acts as prominent collagen I receptor in a subset of dermal FBs and is closely involved in TGF β signaling. Its expression is enhanced in wounds, and was found to interact with tenascin X, thereby paving the way for latent TGF β activation (193).

Of all integrins, αv were found to be the most important regulators of latent TGF β activation from tissues. All cells express one or more type of αv of integrins, thus, they also drive the activation of FBs and promote tissue fibrosis via TGF β (217). $\alpha v\beta 6$ integrin mediates the stress-triggered mechanical release of TGF β from its latent complex, enabling TGF β paracrine signaling. In turn, the stiffer ECM further

enhances the mechanical force onto the bound TGF β latent complexes, in turn again increasing the liberation of TGF β . This creates a positive feedback loop, further stiffening the matrix and driving fibrosis (193). Integrin $\alpha\beta 5$ was also found to contribute to autocrine TGF β signaling in localized scleroderma, and Anti- $\alpha\beta 5$ antibody partially reversed expression levels of type I procollagen and MMP-1 and constitutive DNA-Smad3 (218).

Extracellular matrix remodeling: MMPs and TIMPs

MMPs are tissue-remodeling and ECM-degrading endopeptidases. The large calcium-dependent zinc-containing enzyme superfamily includes collagenases, adamalysins, serralysins, and astacins, and belongs to an even larger family of proteases known as the metzincin superfamily (219). MMPs are secreted by FBs, osteoblasts, macrophages, neutrophils and lymphocytes, and degrade collagens, elastin, gelatin, glycoproteins and proteoglycans (219). MMPs typically contain a propeptide of about 80 amino acids, a catalytic metalloproteinase domain of about 170 amino acids, and linker peptide of variable length, called the 'hinge region', and a hemopexin domain of about 200 amino acids (220, 221).

Aside from 13 MMPs that are directly secreted as proMMPs, MMPs are secreted as pre-proenzymes, and the signal peptide is removed during translation, generating proMMPs. Tissue and bacterial proteases can activate these proMMPs, and the activation of these zymogens tightly regulates MMP activity (220, 221). MMPs display a plethora of different actions, dependent on the substrates, and each MMP has distinct biological effects. E.g., MMP1 cleaves collagen I and fibronectin facilitating cell migration, keratinocyte migration and reepithelialization. MMP13 also cleaves collagen I and activates osteoclasts. MMP2 cleaves chondroitinsulphate proteoglycan, facilitating neurite outgrowth. Several MMPs cleave plasminogen, and MMP9 can cleave latent TGF β and activate it, and also activate latent IL-1 β , and inactivate active IL-1 β (220, 222). MMPs tightly interact with integrins via several mechanisms.

For example, integrin $\alpha 1\beta 1$ mitigates the expression of MMP13, but activation of integrin $\alpha 2\beta 1$ enhances in turn the expression of MMP1 and MMP13 (193). $\alpha 2\beta 1$ enhances NF κ B signaling, which also promotes the secretion of collagen I (193). When MMP expression increases, this is usually concomitant with more FB migration and invasion, further promoting the remodeling of provisional ECM (193).

TIMPs are the natural inhibitors and thus counteracting opponents of MMPs, thus also tightly regulating ECM remodeling and degradation (223). Aside from MMPs, TIMPs also inhibit ADAMs and ADAMTs. Four members of the TIMP family were identified thus far, and TIMPs are capable of inhibiting all known MMPs, but the efficacy of MMP inhibition varies with each TIMP (224). While TIMP-1, TIMP-2 and TIMP-4 are present in soluble forms, TIMP-3 is tightly bound to the matrix (223). TIMPs exert various functions: they were found to promote cell growth, inhibit apoptosis, regulate steroidogenic activity, hematopoiesis, and embryogenesis, and prevent angiogenesis (223). However, their key role is regulation of ECM remodeling. As TIMPs inhibit the breakdown of ECM, increased TIMP levels result in ECM accumulation and fibrosis, while lack of TIMPs leads to increased matrix proteolysis (224). In scars, TIMP-1 and TIMP-2 are increased while MMP1, MMP2, MMP9 and MMP13 are reduced compared to normal skin. Moreover, TIMPs can regulate TGF β activity in tissues, as they prevent release of TGF β from the matrix by MMPs (223).

Proteases

In tissue remodeling, several serine proteases are critically involved. Serine proteases are ubiquitously found enzymes that cleave peptide bonds in proteins with serine serving as the nucleophilic amino acid at the active site (225). Urokinase or tissue-type plasminogen activator (*PLAU*) regulates cellular proteolytic degradation of ECM proteins and maintenance of tissue homeostasis by cleaving proMMPs to active MMPs and latent TGF β to active TGF β . Its most potent inhibitor is plasminogen activator inhibitor-1 (PAI-1, *SERPINE1*), a member of the *serpin* serine protease inhibitor gene family. Thus, PAI-1 is crucial for protecting ECM from proteolytic breakdown (226). On the other hand, PAI-1 deficiency and pharmacological inhibition of PAI-1 protects against fibrosis in animal models (226).

Other members of the family of serine proteases involved in ECM remodeling and fibrosis are elastases. The family of elastase proteases comprises several different members, namely chymotrypsin-like pancreatic elastase (*CELA1/2A/2B/2C/3A/3B*), also called pancreatic elastase, chymotrypsin (*CTRC*),

neutrophil elastase (*ELANE*), and macrophage metalloelastase (*MMP12*) (227). Chymotrypsin-like elastase 1 (*CELA1*), also referred to as pancreatic elastase, (but not expressed in pancreas), is expressed in lung epithelial cells and macrophages during development and in lung regeneration (227). *Cela1* plays a role in stretch-dependent remodeling and fibrotic processes in the lung, particularly elastin fiber organization and function (227).

Neutrophil elastase (NE) endopeptidase contains serine in the active tripeptide catalytic site: Asp, His, Ser, and it is the most abundant of four serine proteases present in neutrophils, others being proteinase 3, cathepsin G, and neutrophil serine protease 4 (*NSP4*). NE is a 29.5 kDa protein, and its substrates are neutral, non-aromatic dipeptides, and thus a broad array of substrates (228). It catalyzes the degradation of elastin, collagens, fibronectin and laminins, and other plasma proteins, e.g. immunoglobulins (227). While neutrophil elastase is hardly present in skin (see Results Chapter 3), it is crucially involved in the pathogenesis of chronic lung disease and fibrosis (228). NE is required for microbial clearance in the airways, however, if dysregulated, NE facilitates prolonged inflammation, impairs the innate immune system, and thus contributes to fibrosis (228).

Lysyl oxidases (LOX) and LOX-like (LOXL) enzymes also contribute to ECM-stiffening and myoFB activation (229). Lysyl Oxidase Like 1 (*LOXL1*) is required for elastin biogenesis and collagen cross-linking and polymerizes tropoelastin monomers into elastin polymers. It regulates elastin homeostasis and matrix remodeling during injury, fibrosis, and cancer development (229). LOX family members are copper dependent monoamine oxidases. *LOX* and *LOXL1* are secreted inactive pro-enzymes, and their pro-regions interact directly with the (ECM), directing the deposition of these enzymes onto elastic tissues. *LOX* and *LOXL1* both regulate in collagen and elastin cross-linking, matrix remodeling in development, injury, fibrosis and cancer, but less is known about the function of the other LOX family members (229). Thus, irregularities of *LOXL1* expression can result in various pathologies due to an imbalance in ECM synthesis and degradation. While decreased *LOXL1* causes increased laxity and impaired elastogenesis, *LOXL1* is a pro-fibrotic factor when overexpressed (229). *LOXL1* deficiency led to elastinopathy and has been observed in ocular and systemic disease, skin aging, chronic obstructive pulmonary disease, emphysema, and aneurysms. On the other hand, an increase of *LOXL1* expression

was found in pulmonary fibrosis, liver cirrhosis, and endometriosis (229). Knockdown of LOXL1 inhibited TGF β 1 induced fibrotic proliferation, and suppressed expression of other pro-fibrotic MMPs and collagen I (230).

1.6. Human skin scarring: translational aspects

Patients with (hypertrophic) scars often suffer from reduced mobility, pain, pruritus, and overall reduced quality of life (53). Various conservative, pharmacological and surgical treatment options are available to treat hypertrophic scars e.g. after (burn) injury or surgery, however, there is no clear consensus on the evidence (56). Conservative treatments and preventive measures to prevent scar hypertrophy include scar massage, pressure therapy, silicone gel/dressing application and hydration, sometimes ultrasound (56). Pharmacological therapies include injection of corticosteroids, most often triamcinolone (TAC), 5-fluorouracil (5-FU), or verapamil. Triamcinolone is most widely used first-line drug, but was shown to cause a series of adverse reactions such as pigmentation and tissue atrophy (58).

Numerous therapeutic agents to tackle (hypertrophic) skin scarring were investigated in clinical trials. However, most of them failed to prove efficacy. E.g., Juvista™ ([clinicaltrials.gov: NCT00742443](https://clinicaltrials.gov/ct2/show/study/NCT00742443)), a recombinant TGF β 3 protein, recombinant IL-10 (NCT00984646), and antisense oligonucleotides (EXC 001; NCT01038297) targeting the expression of connective tissue growth factor (CTGF). Juvista™ failed phase III clinical trial in 2011, IL10 showed no efficacy, and clinical trials for EXC001 were ceased in 2012 with no further update (196). Taken together, although there are numerous methods for treating keloids and hypertrophic scars, there is no satisfactory general method for all (53).

1.6.1. Stem cell-based therapies

Mesenchymal stem cells (MSCs) are multipotent cells with the ability to regenerate and differentiate into a wide range of types. These abilities play key roles in tissue healing and regenerative medicine. In cell therapy and tissue engineering, bone marrow-derived mesenchymal stem cells (BMSCs) are the most often applied stem cells (135, 231). MSCs can migrate into injured sites, differentiate into local components of injured sites, and secrete chemokines, cytokines, and growth factors that assist in tissue regeneration (231). In response to injury signals, BMSCs can move from their location into the peripheral circulation and pass through vessel walls to reach target tissues. BMSCs migration is

regulated by chemical factors, e.g., the *CXCR4*-axis, osteopontin, FGF, VEGF, HGF, IGF1, TGF β , and PDGF, but also by mechanical forces such as stretch, shear stress and ECM stiffness (135).

During the last years, stem cells from bone marrow, adipose tissue, adult blood, cord blood, epidermis, and hair follicle have been investigated in numerous preclinical studies and a few clinical pilot studies for their efficacy in tissue regeneration, wound healing, and various pathologies (79). MSCs from different sources were used in a wide variety of skin diseases in human and in animals. In humans, mesenchymal stem cells (MSCs) from bone marrow- and adipose tissue were found to augment repair in skin wounds in patients (232-234). MSC are now well recognized therapeutics for skin regeneration and rejuvenation. Their application can support collagen and elastin production, tackle MMPs, and attenuate cell damage and senescence caused by UV-irradiation (235).

Autologous adipose-derived cells are often used as treatment for hypertrophic scarring, showing promising clinical results (236). They inherently contain adipose-derived MSCs, or stromal cell-derived factors, and beneficial are mostly mediated by paracrine signaling, modifying the activity of the TGF β /Smad pathway, and normalizes functioning of FBs and KCs in the recipient scar (236). Adipose-derived MSCs inhibited cell proliferation and migration and the expression of ECM proteins and suppressed the expression of TGF β 1 in keloid and hypertrophic scar FBs (237).

As bone marrow- or adipose derived MSC are invasively and difficult to obtain, recent developments in reprogramming skin and other differentiated cells into induced pluripotent stem cells (iPSCs) might provide an alternative cell source of MSCs (238). Human skin equivalents can be generated from iPSCs, and epidermolysis bullosa patients received keratinocyte transplants with *COL17A1*-reprogrammed iPSCs (238). However, FDA-approved cellular therapies use primary human cells, which have strong limitations. They are difficult and invasive to obtain, need certified, expensive laboratories, and proliferation rates are low (238). For the treatment of skin wounds, there is currently no approved stem cell product (238).

1.6.2. Conditioned medium and cell-free therapies

The conditioned medium (CM), i.e. the supernatant of cultivated MSCs (MSC-CM) was investigated extensively and was applied intravenously, intraperitoneally, subcutaneously, intradermally, or

intralesionally injected or topically applied in both animals and humans (239). MSC-CM was shown to improve wound healing, skin rejuvenation, atopic dermatitis, hair restoration, and psoriasis in various human and animal experimental settings.

Moreover, application of MSC-CM decreased hypertrophic scars and flap ischemia in animal models (239). MSC-conditioned medium inhibited cell proliferation and migration of hypertrophic scar and keloid FBs, and attenuated the proliferative and profibrotic phenotype associated with hypertrophic and keloid FBs and inhibit ECM synthesis through paracrine signaling (240). Application of secretome/ CM showed improved wound healing, anti-aging effects, improved cell proliferation, migration, and angiogenesis, suppress cell apoptosis, and inflammation, as well as reduce oxidative stress and immune regulation (234, 239).

Several studies assessed CM injected mainly subcutaneously (241-243) but also intradermally in wounds (239, 244), and several in hypertrophic scar/keloid models (245-247). Other authors compared topical application versus the injection of human embryonic stem cell derived endothelial precursor cells and thereof CM in cutaneous excisional wound models (248). They authors found that the subcutaneous injections is not as effective as the topical application (248).

A recent review by Bormann et al. extensively lists applications of various applications of cell secretomes in dermal wound healing, assessing secretomes from adipose mesenchymal, umbilical cord, antler, amniotic mesenchymal and BMSCs (Figure 4) (49). Numerous clinical trials for the use of MSCs in topical applications are conducted, many of them for cosmetic and aesthetic purposes but hardly any studies were found that investigated the effect of the secretome in human chronic wound healing (49). In contrast to the use of cellular therapies, secretomes offer some advantages: secretome-based biologicals can be virally pathogen cleared, not necessarily stem cells are needed for their production (i.e., PBMCs), enabling easier accessibility, and the secretome of numerous donors can be pooled, thereby smoothing our donor variabilities (49).

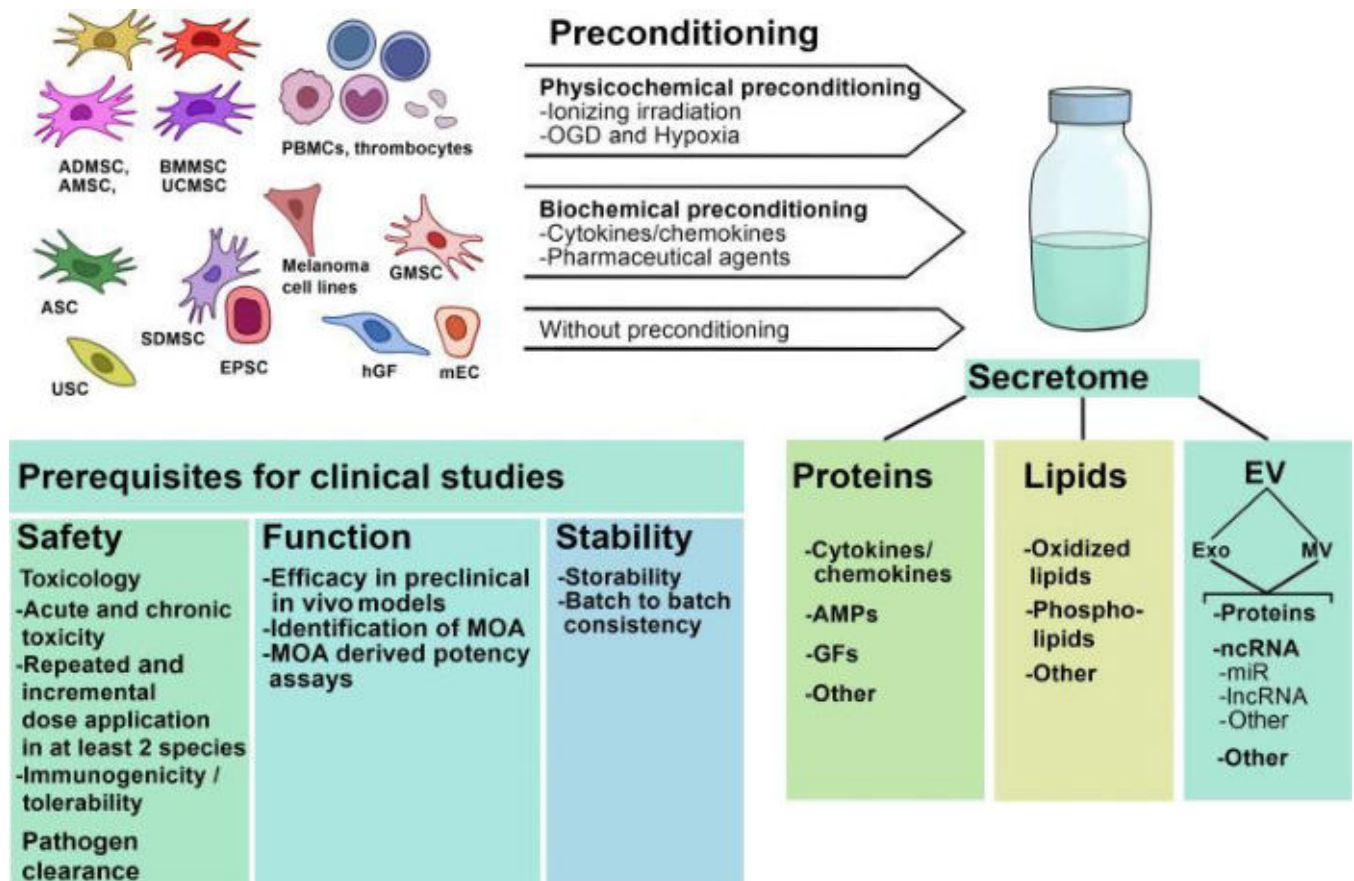


Figure 4: Therapeutic secretomes and their components. Secretomes from various MSCs and their components (ADMSC, adipose tissue-derived mesenchymal stem/stromal cell; AMP, antimicrobial peptide; AMSC, amniotic mesenchymal stem/stromal cell; ASC, antler stem cell; BMSC, bone marrow-derived mesenchymal stem/stromal cell; EPSC, epidermal stem cell; Exo, exosome; GMSC, gingival mesenchymal stem cell; hGF, human gingival fibroblast; lncRNA, long noncoding RNA; mEC, mucosal epithelial cell; miR, microRNA; MOA, mechanism of action; MV, microvesicle; ncRNA, noncoding RNA; OGD, oxygen glucose deprivation; SDMSC, skin-derived multipotent stem/stromal cell; UCMSC, umbilical cord-derived mesenchymal stem/stromal cell; USC, urine-derived stem cell) (49). Use of graphic permitted according to CC BY 4.0 license.

1.7. Aims of the thesis

This thesis aims to characterize the potentially beneficial effect of PBMCsec and its mechanisms of action in healthy human skin and in (hypertrophic) scarring on a single-cell level. Thus, this thesis aims:

- **The transcriptomic landscape of healthy skin**

to establish the characterization of skin cells, particularly FB subpopulations. As discussed above, FB subpopulations are difficult to study, as isolation and cultivation strongly affects their properties. scRNAseq first enables unbiased selection and clustering of FB populations without prior marker definition.

- **Characterization of hypertrophic scars and identification of promising new drug targets**

to use scRNAseq to investigate gene expression and mechanisms involved in hypertrophic scar formation. Although there are several treatment options for hypertrophic scars available, many lack evidence of efficacy and safety, and mechanisms of actions are still unclear. Recently, several proteases have become the focus of drug development in fibrotic diseases, including serine proteases/peptidases such as trypsins and DPP4. However, their role in human scar formation and the underlying anti-fibrotic mechanisms are not yet known. Therefore, this study aimed to provide a genetic landscape of hypertrophic scar tissue and discover potential novel targets for drug development toward scar-free wound healing or regeneration of a present scar.

- **Investigating the anti-fibrotic mechanisms of PBMCsec in skin scarring**

to investigate the potential mechanisms of action of PBMCsec on skin scarring. PBMCsec has shown promising results in pre-clinical studies as a potential treatment option for various conditions, including wound healing and tissue regeneration. The study used a multi-model murine and human approach on a scRNAseq level to unravel the anti-fibrotic activity of PBMCsec and provide mechanistic description of its effects. The study aimed to enable the investigation of PBMCsec for its future clinical use as a treatment option in skin scarring.

2. Results

2.1. Chapter 1: Deciphering the functional heterogeneity of skin fibroblasts using single-cell RNA sequencing

The role of dermal fibroblasts (FBs) in skin homeostasis, wound healing, scar formation, cancer invasion, and aging has gained increasing attention in recent years. Two distinct populations of dermal FBs, papillary and reticular, have been identified based on their anatomical localization in the skin, but recent literature suggests heterogeneity in FB populations in the skin, and classification based solely on anatomical localization may not be sufficient to understand their specific roles in skin homeostasis and tissue regeneration after injury (172). Several markers have been suggested to discriminate between papillary and reticular FBs, including DPP4, an enzyme that cleaves a broad range of substrates. Previous studies have shown conflicting results on the expression and properties of DPP4 in human skin, complicating clinical translation of findings on its role in wound healing and scar formation.

In this study, we used single-cell RNA sequencing to examine the functional heterogeneity of human skin FBs in a manner that mimicked the in vivo scenario. We sought to delineate the complex diversity of FB populations in human skin and characterize the DPP4-expressing FB subpopulation in detail, considering its presumptive role in wound healing and scar formation.

Overall, this study adds to our understanding of the heterogeneity of FB populations in human skin and provides insights into the potential role of DPP4-expressing FBs in wound healing and scar formation. These findings may have implications for the development of new therapies targeting FBs in skin diseases.

RESEARCH ARTICLE

Deciphering the functional heterogeneity of skin fibroblasts using single-cell RNA sequencing

Vera Vorstandlechner¹ | Maria Laggner¹ | Polina Kalinina² | Werner Haslik³ |
Christine Radtke³ | Lisa Shaw⁴ | Beate Maria Lichtenberger⁵ | Erwin Tschachler² |
Hendrik Jan Ankersmit¹ | Michael Mildner²

¹Division of Thoracic Surgery, Medical University of Vienna, Vienna, Austria

²Research Division of Biology and Pathobiology of the Skin, Department of Dermatology, Medical University of Vienna, Vienna, Austria

³Division of Plastic and Reconstructive Surgery, Department of Surgery, Medical University of Vienna, Vienna, Austria

⁴Department of Dermatology, Medical University of Vienna, Vienna, Austria

⁵Skin and Endothelium Research Division, Department of Dermatology, Medical University of Vienna, Vienna, Austria

Correspondence

Michael Mildner, Research Division of Biology and Pathobiology of the Skin, Department of Dermatology, Medical University of Vienna, Lazarettgasse 14, 1090 Vienna, Austria.
Email: michael.mildner@meduniwien.ac.at

Funding information

Österreichische Forschungsförderungsgesellschaft (FFG), Grant/Award Number: 852748/862068; Wirtschaftsagentur Wien, Grant/Award Number: 2343727; ÖAD Sparling Science, Grant/Award Number: SPA06/055

Abstract

Though skin fibroblasts (FB) are the main cell population within the dermis, the different skin FB subsets are not well characterized and the traditional classification into reticular and papillary FBs has little functional relevance. To fill the gap of knowledge on FB diversity in human skin, we performed single-cell RNA sequencing. Investigation of marker genes for the different skin cell subtypes revealed a heterogeneous picture of FBs. When mapping reticular and papillary FB markers, we could not detect cluster specificity, suggesting that these two populations show a higher transcriptional heterogeneity than expected. This finding was further confirmed by in situ hybridization, showing that DPP4 was expressed in both dermal layers. Our analysis identified six FB clusters with distinct transcriptional signatures. Importantly, we could demonstrate that in human skin DPP4⁺ FBs are the main producers of factors involved in extracellular matrix (ECM) assembly. In conclusion, we provide evidence that hitherto considered FB markers are not ideal to characterize skin FB subpopulations in single-cell sequencing analyses. The identification of DPP4⁺ FBs as the main ECM-producing cells in human skin will foster the development of anti-fibrotic treatments for the skin and other organs.

KEYWORDS

CD26, DPP4, extracellular matrix, fibrosis, transcriptome

Abbreviations: BEAM, branched expression analysis and modeling; DC, dendritic cells; DPP4, dipeptidyl-peptidase 4; EC, endothelial cells; ECM, extracellular matrix; FB(s), fibroblast(s); LC, Langerhans cells; LEC, lymphatic endothelial cells; Mac, macrophages; MC, mast cells; PC, pericytes; PC(A), principal component (analysis); scRNAseq, single-cell RNA sequencing; SMC, smooth muscle cells; TC, T-cells; tSNE, t-stochastic neighbor embedding; UMI, unique molecular identifier.

This is an open access article under the terms of the Creative Commons Attribution-NonCommercial-NoDerivs License, which permits use and distribution in any medium, provided the original work is properly cited, the use is non-commercial and no modifications or adaptations are made.

© 2020 The Authors. *The FASEB Journal* published by Wiley Periodicals, Inc. on behalf of Federation of American Societies for Experimental Biology

1 | INTRODUCTION

In the past, dermal fibroblasts (FBs) had been considered to play a rather marginal role with the exclusive responsibility of producing components of the extracellular matrix (ECM), such as collagens and elastin.¹ In recent years, however, FBs have gained increasing attention as their involvement in matrix remodeling during wound healing and scar formation, cancer invasion,² and skin aging has been discovered.^{3,4}

Based on their anatomical localization in the skin, two distinct populations of dermal FBs with different shape and function, *that is*, papillary and reticular FBs, have been identified.^{1,5-10} While the papillary dermis (uppermost 300 μm) displays high cell density, the reticular dermis is characterized by a dense ECM network and rather low cell density.⁵ The majority of previous studies have investigated their functions *in vitro*, which strongly affects phenotype and function of FBs.¹¹ Recently, other strategies have been employed to decipher the roles of papillary and reticular FBs. For instance, Korosec et al have used a dermatome to mechanically separate papillary and reticular dermis and characterized the major FB population in each dermal layer by the expression levels of Thy-1 cell surface antigen (THY1) and fibroblast activation protein-alpha (FAP).¹² Although the so defined populations show all characteristics of either papillary or reticular FBs, their appearance is not strictly limited to the respective skin layer. Furthermore, they showed that the location within the dermis affects the expression of various enzymes and likely also their function. A study by Tabib and colleagues suggests a more diverse picture than initially expected.¹³ Their work revealed, next to several smaller FB populations, the presence of two major FB populations in human skin, which do not coincide with their location in either the papillary or reticular dermis.¹³ Together, recent literature on skin FBs suggests FB heterogeneity in the skin, and a sole classification of skin FBs based on the anatomical localization into papillary and reticular FBs might not be sufficient to fully understand their specific roles in skin homeostasis and tissue regeneration after injury.

So far, several markers have been suggested to discriminate between papillary and reticular FBs, including podoplanin (PDPN), netrin-1 (NTN1), matrix Gla protein (MGP),^{1,5,8} and dipeptidyl peptidase 4 (DPP4).¹² DPP4 is an enzyme which cleaves a broad range of substrates, including chemokines and vasoactive peptides.¹⁴ While DPP4 was previously found in mouse papillary dermis during embryonic and early postnatal development, in adult mice DPP4 expression was mainly located in the reticular dermis.^{15,16} In contrast, Korosec et al have recently demonstrated that DPP4⁺ FBs in human skin are mainly located in the papillary dermis, but also detectable at lower levels in the reticular dermis.¹² In addition, Tabib et al¹³ show DPP4 expression in FBs of both dermal layers in human skin, and suggest a novel major

FB population characterized by co-expression of *DPP4* and secreted frizzled related protein 2 (*SFRP2*), a soluble modulator of Wnt signaling.^{17,18} However, most of the relevant literature on the role of DPP4-expressing skin fibroblasts still originates from mouse studies. Rinkevich et al demonstrated that a distinct DPP4-expressing lineage of FBs in the mouse skin was responsible for elevated ECM deposition and fibrosis during scar formation.¹⁹ Interestingly, inhibition of DPP4 activity results in attenuated matrix secretion and reduced transforming growth factor beta 1 (TGFB1)-mediated pro-fibrotic effects, indicating a prominent role of DPP4 in wound healing and scar formation.^{20,21} In contrast to mouse studies, reports on the expression and the properties of DPP4 in human skin are scarce and inconsistent,^{12,13,22-26} complicating clinical translation of these findings. Moreover, the existence of a DPP4⁺ FB subset responsible for the production of the ECM has not been confirmed in human skin so far.

In the present study, we sought to investigate the functional heterogeneity of human skin FBs in a setting mimicking the *in vivo* situation using single-cell RNA sequencing. Considering the presumptive, yet elusive role of DPP4 in wound healing and scar formation, we delineated the complex diversity of FB populations in human skin and characterized the DPP4-expressing FB subpopulation in detail.

2 | METHODS

2.1 | Ethical statement

This study was approved by the ethics committee of the Medical University of Vienna (Vote Nr 217/2010), and all donors gave written informed consent.

2.2 | Generation of single-cell suspension for single-cell RNA sequencing

Skin samples for single-cell RNA sequencing (scRNAseq) analysis were obtained from three healthy female donors, 30, 36, and 43 years old, from surplus trunk skin removed during abdominoplasty. From each skin sample, three biopsies were taken, enzymatically digested using GentleMACS Human Whole Skin dissociation kit (Miltenyi Biotec, Bergisch-Gladbach, Germany) for 2.5 hours according to the manufacturer's protocol, and processed on a GentleMACS OctoDissociator (Miltenyi). Cell suspensions were passed through 70- and 40- μm filters, and stained with DAPI-dye for 10 seconds. Cells were resuspended in phosphate-buffered saline (PBS) containing 0.04% bovine serum albumin and washed twice. Cells were sorted for viability using an AriaFusion (BD Biosciences, San Jose, CA, USA) high-speed cell sorting device.

2.3 | Single-cell RNA sequencing (scRNAseq)

Immediately after cell sorting, the single-cell suspension was processed for single-cell separation and cDNA library preparation. For generation of Gel Bead-in Emulsion (GEMs), the 10X Genomics Chromium instrument (Single-cell gene expression 3'v2, 10X Genomics, Pleasanton, CA, USA) was used. Processing of the single-cell suspension to a GEM emulsion, library preparation, and RNA sequencing were performed by the Biomedical Sequencing Core Facility of the Center for Molecular Medicine (Center for Molecular Medicine, Vienna, Austria). Obtaining biopsies and acquiring cell suspensions by Chromium instrument occurred within 3.5 hours. In total, data from ~5000 cells were isolated. Sequencing was performed using Illumina HiSeq 3000/4000 (Illumina, San Diego, CA, USA).

2.4 | Data analysis

Raw sequencing data from all samples were demultiplexed and aligned to a reference genome (GrCh38) using the Cell Ranger Fastq pipeline by 10X Genomics. In the fastq-files generated by the fastq-pipeline, cell barcodes, and unique molecular identifiers (UMIs) were counted using the Cell Ranger Count pipeline to generate a gene-barcode matrix. To compare the three donor datasets, the gene-barcode matrices were loaded into Seurat individually, integrated with the recommended standard workflow, and tested for their donor variations (Data not shown). Ultimately, the samples were aggregated in the Cell Ranger Aggregate pipeline, yielding a single gene-barcode matrix of all cells as the basis for secondary analysis.

For secondary analysis, the R-package “Seurat” was used (Seurat v2, Satija Lab, NYU, New York, USA)^{27,28} with R-Studio software in R (The R Foundation, Vienna, Austria).²⁹ To remove unwanted variations in the scRNAseq data, cells were first analyzed for their UMI and mitochondrial gene counts, and cells with low or very high UMI count or high percentage of mitochondrial genes were excluded from the data set. Data were scaled³⁰ and principal component analysis (PCA) was performed. Statistically significant principal components (PCs) were identified by visual inspection and by using the JackStraw Procedure.³¹ Based on significant PCs, clusters were identified using the Louvain algorithm at a resolution of 1.2 and 10 iterations. The preselected PCs and identified clusters served as the basis for t-stochastic neighbor embedding (tSNE), which visually clusters cells in an unsupervised manner according to the similarity of their PCA signature. To identify significant changes in expressed genes in DPP4⁺ versus DPP4⁻ FB, all cells assigned to “FB-clusters were grouped together, and cells with DPP4-log2 fold change higher than 0.5 (scaled data compared to the entire data set)

were defined as “DPP4⁺”. Differentially expressed genes in all DPP4⁺ versus DPP4⁻ FBs in multivariate testing were calculated using the Wilcoxon rank sum test. Adjusted *P* value was calculated by Bonferroni correction based on the total number of genes in the dataset. To confirm statistical significance, an implementation of the Student's *t*-test was employed for each gene of interest in all DPP4⁺ versus DPP4⁻ cells.

2.5 | GO-term analysis and functional network analysis

For functional analysis of differentially expressed genes, gene lists were filtered for significance with adjusted *P* values <.05 (adjusted by Bonferroni correction), and log2 expression fold changes >0.25. Filtered lists were then submitted to ClueGO-tool³² in Cytoscape,³³ and GO-term analysis for biological processes, immune system processes, and molecular functions were included in the calculation. The analysis was calculated with medium network specificity, GO-term fusion was applied and only pathways with *P* values of <.05 were calculated and visualized in the resulting network.

2.6 | Pseudotime and trajectory analysis

To calculate pseudotime values and trajectories, the ‘Seurat’ object was converted to a CellDataSet and loaded into Monocle2.³⁴ Size factors and dispersions were estimated, outliers removed, and clustering was performed after tSNE-reduction. As model formula input for trajectory construction, differentially expressed genes between FB clusters were used, and trajectories were constructed with DDRTree. Branched expression analysis model (BEAM)³⁵ was applied to the branching point, and genes with *q*-value 10⁻³⁰ were displayed in the heatmap.

2.7 | Isolation of skin cell subsets for affymetrix chip analysis

Cells were isolated from abdominal skin as described previously.³⁶ Briefly, epidermis and dermis were separated by incubation with Dispase II (2,4 U/mL; Roche Diagnostics GmbH, Mannheim, Germany) for 18 hours at 4°C. KC, LC, and MC were separated from the epidermis by incubation with Trypsin-EDTA (0.05%; Gibco by Life Technologies, Carlsbad, CA, USA) and DNase I (BD Biosystems) for 30 minutes at 37°C. A suspension of dermal cells was prepared by incubation of the tissue with Liberase Research Grade (400 µg/mL, Roche Diagnostics GmbH, Mannheim, Germany) and DNase I for 3 hours at 37°C. Different subtypes of skin cells were purified by subsequent incubation with the following MicroBeads: CD1a MicroBeads, CD117 MicroBeads, CD2 MicroBeads,

and CD31 MicroBeads. All MicroBeads were obtained from Miltenyi Biotec. Cells were separated on the autoMACS Pro Separator according to the manufacturer's protocols. FB were obtained as a negative fraction after removal of other cell types, including mast cells, schwann cells, T-cells, and endothelial cells from the suspension of dermal cells.

2.8 | Affymetrix gene chip analysis

Total RNA was extracted from the purified cell samples using peqGOLD TriFast (VWR International, Radnor, PA, USA) according to the manufacturer's instructions. Transcriptome analysis was performed at the Core Facility Genomics of the Medical University of Vienna, Austria, using Affymetrix Human Gene 2.1 ST Array (Thermo Fisher, Santa Clara, CA, USA).

2.9 | Venn diagram

A Venn diagram was constructed using the InteractiVenn browser tool.³⁷ Differentially expressed genes of each FB cluster compared to the rest of the FBs with log fold change >0.25 and adjusted *P* value <.05 were used.

2.10 | Immunofluorescence staining

Immunofluorescent staining of DPP4 was performed in normal human skin using samples of healthy human surplus skin obtained from plastic surgeries (usage approved by ethics committee Medical University of Vienna Vote Nr 1149/2011). Samples were fixed in formalin and embedded in paraffin, or frozen in OCT compound using liquid nitrogen for cryosections. Sections of 5 μ m thickness were used for immunostaining according to protocol as described³⁸ with primary and secondary antibodies used as listed in Tables S1 and S2. All staining experiments were performed with mouse or rabbit IgG as negative control. Blocking experiments were done using full-length human DPP4 protein (ab79138, Abcam, Cambridge, USA). Images were acquired by AX70 microscope (Olympus, Hamburg, Germany) using the imaging software MetaMorph (Olympus).

2.11 | RNAScope In situ hybridization

Healthy human skin was formalin fixed and paraffin embedded (FFPE) for RNAScope In Situ Hybridization (Advanced Cell Diagnostics by biotechne, Minneapolis, USA) according to the manufacturer's pretreatment protocol for FFPE samples.³⁹ Samples were hybridized with RNAScope probe Hs-DPP4-CDS-XMm, and signals were visualized by RNAScope 2.5 HD Assay—RED, and counterstained with hematoxylin for 10 seconds. Images were acquired as described above.

2.12 | Magnetic-activated cell sorting of DPP4⁺ and DPP4⁻ fibroblasts

To isolate DPP4⁺ FB, we dissociated full-thickness skin biopsies with MACS Whole Skin Dissociation Kit as described above. Cell suspensions were incubated with rabbit-anti-human-DPP4 antibodies (see Table S1) for 30 minutes at 4°C, washed twice, and incubated with magnetic bead-labeled anti-rabbit antibodies (Table S2) for 30 minutes at 4°C. Cells were washed twice, loaded into an AutoMACS-device (Miltenyi, Biotech), and DPP4⁺ and DPP4⁻ cell populations were separated with the “possel”-program provided by the manufacturer. Both cell fractions were seeded into six-well plates and cultured in DMEM with 10% heat-inactivated fetal bovine serum and 1% penicillin/streptomycin. Supernatants were stored at -80°C, and cells were lysed in 1x Laemmli Buffer (Bio-Rad, Hercules, USA) for western blotting.

2.13 | Western blot analysis

Lysates from DPP4⁺ and DPP4⁻ FB were separated by SDS-PAGE using 4%-15% gradient gels (Bio-Rad). Proteins were transferred onto nitrocellulose membranes (Bio-Rad), blocked with non-fat dry milk, and incubated with primary antibodies (Table S1) overnight at 4°C. Membranes were washed 3 times and incubated with horseradish peroxidase-conjugated secondary antibody (Table S2) for 30 minutes at room temperature. Signals were visualized with SuperSignal West Dura Extended Duration Substrate (ThermoFisher Scientific) and detected by a ChemiDoc XRS+ (Bio-Rad).

2.14 | Enzyme-linked Immunosorbent Assay (ELISA)

Human pro-collagen Ia1 ELISA (R&D Systems, Biotechne, Minneapolis, USA) and human fibronectin ELISA (R&D Systems) were performed in duplicates using supernatants obtained from cultured DPP4⁺ and DPP4⁻ FBs according to the manufacturer's manual. For collagen Ia1 and fibronectin, samples were diluted 1:100 and 1:10, respectively. Absorbance was detected by FluoStar Optima microplate reader (BMG Labtech, Ortenberg, Germany).

3 | RESULTS

3.1 | scRNAseq identifies six transcriptionally distinct FB populations in healthy human skin

To obtain detailed information on FB populations in healthy human skin, we performed scRNAseq of three healthy

donors. After t-SNE-clustering based on principal component analysis, we were able to discriminate between 18 different cell populations in the human skin, including T-cells (TC), dendritic cells (DC), macrophages (Mac), Langerhans cells (LC), mast cells (MC), endothelial cells (EC), lymphatic EC (LEC), pericytes (PC), smooth muscle cells (SMC), four distinct keratinocyte (KC), and six different FB populations (Figure 1A). All clusters were confirmed by visualization of marker gene expressions (Figure 1B) and showed distinct transcriptional patterns when displayed in a heatmap (Figure S1A,B). Separate analysis of all three donors revealed presence of all clusters and comparable cluster marker gene expression in each donor with only minor differences observed in cell numbers (data not shown). Identification of FB clusters by commonly used FB markers, such as vimentin (*VIM*), S100 calcium binding protein A4 (*S100A4*) or fibrillin 1 (*FBNI*) failed, as they were either also detected in several other cell clusters or did not cover all FB subsets (Figure S2). To identify genes that specifically mark the respective FB clusters, we compared the transcriptome of the FB clusters to that of all other cells and screened the resulting gene list for reliable new candidates. Interestingly, we found several marker genes, encoding cytoplasmic [fibulin-1 (*FBLN1*), lumican (*LUM*), and procollagen C-endopeptidase enhancer (*PCOLCE*) Figure 1C-E] and transmembrane proteins [phospholipid phosphatase 3 (*PLPP3*), syndecan 2 (*SDC2*), and matrix remodeling associated 8 (*MXRA8*) (Figure 1F-H)] that were expressed by all FB clusters. *LUM* and *MXRA8* showed the most FB-specific expression pattern. Comparison of all subsets in a Venn diagram identified serpin family G member 1 (*SERPING1*) as the only gene strongly expressed in all six subpopulations (Figure S3). However, its expression was not confined to FBs, since it was also detected in pericytes, smooth muscle cells, and endothelial cells. To further investigate this, we used an alternative method and enriched different skin cell populations using magnetic beads. As shown in Figure S4, we found expression of *LUM*, *PCOLCE*, *SDC2*, and *MXRA8* specifically in FBs, confirming the specificity of these markers.

3.2 | scRNAseq does not mirror identities of papillary and reticular FB

As FBs have been described to show phenotypic heterogeneity, gene expression, and ability to synthesize ECM,^{5,6,13,40} we next wanted to compare the transcriptomes of every identified FB cluster (Data will be made available upon request). Interestingly, this comparison did not reveal the classical discrimination of papillary and reticular FBs, since markers for these FB subsets, such as netrin 1 (*NTN1*), podoplanin (*PDPN*), and matrix Gla protein (*MGP*),^{5,12,41} were detected in all FB clusters (Figure S5). We also screened our data set

for genes which have recently been shown to identify major FB subsets in the skin, such as *THY1*, *FAP*, secreted frizzled-related protein 2 (*SFRP2*), and flavin containing monooxygenase 1 (*FMO1*).^{12,42,43} Remarkably, *THY1* (Figure 2A), *FAP* (Figure 2B), and *FMO1* (Figure 2C) showed only marginal expression in our dataset (15,4% *THY1*⁺, 16,3% *FAP*⁺, and 3% *FMO1*⁺ FB). By contrast, *SFRP2* expression was detected in 60% of all FBs (Figure 2D). These data indicate that, in contrast to identification of FB subsets by marker protein expression, other, strongly expressed marker genes are necessary to properly identify FB subsets in single-cell sequencing analyses. Our analysis identified several other genes, including microfibril-associated protein 5 (*MFAP5*), apolipoprotein E (*APOE*), APC down-regulated 1 (*APCDD1*), beta-1,4-galactosyltransferase 1 (*BGALTI*), C-X-C motif chemokine ligand 1 (*CXCL1*), and WNT inhibitory factor 1 (*WIFI*), as most suitable to discriminate between the different FB clusters present in human skin (Figure 2E-J). Although we observed a clear discrimination of FB1 (Figure 2E) and FB4 (Figure 2H), the clusters FB2 (Figure 2F), FB3 (Figure 2G), FB5 (Figure 2I), and FB6 (Figure 2J) were not clearly distinguishable from each other on the RNA level, suggesting a high transcriptional similarity.

3.3 | FB clusters are functionally heterogeneous

To bioinformatically investigate possible functional differences between the six FB clusters, we performed GO-term analysis using the network visualization and clustering tool ClueGO [25], a Cytoscape plugin [26]. Networks of functionally clustered GO-term groups were generated using genes significantly enriched in each FB cluster. As shown in Figure 3 and Supporting Information Figures S6-S11, we indeed detected significant functional differences. We found strong associations of FB1 with ECM assembly (Figure 3A,B), wound healing (Figure 3C), and angiogenesis (Figure 3D and Figure S6). FB2 and FB5 were mainly associated with immunological processes, including antimicrobial immune response (Figure 3E) and leukocyte migration (Figures 3F, S7 and S10). By contrast, FB3 showed a very specific association with cartilage development (Figure 3G) and leptin signaling (Figures 3H and S8). FB4 was mainly characterized by its response to growth factors (Figures 3I and S9), whereas FB6 was distinguished by its association with interferon-gamma (IFNG) response and p38 and NFκB signaling (Figures 3J-I, S11). Together, our analysis identified six dermal FB subsets which differ significantly from each other with regard to their putative functional properties. Since one of the main functions of FB is the production and assembly of the ECM, to confirm our findings obtained by GO-term enrichment analysis,^{1,5} we investigated this particular process in more detail

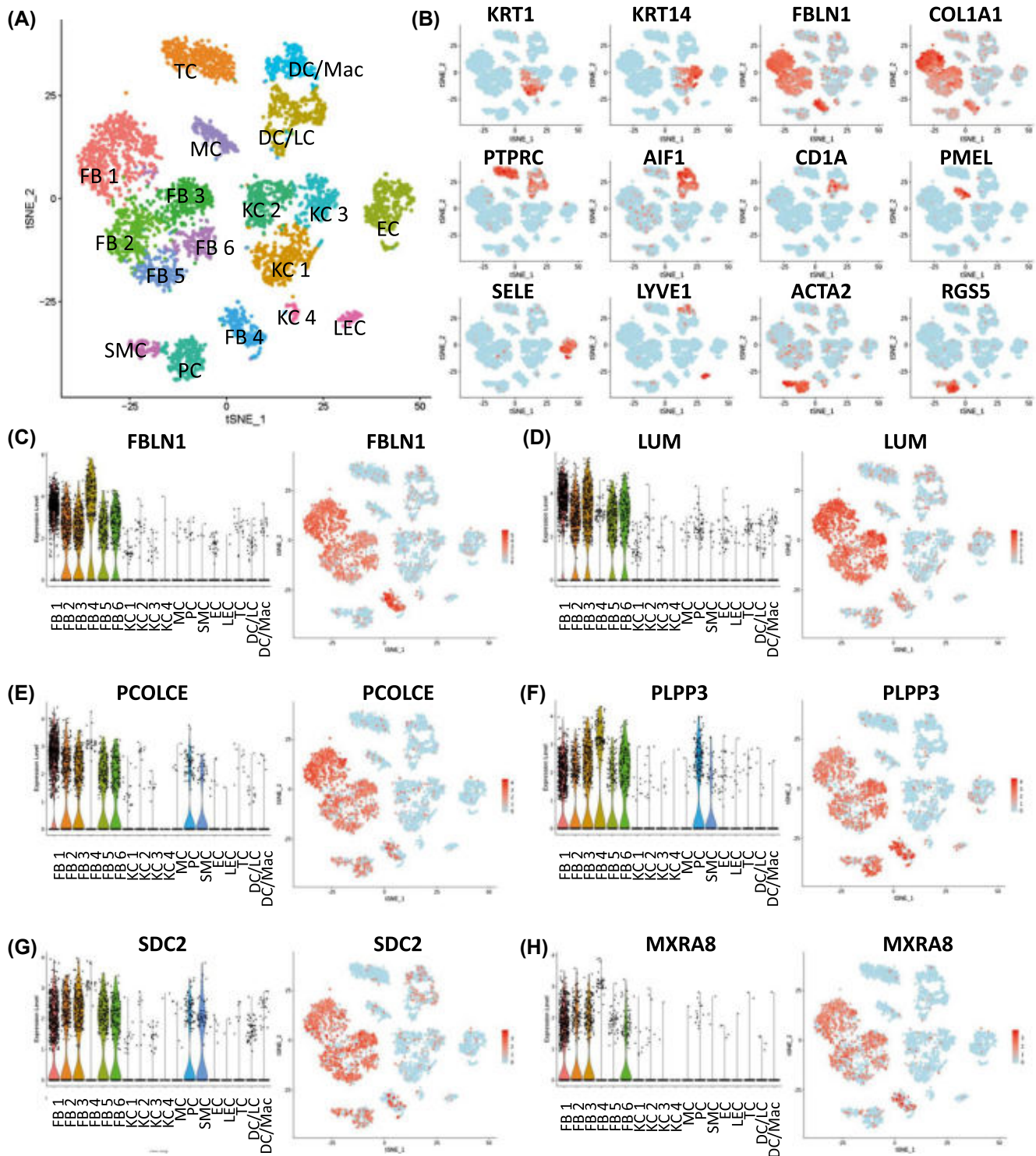


FIGURE 1 Identification of cell types and fibroblast markers in a scRNAseq data set of human skin. A, tSNE-Plot after unsupervised tSNE clustering of 4764 cells yielded 18 cell clusters comprising 6 fibroblast clusters (FB 1-6), 4 keratinocyte clusters, (KC 1-4) melanocytes (MC), smooth muscle (SMC), endothelial (EC) and lymphatic endothelial cells (LEC), pericytes (PC), dendritic cells and Langerhans cells (DC/LC) and dendritic cells/macrophages (DC/Mac), and T-cells (TC). B, Feature plots of marker genes for cell type identification. Keratin 1 (*KRT1*), keratin 14 (*KRT14*), fibulin 1 (*FBLN1*), collagen I (*COL1A1*), protein tyrosine phosphatase receptor type C (*PTPRC*), allograft Inflammatory Factor 1 (*AIF1*), premelanosome protein (*PMEL*), selectin E (*SELE*), lymphatic vessel endothelial hyaluronan receptor 1 (*LYVE1*), actin alpha 2 (*ACTA2*), and regulator of signaling protein 5 (*RGS5*). Feature plots and violin plots of newly identified fibroblast cytosolic FB markers (C-E), and membrane-bound FB markers (F-H). In feature plots, expression of the respective gene is mapped onto the tSNE-plot. Color intensity indicates level of gene expression. In violin plots, dots represent individual cells. y-axis represents log₂ fold change of normalized genes and log-transformed single-cell expression. Vertical lines in violin plots represent maximum expression, shape of each violin represents all results, and width of each violin represents frequency of respective expression level. tSNE, t-stochastic neighbor embedding

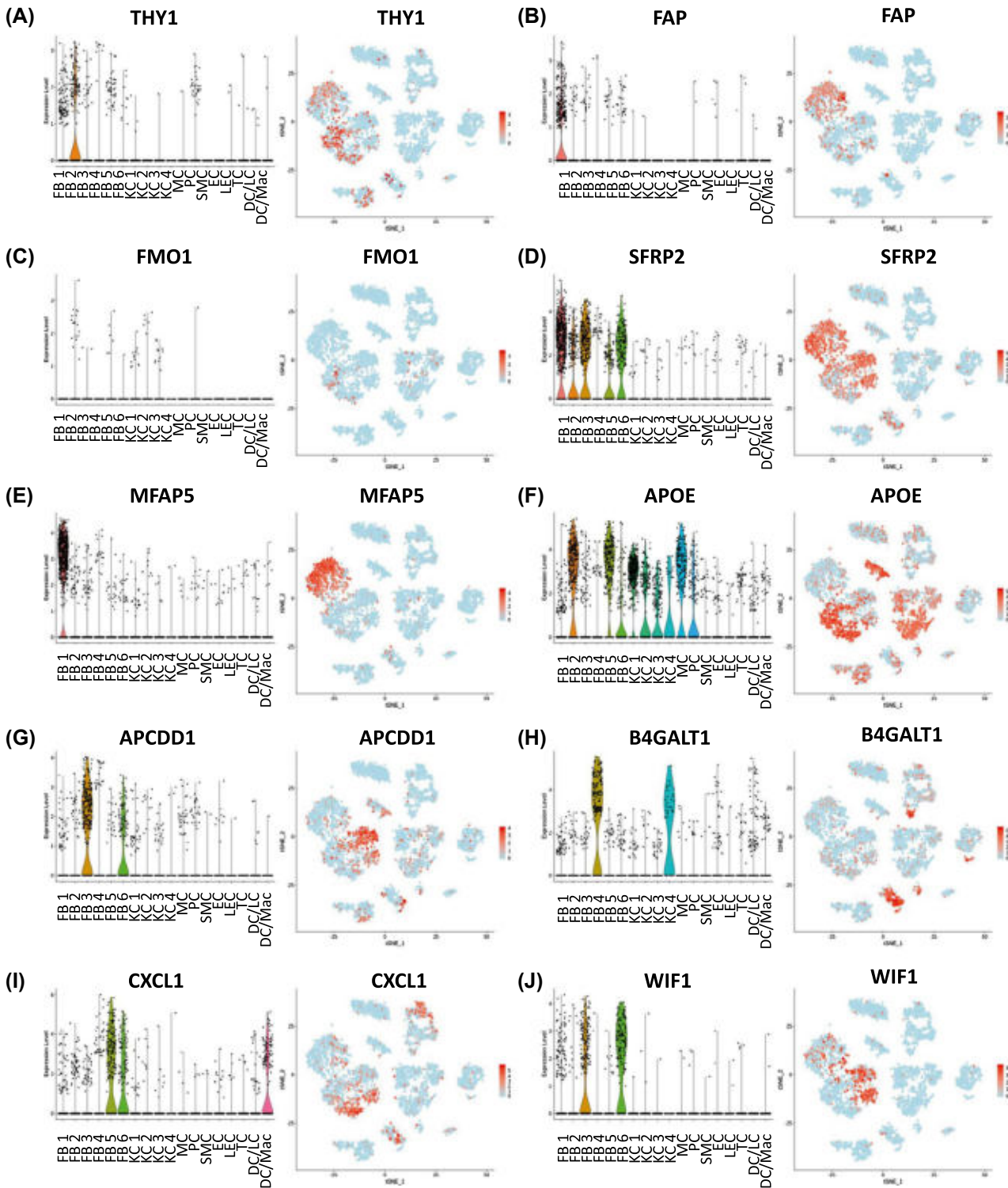


FIGURE 2 Differential gene expression analysis reveals specific genes distinguishing FB clusters. A,B, Feature plots and violin plots of previously described FB marker genes, Thy-1 cell surface antigen (*THY1*), and fibroblast activation protein alpha (*FAP*). C,D, Feature plots and violin plots of previously described FB clustering genes, Flavin-containing monooxygenase 1 (*FMO1*), and secreted frizzled-related protein 2 (*SFRP2*). E-J, Feature plots and violin plots of genes characterizing each FB cluster. Microfibril-associated protein 5 (*MFAP5*), apolipoprotein E (*APOE*), APC downregulated 1 (*APCDD1*), beta-1,4-galactosyltransferase 1 (*B4GALT1*), C-X-C motif chemokine ligand 1 (*CXCL1*), and WNT inhibitory factor 1 (*WIF1*). In violin plots, dots represent individual cells. y-axis represents log₂ fold change of the normalized genes and log-transformed single-cell expression. Vertical lines in violin plots represent maximum expression, shape of each violin represents all results, and width of each violin represents frequency of respective expression level. In feature plots, expression of the respective gene is mapped onto the tSNE-plot. Color intensity indicates level of gene expressions. tSNE, t-stochastic neighbor embedding

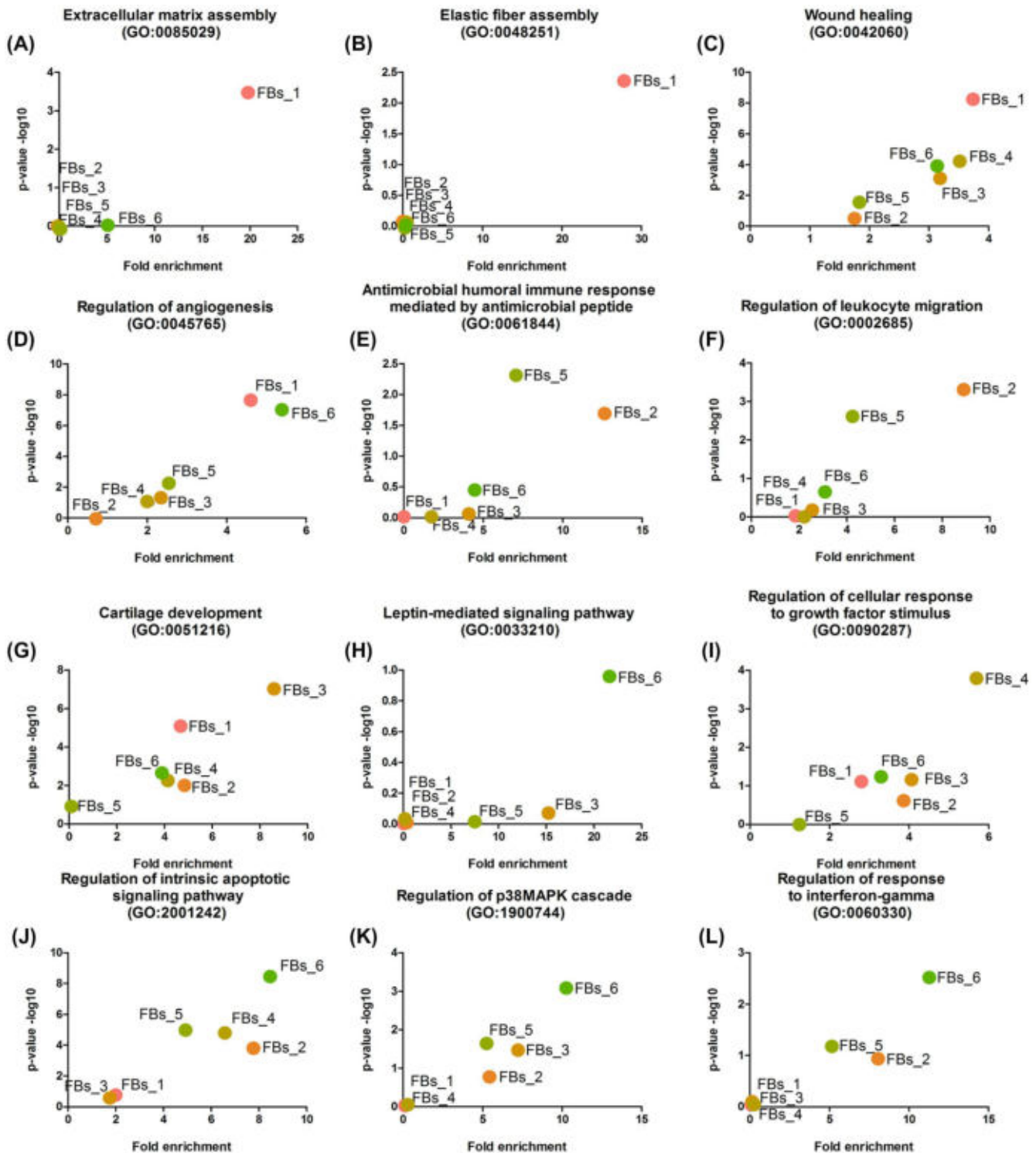


FIGURE 3 FB clusters show distinct functional properties. Scatter plots display fold enrichment and significance of selected relevant gene ontology (GO)-term for each cluster. Lists of differentially upregulated genes of each FB cluster compared to all other FB with log fold change >0.25 and adjusted P value $<.05$ were analyzed by PantherGO tool and calculated fold enrichment and P values were used for graphical depiction. Color code indicates FB subpopulations

by analyzing the expression of components of the ECM and factors important for ECM remodeling in all human FB populations. Interestingly, most of the ECM-related genes investigated showed highest expression levels in FB1 (Figure 4).

Strikingly, among the highest differentially expressed mRNAs, we found many components of the ECM, including the collagens *COL1A1*, *COL1A2*, *COL3A1*, *COL12A1*, as well as elastin (*ELN*), fibronectin (*FNI*), and fibrillin (*FBN1*).

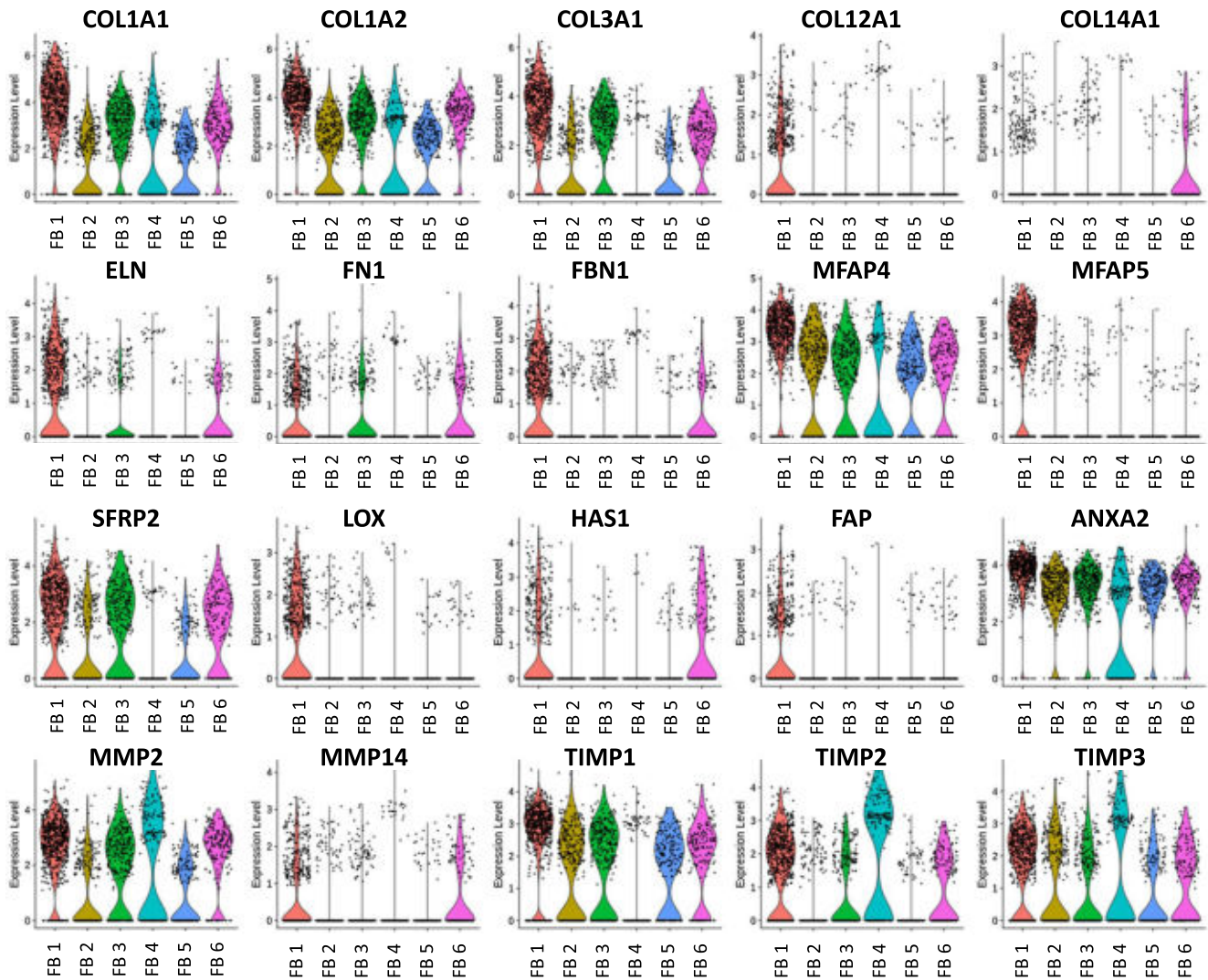


FIGURE 4 ECM-related gene expression differs among FB clusters. Violin plots of genes associated with ECM formation and ECM assembly in all FB clusters. Genes were selected according to GO-terms of ECM-secretion/formation/assembly. Collagens (*COL1A1*, *COL1A2*, *COL3A1*, *COL12A1*, and *COL14A1*), elastin (*ELN*), fibronectin (*FNI*), fibrillin (*FBN1*), microfibril-associated proteins 4 and 5 (*MFAP4* and *MFAP5*), secreted frizzled-related protein 2 (*SFRP2*), lysyl oxygenase (*LOX*), hyaluronan synthase 1 (*HAS1*), fibroblast activation protein alpha (*FAP*), annexin 2 (*ANXA2*), matrix metalloproteinases 2 and 4 (*MMP2* and *MMP14*), tissue inhibitor of metalloproteinases 1, 2, and 3 (*TIMP1*, *TIMP2*, and *TIMP3*). In violin plots, dots represent individual cells. y-axis represents log₂ fold change of the normalized genes and log-transformed single-cell expression. Vertical lines in violin plots represent maximum expression, shape of each violin represents all results, and width of each violin represents frequency of respective expression level. Color code indicates FB subpopulations

We also found overexpression of several factors involved in matrix assembly, such as *MFAP4* and *MFAP5*, *SFRP2*, lysyl oxidase (*LOX*), hyaluronan synthase 1 (*HAS1*), *FAP*, and annexin A2 (*ANXA2*). Interestingly, factors involved in matrix remodeling, such as matrix metalloproteinases (*MMP2*, *MMP14*), as well as the TIMP metalloproteinase inhibitors (*TIMP1*, *TIMP2*, *TIMP3*) were not specifically expressed in FB1. Some of the investigated factors, such as *COL14A1*, *FNI*, *HAS1*, and *MMP14* were either specifically expressed in FB cluster 6 or in both FB clusters 1 and 6, suggesting a contribution of FB cluster 6 to matrix assembly (Figure 4).

3.4 | Functional clustering of *DPP4*⁺ FB reveals a role in ECM assembly, tissue regeneration, and immune defense

Since *DPP4*⁺ FBs were identified as the culprits of ECM deposition and fibrotic scar formation in mice,¹⁹ we next sought to confirm their presence in human skin and closely investigate their properties. Our single-cell sequencing dataset revealed highest expression of *DPP4* in FB1 (Figures 5A,B and S12). In contrast, only minute *DPP4* positivity was detected in other FB clusters, T-cells, dendritic

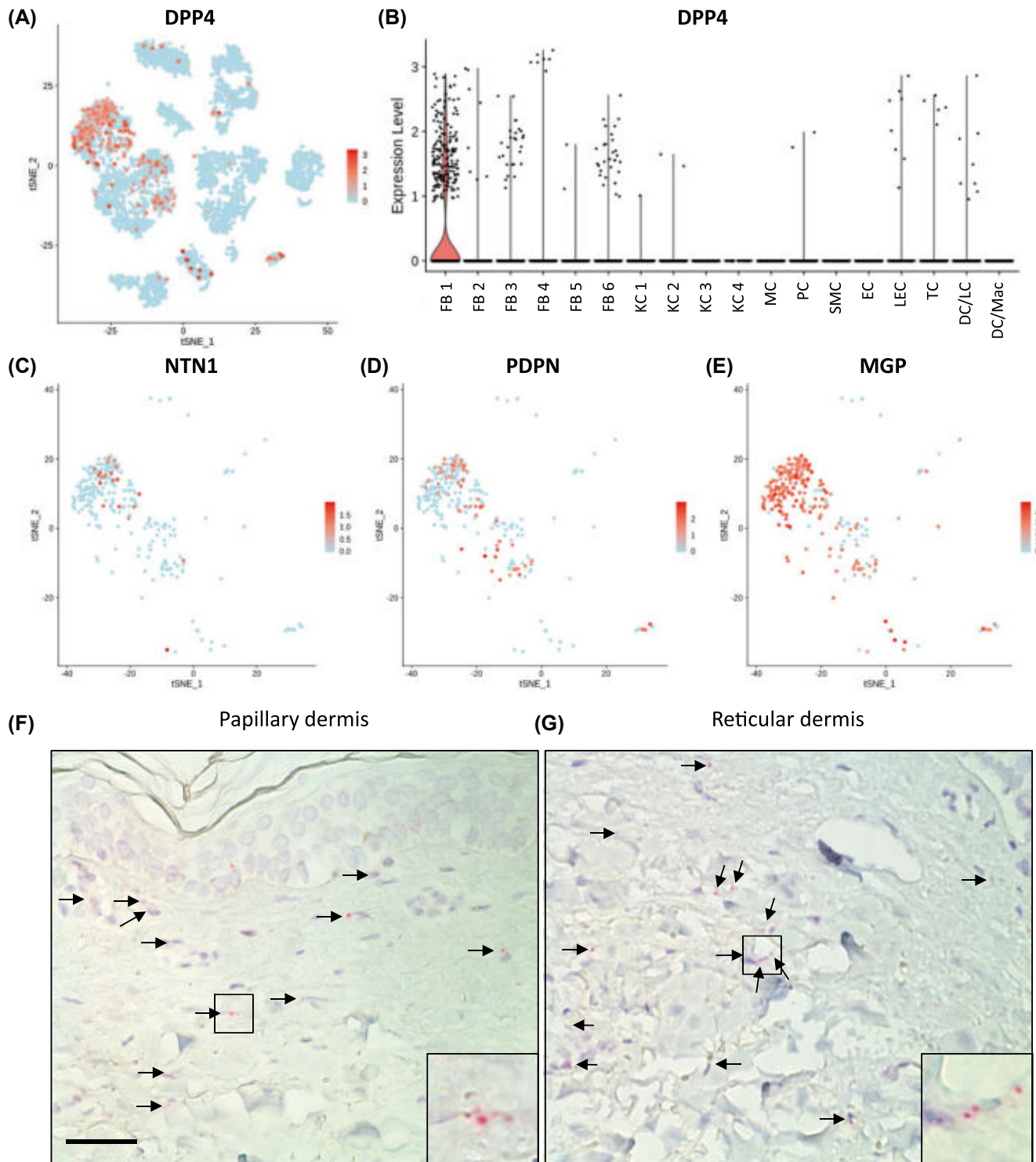


FIGURE 5 $DPP4^+$ FBs are present in reticular and papillary dermis. A,B, Feature plot and violin plot of dipeptidyl peptidase 4 (*DPP4*). Color code indicates subpopulations. C-E, Feature plot of papillary [netrin 1 (*NTN1*), podoplanin (*PDPN*)] and reticular marker genes and matrix Gla protein (*MGP*) in $DPP4^+$ cells only. F,G, RNAScope In situ hybridization of papillary and reticular dermis of paraffin-embedded healthy human skin is shown. Red dots, representing *DPP4*-mRNA molecules, are indicated by arrows. Scale bar 25 μ m

cells, and lymphatic endothelial cells (Figure 5A,B). When analyzing co-expression of *DPP4* with traditional gene markers for FB of the papillary and reticular dermis, we

detected *DPP4^+* FBs in both subsets, suggesting that a clear assignment of *DPP4^+* FBs to either of the two dermal compartments in the human skin, as suggested previously in

mouse skin,^{15,16} is not possible on the transcriptional level (Figure 5C-E). Since data on DPP4 expression in the skin are controversial^{24,34} and to confirm our findings of DPP4⁺ FBs on protein level, we next investigated DPP4 protein expression in human skin by immunofluorescence staining. Strikingly, all antibodies used showed different expression patterns (Figure S13). While antibody #1 exclusively stained tryptase-positive mast cells (Figure S13A) and antibodies #2 and #3 showed only diffuse staining of KCs (Figure S13B,C), antibody #4 revealed strong staining in all FBs. Antibody #5 showed DPP4-positivity in mast cells, blood vessels and melanocytes (Figure S13E), and antibody #6 in mast cells and FBs. Together, our analysis shows that detection of DPP4 in human skin is difficult and results should be interpreted with caution. Since immunostaining was not reliable, we wanted to verify our data by assessing localization of DPP4 mRNA expression in healthy human skin by in situ hybridization using RNAscope. As shown in Figure 5, DPP4⁺ FBs were found in both papillary (Figure 5F) and reticular dermis (Figure 5G), confirming our single-cell sequencing data.

We next analyzed expression of the ECM-related factors shown in Figure 4 in the DPP4⁺ FBs and found that, in comparison to DPP4⁻ FBs, all genes were significantly up-regulated in the DPP4⁺ FB, corroborating the role of DPP4⁺ FB in matrix assembly (Figure 6A). To further characterize DPP4⁺ FBs, we performed GO-term analysis (Figure 6B). Besides the expected association of DPP4⁺ FBs with ECM formation and the pool of active proteases in the skin, our bioinformatics analysis revealed a possible functional involvement of DPP4⁺ FBs in tissue regeneration and immunological processes. Interestingly, our data suggest an antiproliferative, yet cell migration-favoring role of DPP4⁺ FBs. Furthermore, we identified a potential contribution of DPP4⁺ FBs to blood vessel formation and blood coagulation, two events involved in wound healing. Our analysis also suggests a role for DPP4⁺ FBs in immune defense by affecting leucocyte activation and neutrophil degranulation. In contrast to DPP4⁺ FBs, DPP4⁻ FBs were mainly associated with the p38/MAPK and NFκB-pathway, suggesting a role in response to growth and inflammatory stimuli (Figure S14). To corroborate our bioinformatics result of ECM overproduction by DPP4⁺ FBs, we isolated DPP4⁺ and DPP4⁻ FBs from three different donors and analyzed the expression of the ECM-proteins collagen Ia1 and fibronectin by ELISA. Of note, also initially DPP4⁻ FBs expressed low levels of DPP4 after cultivation for several days (Figure 6C), suggesting a positive regulation of DPP4 expression in cultivated FBs. Our analyses revealed a significantly enhanced production of collagen Ia1 and a trend for increased fibronectin production in DPP4⁺ FBs compared to DPP4⁻ FBs (Figure 6D), indicating the DPP4⁺ FB population as the main producer of ECM components in humans.

3.5 | Pseudotime ordering and trajectory construction reveals two possible FB cell fates

To obtain more information on FB cell fates, differentiation, and temporal gene expression changes, we performed pseudotime trajectory analysis by submitting our data set to Monocle2, and constructing a trajectory (Figure 7A) based on pseudotime-sorted cells (Figure 7B). This analysis revealed one branching point splitting FB populations into two directions. Interestingly, FB4 was located at the beginning of the trajectory, suggesting that FB4 is the least differentiated FB population. Conversely, FB5 was located at the end of branch 1, and FB1 at the end of branch 2 (Figure 7A,B). As expected, DPP4 expression was more prominent in branch 2, and increased over pseudotime (Figure 7C). FB clusters 2, 3, and 6 were distributed equally along all branches. Subsequently, BEAM³⁵ identified the most significant pseudotime-dependent genes in the trajectory branches, and assembled them in five gene groups (Figure 7D). While group 1 is defined by high pseudotime-dependent expression of the respective gene at the beginning of the prebranch and at the end of branch 1, group 2 shows high expression at the end of branch 2 only. In contrast, gene groups 3, 4, and 5 show highest expression at the end of branch 2, with gene group 4 additionally at the beginning of the prebranch. As expected, DPP4- and ECM-related genes were pseudotime dependently expressed at the end of branch 2. Interestingly, we identified several other genes similarly regulated that have been described in skin scarring or organ fibrosis, such as *ASPNI* (Asporin),⁴⁴ *PDGFR* (platelet-derived growth factor receptor),⁴⁵ *CTHRC1* (collagen triple helix repeat containing 1),⁴⁶ *AEBP1* (adipocyte enhancer-binding protein 1),⁴⁷ and *TPM1* (Tropomyosin 1),⁴⁸ further underpinning the fibrogenic properties of FB1.

4 | DISCUSSION

Although recent studies on dermal FB populations in the skin have already shed some light on their heterogeneity, little is known about the functional differences of these subpopulations. In the present study, we therefore investigated FB subpopulations and their biological properties in healthy human skin. Using single-cell sequencing, we identified three large FB clusters, one of which can be further subdivided into four smaller clusters (FB2, FB3, FB5, FB6), depicting a far more complex picture of skin FB subpopulations beyond the traditional subsets of papillary and reticular FB.^{1,5,9,10}

Our attempt to identify genes that specifically define all FB populations in single-cell analysis indicated that well-recognized FB markers, such as *VIM*, *S100A4*, *THY1*, or *FAP* [1, 5, 11, 26, 40], are not ideal for this type of analysis, since expression was either not confined to all FB subsets

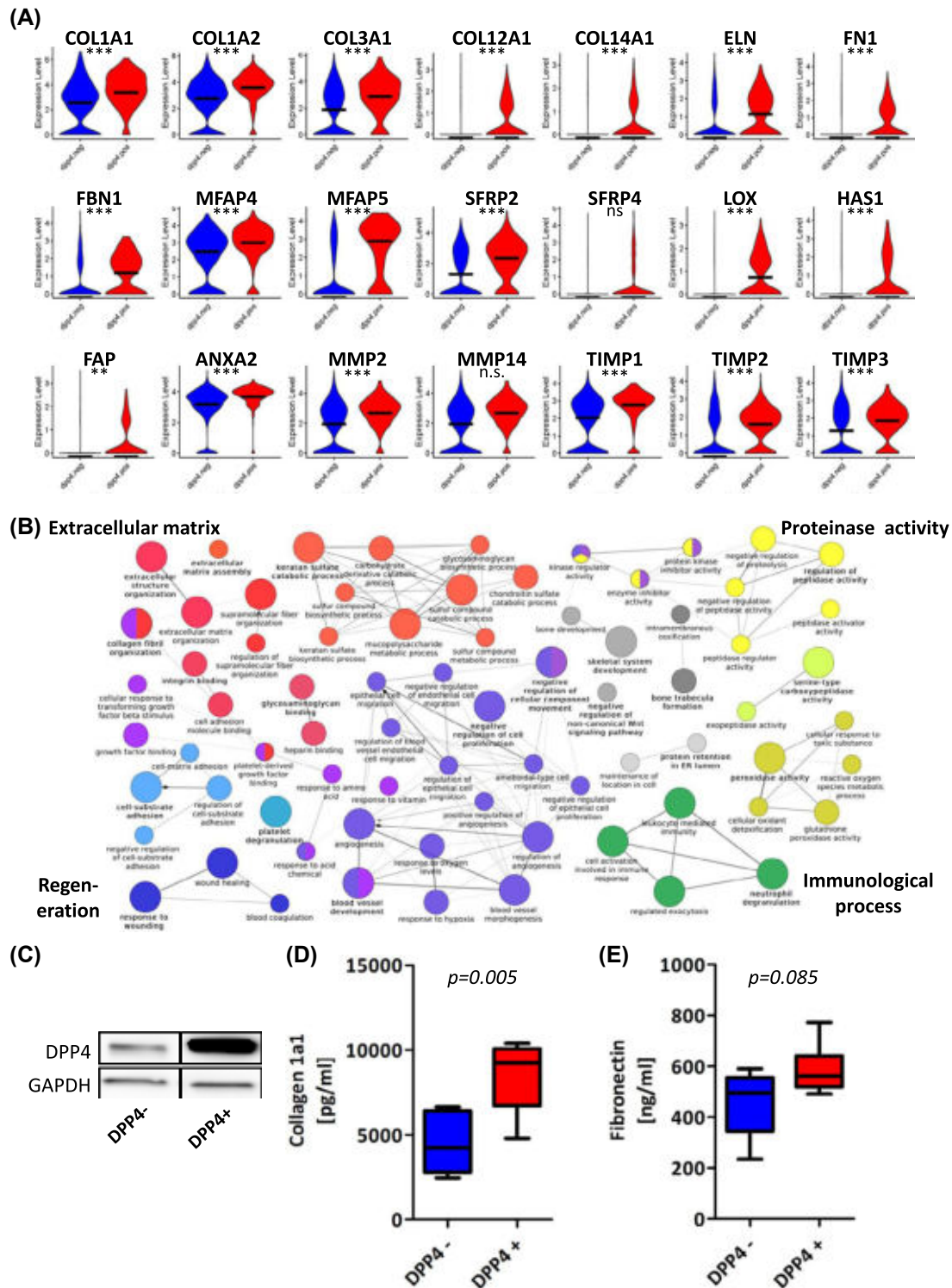


FIGURE 6 DPP4⁺ FBs overexpress ECM-related genes in silico and in vitro. A, Violin plots of selected genes associated with ECM-formation. Blue violins represent respective gene expression in DPP4⁻ FBs, red violins represent respective gene expression in DPP4⁺ FBs. y-axis represents log₂ fold change of normalized genes and log-transformed single-cell expression. Vertical lines in violin plots represent maximum expression, shape of each violin represents all results, and width of each violin represents frequency of respective expression level. Black line indicates mean; ***represents Bonferroni-adjusted *P* value <.001 in Wilcoxon rank-sum test for differential gene expression. B, Network analysis of GO-terms was created using the Cytoscape-plugin ClueGO medium GO-specificity, with GO-term fusion. Only significant (*P* value <.05) GO-terms are shown. Circle size correlates with *P* value, lines (“edges”) represent functional connection of respective GO-terms with input of all genes upregulated in DPP4⁺ FBs compared to DPP4⁻ FBs with fold change >0.25 and adjusted *P* values <.05. C, Western blot analysis of DPP4⁻ and DPP4⁺ FB lysates. One representative of three independent experiments is shown. D,E, ELISA of collagen Ia1 and fibronectin from supernatants of confluent DPP4⁻ and DPP4⁺ FBs. Assay was performed in duplicate from three independent experiments. *P* value was calculated with Student's *t*-test

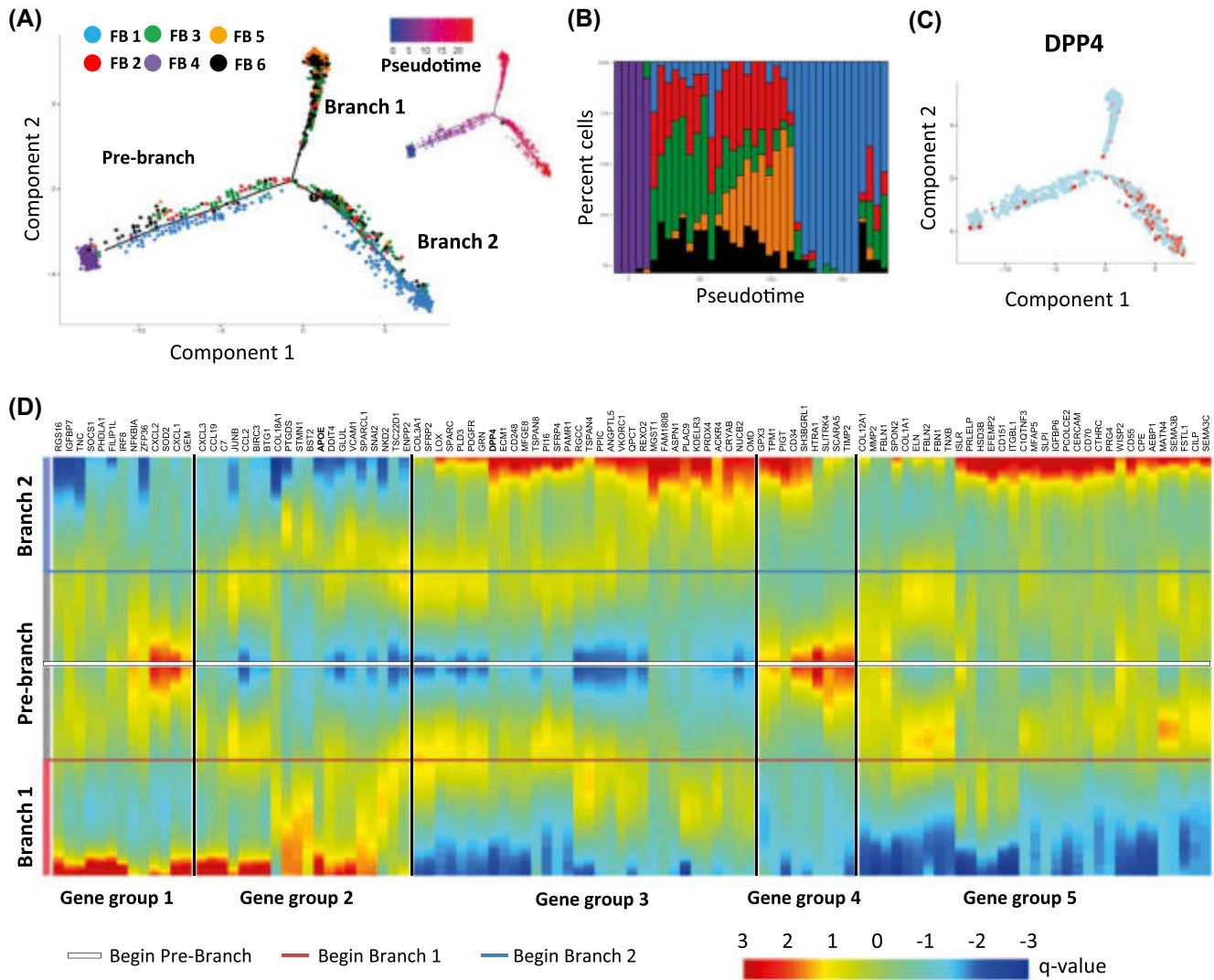


FIGURE 7 Pseudotime ordering and trajectory construction reveal two FB cell fates. A, Trajectory plot of all FBs, color coded by FB clusters 1-6. Lower left corner is the beginning of pseudotime, as indicated in the legend. B, Binplot of FBs across pseudotime. *x*-axis represents pseudotime, *y*-axis represents percentage of cells in respective pseudotime bin. C, Trajectory plot of DPP4 expression. D, BEAM expression of pseudotime-dependent genes in trajectory branches. Colors represent *q*-value

or present in too many other cell types. By contrast, other genes, including *SERPING1*, *FBLN1*, *PLPP3*, *LUM*, *SDC2*, *PCOLCE*, and *MXRA8* reliably identified all FB subpopulations. Interestingly, some of these genes (*PCOLCE*, *PLPP3*, *SDC2*, *SERPING1*) were also found in the pericyte and smooth muscle cell clusters, confirming their high genetic similarity, due to their common mesenchymal progenitor cells.⁴⁹ The membrane-associated factors (*PLPP3*, *SDC2*, *MXRA8*) identified in our study are of special interest, since they could be used to solve a common problem observed in tissue cultures. Purified cell types of enzymatically digested organs are often contaminated with FBs.^{50,51} The newly identified membrane-associated FB markers might represent a novel tool to specifically label and remove unwanted FBs from isolated primary cell suspensions. The feasibility of such an approach merits further investigations.

Recent work by Tabib et al already suggested a higher heterogeneity of dermal FBs than previously expected.¹² Although our study revealed some similarities with their work, we found major differences between our and their analyses. Tabib et al suggested *SFRP2* and *FMO1* as marker genes identifying the two major subset of human skin FBs. By contrast, our analysis showed virtually no expression of *FMO1* in any cell and *SFRP2* expression in almost every FB subset. When analyzing our data set together with that published by Tabib et al using the same settings, the two data sets differed substantially from each other, which could be due to technical reasons, such as different cell numbers or different RNA reads per cell (data not shown). In contrast to the six FB clusters identified in our data set, the dataset by Tabib et al only revealed four different FB subsets. Since site-specific differences in FBs have been described before,⁵²⁻⁵⁴ a further

possible explanation for the observed differences could be that we performed our analyses on abdominal skin, while Tabib et al analyzed sun-exposed skin from the dorsal forearm. In contrast to Tabib et al, who had a more heterogeneous donor cohort (three females and three males; 23–66 years old) at their disposal, we focused on Caucasian female donors younger than 45 years. More studies are needed to fully address the gender-specific and ethnological differences contributing to data variability.

Until now, skin FBs have been characterized as papillary and reticular FB.^{5,8,10,12} Our analysis suggests a novel classification of dermal FB subsets, not solely due to their anatomical location within the skin, but, more importantly, based on their transcriptional signature. Interestingly, our newly identified FB subsets do not overlay with common markers used to identify papillary and reticular FBs, suggesting that FBs with similar functions are distributed over all dermal layers. We identified six FB subsets, each characterized by specific putative biological functions. As shown by our marker gene identification, FB2, FB5, and FB6 showed high similarities on the transcriptional level. Intriguingly, a high similarity of FB2 and FB5 was also observed on the functional level, making a clear distinction difficult. Our GO-term analysis revealed a strong association of these two clusters with leucocyte migration and innate immune defense. Cluster 6, however, showed unique biological functions, including p38/MAPK signaling, response to TNF α and IFN γ as well as response to starvation and hypoxia. In contrast, our analysis suggests a very specific role for FB3 in tissue regeneration. This cluster is mainly characterized by its response to leptin (LEP), which was also identified as one of the main functions of FB6. LEP is a pro-hormone secreted by white adipocytes, targeting the hypothalamus and thereby regulating the energy balance of the body.^{55,56} Interestingly, our transcriptome analysis revealed that FB3 and FB6 highly and FB1 to a minor degree express the LEP-receptor (*LEPR*, Figure S15). Since application of LEP on mouse wounds has been shown to promote wound healing,^{57,58} and blocking of LEP delays wound healing,⁵⁷ our data suggest a contribution of FB3 and FB6 to wound healing in response to LEP.

In contrast to FB2, 3, 5, and 6, FB1 and FB4 displayed the most distinct transcriptomes. While FB4 are functionally associated with response to growth factors, epithelial cell proliferation, and cell morphogenesis, FB1 represents FBs mainly involved in the production and assembly of the ECM. Interestingly, our pseudotime trajectory analysis identified FB4 as the least differentiated and FB1 as one of the more terminally differentiated FB cluster, explaining the vast transcriptional differences. Our analysis suggests a particular function of these FB clusters in wound healing and scar formation. Since DPP4⁺ FBs have been shown to be responsible for augmented ECM production and fibrosis in mice,^{15,19,20,59}

we searched for the DPP4⁺ FB population in our data set and found that *DPP4* expression was almost exclusively restricted to FB1. To the best of our knowledge, our analysis is the first to show that DPP4⁺ FBs are the main producers of factors involved in ECM assembly in human skin. We hypothesize that cells acquiring this cell fate are involved in scar formation after injury and studies comparing human healthy skin and scar tissue could elucidate the real impact of each FB subset on fibrotic processes. Since FBs also constitute the center of fibrotic disease etiology in other organs, this finding might have important implications beyond the skin.^{1,60} In animal studies, DPP4⁺ FBs have been shown to be involved in fibrotic pathologies of several other organs, and inhibition of DPP4 activity by gliptins attenuated fibrotic processes in the lung,⁶¹ heart,^{62,63} kidney,⁶⁴ and liver.⁶⁵ Therefore, our transcriptome analysis of DPP4⁺ FBs in the human skin might represent an important step toward the development of novel anti-fibrotic therapeutic approaches, specifically targeting the DPP4⁺ FB subset. However, further studies are needed to investigate whether such a FB subset with comparable contribution to fibrotic processes indeed exists in other organs in humans.

In summary, we show that dermal FBs are more heterogeneous in terms of their gene expression and function than previously expected. We therefore suggest that the old classification of dermal FBs into papillary and reticular FBs due to their anatomical location should be properly revisited, and believe that a functional classification could lead to more accurate investigations in the future. This could help decipher the exact contribution of FBs to physiological and pathological processes in the skin. In addition, we identified a specific subset of FB as the main producer of ECM in human skin. Our study has built a base for further, more detailed analyses elucidating the roles of the diverse FB populations in the healthy human skin and in fibrotic skin conditions.

ACKNOWLEDGMENTS

This research project was financed in part by the FFG Grant “APOSEC” (852748 and 862068; 2015–2019), by the Vienna Business Agency “APOSEC to clinic,” (ID 2343727, 2018–2020), and by the Aposcience AG under group leader HJA. MM and PK were funded by the Sparkling Science Program of the Austrian Federal Ministry of Education, Science and Research (SPA06/055). We thank HPH for his belief in this private-public partnership to augment patients' health. We thank Prof. Andreas Spittler from the Core Facility Flow Cytometry and Prof. Martin Bilban and Marcus Jeitler from the Core Facility Genomics, Medical University of Vienna, for excellent technical support. We thank the Biomedical Sequencing Facility, Center for Molecular Medicine, Vienna, Austria, for the processing and sequencing of our samples. The authors acknowledge the core facilities of the Medical University of Vienna, a member of VLSI.

CONFLICT OF INTEREST

The authors declare no conflicts of interest.

AUTHOR CONTRIBUTIONS

M. Mildner, E. Tschachler, and H.J. Ankersmit provided study conception and design; W. Haslik and C. Radtke provided patient sample material; H.J. Ankersmit and M. Mildner acquired funding; V. Vorstandlechner and P. Kalinina conducted experiments and prepared samples; V. Vorstandlechner performed data analysis and visualization; M. Laggner, B.M. Lichtenberger, E. Tschachler, and M. Mildner participated in data interpretation; V. Vorstandlechner, M. Laggner, L. Shaw, B.M. Lichtenberger, E. Tschachler, H.J. Ankersmit, and M. Mildner drafted, reviewed, and edited the manuscript.

REFERENCES

- Sorrell JM, Caplan AI. Fibroblasts—a diverse population at the center of it all. *Int Rev Cell Mol Biol*. 2009;276:161-214.
- Kalluri R, Zeisberg M. Fibroblasts in cancer. *Nat Rev Cancer*. 2006;6:392-401.
- Maier AB, Westendorp RG. Relation between replicative senescence of human fibroblasts and life history characteristics. *Ageing Res Rev*. 2009;8:237-243.
- Haydout V, Neiveyans V, Fortunel NO, Asselineau D. Transcriptome profiling of human papillary and reticular fibroblasts from adult interfollicular dermis pinpoints the ‘tissue skeleton’ gene network as a component of skin chrono-ageing. *Mech Ageing Dev*. 2019;179:60-77.
- Janson DG, Saintigny G, van Adrichem A, Mahé C, El Ghalbzouri A. Different gene expression patterns in human papillary and reticular fibroblasts. *J Invest Dermatol*. 2012;132:2565-2572.
- Hiraoka C, Toki F, Shiraishi K, et al. Two clonal types of human skin fibroblasts with different potentials for proliferation and tissue remodeling ability. *J Dermatol Sci*. 2016;82:84-94.
- Janson D, Saintigny G, Mahe C, El Ghalbzouri A. Papillary fibroblasts differentiate into reticular fibroblasts after prolonged in vitro culture. *Exp Dermatol*. 2013;22:48-53.
- Nauroy P, Barruche V, Marchand L, et al. Human dermal fibroblast subpopulations display distinct gene signatures related to cell behaviors and matrixome. *J Invest Dermatol*. 2017;137:1787-1789.
- Schafer IA, Pandey M, Ferguson R, Davis BR. Comparative observation of fibroblasts derived from the papillary and reticular dermis of infants and adults: growth kinetics, packing density at confluence and surface morphology. *Mech Ageing Dev*. 1985;31:275-293.
- Pageon H, Zucchi H, Asselineau D. Distinct and complementary roles of papillary and reticular fibroblasts in skin morphogenesis and homeostasis. *Eur J Dermatol*. 2012;22:324-332.
- Walmsley GG, Rinkevich Y, Hu MS, et al. Live fibroblast harvest reveals surface marker shift in vitro. *Tissue Eng Part C Methods*. 2015;21:314-321.
- Korosec A, Frech S, Gesslbauer B, et al. Lineage identity and location within the dermis determine the function of papillary and reticular fibroblasts in human skin. *J Invest Dermatol*. 2019;139:342-351.
- Tabib T, Morse C, Wang T, Chen W, Lafyatis R. SFRP2/DPP4 and FMO1/LSP1 define major fibroblast populations in human skin. *J Invest Dermatol*. 2018;138:802-810.
- Klemann C, Wagner L, Stephan M, von Horsten S. Cut to the chase: a review of CD26/dipeptidyl peptidase-4's (DPP4) entanglement in the immune system. *Clin Exp Immunol*. 2016;185:1-21.
- Driskell RR, Lichtenberger BM, Hoste E, et al. Distinct fibroblast lineages determine dermal architecture in skin development and repair. *Nature*. 2013;504:277-281.
- Driskell RR, Watt FM. Understanding fibroblast heterogeneity in the skin. *Trends Cell Biol*. 2015;25:92-99.
- Sun Y, Zhu D, Chen F, et al. SFRP2 augments WNT16B signaling to promote therapeutic resistance in the damaged tumor microenvironment. *Oncogene*. 2016;35:4321-4334.
- Heinosalo T, Gabriel M, Kallio L, et al. Secreted frizzled-related protein 2 (SFRP2) expression promotes lesion proliferation via canonical WNT signaling and indicates lesion borders in extraovarian endometriosis. *Hum Reprod*. 2018;33:817-831.
- Rinkevich Y, Walmsley GG, Hu MS, et al. Skin fibrosis. Identification and isolation of a dermal lineage with intrinsic fibrogenic potential. *Science*. 2015;348:aaa2151.
- Thielitz A, Vetter RW, Schultze B, et al. Inhibitors of dipeptidyl peptidase IV-like activity mediate antifibrotic effects in normal and keloid-derived skin fibroblasts. *J Invest Dermatol*. 2008;128:855-866.
- Thielitz A, Ansoorge S, Bank U, et al. The ectopeptidases dipeptidyl peptidase IV (DP IV) and aminopeptidase N (APN) and their related enzymes as possible targets in the treatment of skin diseases. *Front Biosci*. 2008;13:2364-2375.
- van Lingen RG, van de Kerkhof PC, Seyger MM, et al. CD26/dipeptidyl-peptidase IV in psoriatic skin: upregulation and topographical changes. *Br J Dermatol*. 2008;158:1264-1272.
- Pantano S, Dubost V, Darribat K, et al. Differential expression of dipeptidyl peptidase IV in human versus cynomolgus monkey skin eccrine sweat glands. *J Mol Histol*. 2013;44:733-747.
- Philippeos C, Telerman SB, Oules B, et al. Spatial and single-cell transcriptional profiling identifies functionally distinct human dermal fibroblast subpopulations. *J Invest Dermatol*. 2018;138:811-825.
- Van den Oord JJ. Expression of CD26/dipeptidyl-peptidase IV in benign and malignant pigment-cell lesions of the skin. *Br J Dermatol*. 1998;138:615-621.
- Novelli M, Savoia P, Fierro MT, Verrone A, Quaglino P, Bernengo MG. Keratinocytes express dipeptidyl-peptidase IV (CD26) in benign and malignant skin diseases. *Br J Dermatol*. 1996;134:1052-1056.
- Stuart T, Butler A, Hoffman P, et al. Comprehensive integration of single cell data. *bioRxiv*. 2018:460147.
- Butler A, Hoffman P, Smibert P, Papalexi E, Satija R. Integrating single-cell transcriptomic data across different conditions, technologies, and species. *Nat Biotechnol*. 2018;36:411-420.
- Freytag S, Tian L, Lonnstedt I, Ng M, Bahlo M. Comparison of clustering tools in R for medium-sized 10x Genomics single-cell RNA-sequencing data. *F1000Research*. 2018;7:1297.
- Buettner F, Natarajan KN, Casale FP, et al. Computational analysis of cell-to-cell heterogeneity in single-cell RNA-sequencing data reveals hidden subpopulations of cells. *Nat Biotechnol*. 2015;33:155-160.
- Macosko EZ, Basu A, Satija R, et al. Highly parallel genome-wide expression profiling of individual cells using nanoliter droplets. *Cell*. 2015;161:1202-1214.

32. Bindea G, Mlecnik B, Hackl H, et al. ClueGO: a cytoscape plug-in to decipher functionally grouped gene ontology and pathway annotation networks. *Bioinformatics*. 2009;25:1091-1093.
33. Lotia S, Montojo J, Dong Y, Bader GD, Pico AR. Cytoscape app store. *Bioinformatics*. 2013;29:1350-1351.
34. Trapnell C, Cacchiarelli D, Grimsby J, et al. The dynamics and regulators of cell fate decisions are revealed by pseudotemporal ordering of single cells. *Nat Biotechnol*. 2014;32:381-386.
35. Qiu X, Hill A, Packer J, Lin D, Ma YA, Trapnell C. Single-cell mRNA quantification and differential analysis with census. *Nat Methods*. 2017;14:309-315.
36. Gschwandtner M, Paulitschke V, Mildner M, et al. Proteome analysis identifies LICAM/CD171 and DPP4/CD26 as novel markers of human skin mast cells. *Allergy*. 2017;72:85-97.
37. Heberle H, Meirelles GV, da Silva FR, Telles GP, Minghim R. InteractiVenn: a web-based tool for the analysis of sets through Venn diagrams. *BMC Bioinformatics*. 2015;16:169.
38. Gschwandtner M, Mildner M, Mlitz V, et al. Histamine suppresses epidermal keratinocyte differentiation and impairs skin barrier function in a human skin model. *Allergy*. 2013;68:37-47.
39. Wang F, Flanagan J, Su N, et al. RNAscope: a novel in situ RNA analysis platform for formalin-fixed, paraffin-embedded tissues. *J Mol Diagn*. 2012;14:22-29.
40. Sriram G, Bigliardi PL, Bigliardi-Qi M. Fibroblast heterogeneity and its implications for engineering organotypic skin models in vitro. *Eur J Cell Biol*. 2015;94:483-512.
41. Lv F-J, Tuan RS, Cheung KMC, Leung VYL. Concise review: the surface markers and identity of human mesenchymal stem cells. *Stem Cells*. 2014;32:1408-1419.
42. Kisselbach L, Merges M, Bossie A, Boyd A. CD90 expression on human primary cells and elimination of contaminating fibroblasts from cell cultures. *Cytotechnology*. 2009;59:31-44.
43. Park JE, Lenter MC, Zimmermann RN, Garin-Chesa P, Old LJ, Rettig WJ. Fibroblast activation protein, a dual specificity serine protease expressed in reactive human tumor stromal fibroblasts. *J Biol Chem*. 1999;274:36505-36512.
44. Ong CT, Khoo YT, Mukhopadhyay A, et al. Comparative proteomic analysis between normal skin and keloid scar. *Br J Dermatol*. 2010;162:1302-1315.
45. Klinkhammer BM, Floege J, Boor P. PDGF in organ fibrosis. *Mol Aspects Med*. 2018;62:44-62.
46. Li J, Wang Y, Ma M, et al. Autocrine CTHRC1 activates hepatic stellate cells and promotes liver fibrosis by activating TGF-beta signaling. *EBioMedicine*. 2019;40:43-55.
47. Gerhard GS, Hanson A, Wilhelmsen D, et al. AEBP1 expression increases with severity of fibrosis in NASH and is regulated by glucose, palmitate, and miR-372-3p. *PLoS ONE*. 2019;14:e0219764.
48. Wu J, Ma B, Yi S, et al. Gene expression of early hypertrophic scar tissue screened by means of cDNA microarrays. *J Trauma*. 2004;57:1276-1286.
49. Bergers G, Song S. The role of pericytes in blood-vessel formation and maintenance. *Neuro Oncol*. 2005;7:452-464.
50. Xiao L, McCann JV, Dudley AC. Isolation and culture expansion of tumor-specific endothelial cells. *J Vis Exp*. 2015;(105):e53072.
51. Halfon S, Abramov N, Grinblat B, Ginis I. Markers distinguishing mesenchymal stem cells from fibroblasts are downregulated with passaging. *Stem Cells Dev*. 2011;20:53-66.
52. Castor CW, Prince RK, Dorstewitz EL. Characteristics of human "fibroblasts" cultivated in vitro from different anatomical sites. *Lab Invest*. 1962;11:703-713.
53. Chang HY, Chi JT, Dudoit S, et al. Diversity, topographic differentiation, and positional memory in human fibroblasts. *Proc Natl Acad Sci U S A*. 2002;99:12877-12882.
54. Rinn JL, Bondre C, Gladstone HB, Brown PO, Chang HY. Anatomic demarcation by positional variation in fibroblast gene expression programs. *PLoS Genet*. 2006;2:e119.
55. Wada N, Hirako S, Takenoya F, Kageyama H, Okabe M, Shioda S. Leptin and its receptors. *J Chem Neuroanat*. 2014;61-62:191-199.
56. D'souza AM, Neumann UH, Glavas MM, Kieffer TJ. The glucoregulatory actions of leptin. *Mol Metab*. 2017;6:1052-1065.
57. Murad A, Nath AK, Cha ST, Demir E, Flores-Riveros J, Sierra-Honigsmann MR. Leptin is an autocrine/paracrine regulator of wound healing. *FASEB J*. 2003;17:1895-1897.
58. Ring BD, Scully S, Davis CR, et al. Systemically and topically administered leptin both accelerate wound healing in diabetic ob/ob mice. *Endocrinology*. 2000;141:446-449.
59. Hu MS, Longaker MT. Dipeptidyl peptidase-4, wound healing, scarring, and fibrosis. *Plast Reconstr Surg*. 2016;138:1026-1031.
60. Rosenbloom J, Macarak E, Piera-Velazquez S, Jimenez SA. Human fibrotic diseases: current challenges in fibrosis research. In: Rittié L, ed. *Fibrosis: methods and protocols*. New York, NY: Springer; 2017:1-23.
61. Suzuki T, Tada Y, Gladson S, et al. Vildagliptin ameliorates pulmonary fibrosis in lipopolysaccharide-induced lung injury by inhibiting endothelial-to-mesenchymal transition. *Respir Res*. 2017;18:177.
62. Hong SK, Choo EH, Ihm SH, Chang K, Seung KB. Dipeptidyl peptidase 4 inhibitor attenuates obesity-induced myocardial fibrosis by inhibiting transforming growth factor-beta1 and Smad2/3 pathways in high-fat diet-induced obesity rat model. *Metab Clin Exp*. 2017;76:42-55.
63. Aroor AR, Habibi J, Kandikattu HK, et al. Dipeptidyl peptidase-4 (DPP-4) inhibition with linagliptin reduces western diet-induced myocardial TRAF3IP2 expression, inflammation and fibrosis in female mice. *Cardiovasc Diabetol*. 2017;16:61.
64. Uchida T, Oda T, Matsubara H, et al. Renoprotective effects of a dipeptidyl peptidase 4 inhibitor in a mouse model of progressive renal fibrosis. *Ren Fail*. 2017;39:340-349.
65. Kaji K, Yoshiji H, Ikenaka Y, et al. Dipeptidyl peptidase-4 inhibitor attenuates hepatic fibrosis via suppression of activated hepatic stellate cell in rats. *J Gastroenterol*. 2014;49:481-491.

SUPPORTING INFORMATION

Additional supporting information may be found online in the Supporting Information section.

How to cite this article: Vorstandlechner V, Laggner M, Kalinina P, et al. Deciphering the functional heterogeneity of skin fibroblasts using single-cell RNA sequencing. *The FASEB Journal*. 2020;34:3677–3692. <https://doi.org/10.1096/fj.201902001RR>

Supplementary tables

Target	Supplier/Product number	Host species	Clonality	Dilution	Tissue	Application
DPP4	Abcam/ab3154	Mouse	monoclonal	1:200	Paraffin	IF
DPP4	Abcam/ab212326	Mouse	monoclonal	1:500	Paraffin	IF
DPP4	BioLegend #302708	Mouse	monoclonal	1:100	cryo, unfixed	IF
DPP4	Thermo Fisher Scientific/MA5-13562	Mouse	monoclonal	1: 50	cryo, PFA-fixed	IF
DPP4	Abcam/ab215711	Rabbit	monoclonal	1:1000 1:100 1:200	Paraffin Cells Membrane	IF MACS-sort WB
DPP4	Abcam/ab86806	Rabbit	polyclonal	1:500	Paraffin	IF
ACTA2	Abcam/ab7817	Mouse	monoclonal	1:200	Paraffin	IF
TPSAB1	Abcam/ab2378	Mouse	monoclonal	1:1000	Paraffin	IF
Melan-A	Agilent/M7196	Mouse	monoclonal	1:500	Paraffin	IF

Table S1: Primary antibodies

Secondary antibody	Dilution	Company	Application
Alexa fluor® 546 goat anti- rabbit IgG (H + L)	1:500	Invitrogen	IF
Alexa fluor® 546 goat anti- mouse IgG (H + L)	1:500	Invitrogen	IF
Alexa fluor® 488 goat anti- mouse IgG (H + L)	1:500	Invitrogen	IF
Anti-Rabbit IgG MicroBeads	10µl per 1 Mio. cells	MACS Miltenyi	MACS-Sort
Goat-anti-rabbit horseradish-peroxidase-conjugated #1706511	1:10000	Bio-Rad	WB

Table S2: Secondary antibodies

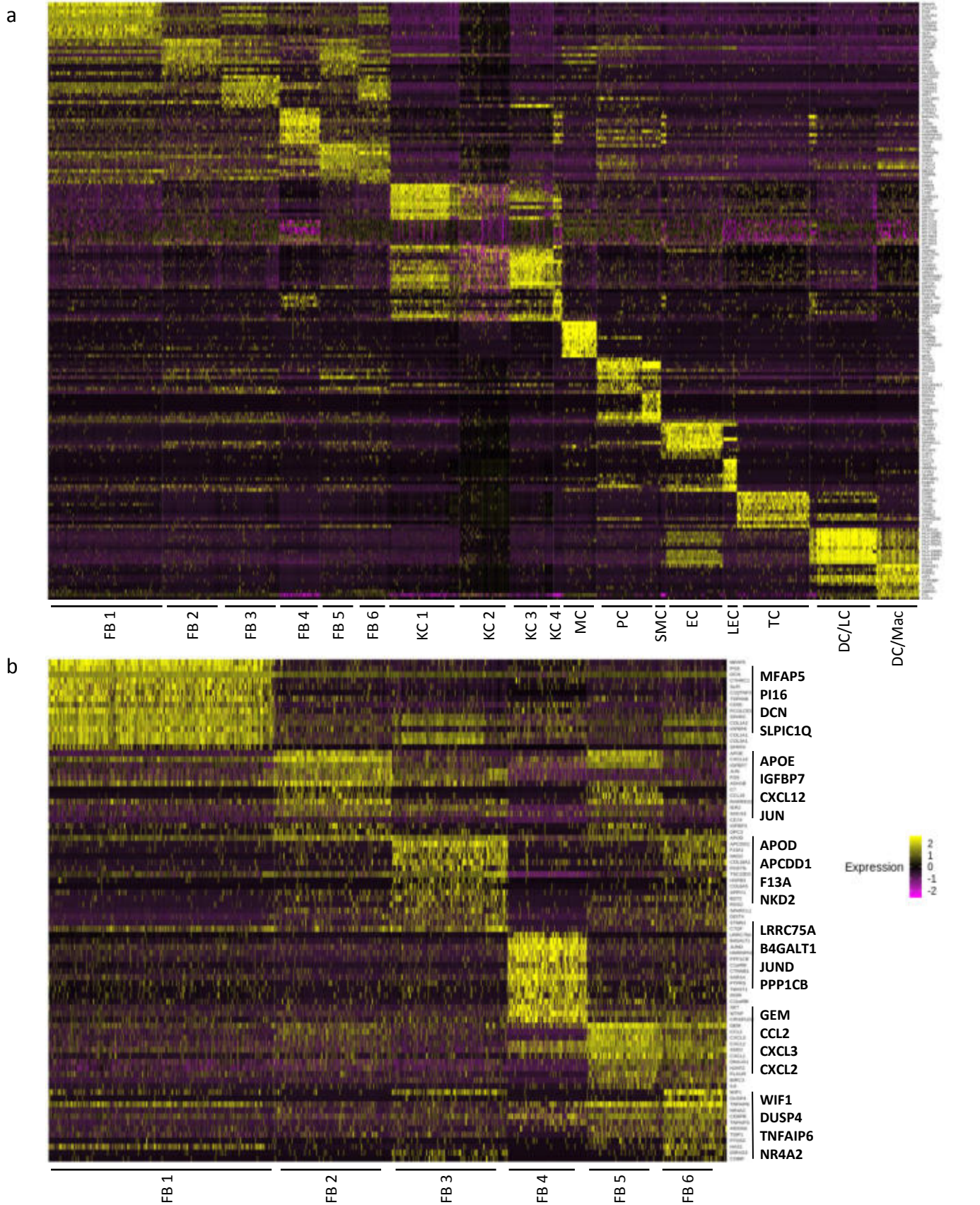


Figure S1: Transcriptional profiles of all cells and of FB. Heatmap of all cells in the dataset clustered by tSNE based on PCA. For each cluster, top ten differentially upregulated genes compared to the rest of the dataset were used to create the heatmap. b) Genes of all FB clusters. Top ten differentially upregulated genes of each FB cluster compared to the rest of the FB. In heatmaps, each column represents one cell, each row represents a gene. Colors represent log-transformed scaled data, with yellow indicating upregulation and violet indicating downregulation of respective gene compared to the rest of the dataset as indicated in the legend. tSNE, t-stochastic neighbor embedding; PCA, principal component analysis.

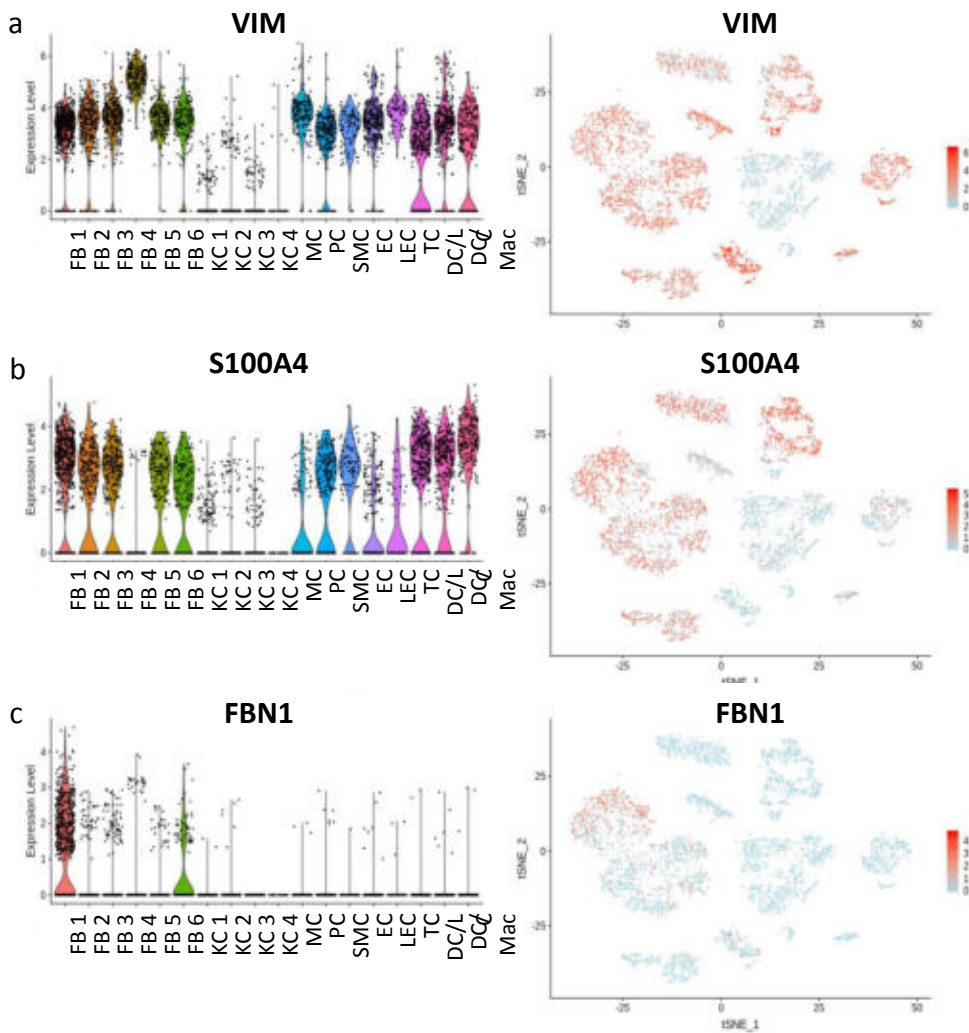


Figure S2: Traditional pan-FB markers do not reliably identify all FB. a-c) Violin plots and feature plots of marker genes traditionally used for FB identification, vimentin (*VIM*), S100 calcium binding protein A4 (*S100A4*), and fibrillin 1 (*FBN1*). In Violin plots, dots represent individual cells. Y-axis represents log₂-fold-change of normalized genes and log-transformed single-cell expression. Vertical lines in violin plots represent maximum expression, shape of each violin represents all results, and width of each violin represents frequency of respective expression level. In feature plots, expression of the respective gene is mapped onto the tSNE-plot. Color intensity indicates level of gene expressions. tSNE, t-stochastic neighbor embedding.

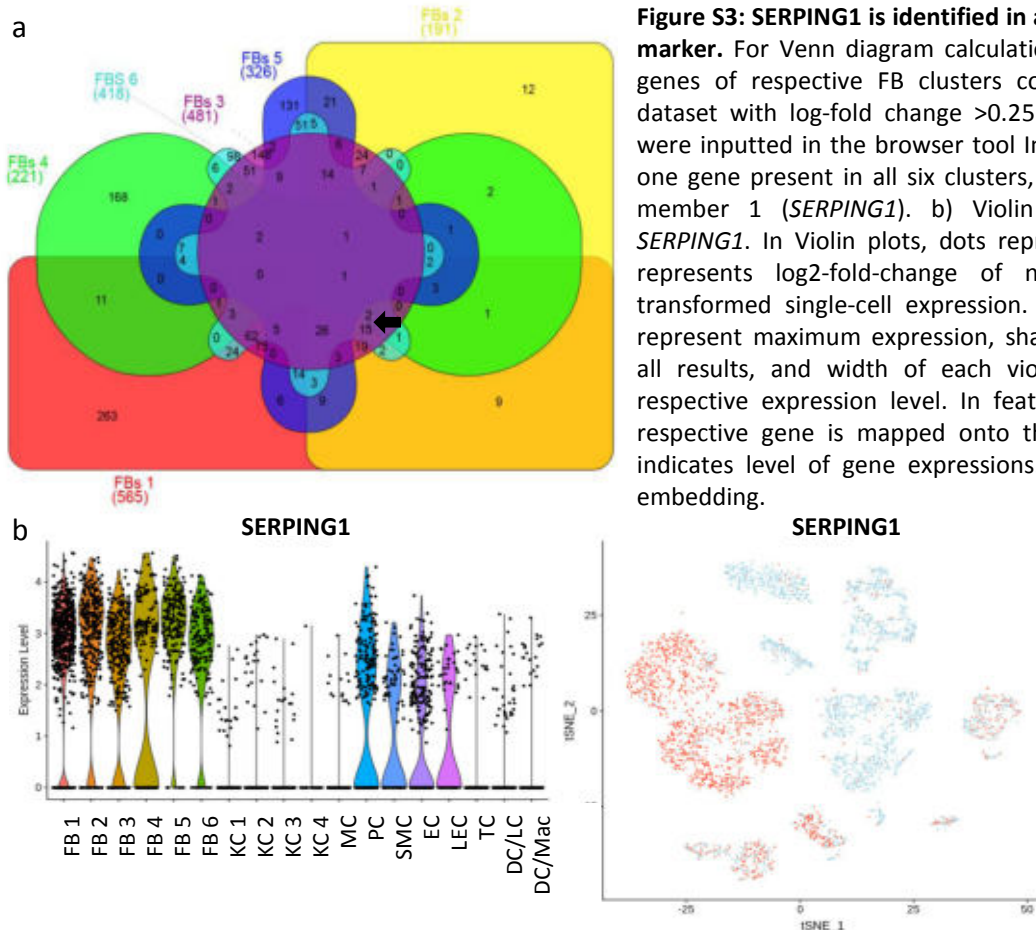


Figure S3: SERPING1 is identified in all FB clusters as a reliable FB marker. For Venn diagram calculation, differentially upregulated genes of respective FB clusters compared to the rest of the dataset with log₂-fold change >0.25 and adjusted p-value <0.05 were inputted in the browser tool InteractiVenn. Arrow indicates one gene present in all six clusters, identified as serpin family G member 1 (*SERPING1*). b) Violin plot and feature plot of *SERPING1*. In Violin plots, dots represent individual cells. Y-axis represents log₂-fold-change of normalized genes and log-transformed single-cell expression. Vertical lines in violin plots represent maximum expression, shape of each violin represents all results, and width of each violin represents frequency of respective expression level. In feature plots, expression of the respective gene is mapped onto the tSNE-plot. Color intensity indicates level of gene expressions. tSNE, t-stochastic neighbor embedding.

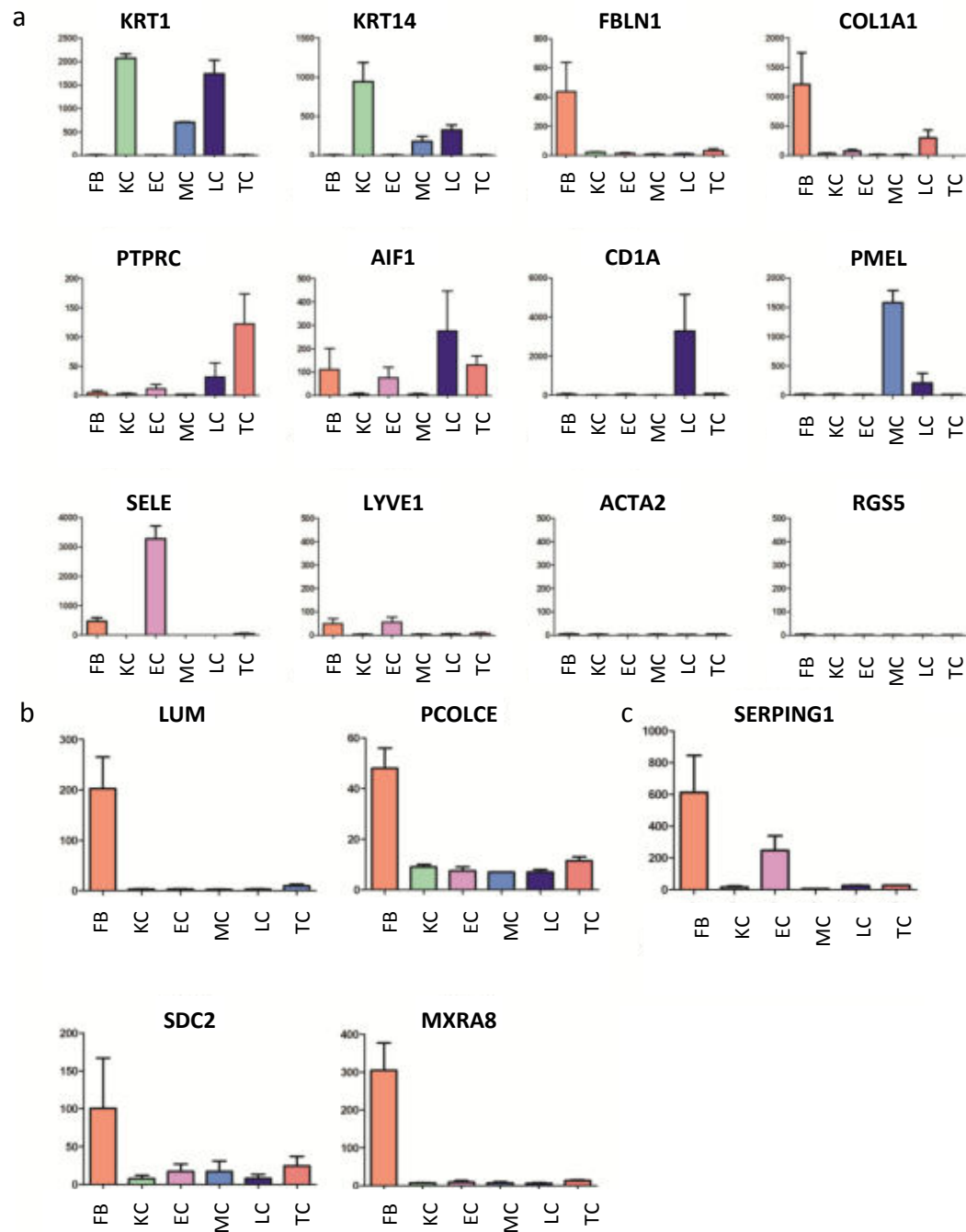


Figure S4: Cluster markers and FB marker expression were confirmed in affymetrix array of isolated skin subsets. Skin cell subsets from human trunk skin (n=2) were isolated using MACS-bead sorting. Fibroblasts (FB), keratinocytes (KC), endothelial cells (EC), melanocytes (MC), langerhans cells (LC) and T-cells (TC) were purified. The transcriptome of each subset was assessed by Affymetrix® Human Gene 2.1 ST Array. a) Bar graphs show cell type marker genes used for celltype identification in figure 1b). Keratin 1 (*KRT1*), keratin 14 (*KRT14*), fibulin 1 (*FBLN1*), collagen I (*COL1A1*), protein tyrosine phosphatase receptor type C (*PTPRC*), allograft Inflammatory Factor 1 (*AIF1*), premelanosome protein (*PMEL*), selectin E (*SELE*), lymphatic vessel endothelial hyaluronan receptor 1 (*LYVE1*), actin alpha 2 (*ACTA2*), regulator of signaling protein 5 (*RGS5*). b) Bar graphs show genes identified as new FB markers. Fibulin-1 (*FBLN1*), lumican (*LUM*), procollagen C-endopeptidase enhancer (*PCOLCE*), matrix remodeling associated 8 (*MXRA8*). Bars represent mean and standard error of the mean (SEM). Y-axes represent fluorescence intensity units from affymetrix® data.

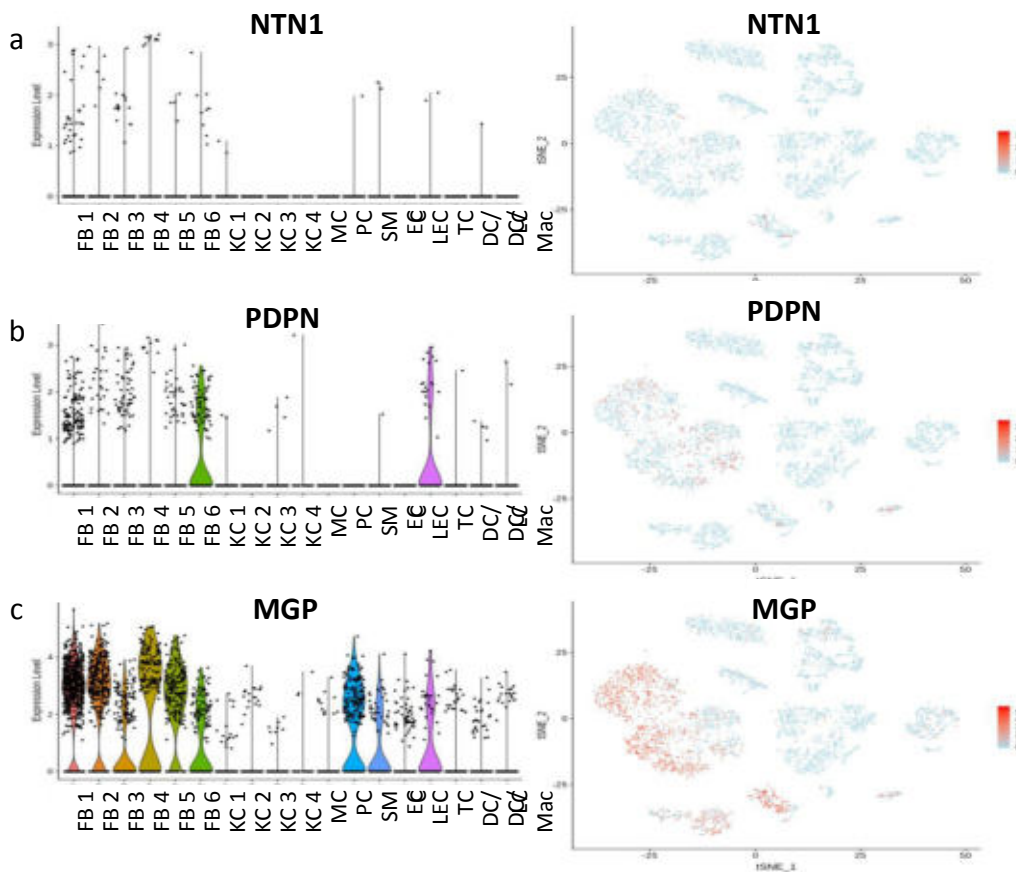


Figure S5: FBs do not cluster into reticular and papillary FBs based on single cell transcriptional data. Violin plot and feature plot of a) netrin 1 (*NTN1*), b) podoplanin (*PDPN*), and c) matrix Gla protein (*MGP*). In violin plots, dots represent individual cells. Y-axis represents log2-fold-change of normalized genes and log-transformed single-cell expression. Vertical lines in violin plots represent maximum expression, shape of each violin represents all results, and width of each violin represents frequency of respective expression level. In feature plots, expression of the respective gene is mapped onto the tSNE-plot. Color intensity indicates level of gene expressions. tSNE, t-stochastic neighbor embedding.

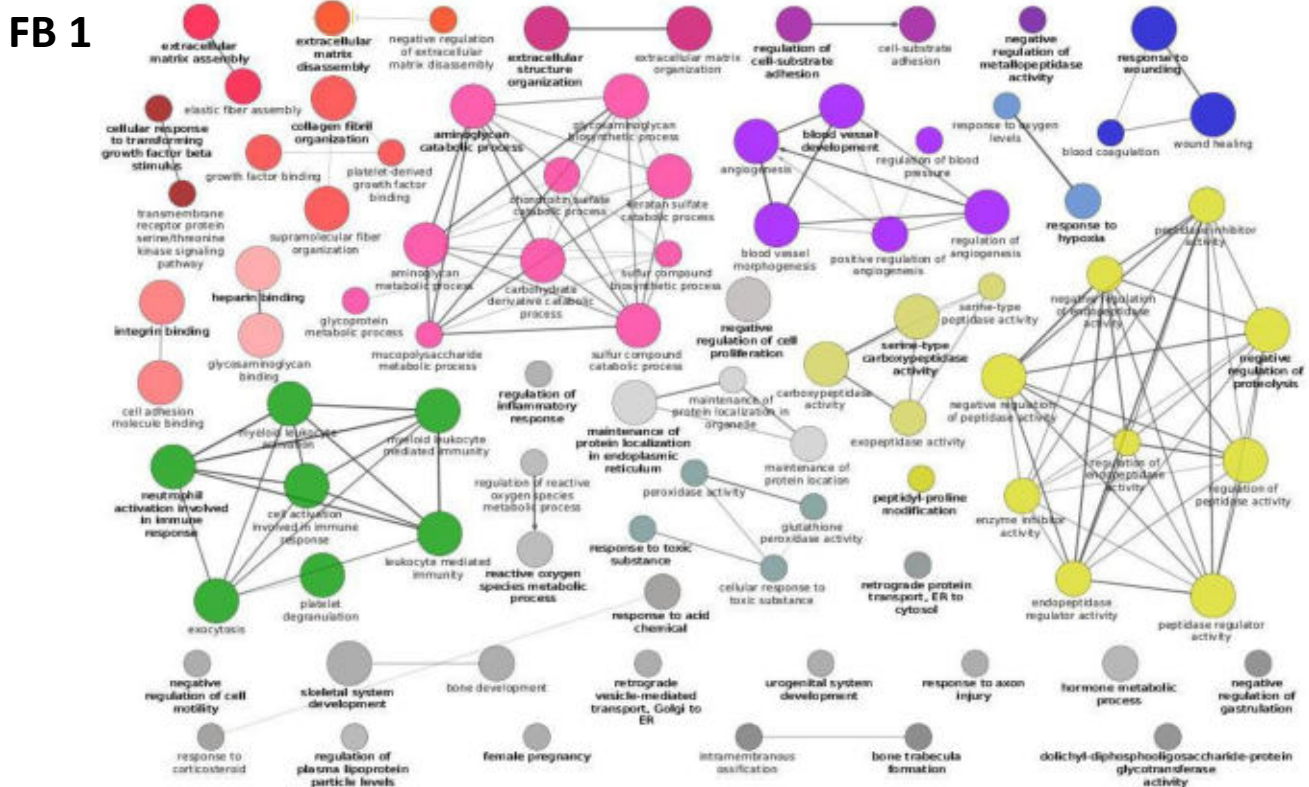


Figure S6 : GO-network analysis of cluster FB1 reveals complex and distinct functional properties. For calculation of GO-term networks, lists of differentially upregulated genes of each FB cluster compared to all other FB with log-fold change >0.25 and adjusted p-value<0.05 were submitted to Cytoscape-plugin ClueGO at medium GO-specificity, with GO-term fusion and with only significant (p-value<0.05) GO-terms shown. Circle size correlates with p-value; lines ('edges') represent functional connection of respective GO-terms. GO-groups were colored for function according to group overview terms (in bold letters). Red represents ECM-formation and ECM-assembly-associated terms, orange signaling pathways, yellow proteinase activity, green immunological function, blue wound healing and regeneration, purple angiogenesis and blood vessel formation, brown developmental processes, and pink metabolism.

FB 2

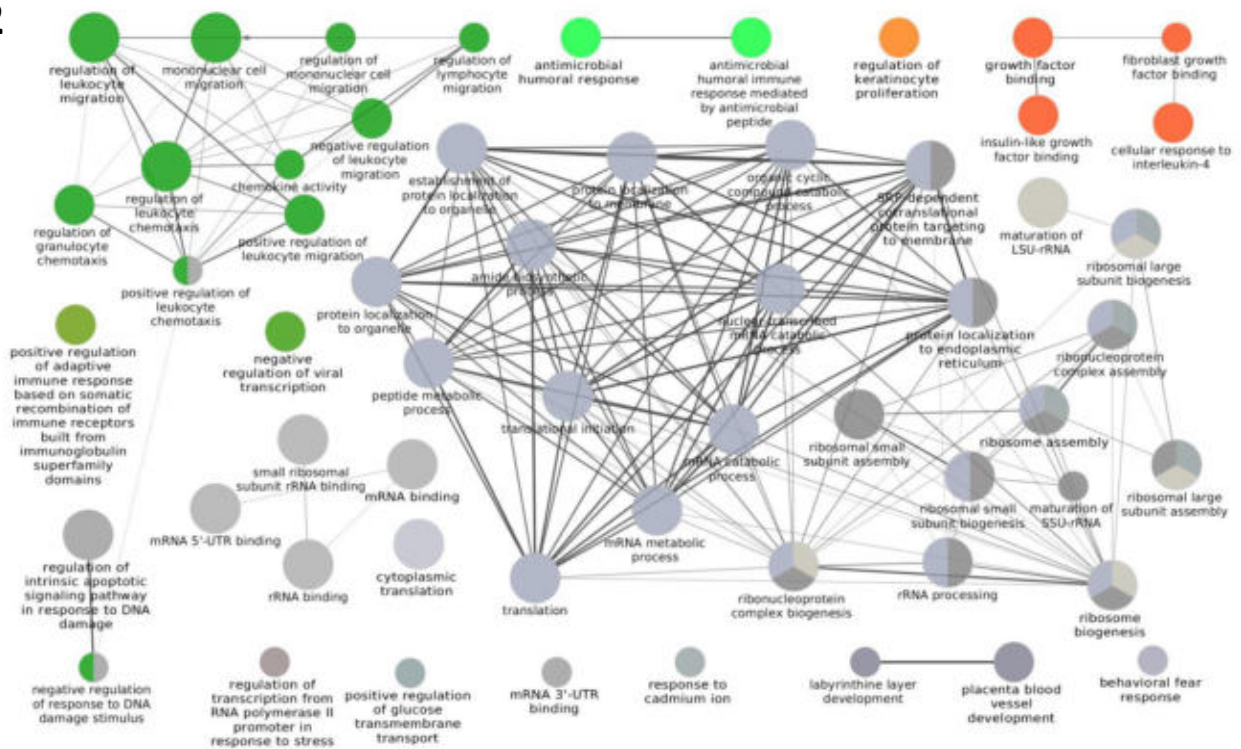


Figure S7: GO-network analysis of cluster FB2 reveals complex and distinct functional properties. For calculation of GO-term networks, lists of differentially upregulated genes of each FB cluster compared to all other FB with log-fold change >0.25 and adjusted p-value<0.05 were submitted to Cytoscape-plugin ClueGO at medium GO-specificity, with GO-term fusion and with only significant (p-value<0.05) GO-terms shown. Circle size correlates with p-value; lines ('edges') represent functional connection of respective GO-terms. GO-groups were colored for function according to group overview terms (in bold letters). Red represents ECM-formation and ECM-assembly-associated terms, orange signaling pathways, yellow proteinase activity, green immunological function, blue wound healing and regeneration, purple angiogenesis and blood vessel formation, brown developmental processes, and pink metabolism.

FB 3

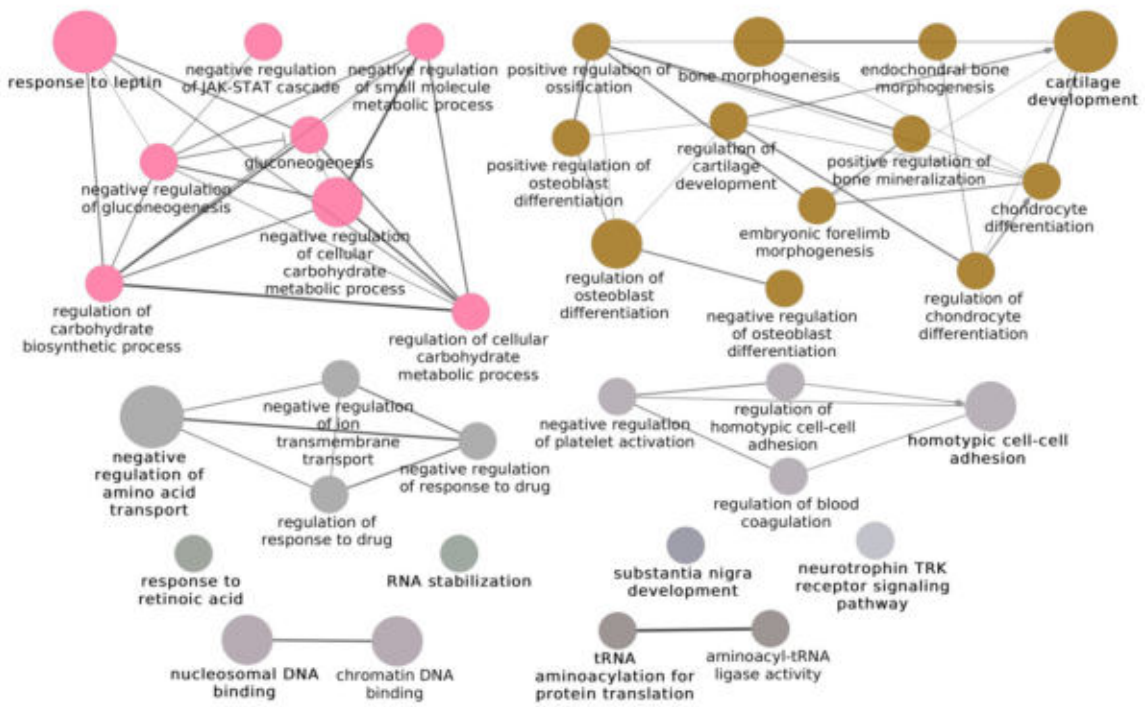


Figure S8: GO-network analysis of cluster FB3 reveals complex and distinct functional properties. For calculation of GO-term networks, lists of differentially upregulated genes of each FB cluster compared to all other FB with log-fold change >0.25 and adjusted p-value<0.05 were submitted to Cytoscape-plugin ClueGO at medium GO-specificity, with GO-term fusion and with only significant (p-value<0.05) GO-terms shown. Circle size correlates with p-value; lines ('edges') represent functional connection of respective GO-terms. GO-groups were colored for function according to group overview terms (in bold letters). Red represents ECM-formation and ECM-assembly-associated terms, orange signaling pathways, yellow proteinase activity, green immunological function, blue wound healing and regeneration, purple angiogenesis and blood vessel formation, brown developmental processes, and pink metabolism.

FB 4

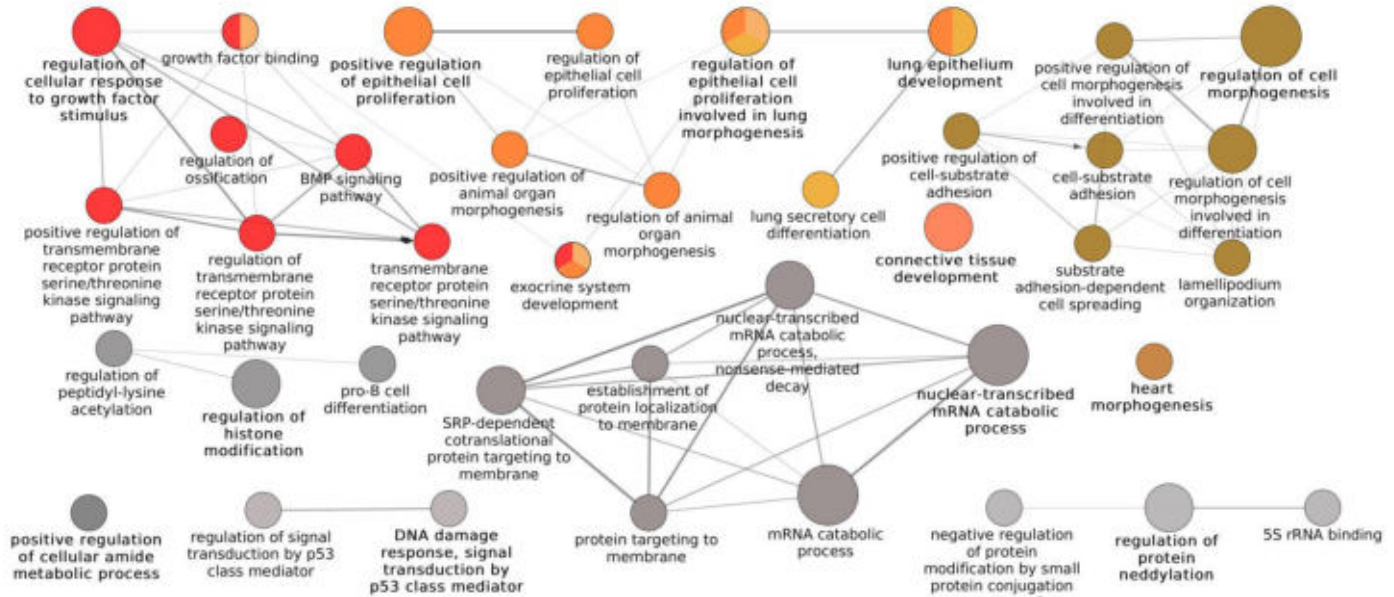


Figure S9: GO-network analysis of cluster FB4 reveals complex and distinct functional properties. For calculation of GO-term networks, lists of differentially upregulated genes of each FB cluster compared to all other FB with log-fold change >0.25 and adjusted p-value<0.05 were submitted to Cytoscape-plugin ClueGO at medium GO-specificity, with GO-term fusion and with only significant (p-value<0.05) GO-terms shown. Circle size correlates with p-value; lines ('edges') represent functional connection of respective GO-terms. GO-groups were colored for function according to group overview terms (in bold letters). Red represents ECM-formation and ECM-assembly-associated terms, orange signaling pathways, yellow proteinase activity, green immunological function, blue wound healing and regeneration, purple angiogenesis and blood vessel formation, brown developmental processes, and pink metabolism.

FB 5

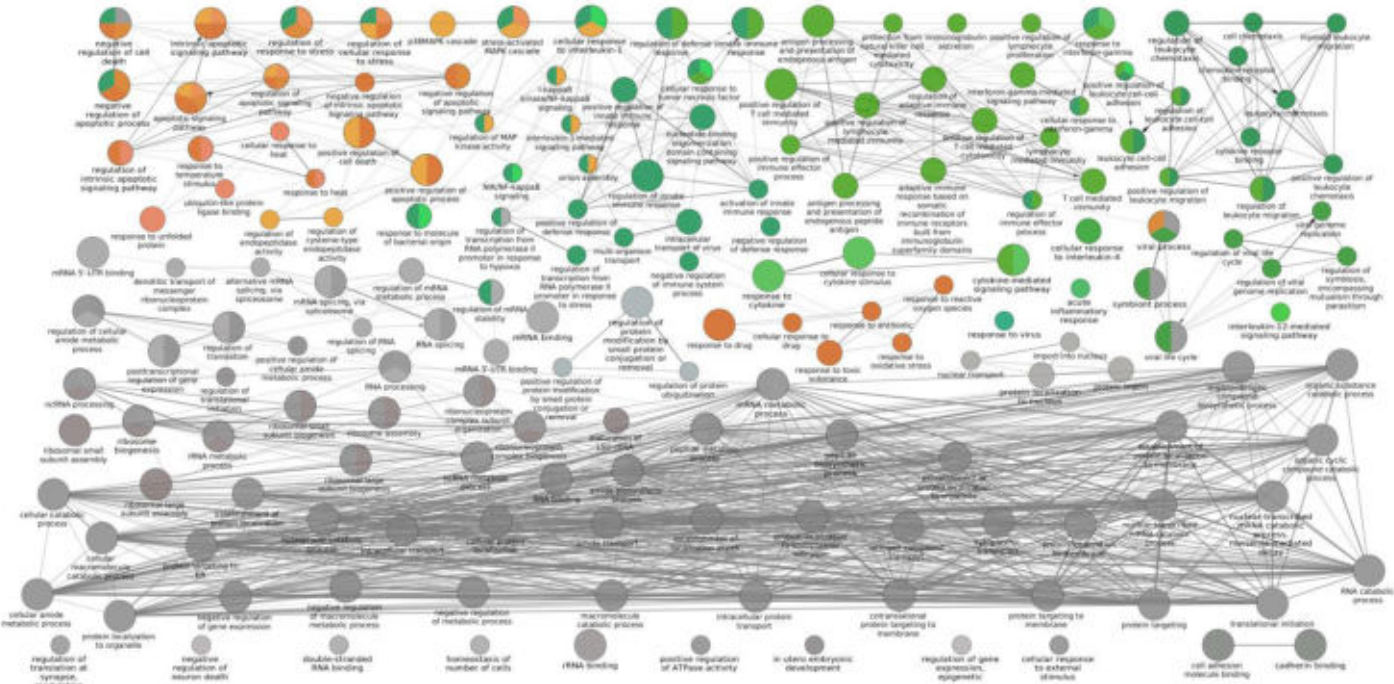


Figure S10: GO-network analysis of cluster FB5 reveals complex and distinct functional properties. For calculation of GO-term networks, lists of differentially upregulated genes of each FB cluster compared to all other FB with log-fold change >0.25 and adjusted p-value<0.05 were submitted to Cytoscape-plugin ClueGO at medium GO-specificity, with GO-term fusion and with only significant (p-value<0.05) GO-terms shown. Circle size correlates with p-value; lines ('edges') represent functional connection of respective GO-terms. GO-groups were colored for function according to group overview terms (in bold letters). Red represents ECM-formation and ECM-assembly-associated terms, orange signaling pathways, yellow proteinase activity, green immunological function, blue wound healing and regeneration, purple angiogenesis and blood vessel formation, brown developmental processes, and pink metabolism.

FB 6

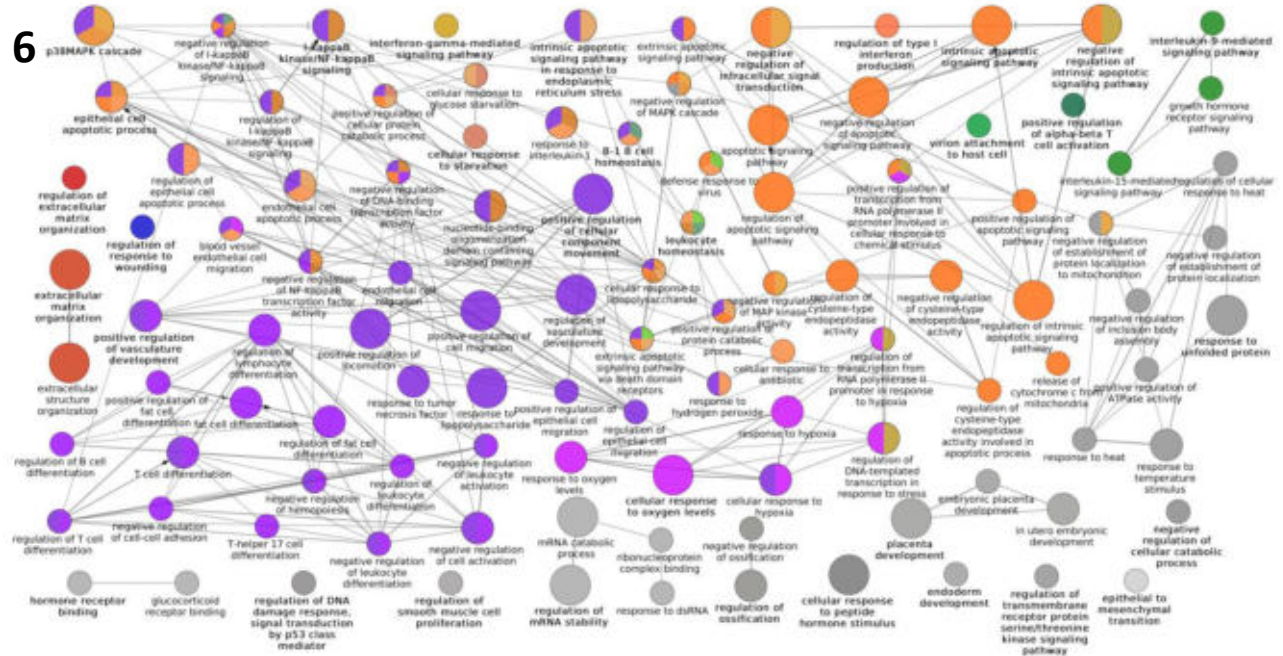


Figure S11: GO-network analysis of cluster FB6 reveals complex and distinct functional properties. For calculation of GO-term networks, lists of differentially upregulated genes of each FB cluster compared to all other FB with log-fold change >0.25 and adjusted p-value <0.05 were submitted to Cytoscape-plugin ClueGO at medium GO-specificity, with GO-term fusion and with only significant (p-value <0.05) GO-terms shown. Circle size correlates with p-value; lines ('edges') represent functional connection of respective GO-terms. GO-groups were colored for function according to group overview terms (in bold letters). Red represents ECM-formation and ECM-assembly-associated terms, orange signaling pathways, yellow proteinase activity, green immunological function, blue wound healing and regeneration, purple angiogenesis and blood vessel formation, brown developmental processes, and pink metabolism.

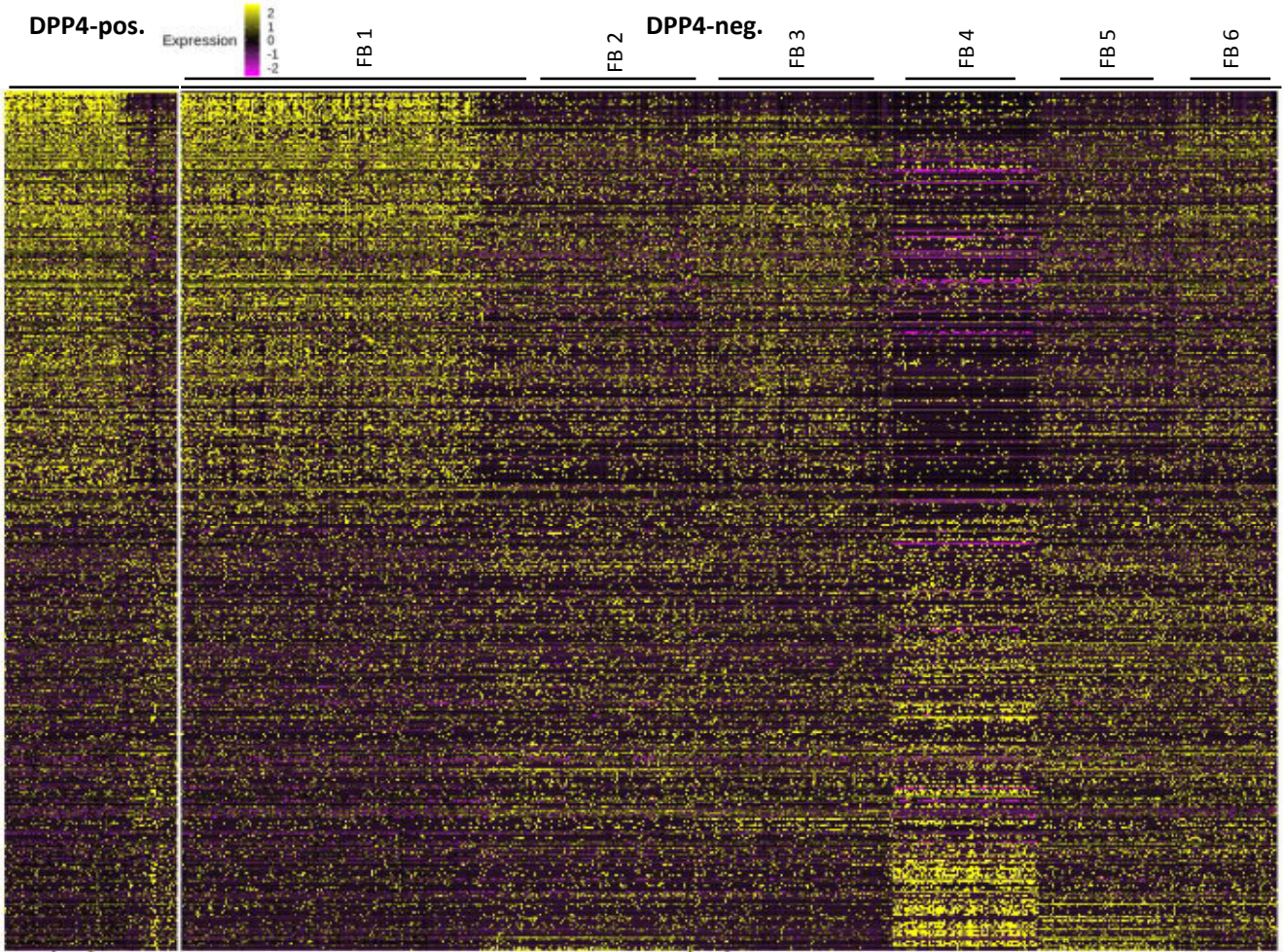


Figure S12: Transcriptional profiles of DPP4⁺ and DPP4⁻ FB. Gene expression of DPP4⁺ and compared to DPP4⁻ FB dataset. In the heatmap, each column represents one cell, each row represents a gene. Colors represent log-transformed scaled data, with yellow indicating upregulation and violet indicating downregulation of respective gene compared to the rest of the dataset as shown in the legend.

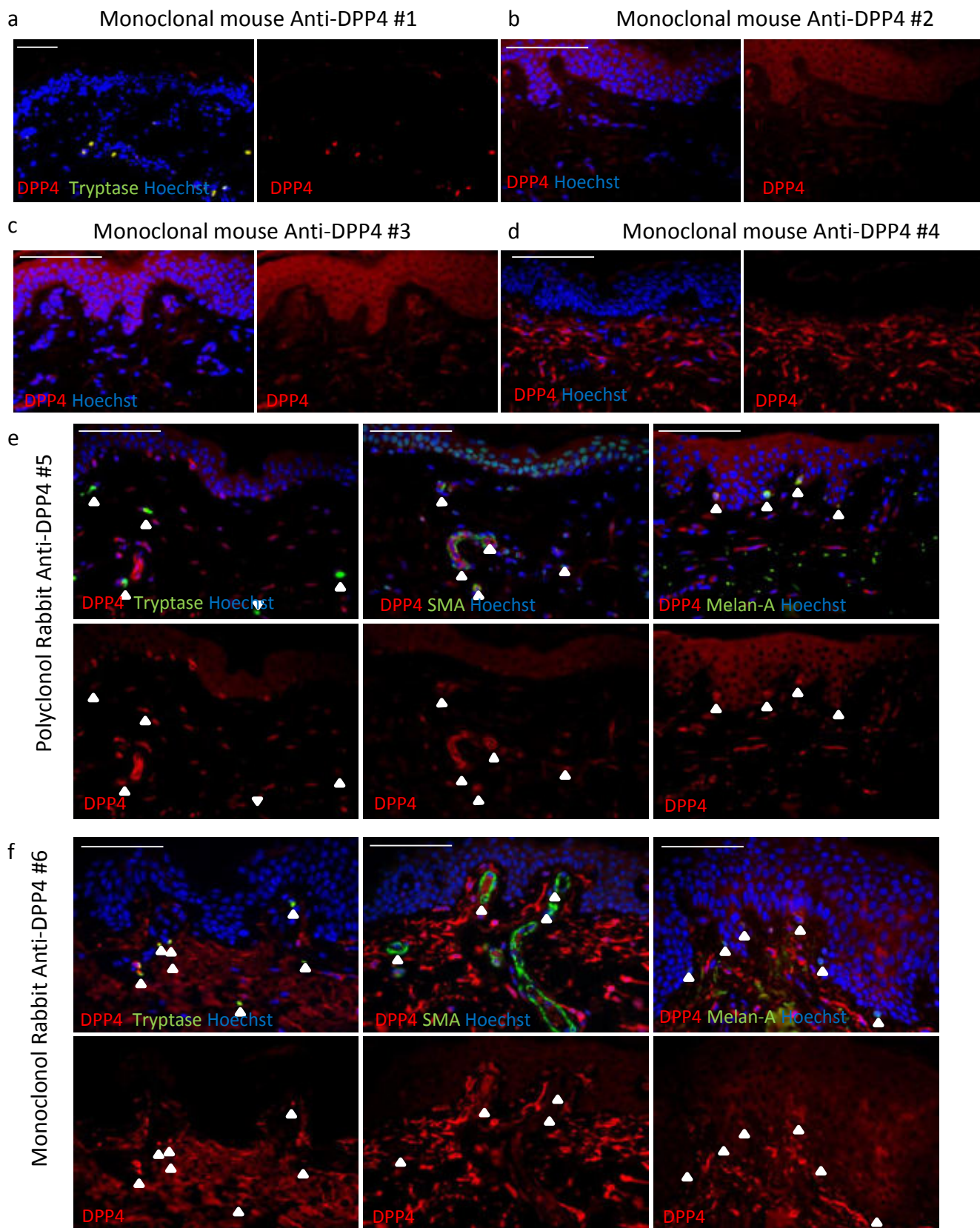


Figure S13. Comparison of expression of DPP4 in healthy human skin using different antibodies. Frozen sections (a,d) or paraffin-embedded (b-e) sections of healthy human skin (5 μ m thickness) were immunofluorescence-stained using a monoclonal mouse-anti human DPP4 antibody (ab3154, Abcam, Cambridge, UK) (a), (ab212326, abcam, Cambridge, UK) (b), (MA5-13562, ThermoFisher, Waltham, USA) (c) of the same clone [202-36], and mouse-anti human DPP4 antibody (#302708, Biolegend, San Diego, USA). Monoclonal Polyclonal rabbit-hosted anti-human DPP4-antibody (ab86806, abcam, Cambridge, UK) (e) and monoclonal rabbit-hosted anti-human DPP4-antibody (ab215711, Abcam, Cambridge, UK) (f). Red shows DPP4, green represents Smooth muscle actin (SMA), mast cell tryptase, or Melan-A. Blue represents Hoechst staining of nuclei (concentration 1:2500). All images were taken at 3000ms exposure time for DPP4, with magnification 20x (A), or 40x (B-F), scale bars represent 100 μ m.

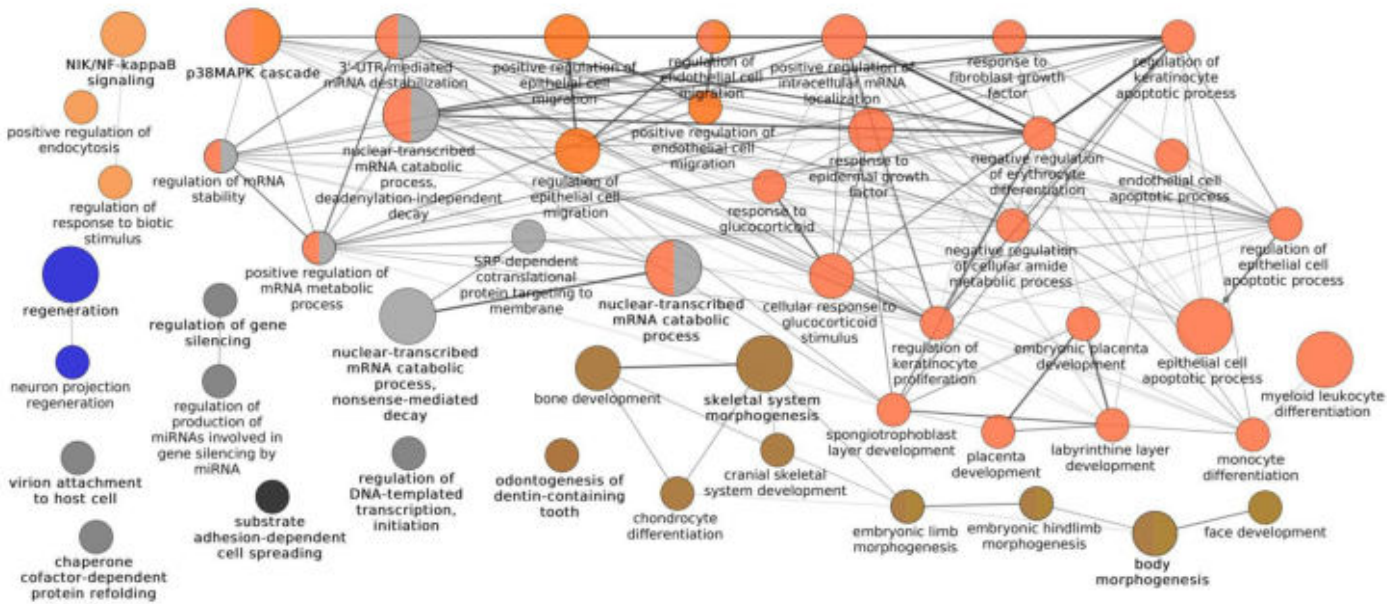


Figure S14: GO-network analysis of DPP4- FB shows association with the p38/MAPK and NFkB-pathway. For calculation of GO-term networks, lists of differentially upregulated genes of each FB cluster compared to all other FB with log-fold change >0.25 and adjusted p-value<0.05 were submitted to Cytoscape-plugin ClueGO at medium GO-specificity, with GO-term fusion and with only significant (p-value<0.05) GO-terms shown. Circle size correlates with p-value; lines ('edges') represent functional connection of respective GO-terms. GO-groups were colored for function according to group overview terms (in bold letters). Red represents ECM-formation and ECM-assembly-associated terms, orange signaling pathways, yellow proteinase activity, green immunological function, blue wound healing and regeneration, purple angiogenesis and blood vessel formation, brown developmental processes, and pink metabolism.

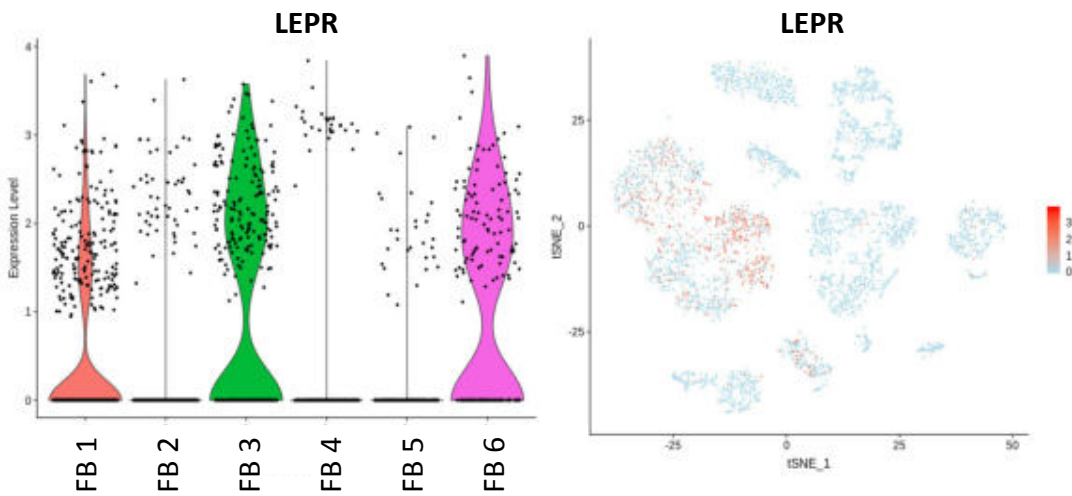


Figure S15: Leptin receptor (*LEPR*) is present in three distinct FB clusters. Violin plot and feature plot of *LEPR*. In Violin plots, dots represent individual cells. Y-axis represents log₂-fold-change of normalized genes and log-transformed single-cell expression. Vertical lines in violin plots represent maximum expression, shape of each violin represents all results, and width of each violin represents frequency of respective expression level. In feature plots, expression of the respective gene is mapped onto the tSNE-plot. Color intensity indicates level of gene expressions. tSNE, t-stochastic neighbor embedding.

2.2. Chapter 2: The serine proteases dipeptidyl-peptidase 4 and urokinase are key molecules in human and mouse scar formation


Hypertrophic scars pose a significant medical challenge and global health burden, affecting millions of people worldwide. Scar formation occurs as a result of an abnormal wound healing process, characterized by prolonged inflammation and excessive fibroblast activity, which leads to the accumulation of excessive extracellular matrix components. Current treatments for hypertrophic scars have limited efficacy, high recurrence rates, and uncertain mechanisms of action. Thus, there is an urgent need to identify new therapeutic targets for hypertrophic scars (249).

Recently, several studies found that proteases may critically regulate ECM turnover and growth factor activation during tissue remodeling, making them an attractive target for drug development in fibrotic diseases (96). The role of serine proteases in particular, however, were hitherto not closely investigated in hypertrophic scar formation.

In the second study, we thus used single-cell RNA sequencing to analyze gene expression and pathways involved in hypertrophic scar formation in an effort to discover novel targets for therapeutic development toward scar-free wound healing or full reversion of a preexisting scar. Furthermore, we aimed to identify genes that are regulated in scar tissue and potentially involved in scar formation.

This work was the first to examine hypertrophic scar tissue at the single-cell level, revealing new information on the molecular processes underlying the development of hypertrophic scars. The findings of this study could have important clinical implications and could inspire the invention of new treatment options for hypertrophic scars.

The serine proteases dipeptidyl-peptidase 4 and urokinase are key molecules in human and mouse scar formation

Vera Vorstandlechner^{1,2,3}, Maria Laggner^{1,2}, Dragan Copic^{1,2}, Katharina Klas^{1,2}, Martin Direder^{1,2}, Yiyang Chen^{4,5}, Bahar Golabi⁴, Werner Haslik³, Christine Radtke³, Erwin Tschachler⁴, Konrad Hötzenecker⁶, Hendrik Jan Ankersmit^{1,2,7}✉ & Michael Mildner^{4,7} ✉

Despite recent advances in understanding skin scarring, mechanisms triggering hypertrophic scar formation are still poorly understood. In the present study, we investigate mature human hypertrophic scars and developing scars in mice at single cell resolution. Compared to normal skin, we find significant differences in gene expression in most cell types present in scar tissue. Fibroblasts show the most prominent alterations in gene expression, displaying a distinct fibrotic signature. By comparing genes upregulated in murine fibroblasts during scar development with genes highly expressed in mature human hypertrophic scars, we identify a group of serine proteases, tentatively involved in scar formation. Two of them, dipeptidyl-peptidase 4 (*DPP4*) and urokinase (*PLAU*), are further analyzed in functional assays, revealing a role in TGF β 1-mediated myofibroblast differentiation and over-production of components of the extracellular matrix in vitro. Topical treatment with inhibitors of DPP4 and PLAU during scar formation in vivo shows anti-fibrotic activity and improvement of scar quality, most prominently after application of the PLAU inhibitor BC-11. In this study, we delineate the genetic landscape of hypertrophic scars and present insights into mechanisms involved in hypertrophic scar formation. Our data suggest the use of serine protease inhibitors for the treatment of skin fibrosis.

¹Laboratory for Cardiac and Thoracic Diagnosis, Regeneration and Applied Immunology, Department of Thoracic Surgery, Medical University of Vienna, Vienna, Austria. ²Aposcience AG (FN 308089y), Dresdner Straße 87/A21, Vienna, Austria. ³Department of Plastic and Reconstructive Surgery, Medical University of Vienna, Vienna, Austria. ⁴Department of Dermatology, Medical University of Vienna, Vienna, Austria. ⁵University of Applied Sciences, FH Campus Wien, Vienna, Austria. ⁶Department of Thoracic Surgery, Medical University of Vienna, Vienna, Austria. ⁷These authors contributed equally: Hendrik Jan Ankersmit, Michael Mildner. ✉email: hendrik.ankersmit@meduniwien.ac.at; michael.mildner@meduniwien.ac.at

Hypertrophic scars are a complex medical problem and a significant global disease burden^{1,2}. In the western world, an estimated number of 100 million people develop scars every year, ~11 million of which bear keloid scars and 4 million suffer from burn scars¹. In the USA, an estimated amount of 12 billion dollars is spent annually on the treatment of skin scarring³. For affected persons, a pathological hypertrophic scar can cause significant functional impairment, pain, pruritus, and a reduction in quality of life^{4,5}.

Wound healing is a tightly coordinated, three-step process, characterized by an acute inflammatory phase, a proliferative phase, and a remodeling phase. Prolonged inflammation results in increased fibroblast (FB) activity, with enhanced secretion of transforming growth factor beta 1 (TGFβ1), TGFβ2, insulin-like growth factor (IGF1), and other cytokines⁶. TGFβ1 drives differentiation of FBs into myofibroblasts, which have a contractile phenotype, are characterized by excessive secretion of ECM-components⁷, and are the major contributors to the formation of hypertrophic scars⁸. Mature hypertrophic scars display strong tissue contraction⁶, and dense, parallel, or whorl-like ECM⁸.

Topical silicone application, compression or massage therapy, intralesional injection of triamcinolone (TAC), corticosteroids, or 5-Fluorouracil (5-FU), laser ablation, and surgery are the most commonly used options for prevention or treatment of hypertrophic scars^{6,9–11}. However, many of these therapies lack evidence of efficacy and safety, show high recurrence rates, and mechanisms of actions are still unclear^{10,12}.

Recently, several proteases became the focus of drug development in fibrotic diseases, as they have been shown to be involved in ECM-breakdown and the activation of growth factors in tissue remodeling^{13,14}. Serine proteases/peptidases constitute a large, diverse group of proteases, divided into 13 clans and 40 families¹⁵. The group of trypsin-like proteases contributing to vital processes such as blood coagulation, fibrinolysis, apoptosis, and immunity¹⁶. Members of this family include urokinase, HTRA1/3 (high-temperature requirement A1/3 peptidase), several coagulation factors and complement components, PRSS-like serine proteases, granzymes, and cathepsin G^{16,17}. Inhibitors of PLA2 have been shown to counteract fibrotic processes in cardiac and pulmonary fibrosis in human in vitro studies and in mouse experiments^{18,19}. Recently, the serine protease DPP4 became the center of attention, since DPP4 inhibitors (gliptins) have been clinically used for the treatment of diabetes mellitus²⁰. DPP4 was also implicated in a variety of fibrotic pathologies, including cardiac, hepatic, renal, and dermal fibrosis^{21–25}, and inhibition of DPP4 activity mitigated fibrotic processes in animal models^{18,19,26–29}. However, the contribution of serine proteases to human scar formation and the underlying anti-fibrotic mechanisms are so far not known. Even though scRNAseq was previously performed to identify factors important for embryonic³⁰ and postnatal³¹ skin development as well as for tissue regeneration³² by investigating murine wound healing³³, scar tissue on single-cell level has not been investigated yet.

Here, we used scRNAseq to thoroughly study gene expression and mechanisms involved in hypertrophic scar formation. We aimed to identify genes regulated in scar tissue, and to uncover potential targets for drug development toward scar-free wound healing or full reversion of a present scar.

Results

The single-cell landscape of hypertrophic scars. To elucidate the complex biological processes of scar formation, we performed droplet-based single-cell transcriptome analysis of human hypertrophic scar tissue and healthy skin³⁴ (Fig. 1A). In both samples, Unsupervised Uniform Manifold Approximation and

Projection (UMAP)-clustering revealed 21 cell clusters, which were further classified as specific cell types by well-established marker genes (Figure S2A), expression patterns of all clusters (Figure S2B), and transcriptional cluster proximity via a phylogenetic clustertree (Fig. 1B). We identified seven FB clusters, smooth muscle cells and pericytes (SMC/Peri), three clusters of endothelial cells (EC), and lymphatic endothelial cells (LECs), two clusters of T cells and of dendritic cells (DC), macrophages (Mac), three keratinocyte (KC) clusters, and melanocytes (Mel). All cells of specific subsets were clustered together, and skin and scar samples displayed comparable cellular cluster composition (Fig. 1C, D). Only cluster FB1 was mainly present in scar tissue. The clusters of skin and scars showed different relative cell number ratios (Fig. 1E, F). Whereas FBs represented 40% of all cells in healthy skin, a significant increase (53%) was observed in scar tissue. Similarly, we detected more ECs (16.31%) in scar tissue as compared to normal skin (8.1%). Contrary, the relative numbers of epithelial cells (6.37%) and immune cells (12.47%) in mature hypertrophic scars were significantly reduced compared to skin (22.47% and 19.97%, respectively).

When comparing scar to skin, we identified considerably more up- (Fig. 1G) than downregulated genes (Fig. 1H), and the most abundant differential gene expression (number of differentially expressed genes, nDEG) was found in FBs, SMC/PCs, macrophages, DC1 and KC1 (Fig. 1G, H). The top 50 up- and downregulated genes for FBs, SMC/PCs, ECs, T cells, DCs, and KCs are listed in Figure S3. Genes related to ECM production (e.g., *COL1A1/2*, *COL3A1*, *COL5A1/2*, *FN1*, *BGN*, *LOX*, *LUM*, *OGN*, *PCOLCE*) were mainly overrepresented in FBs, but notably also in PCs and ECs (Figure S3A–C). Several significantly regulated genes with so far undescribed roles in fibrosis and scar formation (e.g., *ARLAC*, *COPZ2*, *CRABP2*, *HSPA1A/B*, *MDK*, *OGN*, among others) were found in all cell types (Figure S3A–F). These distinctly regulated genes might provide valuable new candidates to understand and modulate skin scarring.

The fibrotic gene expression pattern of fibroblasts in hypertrophic scars. Since FBs showed the strongest gene regulation in our scRNAseq dataset, and have been considered as the major drivers of skin scarring and an important source for myofibroblasts⁷, we focused our further analysis on differences between FBs of healthy skin and hypertrophic scars (Fig. 2).

After subsetting and reclustering of all FBs, we identified 11 separate clusters (Fig. 2A–C) showing 110 significantly up- and 85 downregulated genes in FBs derived from scar tissue compared to healthy skin. The top 50 differentially up- and downregulated genes are shown in Fig. 2D. Interestingly, one FB cluster (FB1) was almost exclusively present in hypertrophic scars, suggesting a specific role in tissue fibrosis. Comparison of FB cluster 1 to all other scar FBs revealed 141 significantly up- and 179 downregulated genes. The top 50 differentially up- and downregulated genes are shown in Fig. 2E. Most of the upregulated genes in scar-derived FBs are well-studied in the context of skin scarring and are functionally related to collagens and ECM-modifying genes, e.g., *BGN*, *COL14A1*, *COL1A1/2*, *COL3A1*, *COL5A1/2*, *FN1*, *MMP23B*, *OGN*, *PCOLCE* (Figure S3). Analysis of the biological processes associated with differentially regulated genes between FB1 and other FB clusters by gene ontology network analysis revealed a strong association of FB1 with TGFβ-signaling (associated genes: *ASPN*, *COL1A1*, *COL1A2*, *FBN1*, *HSPA1A*, *HTRA1*, *INHBA*, *JUN*, *LOX*, *POSTN*, red circles) and ECM-formation (associated genes: *AEBP1*, *BGN*, *CCN2*, *COL12A1*, *COL14A1*, *COL1A1*, *COL1A2*, *COL3A1*, *COL5A1*, *COL5A2*, *COL6A1*, *COL6A2*, *COMP*, *CREB3L1*, *DPP4*, *EGFL6*, *FBN1*, *FN1*, *HTRA1*, *LOX*, *LUM*, *MFAP2*, *MMP11*, *PHLDB2*,

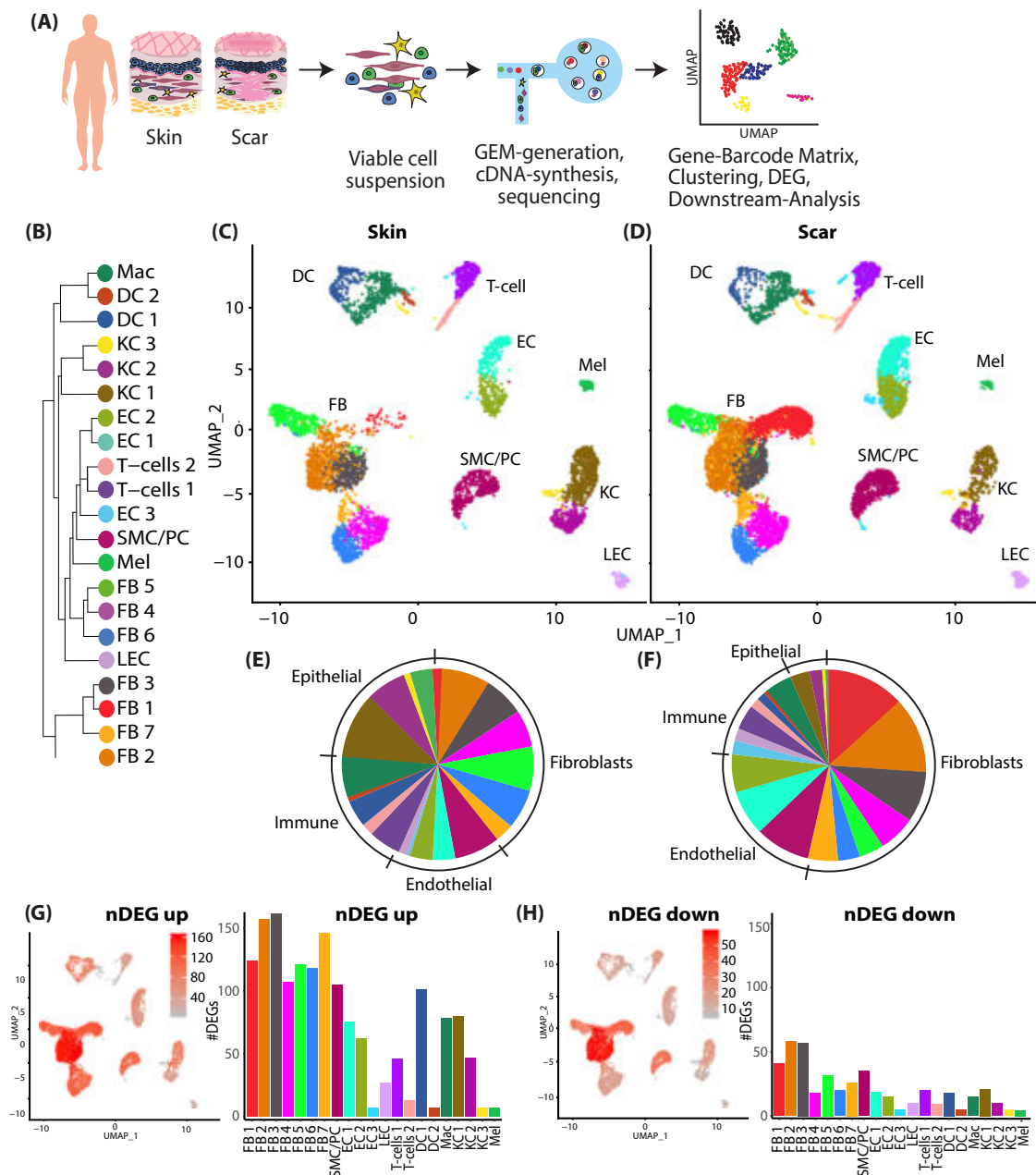


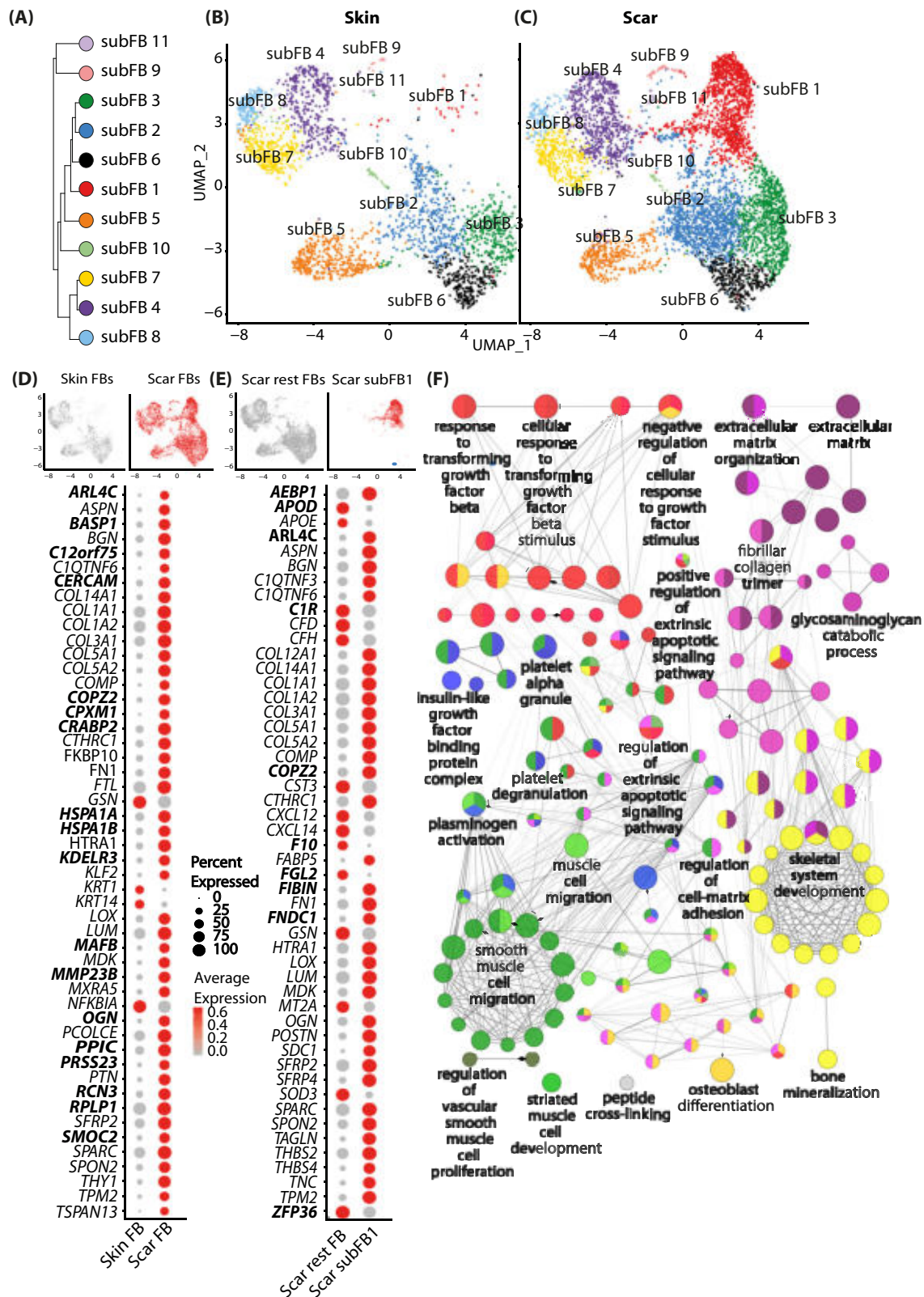
Fig. 1 Characterization of human skin and scar samples with scRNAseq identifies specific cell clusters and a distinct fibrotic gene signature.

A Workflow of scRNAseq in human skin ($n = 3$) and scar ($n = 3$) samples. **B** Phylogenetic clustertree calculated based on UMAP-clustering. **C, D** UMAP-plots of human skin and scar samples, split by tissue, after integration of all samples, identifying seven fibroblast clusters (FB1-7), smooth muscle cells and pericytes (SMC/Peri), endothelial cells (EC1 + 2), lymphatic endothelial cells (LEC), T cells, macrophages (Mac), dendritic cells (DC1 + 2), three keratinocyte clusters (KC1-3), and melanocytes (Mel). **E, F** Pie charts showing ratios of cell clusters in skin and scars. Feature plots and bar graphs of number of differentially expressed genes (nDEG) per cluster of **G** up- and **H** downregulated genes. DEGs were calculated per cluster comparing scar versus skin using Wilcoxon rank-sum test, including genes with average logarithmic fold change (avglogFC) of >0.1 or <-0.1 and Bonferroni-adjusted p -value <0.05 . Feature plots show projection of nDEG onto the UMAP-plot, color intensity represents nDEG. Bar graphs show absolute numbers of nDEG per cluster, y-axis represents nDEG. UMAP, uniform manifold approximation and projection.

POSTN, *SERPINE1*, *SFRP2*, *SPARC*, *TGFBI*, *THBS1*, *TNC*, *VCAN*, purple circles) (Fig. 2F), further corroborating its role in skin fibrosis. In addition, our analysis indicated a role of FB1 in processes important for several other cell types, including platelets, smooth muscle cells (associated genes: *CCN3*, *CHN1*, *IGF1*, *IGFBP3*, *PLAT*, *PLAU*, *POSTN*, *SERPINE1*, green circles), and cells of the skeletal system (associated genes: *CCN2*, *CCN3*, *COL12A1*, *COL14A1*, *COL1A1*, *COL1A2*, *COL3A1*, *COL5A2*, *COL6A1*, *COL6A2*, *COMP*, *ECM1*, *FBN1*, *FRZB*, *HYAL2*, *IGF1*,

INHBA, *LOX*, *LUM*, *PAPSS2*, *POSTN*, *SFRP2*, *SFRP4*, *SOX4*, *SPARC*, *TGFBI*, *VCAN*, yellow circles), suggesting paracrine actions of FB1.

Pseudotime calculation and trajectory construction effectively identified possible cell fates and time-regulated genes, even when analyzing cells of only one timepoint^{35,36}. Thus, we next sorted human skin and scar FBs along a pseudotime axis and constructed trajectories (Fig. 3A, B). The trajectories revealed a division at a certain timepoint where FBs divided into two



branches (Fig. 3C). Whereas the majority of FBs preferentially aligned with branch 1 in normal skin (Fig. 3D), we observed a significantly longer branch 2 with FBs of hypertrophic scar tissue (Fig. 3E). Branched expression analysis identified genes most regulated in a pseudotime-dependent manner in normal skin and hypertrophic scars (Fig. 3F). Interestingly, the collagens *COL1A1*, *COL1A2*, and *COL3A1*, known to contribute to all fibrotic

processes, are most upregulated at the end of Branch 2, but are not among the most pseudotime-regulated genes in scar (Fig. 3F). In contrast, other collagens, including *COL5A1/2*, *COL8A1*, *COL11A1*, and *COL12A1*, dominated the late pseudotime-dependent gene expression in branch 2. The role of these collagens in (hypertrophic) scar is scarcely investigated, and merits further exploration. Together, our trajectory analysis

Fig. 2 Analysis of fibroblast subsets. **A** Phylogenetic clustertree calculated based on UMAP-clustering of subsetted fibroblasts only. **B, C** UMAP-plots of re-clustered skin and scar fibroblasts, split by tissue, reclustering identified 11 fibroblast clusters (subFB1-11). **D** Feature plots illustrating computational basis for dotplots. Dotplots of top 50 regulated genes (according to lowest adjusted p -value) comparing scar FBs versus skin FBs. **E** Dotplot of top 50 regulated genes (according to lowest adjusted p -value) cluster subFB1 compared to all other scar FBs. **F** Gene ontology-term network was calculated based on significantly upregulated (adj. p -value < 0.05, avg.logFC > 0.1) genes comparing subFB1 to all other scar FBs. Gene list was imputed in ClueGO plug-in in Cytoscape with medium GO-specificity, with GO-term fusion, only significant (P value < 0.05) GO terms are shown. Circle size correlates with P value, lines ("edges") represent functional connection of respective GO terms. Red circles represent association of GO-term with TGF β -signaling, purple, with extracellular matrix, green, with smooth muscle differentiation, blue, with signaling factors, and yellow with bone formation and -development. UMAP, uniform manifold approximation and projection.

models the temporal dynamics of gene expression in scars and might provide a basis to target respective genes at different stages of scar development. Interestingly, no genes were strongly regulated directly at the branching point, suggesting cell-fate is already determined at the beginning of pseudotime.

scRNAseq of murine scars identifies genes involved in scar maturation. As our approach so far only gave information on the current state of mature scars, we further investigated mechanisms leading to scar formation and maturation, using a murine full-thickness skin wound model (Figure S4A). Whereas scar formation and maturation in humans is a long-lasting process³⁷, it only takes up to 80 days in rodents³⁸. Although the here used murine scar model does not completely reflect hypertrophic scar formation in humans, the analysis of genes that are regulated in both, human hypertrophic scars and during normal scar formation in mice, might identify the most evolutionary conserved and most interesting targets for therapeutic interventions.

In order to detect dynamic differences in gene expression related to scar formation rather than wound healing, we compared samples from normal mouse skin, and from mice 6 and 8 weeks after wounding (Fig. 4A). Analogously to the human dataset, the murine scRNAseq dataset was clustered, and cell types were identified using established marker genes (Figure S4B), expression patterns of all clusters (Figure S4C), and transcriptome proximity of clusters via a phylogenetic clustertree (Fig. 4B). All clusters aligned homogeneously, and all major skin cell types were represented in normal skin and at both time points after scar development (Fig. 4C, Figure S4). In accordance with human scar tissue, 8-week-old mouse scars contained a higher proportion of murine FBs (mFBs) (32.6%) compared to 6-week-old scars (17.39%), and more immune cells (9.6 versus 6.3%). In contrast, less of the endothelium (2.8 versus 1.5%) and less keratinocytes (63.3 vs 45%) were present (Fig. 4D). We next calculated up- and downregulated genes for FBs, PCs, ECs, T cells, DCs, and KCs, comparing 8 weeks to 6-week-old scars (top 50 are shown in Figure S5A-F). In contrast to human scars, the highest number of differentially expressed genes was found in mFBs and mKCs (Fig. 4E, F), which was most likely due to ongoing epidermal tissue regeneration. Expression of *Acta2* and collagens showed only minor regulation between 6 and 8 weeks in mFBs (Fig. 4G). In addition, expression of several other matricellular and ECM-modulating proteins, e.g., *Fbln1* (Fibulin1), *Ogn* (osteoglycin), *Lum* (Lumican), and *Pcolce* (Procollagen C-Endopeptidase Enhancer), and *Tgfbi* (transforming growth factor, beta-induced) increased in mFBs during scar maturation (Fig. 4H). Together, our scRNAseq identified a gene profile specific for scar maturation in mice.

Serine proteases are strongly upregulated during scar maturation. To identify genes that are crucial for scar maturation, we next compared our human scar dataset with genes upregulated in mouse scars 8 weeks after wounding in

comparison to mouse scars 6 weeks after wounding (Fig. 5A). While in both datasets only one gene (*LEPR*) was downregulated, 16 genes were mutually upregulated (Fig. 5B-D). Stunningly, 5 of these genes (*AEBP1*, *DPP4*, *HTRA1*, *PLAU*, and *PRSS23*) were members of the superfamily of serine proteases (Fig. 5C, E). All five serine proteases were upregulated in scRNAseq in human scar tissue, particularly in FBs, but also in other cell types (Fig. 5E-J). *AEBP1* and *PRSS23* expression also increased in ECs and melanocytes, *HTRA1* in ECs and KC3, and *PLAU* in DCs. Several additional serine proteases, *HTRA3* (high-temperature requirement A serine peptidase 3), *DPP7* (dipeptidyl-peptidase 7), *FAP* (fibroblast activation protein alpha), were upregulated in human scars (Figure S6), and also showed a trend in mouse scars. Analysis of these serine proteases by pseudotime trajectories in human FBs revealed that their expression mainly increased over time and *AEBP1* and *HTRA1* significantly enriched at the end of branch 2 (Figure S7). Together, these data suggest a major role of serine proteases in scar formation and/or maturation.

The serine proteases DPP4 and urokinase regulate TGF β 1-mediated myofibroblasts differentiation and ECM overproduction. We next wanted to investigate the contribution of the identified serine proteases to scar formation. Since specific inhibitors are commercially available only for DPP4 and urokinase, we focused our further functional studies on these two serine proteases. First, we corroborated our scRNAseq data by analyzing RNA and protein expression of DPP4 and urokinase (*PLAU*) using in situ hybridization (Figure S8), and immunofluorescence staining of human (Fig. 6A-C) and murine (Figure S8E-G) skin and scars. Immunofluorescence staining revealed expression of urokinase in the dermis and epidermis of healthy skin. In contrast, DPP4 was only present in the dermal compartment of healthy skin. Whereas the expression of DPP4 was significantly increased in the epidermis and dermis of hypertrophic scars in both species, immunofluorescence staining revealed only a slight, not significant upregulation of *PLAU* in the dermal compartment of hypertrophic scars. Since detection of released proteins by immunofluorescence often shows difficulties, we further quantified urokinase and DPP4 in human tissue biopsies using ELISA. Interestingly, both urokinase and DPP4 were significantly increased in human scar tissue compared to normal skin (Fig. 6F, G).

As TGF β 1 is one of the key inducers of scarring and tissue fibrosis, causing differentiation of FBs to profibrotic myofibroblasts^{19,39-41}, we hypothesized that the serine proteases interact with TGF β -signaling. To test this, we performed siRNA-mediated gene knockdown of *DPP4* and *PLAU* in primary FBs from healthy human skin. The knockdown significantly downregulated *DPP4* and *PLAU* mRNA expression levels (Figure S9A, B) and almost completely abolished the production of the respective proteins (Fig. 7A). Knockdown of both genes strongly reduced TGF β 1-mediated expression of alpha-smooth muscle actin (α SMA), a marker for myofibroblasts (Fig. 7B). The reduced α SMA expression was accompanied by a reduced ability to

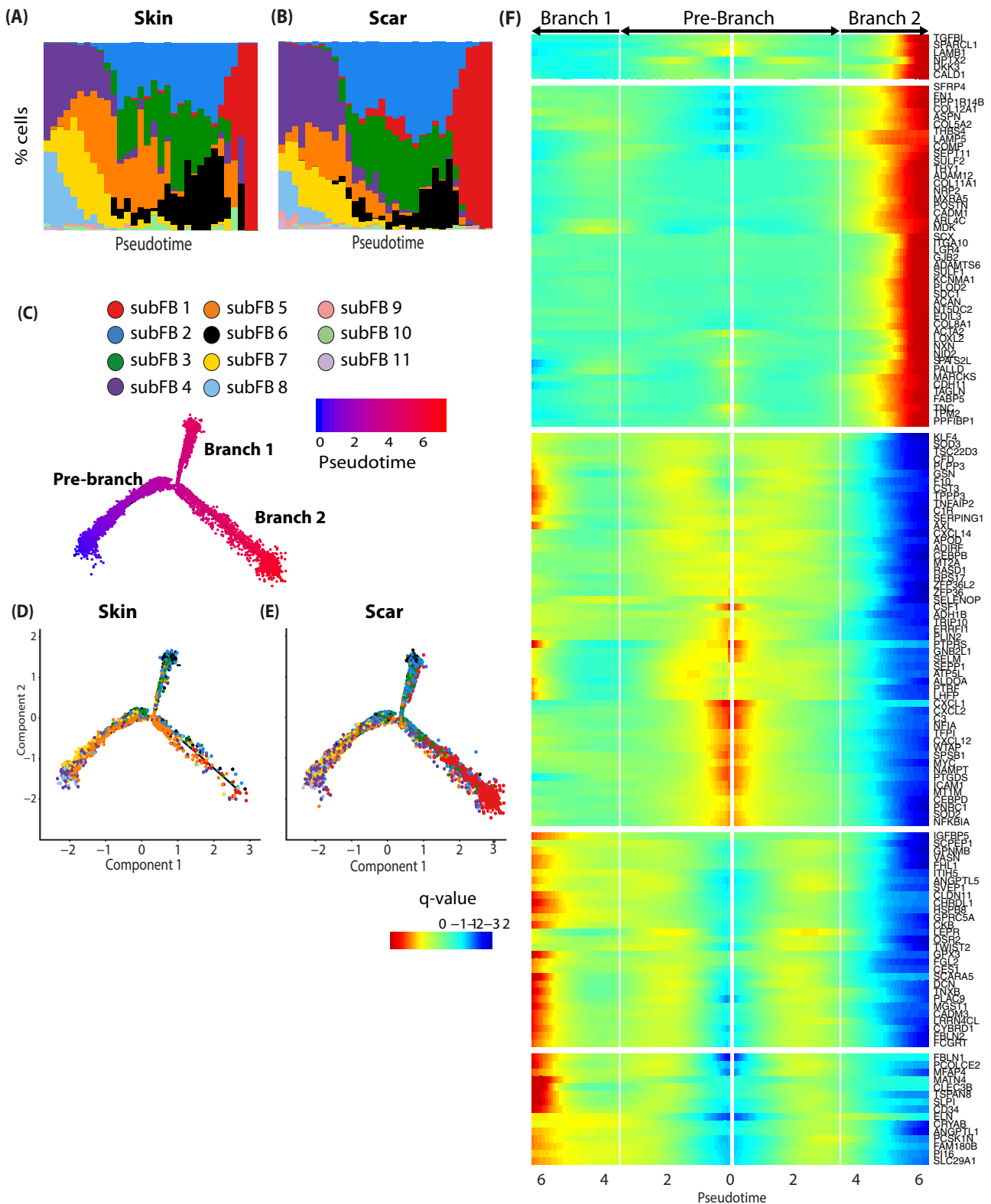
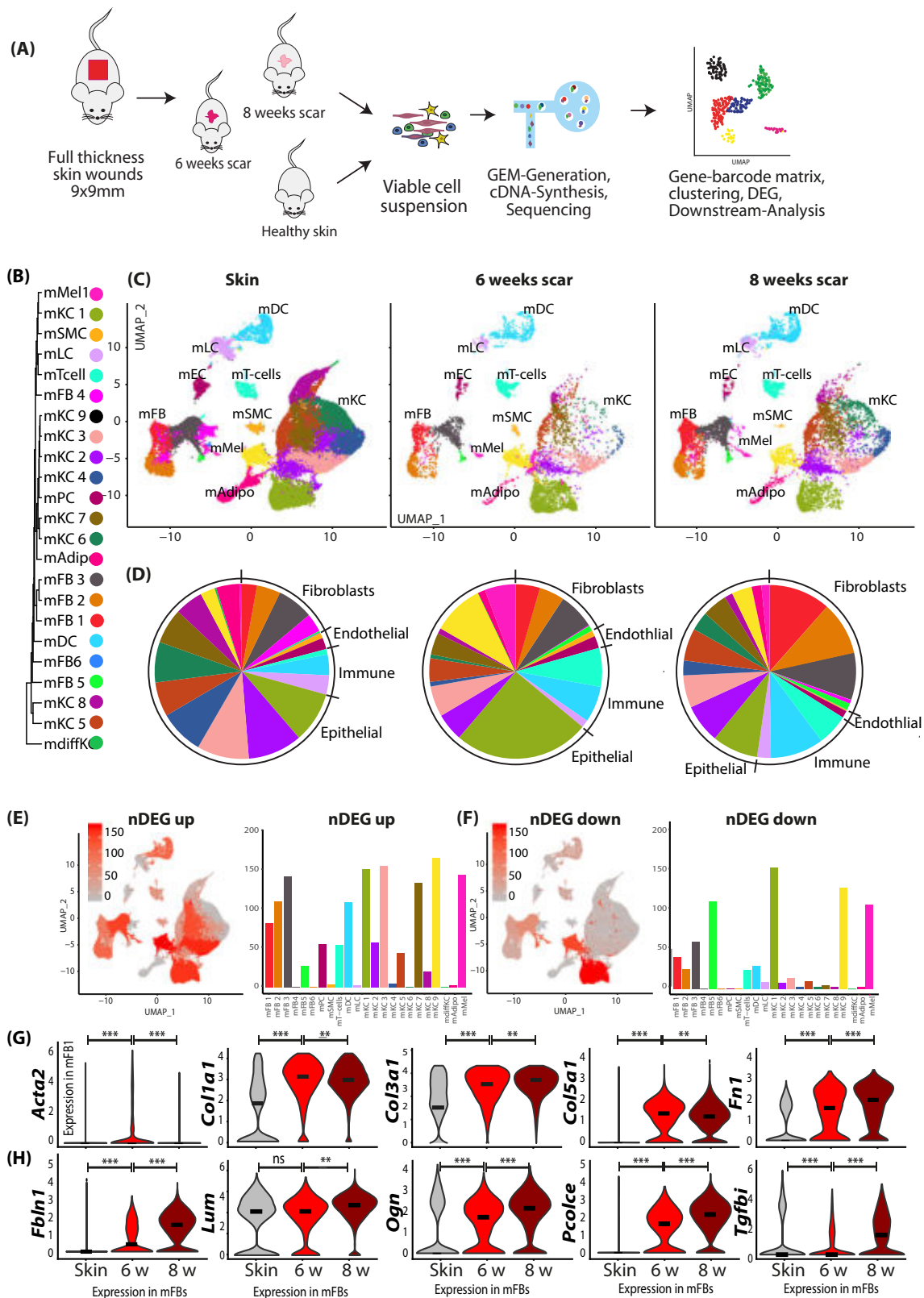


Fig. 3 Pseudotime analysis of human scar FBs identifies cell fates and pseudotime-regulated genes. **A, B** Ordering skin and scar FBs along a pseudotime axis. X-axis, pseudotime. y axis, % of cells in respective pseudotime-bin. Cell trajectory with pre-branch and branches is shown. **C** Color code represents pseudotime progression. **D, E** Cell trajectories were calculated based on pseudotime values, split by tissue. **F** Branched expression analysis modeling (BEAM) of skin and scar fibroblasts. Colors represent q -value, the expression of the respective gene in relation to pseudotime.



contract a matrix of collagen in vitro (Fig. 7C). We also analyzed components of the ECM and found significantly lower expression of different collagens and fibronectin (FN1) in knockdown FBs (Figure S9C-F). While FN1 protein release was strongly reduced (Fig. 7E), protein levels of COL1a1 were not reduced 48 h after gene silencing (Fig. 7D). Of note, transfection of cells led to a strong increase of baseline levels of FN1 and

COL1a1, which might be the reason for the weak response to TGFβ1 stimulation.

Next, we assessed these effects using the specific inhibitors for DPP4 (Sitagliptin) and PLAU (BC-11). Both inhibitors were able to abolish TGFβ1-induced αSMA production to a comparable degree as the specific gene knockdown (Fig. 7F, G). Surprisingly, collagen contraction was not inhibited with the inhibitors

Fig. 4 Two-timepoint mouse scar model identifies genes regulated in scar maturation. A Workflow of mouse skin scar model and two-timepoint ($n = 2$ per timepoint) scRNAseq. **B** Phylogenetic clustertree calculated unsupervised based on unsupervised UMAP-clustering. **C** UMAP-plots of mouse scar tissue, split by timepoint, after integration of all samples, identifying four fibroblast clusters (mFB1-4), smooth muscle cells and pericytes (mPC/SMC), endothelial cells and lymphatic endothelial cells (mEC/LEC), T cells, dendritic cells (mDC), Langerhans cells (mLC), nine keratinocyte clusters (KC1-9), adipocytes (mAdipo), and melanocytes (Mel). **D** Pie charts show relative numbers of cells in clusters, split by timepoint. Feature plots and bar graphs of number of differentially expressed genes (nDEG) per cluster of **E** up- and **F** downregulated genes per cluster. **G, H** Violin plots of ECM-associated genes. *Acta2* skin vs 6w $p = 2.22e-16$; 6w vs 8w $p = 1.4e-6$; *Col1a1* $p = 2.22e-16$, $p = 0.23$; *Col3a1* $p = 2.22e-16$, $p = 0.0079$, *Col5a1* $p = 2.22e-16$; $p = 5e-5$, *Fln1* $p = 2.22e-16$; $p = 5.5e-10$; *Fbln1* $p = 1.3e-10$, $2.22e-16$; *Lum* $p = 0.065$, $p = 2.22e-16$; *Ogn* $p = 9.3-0.5$, $p = 2.22e-16$; *Pcolce* $p = 2.22e-16$, $2.22e-16$; *Tgfb1* $p = 0.023$, $p = 2.22e-16$. Vertical lines in violin plots represent maximum expression, shape of each violin represents all results, and width of each violin represents frequency of cells at the respective expression level. DEGs were calculated per cluster comparing 8- vs 6-week-old scars using a two-sided Wilcoxon-signed rank test, including genes with average logarithmic fold change (avg_logFC) of >0.1 or <-0.1 and Bonferroni-adjusted p -value <0.05 . Feature plots show projection of nDEG onto the UMAP-plot, color intensity represents nDEG. Bar graphs show absolute number of nDEG per cluster, y-axis represents nDEG. UMAP uniform manifold approximation and projection.

(Fig. 7H), indicating off-target or unspecific inhibitor effects. Moreover, Sitagliptin and BC-11 attenuated TGF β 1-induced overproduction of the ECM-proteins Col1a1 (Fig. 7I), and fibronectin (Fig. 7J) by FBs. These results demonstrate that serine proteases are involved in TGF β 1-induced myofibroblast differentiation. Of note, not all observed effects found in FBs deficient for PLAU or DPP4, were mirrored with pharmacological inhibitors.

To investigate whether the serine protease inhibitors interfere with TGF β 1 signaling, we analyzed the TGF β 1-induced SMAD and ERK signaling pathways⁴². Neither knockdown of *DPP4* or *PLAU* nor addition of the inhibitors led to a significant inhibition of the SMAD and ERK1/2 signaling pathway (Figure S10A). To further identify other signaling pathways that might be involved in the action of the serine protease inhibitors, we used a signaling proteome profiler, showing that none of the signaling molecules were blocked by the inhibitors (Figure S10B). Interestingly, the GSK α/β -pathway, known to attenuate fibrotic processes in the heart⁴³ was significantly activated by BC-11 (Figure S10B-D), indicating a counter-regulatory action. Together, these data suggest that sitagliptin and BC-11 do not interfere with canonical or known non-canonical TGF β 1 signaling.

The serine protease inhibitors Sitagliptin and BC-11 improve scar formation by interfering with production and organization of the ECM. We next attempted to assess the effects of Sitagliptin and BC-11 in in vivo scar formation in mice (Fig. 8A). Application of the inhibitors did not interfere with wound healing (Fig. 8B), and even showed a slight, non-significant trend toward faster wound closure after application of BC-11 (Fig. 8C). scRNAseq of scars (Fig. 8D–J) showed a lower number of the main matrix producing FB clusters mFB1 and mFB2 in BC-11 stimulated scars after 8 weeks (Fig. 8F, I). The top 50 regulated genes are shown in Figure S11. Treatment of mice scars with BC-11 and Sitagliptin resulted in a slightly higher expression of *Col1a1*, but significantly lower expression of *Col3a1*, *Col5a1*, and *Fln1*. Interestingly, both inhibitors reduced the expression of their target proteases. Of note, BC-11 treatment also strongly reduced *Dpp4* expression (Fig. 8K).

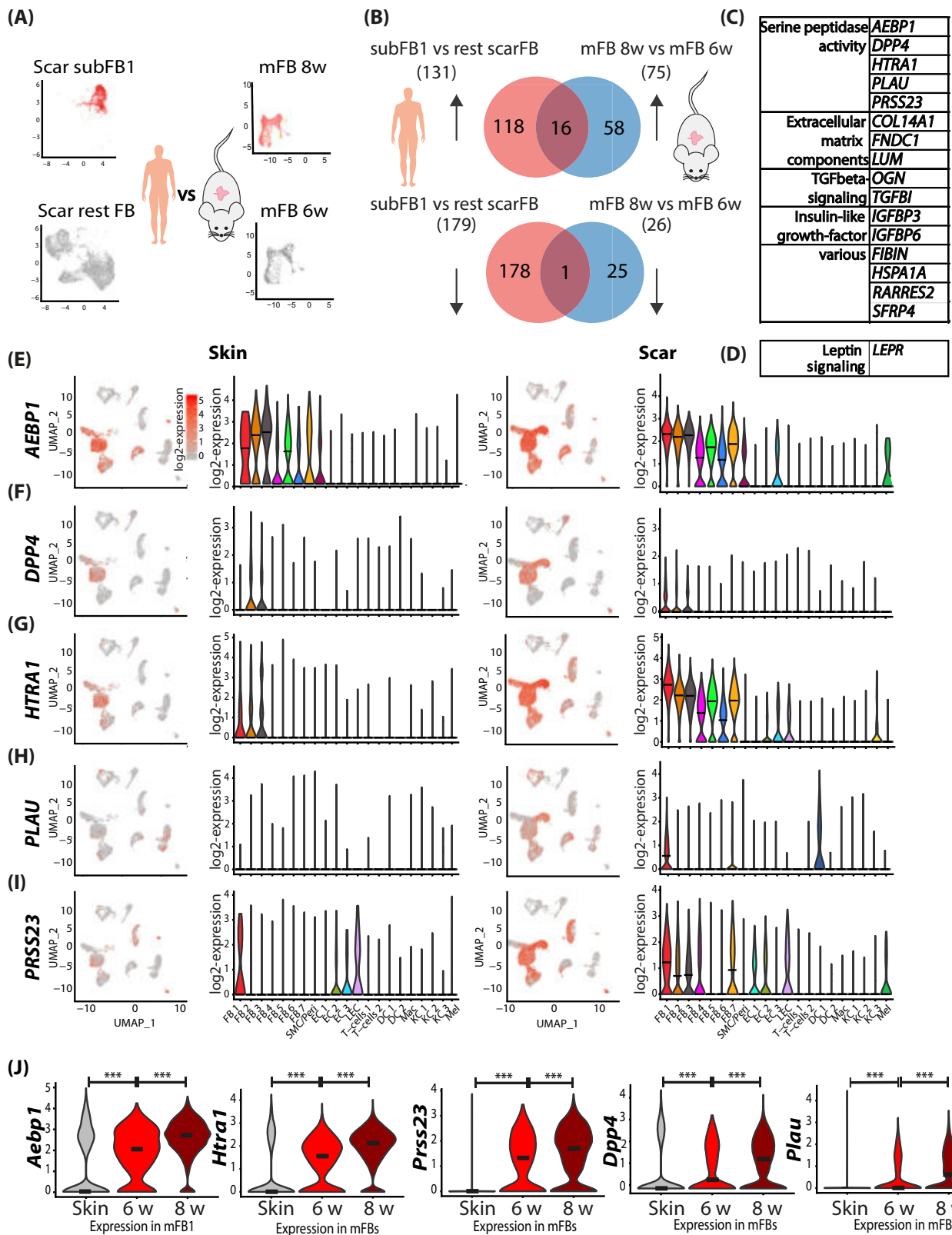
To assess formation of the ECM and collagen deposition, we stained skin and scar samples with picrosirius red (Fig. 9A) and with antibodies against collagen 3 (Fig. 9B), and fibronectin (Fig. 9C). Sirius red staining showed a reduction in total collagen deposition after treatment with both inhibitors (Fig. 9A). Immunofluorescence stainings revealed a significant alteration in collagen alignment and size of the collagen bundles between skin and scars but also between untreated scars and scars treated with inhibitors. As shown in Fig. 9B and C, both inhibitors strongly reduced the thickness of collagen bundles. To assess the quality of the resulting scar tissue, we used CurveAlign, a tool

designed to measure orientation of the ECM. Comparable areas directly adjacent and parallel to the epidermis were analyzed in H&E-stained sections of skin and scars (Fig. 9B). An alignment coefficient was calculated from orientation and alignment of collagenous fibers. A lower coefficient indicated less parallelism and thus less dense dermis. Strikingly, BC-11 treated scars showed a significantly lower alignment coefficient than control scars (Fig. 9C). This effect was not observed in sitagliptin-treated scars. Together, our data suggest that Sitagliptin, and even more prominently BC-11 interfere with matrix deposition in vivo, representing promising candidates for the improvement of (hypertrophic) skin scar formation.

Discussion

Although skin fibrosis has been extensively studied, key mechanisms leading to the development of hypertrophic scars are still not well understood. In addition, treatment options to prevent or treat (hypertrophic) scars are still scarce⁴⁴ and not exceptionally effective. In the present study, we used scRNAseq to elucidate the genetic landscape of hypertrophic scar tissue at a hitherto unmet single-cell resolution.

As expected, our scRNAseq analysis confirmed a plethora of previous studies, but also identified numerous genes, which have so far not been described in the context of skin scarring or tissue fibrosis. For example, the cytokines *MDK* (midkine) and *PTN* (pleiotrophin), both involved in cell growth, migration, and angiogenesis⁴⁵, were strongly upregulated in scar FBs. In contrast, *SOD2/3* (superoxide dismutase 2/3), an enzyme controlling the release of reactive oxygen species (ROS), hence acting as important antioxidant⁴⁶, was strongly downregulated in scar FBs. Intriguingly, failure of ROS-scavenging has already been shown to contribute to hypertrophic scar formation⁴⁷. Another interesting and significantly downregulated gene in scars was *SFN* (stratifin). As stratifin has been identified as potent collagenase-stimulating factor in FBs, its downregulation in scars suggests a contribution to the maintenance and/or progression of the fibrotic phenotype by preventing matrix degradation. However, we also identified interesting, so far undescribed differences in other cell types. In human SMC/Pericytes for example, we found a strong upregulation of a group of methallothionins (*MT1G*, *MT1E*, *MT2A*, *MT1A*), which were previously found to be increased in keloid FBs and concomitantly regulated with collagens upon treatment with TGF β ⁴⁸, however, their role in hypertrophic scars has yet to be determined. We also identified a rearrangement of T-cell subsets in mouse scar tissue (Figure S12). In the light of a previous publication by Kalekar et al.⁴⁹, demonstrating that *GATA3*-expressing regulatory T cells contribute to FB activation in murine dermal fibrosis, and our finding, that *Gata3* is strongly upregulated in mouse scars, it is likely that T-cell subsets contribute significantly to scar formation. However, we were not able



to identify comparable variations in T-cell subsets in human mature hypertrophic scars (Figure S13). It is therefore conceivable that these T-cell subsets play a role in initial scar formation processes rather than in established mature hypertrophic scars. In addition, species-dependent variances cannot be ruled out. Of note, *Serp1nb2*, a specific urokinase inhibitor was downregulated in both species in specific T-cell subsets. Less endogenous

urokinase inhibitors in scars might be an additional explanation for the high efficacy of BC-11, which was not only found in T cells but also in several other cell clusters in human scars and mouse scars (Figure S14). Together, these and many other novel factors identified in our study could be important, decisive molecules for the development and/or maturation of hypertrophic scars. Thus, our study has built a basis for future studies

Fig. 5 Comparing human scar gene expression and mouse scar maturation identifies mutual drivers of skin fibrosis. **A** Illustration of computational basis for comparison human and mouse. Human cluster subFB1 vs remaining scar FBs significantly (adj. p -value < 0.05) regulated genes were compared with mouse scar FBs 8 weeks vs 6 weeks significantly regulated genes. **B** Venn diagrams of human and mouse up- (upper panel) and down- (lower panel) regulated genes. **C** Table of mouse and human mutually up and **D** downregulated genes. **E–I** Violin plots and feature plots of serine proteases in mouse skin and scars. Vertical lines in violin plots represent maximum expression, shape of each violin represents all results, and width of each violin represents frequency of cells at the respective expression level. **J** Feature plots and violin plots of serine proteases in human skin and scar. *AEBP1* (adipocyte enhancer-binding protein 1) ($p = 2.22e-16$, $p = 2.22e-16$), *DPP4* (dipeptidyl-peptidase 4) ($p = 6.8e-9$, $p = 1.1e-15$), *HTRA1* (high-temperature requirement A serine peptidase 1) ($p = 2.22e-16$, $p = 2.22e-16$), *PLAU* (urokinase) ($p = 2.22e-16$, $p = 2.22e-16$), *PRSS23* (serine protease 23) ($p = 2.22e-16$, $p = 4e-14$). In violin plots, dots represent individual cells, y -axis represents \log_2 fold change of the normalized genes and \log -transformed single-cell expression. Vertical lines in violin plots represent maximum expression, shape of each violin represents all results, and width of each violin represents frequency of cells at the respective expression level. In feature plots, normalized \log expression of the respective gene is mapped onto the UMAP-plot. Color intensity indicates level of gene expressions. UMAP, uniform manifold approximation and projection. A two-sided Wilcoxon-signed rank test was used in R. NS $p > 0.05$, * $p < 0.05$, ** $p < 0.01$, *** $p < 0.001$.

describing the role of these molecules in skin scarring and tissue fibrosis.

Our combined study of human mature hypertrophic scars and scar maturation in mice identified a group of serine proteases as key player for scar development and maturation. Although *DPP4*-positive FBs have previously been identified as the main source of ECM production in the skin⁵⁰, and urokinase has been shown to be involved in lung fibrosis¹⁹, their roles in myofibroblast differentiation and production of ECM are still unclear. Our finding that siRNA-mediated gene knockdown and addition of specific *DPP4* and urokinase inhibitors to TGF β 1-stimulated FBs almost completely inhibited myofibroblast differentiation and upregulation of matrix proteins was striking. Sitagliptin, the here used *DPP4* inhibitor, is an effective drug widely used for the treatment of diabetes mellitus⁵¹. Recently, Li et al. showed that exposure of FBs derived from hypertrophic scars to high glucose led to activation of the IGF/Akt/mTOR signaling pathway, suggesting a possible mechanism by which gliptins interfere with fibrotic processes⁵². Based on our study, it might be very interesting to systemically evaluate differences in scar formation and scar quality of diabetic patients treated with either gliptins or other drugs with serine protease inhibitory action. Indeed, an initial investigation on hypertrophic scar formation in Japanese patients receiving gliptins showed already promising results⁵³. As gliptins are already approved for clinical use, an off-label topical application including non-diabetic patients would be a promising step forward to fully elucidate its efficacy on skin scarring.

The urokinase inhibitor BC-11 showed more pronounced effect on scar formation compared to sitagliptin. Strikingly, BC-11 also inhibited the expression of both, *PLAU* and *DPP4*. The exact underlying mechanism needs further investigations; however, the combined action of BC-11 on both serine proteases might explain its better performance on collagen deposition in vivo. So far BC-11 has only been used in vitro, and further in vivo testing for efficacy and safety is still required. Inhibition of urokinase to attenuate tissue fibrosis per se might appear counterintuitive, as urokinase facilitates fibrinolysis and regulates ECM-turnover, eliciting anti-fibrotic action⁵⁴. However, literature on urokinase inhibitors and fibrosis is contradictory. The best investigated endogenous urokinase-inhibitor, plasminogen activator inhibitor-1 (PAI-1, *SERPINE1*), was found to cause excessive matrix deposition after injury⁵⁵. By contrast, and in line with our results, inhibition of urokinase by PAI-1 suppressed profibrotic response in FBs from fibrotic lungs and prevented cardiac fibrosis in mice¹⁸. Therefore, our study suggests the use of urokinase inhibitor BC-11 as a possible therapeutic strategy for the treatment of skin scars. Further studies are necessary to fully elucidate its efficacy in vivo.

Surprisingly, our analyses revealed no influence of the inhibitors and knockdown of the serine proteases on the canonical

TGF β 1 signaling pathway. Although *DPP4* inhibition has previously been demonstrated to directly inhibit canonical TGF β signaling via Smad2 in renal fibrosis⁵⁶ and TGF β -mediated myoFB-differentiation by interfering with ERK signaling⁵⁷, we were not able to confirm these mechanisms in skin FBs. Regarding BC-11, we found a significant activation of GSK3 α/β in TGF β 1-stimulated FBs. Since GSK3 β was previously found to interact with WNT/ β -catenin signaling^{58,59}, and deletion of GSK3 β induced a profibrotic myofibroblast phenotype in isolated cardiac FBs in mice⁴³, the activation of GSK3 α/β suggests a counter-regulation of TGF β 1 signaling. It is therefore conceivable that BC-11, at least partially, exerts its anti-fibrotic action via activation of GSK3 α/β . Deciphering the exact underlying mechanism by which the inhibitors interfere with TGF β signaling will be the scope of further studies.

In this study, we analyzed human hypertrophic scars and mouse scar formation on a single-cell level. However, several limitations should be considered. Due to the high costs and the fact that scRNAseq yields large datasets of tens of thousands of cells, thereby smoothening donor and technical variances⁶⁰, low donor numbers are usually justifiable^{61–63}. Nevertheless, the relatively small sample size in our study should be considered as a limitation of our study. Differences in body sites between scar tissue and healthy skin, and the fact that healthy skin and scars were not taken from the same donors could affect comparability of the data. However, a recent study by Ascension et al.⁶⁴, comparing different single-cell datasets of skin samples from different body regions showed that the major FB populations were consistently present in all donors and body sites, suggesting high comparability.

Furthermore, there are certainly considerable differences between human and murine wound healing; while mouse wounds heal predominantly via contraction promoted by the subcutaneous *panniculus carnosus*, de novo formation and deposition of ECM and subsequent re-epithelialization prevails in human wound healing⁶⁵. However, a study assessing contribution of epithelialization and contraction in mice found that each accounted for 40–60%, and that mouse wound models can thus be considered a valid model also for human wound healing⁶⁶. Moreover, our mouse scarring model does not fully reflect the pathological fibrotic state of human hypertrophic scars. Although mouse models for hypertrophic scars, e.g., subcutaneous bleomycin injection⁶⁷, or tight-skin mice⁶⁸ have been described, their transcriptome comparability with human hypertrophic scars is not well investigated. We therefore suggest that future studies testing the efficacy of serine protease inhibitors should be performed in large animal models, e.g., pigs, which better reflect the pathology of human hypertrophic scars⁶⁸. In our experimental model, creams containing protease inhibitors were topically applied on wounds and scar tissue after complete wound closure.

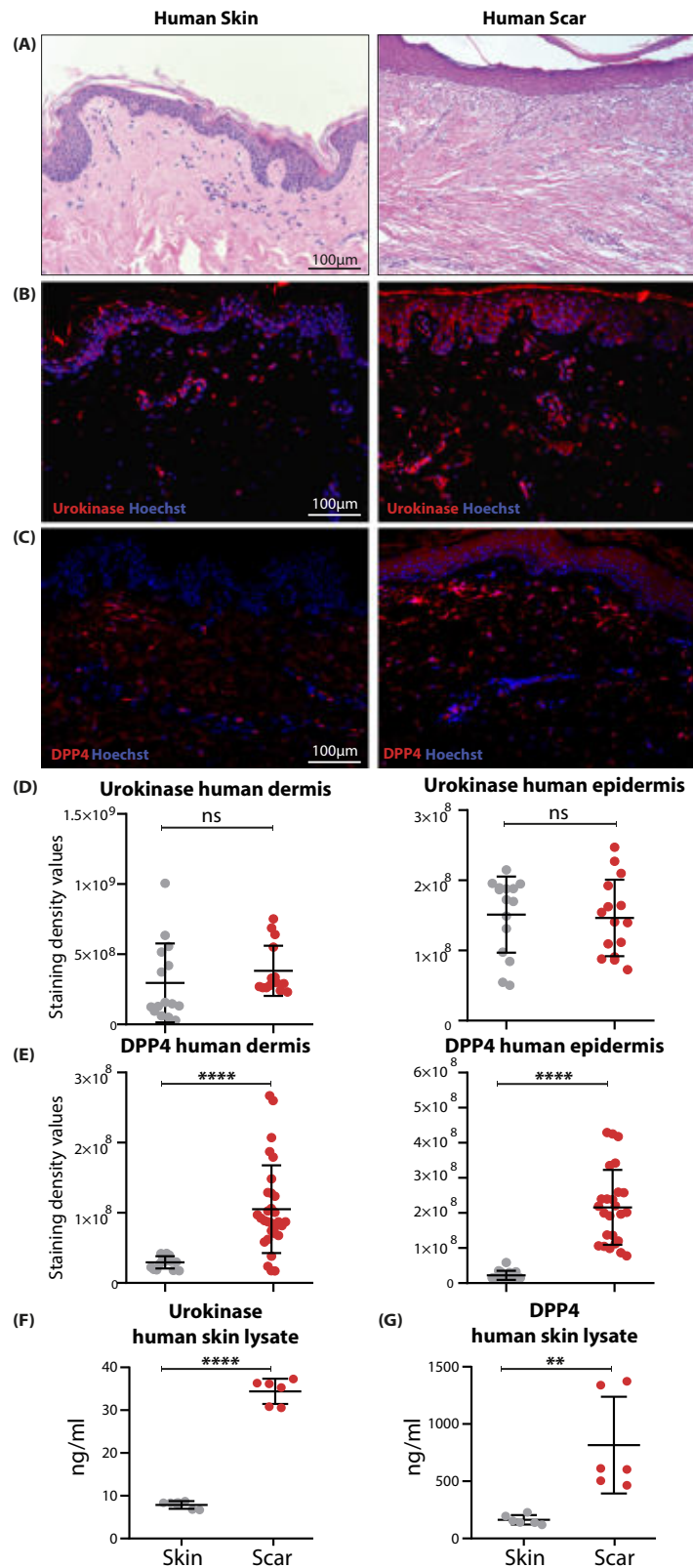
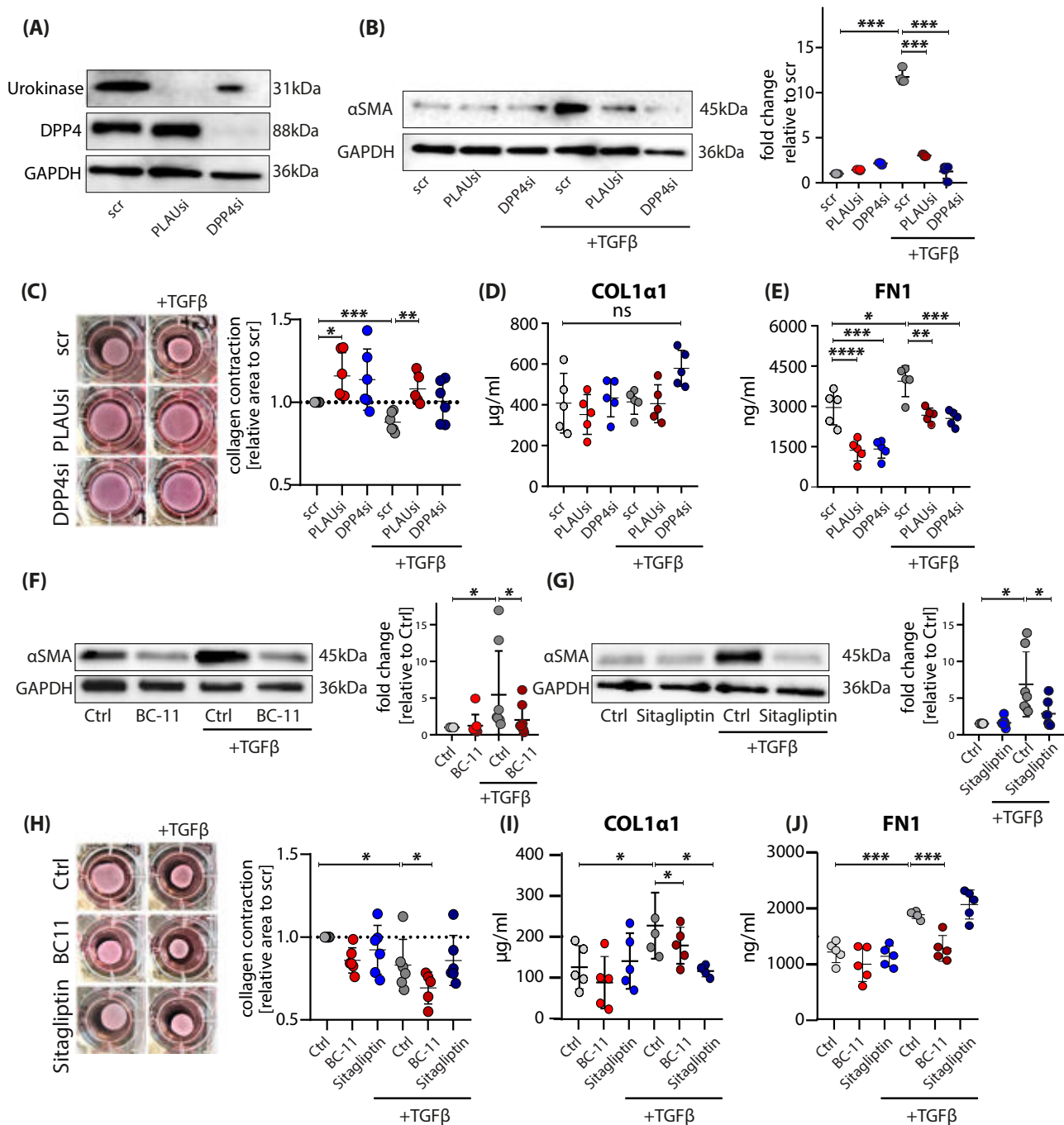


Fig. 6 Immunofluorescence staining confirms elevated expression of *PLAU* and *DPP4* in human and mouse skin and scar. **A** H&E staining of human skin and scar; immunofluorescent staining of **B** Urokinase and **C** DPP4 in human skin and scar. Quantification of staining intensity separate for epidermis and dermis for **D** urokinase ($p = 0.329$ dermis, $p = 0.815$ epidermis) and **E** DPP4 ($p < 0.0001$ dermis, $p < 0.0001$ epidermis). For all stainings, $n = 2-3$ normal skin samples were analyzed, and $n = 4$ scars. From each sample, five regions of interest per sample were quantified. ELISA from human whole skin ($n = 6$) and scar ($n = 6$) lysate for **F** urokinase ($p < 0.0001$) and **G** DPP4 ($p = 0.0037$) is shown. Statistical significance was tested using two-tailed unpaired Student *t*-test. Lines and error bars indicate mean and standard deviation. NS $p > 0.05$, * $p < 0.05$, ** $p < 0.01$, **** $p < 0.0001$. Source data are provided as a Source data file.



Whether the actives are able to penetrate wound scabs and/or scar tissue, or the initial treatment on open wounds is already enough to improve scar formation is currently not known. A recent study investigating transdermal resorption of Sitagliptin⁶⁹, however, indicates sufficient skin penetration. As literature for BC-11 is scarce, future studies are needed to evaluate its pharmacodynamics and pharmacokinetics properties.

Since we have demonstrated significant differences between specific knockdown of *PLAU* and *DPP4* and the inhibitors with regard to collagen contraction, it is conceivable that both inhibitors show side effects which have to be fully elucidated in further studies. Finally, histological analysis revealed up to 10% normal adjacent skin in the mouse scar samples, which slightly impacts our single-cell analysis.

Together, our study provides a genetic landscape of hypertrophic scars which is the basis for further investigations on genes

and fibrotic processes hitherto not studied in the context of skin scarring. Our in vitro and in vivo approaches suggest the use of serine protease inhibitors as treatment option for the prevention or improvement of hypertrophic scar development.

Methods

Ethical statement. The Vienna Medical University ethics committee approved the use of healthy abdominal skin (Vote Nr. 217/2010) and of scar tissue (Vote Nr. 1533/2017) and all donors provided written informed consent. Animal experiments were approved by the Medical University of Vienna ethics committee and by the Austrian Federal Ministry of Education, Science and Research (Vote Nr. BMBWF-66.009/0075-V/3b/2018) and performed in accordance with the Austrian guidelines for the use and care of laboratory animals. Mouse experiments were performed once, repetition of the experiment was not permitted by the ethics committee.

Scar and skin samples. Resected scar tissue ($n = 3$) was obtained from patients who underwent elective scar resection surgery (donor information is provided in

Fig. 7 Knockdown and pharmacological inhibition of DPP4 or urokinase prevents TGF β -induced myofibroblast differentiation. **A, B** Western blot of primary FBs after knockdown of PLAUI or DPP4. **B** Western blot of primary FBs after knockdown of DPP4 or PLAUI stimulated with active TGF β 1 for 24 h to differentiate FBs into alpha-smooth muscle actin-expressing (α SMA) myofibroblasts, and western blot quantification ($n = 3$). scr vs scr+TGF β 1, $p = 0.0006$; scr+TGF β 1 vs PLAUI+TGF β 1 $p = 0.0010$; scr+TGF β 1 vs DPP4si + TGF β 1 $p = 0.0017$. **C** Collagen contractility with FBs after knockdown of PLAUI or DPP4 and stimulation with or without active TGF β 1. scr vs PLAUIsi $p = 0.0194$; scr vs scr+TGF β 1 $p = 0.0005$; scr+TGF β 1 vs PLAUIsi+TGF β 1 = 0.0018. **D** Collagen I ($p > 0.05$) and **E** fibronectin (scr vs scr+TGF β 1, $p = 0.0193$; scr vs PLAUIsi $p < 0.0001$; scr vs DPP4si $p = 0.0001$; scr+TGF β 1 vs PLAUIsi + TGF β 1 = 0.0017; scr+TGF β 1 vs DPP4si + TGF β 1 = 0.0006) concentrations in supernatants of TGF β 1-stimulated primary skin FBs after knockdown with PLAUI or DPP4. **F, G** Western blot of primary FBs stimulated with active TGF β 1 for 24 h to differentiate FBs into alpha-smooth muscle actin-expressing (α SMA) myofibroblasts, and quantification of western blot ($n = 5-6$). Myofibroblast differentiation inhibited with **F** urokinase inhibitor BC-11 (Ctrl vs Ctrl+TGF β 1 $p = 0.049$, Ctrl+TGF β 1 vs BC-11 + TGF β 1 $p = 0.020$) or **G** DPP4 inhibitor Sitagliptin (Ctrl vs Ctrl+TGF β 1 $p = 0.0183$, Ctrl+TGF β 1 vs Sitagliptin+TGF β 1 $p = 0.0356$). **H** Collagen contractility with FBs after inhibition with BC-11 or Sitagliptin and stimulation with or without active TGF β 1 (Ctrl vs Ctrl+TGF β 1 $p = 0.024$; Ctrl + TGF β 1 vs BC-11 + TGF β 1 $p = 0.037$). **I** Collagen I (Ctrl vs Ctrl+TGF β 1 $p = 0.0465$; Ctrl+TGF β 1 vs BC-11 + TGF β 1 $p = 0.021$) or **J** fibronectin (Ctrl vs Ctrl+TGF β 1 $p = 0.0009$; Ctrl vs Sitagliptin+TGF β 1 $p = 0.0002$) in supernatants of stimulated primary skin FBs, detected by enzyme-linked immunosorbent assay (ELISA). Quantification from western blot was calculated by pixel density measurement in ImageLab, adjusted to GAPDH and normalized to respective Ctrl values. Experiments were performed in duplicates of $n = 5$ each. Whiskers represent range maximum and minimum values with <1.5 interquartile range, boxes represent 25th-75th quartiles, line represents mean. Statistical significance was tested using two-way ANOVA with Tukey post-test. NS $p > 0.05$, * $p < 0.05$, ** $p < 0.01$, *** $p < 0.001$. Source data are provided as a Source data file.

Table S1). Scars were classified as hypertrophic, pathological scars according to POSAS⁷⁰ by a plastic surgeon. Only mature scars, which had not been treated before and persisted for more than 2 years were used for all experiments. All donors had no known chronic diseases and received no chronic medication. The quality of scar tissue was assessed by histological analysis. No adjacent normal skin was observed in any of the scar samples. Healthy skin ($n = 3$) was obtained from female donors between 25 and 45 years from surplus abdominal skin removed during elective abdominoplasty.

Mouse full skin wounding and scar maturation. Female Balb/c mice bred at the animal facility of the Medical University of Vienna (Himberg, Austria) were housed under specific-pathogen-free conditions at 22 ± 2 °C room temperature and $55 \pm 10\%$ humidity, with 12 h/12 h light/dark cycles and food and water access ad libitum. Female mice were used due to easier handling and better experimental compliance, which was necessary to enable frequent handling and application of treatment. For full-thickness skin wounds, mice were anesthetized with 100 mg/kg Xylazin and 5 mg/kg ketamin (both Sigma-Aldrich, St. Louis, MO, USA) intraperitoneally. Postoperative analgesia was provided with 0.1 mg/kg Buprenorphin (Temgesic®, Indivior Inc., North Chesterfield, VA, USA) subcutaneously and 0.125 mg/ml Piritramid (Janssen-Cilag Pharma, Vienna, Austria) in drinking water ad libitum. A 9×9 mm² area was marked on shaved backs and excised with sharp scissors. The wounds were left to heal uncovered without any further intervention. Mice were sacrificed 6 or 8 weeks after wounding, and scar tissues were isolated. Four-millimeter biopsies were taken from the scar tissue and analyzed individually for scRNAseq as described below. The quality of scar tissue was assessed by histological analysis. Samples with a maximum of 20% normal adjacent skin were used for further analyses.

Serine protease inhibitor treatment. Mouse full-thickness skin wounds were induced as described above. Ultrascic/Ultrabas ointment (1:2; Hecht-Pharma, Bremervörde, Germany) was used as carrier substance for all treatments. Four parts Ultrascic/Ultrabas and 1 part water were mixed and used as control treatment. For protein inhibitors, Sitagliptin (final concentration 1 mM) or BC-11 (final concentration 5 mM) were dissolved in water and mixed with the ointment. Immediately after wounding, mice were treated with control or inhibitors by applying 100 μ l ointment on each wound. After application, mice were put individually in empty cages without litter for 30 min and monitored closely to prevent immediate removal of the treatments and allow sufficient tissue resorption. Scabs were left intact to prevent wound infections. Mice were treated daily for the first 7d, and thrice a week for 7 weeks. After scar formation, 4 mm biopsies of the scar tissue were taken and cut in half. One half each scar sample was used for histological analysis, and the other biopsy halves from each treatment group were pooled and analyzed together with scRNAseq as described below.

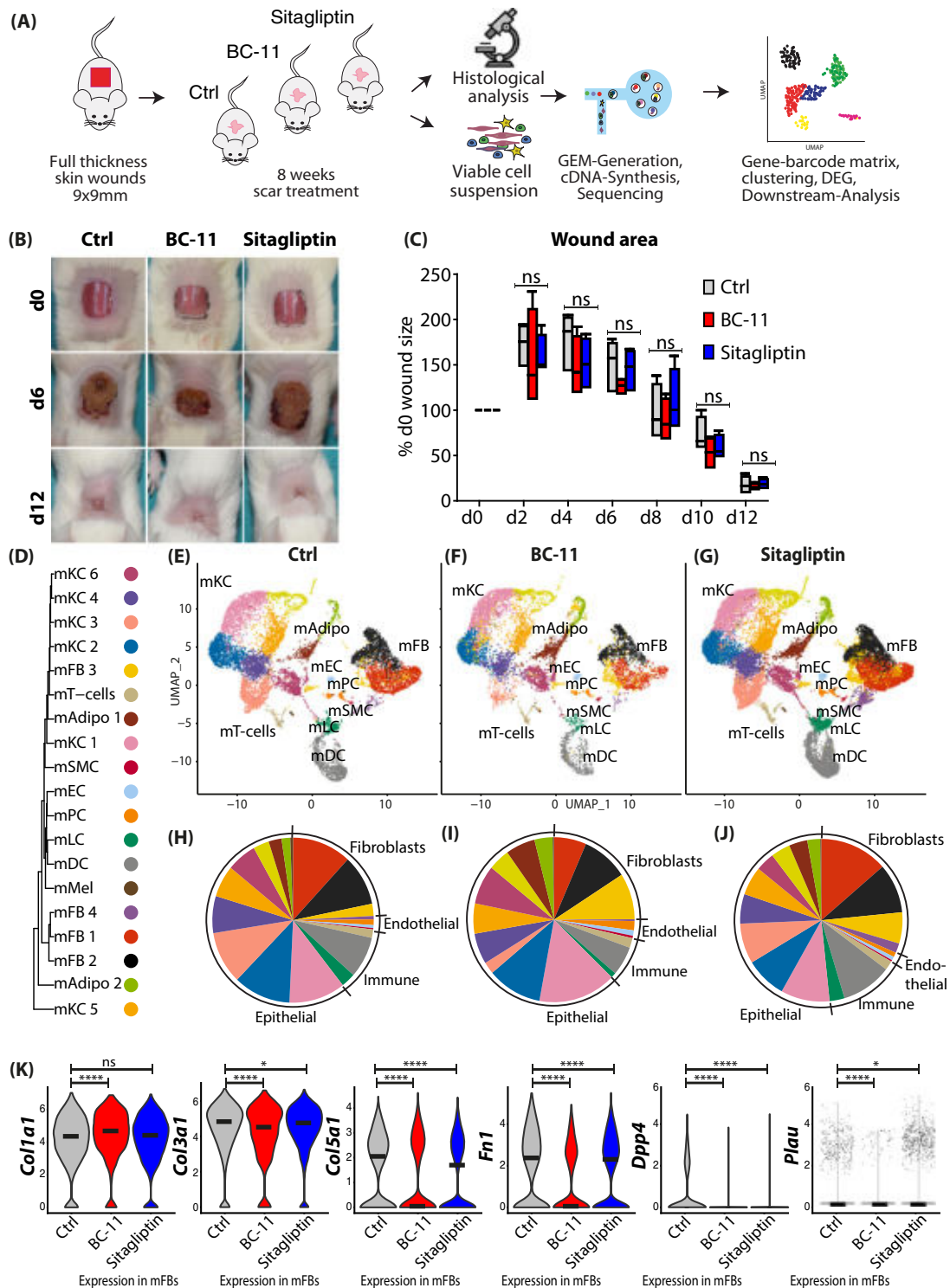
Single-cell isolation and fluorescence-activated cell sorting (FACS). Biopsies from human skin, human scars, and from naturally matured or treated mouse scar tissue were enzymatically digested with MACS Miltenyi Whole Skin Dissociation Kit (Miltenyi Biotec, Bergisch-Gladbach, Germany) for 2.5 h according to the manufacturer's protocol. After processing on a GentleMACS OctoDissociator (Miltenyi), cell suspensions were passed through a 70 μ m and a 40 μ m filter and stained with DAPI nuclear dye. Cells were sorted on a MoFlo Astrios high-speed cell sorting device (Beckman-Coulter, Brea, CA, USA), and only DAPI-negative cells, representing viable cells, were used for single-cell RNAseq (Figure S1).

Generation of single-cell gel-bead in emulsions (GEMs) and library preparation. Immediately after sorting, viable cells were loaded on a 10X-chromium instrument (single-cell gene expression 3'v2/3, 10X Genomics, Pleasanton, CA, USA) to generate GEMs. GEM-generation, library preparation, RNA-sequencing, demultiplexing, and counting were done by the Biomedical Sequencing Core Facility of the Center for Molecular Medicine (CeMM, Vienna, Austria). Sequencing was performed on an Illumina HiSeq 3000/4000 (Illumina, San Diego, CA, USA) with 3 samples per lane, 2×75 bp, and paired-end sequencing.

Cell-gene matrix preparation and downstream analysis. Raw sequencing files were demultiplexed, aligned to the human or mouse reference genome (GrCh38/mm10) and counted using the Cellranger pipelines (Cellranger v3, 10X Genomics). The resulting cell-gene matrices were processed using the 'Seurat'-package (Seurat v3.1.0, Satija Lab, New York, NY, USA) in R-studio in R (R v3.6.2, The R Foundation, Vienna, Austria). From each sample, unwanted variations and low-quality cells were filtered by removing cells with high and low (>3000 and <200) unique molecular identifier (UMI)-counts. First, healthy skin and scar samples were integrated separately to avoid clustering according to donors, and for batch correction. Subsequently, skin and scar data were integrated again into one dataset. Data integration was performed according to the recommended workflow by Butler et al. and Stuart et al.^{60,71} After quality control comparing all donors, we obtained transcriptome data from a total of 25,083 human skin and scar cells, with a median of 24,943 reads and 851 detected genes per cell. In mice, we obtained data from 6561 cells 6 weeks after wounding, and 9393 cells 8 weeks after wounding. The samples displayed a median of 24,774 reads per cell, and median of 1969 detected genes per cell. After quality control, all mouse samples were integrated together in one integration step. In both datasets, normalized count numbers were used for differential gene expression analysis, for visualization in violin plots, feature plots, dotplots, and heatmaps, when displaying features that vary across conditions, as recommended by current guidelines⁷². In both datasets, cell types were identified by well-established marker gene expression (Figures S2A and S4A). For identification of differentially expressed genes (DEGs), normalized count numbers were used, including genes present in the integrated dataset to avoid calculation of batch effects. As keratin and collagen genes were previously found to contaminate skin biopsy datasets and potentially provide a false-positive signal⁷³, these genes (*COL1A1*, *COL1A2*, *COL3A1* and *KRT1*, *KRT5*, *KRT10*, *KRT14*, *KRTDAP*) were excluded from DEG calculation in non-fibroblast clusters (collagens) or non-keratinocyte clusters (keratins), respectively. Moreover, genes *Gm42418*, *Gm17056*, and *Gm26917* caused technical background noise and batch effect in mouse scRNAseq, as described before⁷⁴, and were thus excluded from the dataset.

Pseudotime analyses. Pseudotime analyses, trajectory construction, and calculation of pseudotime-dependent gene expression were performed in Monocle2 (Monocle2, v2.14.0, Trapnell Lab, University of Washington, Seattle, WA, USA)^{35,75}. From the integrated FB subset Seurat-object, data were converted into a monocle-compatible CellDataSet. Analysis was then performed according to the recommended pipeline. Cells with mRNA counts two standard deviations above or below the mean were excluded. Size factors and dispersions were estimated, tSNE-reduction and clustering were performed^{35,36,75}. As input for pseudotime ordering, differentially expressed genes between skin and scar were used, and trajectories were constructed with DDRTree (R-package 'DDRTree' v0.1.5, 2015)³⁶.

Gene ontology (GO)-networks. Gene lists of significantly regulated genes (adjusted p -value <0.05, average log fold change [avg_logFC] >0.1) were imputed in ClueGO v2.5.5⁷⁶ plug-in in Cytoscape v3.7.2⁷⁷ with medium GO-specificity, with



GO-term fusion, and only significant (P value < 0.05) GO terms are depicted as circles, whereby circle size correlates with P value, and lines represent functional connection of respective GO terms.

Immunofluorescence staining. Immunofluorescence staining on formalin-fixed, paraffin-embedded (FFPE) sections of skin and scar tissue were performed according to the protocol provided by the respective antibody manufacturer as described previously⁷⁸. In brief, sections were deparaffinized in xylene and alcohol, antigen retrieval was performed with pH6 citric acid buffer, sections were washed in phosphate-buffered saline, and incubated with antibodies overnight at 4 °C. Sections were washed again, and incubated with secondary antibodies, blocking

sera of secondary antibodies species, and Hoechst, for 1 h at room temperature. Antibodies were used as indicated in Table S2. After the last wash, sections were mounted in aqueous mounting medium. Stainings were photographed using an Olympus BX63 microscope (Olympus, Tokyo, Japan) with Olympus CellSens Dimension v2.3 (Olympus) software with standardized exposure time for all samples. Staining intensity was quantified separately in dermis and epidermis using ImageJ v1.53c⁷⁹. For dermal quantification, regions of interest (ROIs) of 70 × 70 pixels were directly adjacent and parallel to the epidermis, contained no hair follicles or blood vessels, and were obtained from all regions of the specimen. For epidermal quantification, ROIs of 30 × 30 pixels located within the epidermis from all regions of each specimen. The total corrected fluorescence was measured by subtracting background values from area integrated density in the respective ROI.

Fig. 8 In vivo application of BC-11 or Sitagliptin reduces expression of ECM and serine proteases. **A** Workflow of mouse scarring and serine protease inhibitors. Biopsies of $n = 4$ mice per group were pooled for scRNAseq. **B** Images of wound healing in control or inhibitor-treated mice after 9, 6, and 12 days. **C** Quantification of wound area every second day after wounding. Four mice per group with three measurements per timepoint per mouse were analyzed. Wound area of d0 of every mouse was used as reference, and area was compared as percent of original wound size. Boxes indicate first and third quartile, whiskers indicate min and max, line indicates median. Statistical significance was tested using two-way ANOVA with Tukey post-test. **D** Phylogenetic clustering based on unsupervised UMAP-clustering. **E–G** UMAP-plots of mouse scar tissue, split by timepoint, after integration of all samples, identifying four fibroblast clusters (mFB1–4), smooth muscle cells and pericytes (mPC/SMC), endothelial cells and lymphatic endothelial cells (mEC/LEC), T cells, dendritic cells (mDC), Langerhans cells (mLC), nine keratinocyte clusters (KC1–9), adipocytes (mAdipo), and melanocytes (Mel). **H–J** Pie charts show relative numbers of cells in clusters, split by treatment. **K** Violin plots of ECM-associated genes. *Col1a1* Ctrl vs BC-11 $p = 4.8e-16$, Ctrl vs Sitagliptin $p = 0.3$; *Col3a1* Ctrl vs BC-11 $p = 3.2e-12$, Ctrl vs Sitagliptin $p = 0.028$; *Col5a1* Ctrl vs BC-11 $p = 1e-9$, Ctrl vs Sitagliptin $p = 1.4e-9$; *Fn1* Ctrl vs BC-11 $p = 2.22e-16$, Ctrl vs Sitagliptin $p = 8.6e-5$; *Dpp4* Ctrl vs BC-11 $p = 2.22e-16$, Ctrl vs Sitagliptin $p = 8.3e-11$; *Plau* Ctrl vs BC-11 $p = 5.04e-6$, Ctrl vs Sitagliptin $p = 0.022$; vertical lines in violin plots represent maximum expression, shape of each violin represents all results, and width of each violin represents frequency of cells at the respective expression level. A two-sided Wilcoxon-signed rank test was used in R. UMAP, uniform manifold approximation and projection. NS $p > 0.05$, * $p < 0.05$, ** $p < 0.01$, *** $p < 0.001$. using one-way ANOVA with Tukey post-test. NS $p > 0.05$, * $p < 0.05$, ** $p < 0.01$, *** $p < 0.001$. Source data are provided as a Source data file.

Picosirius red staining. Picosirius Red staining was performed according to the manufacturer's protocol of the staining kit (ab150681, Abcam, Cambridge, UK).

Isolation of primary skin fibroblasts. Five mm biopsies were taken from fresh abdominal skin, washed in phosphate-buffered saline (PBS), and incubated in 2.4 U/ml Dispase II (Roche, Basel, Switzerland) overnight at 4 °C. The next day, epidermis was separated from dermis, and dermis was incubated with Liberase TM (Merck Millipore, Burlington, MA, USA) in Dulbeccos modified eagle medium (DMEM, Thermo Fisher Scientific, Waltham, MA, USA) without supplements at 37 °C for 2 h. Next, the dermis was passed through 100 μ m and 40 μ m filters, rinsed with PBS, and cells were plated in a T175 cell culture flask. Medium was changed the next day, and then every other day until FBs reached 90% confluency. First passage FBs were used for TGF β 1-stimulation experiments.

TGF β 1-induced myofibroblast differentiation. After the first passage, isolated primary FBs were plated in 6-well plates, supplied with DMEM + 10% fetal bovine serum (FBS, Thermo Fisher Scientific) and 1% penicillin/streptomycin (Thermo Fisher Scientific) and grown until 100% confluency. FBs were then stimulated with 10 ng/ml TGF β 1 (HEK-293-derived, Peprotech, Rocky Hill, NJ, USA), and with or without DPP4 inhibitor Sitagliptin (10 μ M) (Thermo Fisher Scientific) or urokinase-inhibitor BC-11 hydrobromide (10 μ M) (Tocris by Bio-Techne, Bristol, UK) for 24 h. Supernatants were removed and medium and inhibitors were resupplied for another 24 h. Supernatants were collected and stored at -80 °C and cells were lysed in 1x Laemmli Buffer (Bio-Rad Laboratories, Inc., Hercules, CA, USA) for further analysis. To analyze signaling pathways, FBs were stimulated with TGF β 1 and inhibitors for 1 h, and then harvested in 1x Laemmli Buffer with protease inhibitor (cOmplete, MiniProtease Inhibitor Cocktail Tablets, Roche, Basel, Switzerland) and phosphatase inhibitor (Pierce™ Phosphatase Inhibitor Mini Tablets, Thermo Scientific).

siRNA-mediated gene silencing. Small interfering RNA (siRNA) transfection was conducted according to the previously published protocol⁸⁰ with minor modifications. siRNAs targeting *PLAU* (#HSS108076, Thermo Fisher Scientific) and *DPP4* (#HSS102892, Thermo Fisher Scientific) were used. Briefly, primary human FBs of 3 donors were transfected using Lipofectamine 2000 (Thermo Fisher Scientific). A total of 5 ml of Opti-MEM medium (+L-Glutamine, 4-[2-hydroxyethyl]-1-piperazineethanesulfonic acid, Phenol Red; Gibco by Life Technologies) were mixed with 50 μ l of Lipofectamine 2000 and 65 μ l of a 20 μ M small interfering RNAs or scrambled control RNA (Low GC Duplex; Thermo Fisher Scientific). After 15 min incubation, the solution was added to 20 ml DMEM medium and transferred to FBs. Protein and RNA samples were prepared 48 h after transfection.

Quantitative real-time PCR. Total RNA was prepared from fibroblast monolayers using TRIzol (Thermo Fisher Scientific) according to manufacturer's instructions. cDNA was synthesized using iScript™ cDNA Synthesis Kit (Bio-Rad, Hercules, CA, USA) according to manufacturer's instructions. Relative quantification was performed by using the LightCycler Master SYBR Green I kit (Roche Applied Science, Basel, Switzerland) on a LightCycler480 II thermocycler (Roche). Primers were designed using the Primer3 software (version 0.4.0, <https://bioinfo.ut.ee/primer3-0.4.0/>) and synthesized by Microsynth AG (Balgach, Switzerland). Samples were normalized to β -2-microglobulin (B2M) levels as reference gene. Primers with the sequences indicated in Table S3 were used.

Gel contraction assay. Primary human FBs or FBs silenced for *DPP4* or *PLAU* (3×10^5 fibroblasts per ml) were mixed purified bovine collagen solution (PureCol, Advanced BioMatrix, San Diego, CA) and 10% 10x Hanks' Balanced Salt Solution

(Thermo Fisher Scientific). Cell suspensions were poured into 6-well plates and allowed to solidify for 2 h at 37 °C in a humidified atmosphere. After equilibration with DMEM medium overnight, the collagen gels containing knockdown fibroblasts were further incubated with DMEM and gels with normal fibroblast were either treated with sitagliptin (10 μ M) and BC-11 (10 μ M) or left untreated. Collagen gels were further maintained in the absence or presence of TGF β 1 (10 ng/ml). After 48 h, gels were photographed, and gel areas were calculated using ImageJ software.

Western blotting. Primary FBs were lysed in 1x Laemmli Buffer (Bio-Rad Laboratories, Inc.) and loaded on 4–15% SDS-PAGE gels (Bio-Rad Laboratories, Inc.). Proteins were transferred on a nitrocellulose membrane (Bio-Rad Laboratories, Inc.), membranes were blocked in non-fat milk with 0.1% Tween 20 (Sigma-Aldrich for 1 h, and incubated with antibodies as indicated in Table S2 at 4 °C overnight. After washing, membranes were incubated with horseradish-peroxidase conjugated secondary antibodies as indicated in Table S2 for 1 h at room temperature. Signals were developed with SuperSignal West Dura substrate (Thermo Fisher Scientific) and imaged with a Gel Doc XR + device (Bio-Rad Laboratories, Inc.). Quantification analysis was performed with the Volume tool in ImageLab 6.0.1 (Bio-Rad), adjusted to GAPDH expression, and normalized to respective Ctrl samples to calculate fold change to Ctrl.

Proteome profiling of signaling pathways. To analyze signaling pathways, we used a proteome profiler for human phospho-kinases (ARY003C, R&D Systems, Biotechne, Minneapolis, MN, USA) according to the manufacturer's instructions.

Enzyme-linked immunosorbent assay (ELISA). Supernatants of TGF β 1-stimulated FBs after gene knockdown and treatment with protease inhibition were collected, centrifuged, and stored at -20 °C for further use. Protein levels of human procollagen Ia1 ELISA (R&D Systems) and human fibronectin ELISA (R&D Systems) were measured according to the manufacturer's manual. Absorbance was detected by FluoStar Optima microplate reader (BMG Labtech, Ortenberg, Germany). Six-millimeter punch biopsies of healthy skin and hypertrophic scar tissue were lysed in 1% Triton X-100 lysis buffer (Sigma) and mechanically homogenized using precellyse tissue homogenizer. After centrifugation, lysates were analyzed using DPP4 and urokinase ELISAs (both R&D Systems) Total protein concentrations were measured using a BCA-kit (Abcam) according to the manufacturer's protocol, and concentrations were normalized to total protein.

Scar planimetry. Collagen bundle alignment has been calculated using Curvealign V4.0 Beta, a curvelet transform-based, open-source MATLAB software. Images of H&E-stained tissues were edited by Adobe Photoshop CS6 (Adobe Inc, San Jose, CA, USA) to adapt the collagen color, contrast, brightness, and in some cases epidermal alignment to the image border. All images have been processed the same way. Collagen alignment has been calculated according to Curvealign V4.0 Beta manual (August 31, 2017)⁸¹. Depending on the tissue section, three or four regions of interest per image were selected for calculation. As region size 256 height, 256 width, 1 ROIx, 1 ROIy was chosen. For statistical evaluation, the coefficient of alignment as comparable value for the relative fiber alignment for every region was calculated. In total, 14 regions of interest calculated from 5 images taken from 4 to 5 animals for each condition.

RNA Scope in situ hybridization. FFPE-sections of human skin and scar tissue were prepared according to RNA Scope (ACDBio, Bio-Techne, Bristol, UK) pre-treatment protocol, hybridized with probes targeting human *DPP4* (RNA Scope® Probe-Hs-DPP4) and *PLAU* (RNA Scope® Probe-Hs-PLAU), and visualized with

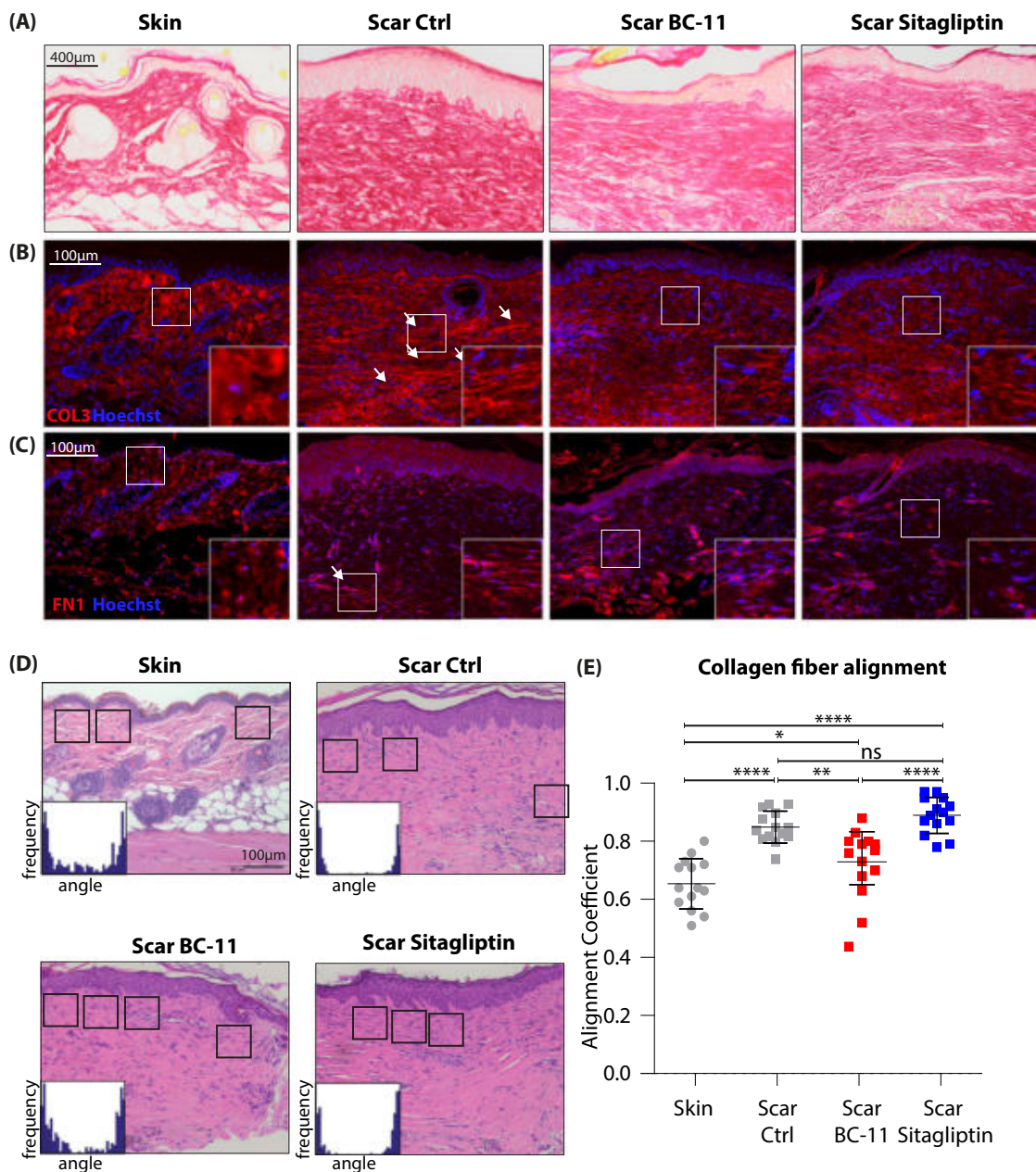


Fig. 9 In vivo application of BC-11 or Sitagliptin improves collagen alignment and fiber orientation in mouse scars. **A** Picrosirius red staining and immunofluorescent staining of **B** Col3a1 and **C** fibronectin in mouse skin and scars are shown. Four mice per group were analyzed. Arrows indicate areas of increased matrix density. **D** H&E images of mouse skin and scars. Squares indicate areas analyzed for collagen alignment. Histograms illustrate measurement of fiber orientation. **E** Calculation of alignment coefficient by CurveAlign in mouse skin and scar. $N = 4$ mice were analyzed per group, and three to four Regions of interest were calculated per image. Whiskers represent range maximum and minimum values with <1.5 interquartile range, boxes represent 25th–75th quartiles, line represents mean. Statistical significance was tested using one-way ANOVA with Tukey post-test. Skin vs Scar untreated $p < 0.0001$; Scar untreated vs Scar+BC-11 $p = 0.0018$; Scar untreated vs Scar+Sitagliptin $p = 0.551$. This mouse experiment was performed once, repetition of the experiment was not permitted by the ethics committee. NS $p > 0.05$, * $p < 0.05$, ** $p < 0.01$, *** $p < 0.001$. Source data are provided as a Source data file.

RNAscope 2.5 HD Assay—RED as suggested by the manufacturer. Images were acquired by AX70 microscope (Olympus, Tokyo, Japan) using the imaging software MetaMorph (Olympus).

Statistical analyses. Two groups with normally distributed data were compared by student's t test. Data of three and more groups were compared by one-way ANOVA with Tukey post hoc test. All statistical analyses were performed in GraphPad Prism v8.0.1 (GraphPad Software, San Diego, USA). P -values were marked in figure using asterisks indicating * $p < 0.05$, ** $p < 0.01$, *** $p < 0.001$, **** $p < 0.0001$.

Reporting summary. Further information on research design is available in the Nature Research Reporting Summary linked to this article.

Data availability

The scRNAseq data generated in this study have been deposited in the NCBI GEO database under accession "GSE156326". The raw sequencing data are protected and are not available due to data privacy laws. If raw sequencing data are absolutely necessary for replication or extension of our research, they will be made available upon request to the corresponding author within a 2-week timeframe. All other relevant data supporting the key findings of this study are available within the article and its Supplementary

Information files or from the corresponding author upon reasonable request. Source data are provided with this paper.

Received: 6 August 2020; Accepted: 8 October 2021;

Published online: 29 October 2021

References

- Bayat, A., McGrouther, D. A. & Ferguson, M. W. J. Skin scarring. *BMJ: Br. Med. J.* **326**, 88–92 (2003).
- Leavitt, T. et al. Scarless wound healing: finding the right cells and signals. *Cell Tissue Res.* **365**, 483–493 (2016).
- Sen, C. K. et al. Human skin wounds: a major and snowballing threat to public health and the economy. *Wound Repair Regen.* **17**, 763–771 (2009).
- Bock, O., Schmid-Ott, G., Malewski, P. & Mrowietz, U. Quality of life of patients with keloid and hypertrophic scarring. *Arch. Dermatol. Res.* **297**, 433 (2006).
- Van Loey, N. E., Bremer, M., Faber, A. W., Middelkoop, E. & Nieuwenhuis, M. K. Itching following burns: epidemiology and predictors. *Br. J. Dermatol.* **158**, 95–100 (2008).
- Lee, H. J. & Jang, Y. J. Recent understandings of biology, prophylaxis and treatment strategies for hypertrophic scars and keloids. *Int. J. Mol. Sci.* **19**, 711 (2018).
- Hinz, B. Myofibroblasts. *Exp. Eye Res.* **142**, 56–70 (2016).
- Nabai, L., Pourghadiri, A. & Ghahary, A. Hypertrophic scarring: current knowledge of predisposing factors, cellular and molecular mechanisms. *J. Burn Care Res.* **41**, 48–56 (2020).
- Anthonissen, M., Daly, D., Janssens, T. & Van den Kerckhove, E. The effects of conservative treatments on burn scars: a systematic review. *Burns* **42**, 508–518 (2016).
- Kafka, M. et al. Evidence of invasive and noninvasive treatment modalities for hypertrophic scars: a systematic review. *Wound Repair Regen.* **25**, 139–144 (2017).
- Tredget, E. E., Shupp, J. W. & Schneider, J. C. Scar management following burn injury. *J. Burn Care Res.* **38**, 146–147 (2017).
- Bao, Y. et al. Comparative efficacy and safety of common therapies in keloids and hypertrophic scars: a systematic review and meta-analysis. *Aesthetic Plast. Surg.* **44**, 207–218 (2020).
- Kanno, Y. The role of fibrinolytic regulators in vascular dysfunction of systemic sclerosis. *Int. J. Mol. Sci.* **20**, 619 (2019).
- Menou, A., Duitman, J. & Crestani, B. The impaired proteases and anti-proteases balance in Idiopathic Pulmonary Fibrosis. *Matrix Biol.* **68–69**, 382–403 (2018).
- Page, M. J. & Di Cera, E. Serine peptidases: classification, structure and function. *Cell. Mol. Life Sci.* **65**, 1220–1236 (2008).
- Di Cera, E. Serine proteases. *IUBMB Life* **61**, 510–515 (2009).
- Rawlings, N. D. & Barrett, A. J. MEROPS: the peptidase database. *Nucleic Acids Res.* **27**, 325–331 (1999).
- Gupta, K. K. & Donahue, D. L. Plasminogen activator inhibitor-1 protects mice against cardiac fibrosis by inhibiting urokinase-type plasminogen activator-mediated plasminogen activation. *Sci. Rep.* **7**, 365 (2017).
- Schuliga, M. et al. The fibrogenic actions of lung fibroblast-derived urokinase: a potential drug target in IPF. *Sci. Rep.* **7**, 41770 (2017).
- Makrilakis, K. The role of DPP-4 inhibitors in the treatment algorithm of type 2 diabetes mellitus: when to select, what to expect. *Int. J. Environ. Res. Public Health* **16**, 2720 (2019).
- Aroor, A. R. et al. Dipeptidyl peptidase-4 (DPP-4) inhibition with linagliptin reduces western diet-induced myocardial TRAF3IP2 expression, inflammation and fibrosis in female mice. *Cardiovasc. Diabetol.* **16**, 61 (2017).
- Hong, S. K., Choo, E. H., Ihm, S. H., Chang, K. & Seung, K. B. Dipeptidyl peptidase 4 inhibitor attenuates obesity-induced myocardial fibrosis by inhibiting transforming growth factor-beta1 and Smad2/3 pathways in high-fat diet-induced obesity rat model. *Metab.: Clin. Exp.* **76**, 42–55 (2017).
- Kaji, K. et al. Dipeptidyl peptidase-4 inhibitor attenuates hepatic fibrosis via suppression of activated hepatic stellate cell in rats. *J. Gastroenterol.* **49**, 481–491 (2014).
- Suzuki, T. et al. Vildagliptin ameliorates pulmonary fibrosis in lipopolysaccharide-induced lung injury by inhibiting endothelial-to-mesenchymal transition. *Respiratory Res.* **18**, 177 (2017).
- Uchida, T. et al. Renoprotective effects of a dipeptidyl peptidase 4 inhibitor in a mouse model of progressive renal fibrosis. *Ren. Fail.* **39**, 340–349 (2017).
- Schuliga, M., Grainge, C., Westall, G. & Knight, D. The fibrogenic actions of the coagulant and plasminogen activation systems in pulmonary fibrosis. *Int. J. Biochem. Cell Biol.* **97**, 108–117 (2018).
- Lay, A. J., Zhang, H. E., McCaughan, G. W. & Gorrell, M. D. Fibroblast activation protein in liver fibrosis. *Front. Biosci.* **24**, 1–17 (2019).
- Shi, S., Koya, D. & Kanasaki, K. Dipeptidyl peptidase-4 and kidney fibrosis in diabetes. *Fibrogenes. Tissue Repair* **9**, 1 (2016).
- Hu, M. S. & Longaker, M. T. Dipeptidyl peptidase-4, wound healing, scarring, and fibrosis. *Plast. Reconstr. Surg.* **138**, 1026–1031 (2016).
- Dong, J. et al. Single-cell RNA-seq analysis unveils a prevalent epithelial/mesenchymal hybrid state during mouse organogenesis. *Genome Biol.* **19**, 31 (2018).
- Dekoninck, S. et al. Defining the design principles of skin epidermis postnatal growth. *Cell* **181**, 604–620.e622 (2020).
- Phan, Q. M. et al. Lefl expression in fibroblasts maintains developmental potential in adult skin to regenerate wounds. *Elife* **9**, e60066 (2020).
- Guerrero-Juarez, C. F. et al. Single-cell analysis reveals fibroblast heterogeneity and myeloid-derived adipocyte progenitors in murine skin wounds. *Nat. Commun.* **10**, 650 (2019).
- Vorstandlechner, V. et al. Deciphering the functional heterogeneity of skin fibroblasts using single-cell RNA sequencing. *FASEB J.* **34**, 3677–3692 (2020).
- Trapnell, C. et al. The dynamics and regulators of cell fate decisions are revealed by pseudotemporal ordering of single cells. *Nat. Biotechnol.* **32**, 381–386 (2014).
- Qiu, X. et al. Reversed graph embedding resolves complex single-cell trajectories. *Nat. Methods.* **14**, 979–982 (2017).
- Kant, S. et al. Duration of scar maturation: retrospective analyses of 361 hypertrophic scars over 5 years. *Adv. Ski. Wound Care* **32**, 26–34 (2019).
- Ferguson, M. W. & O’Kane, S. Scar-free healing: from embryonic mechanisms to adult therapeutic intervention. *Philos. Trans. R. Soc. Lond. Ser. B, Biol. Sci.* **359**, 839–850 (2004).
- Carthy, J. M. TGFbeta signaling and the control of myofibroblast differentiation: implications for chronic inflammatory disorders. *J. Cell. Physiol.* **233**, 98–106 (2018).
- Roberts, A. B. et al. Transforming growth factor type beta: rapid induction of fibrosis and angiogenesis in vivo and stimulation of collagen formation in vitro. *Proc. Natl Acad. Sci. USA* **83**, 4167–4171 (1986).
- Lodyga, M. & Hinz, B. TGF-beta1—A truly transforming growth factor in fibrosis and immunity. *Semin. Cell Dev. Biol.* **101**, 123–39 (2020).
- Hata, A. & Chen, Y. G. TGF-β signaling from receptors to Smads. *Cold Spring Harbor Perspec. Biol.* **8**, a022061 (2016).
- Lal, H. et al. Cardiac fibroblast glycogen synthase kinase-3β regulates ventricular remodeling and dysfunction in ischemic heart. *Circulation* **130**, 419–430 (2014).
- Sidgwick, G. P., McGeorge, D. & Bayat, A. A comprehensive evidence-based review on the role of topicals and dressings in the management of skin scarring. *Arch. Dermatol. Res.* **307**, 461–477 (2015).
- Muramatsu, T. Midkine, a heparin-binding cytokine with multiple roles in development, repair and diseases. *Proc. Jpn. Acad. Ser. B, Phys. Biol. Sci.* **86**, 410–425 (2010).
- Miao, L. & St Clair, D. K. Regulation of superoxide dismutase genes: implications in disease. *Free Radic. Biol. Med.* **47**, 344–356 (2009).
- Carney, B. C. et al. Reactive oxygen species scavenging potential contributes to hypertrophic scar formation. *J. Surg. Res.* **244**, 312–323 (2019).
- Toh, P. P. et al. Modulation of metallothionein isoforms is associated with collagen deposition in proliferating keloid fibroblasts in vitro. *Exp. Dermatol.* **19**, 987–993 (2010).
- Kalekar, L. A. et al. Regulatory T cells in skin are uniquely poised to suppress profibrotic immune responses. *Sci. Immunol.* **4**, eaaw2910 (2019).
- Vorstandlechner, V. et al. Deciphering the functional heterogeneity of skin fibroblasts using single-cell RNA sequencing. *FASEB J.* **34**, 3677–3692 (2020).
- Juillerat-Jeanneret, L. Dipeptidyl peptidase IV and its inhibitors: therapeutics for type 2 diabetes and what else? *J. Med. Chem.* **57**, 2197–2212 (2014).
- Li, Y. et al. Linagliptin inhibits high glucose-induced transdifferentiation of hypertrophic scar-derived fibroblasts to myofibroblasts via IGF/Akt/mTOR signalling pathway. *Exp. Dermatol.* **28**, 19–27 (2019).
- Suwanai, H., Watanabe, R., Sato, M., Odawara, M. & Matsumura, H. Dipeptidyl peptidase-4 inhibitor reduces the risk of developing hypertrophic scars and keloids following median sternotomy in diabetic patients: a nationwide retrospective cohort study using the national database of health insurance claims of Japan. *Plast. Reconstr. Surg.* **146**, 83–89 (2020).
- Behrendt, N. The urokinase receptor (uPAR) and the uPAR-associated protein (uPARAP/Endo180): membrane proteins engaged in matrix turnover during tissue remodeling. *Biol. Chem.* **385**, 103–136 (2004).
- Rabieian, R. et al. Plasminogen activator inhibitor type-1 as a regulator of fibrosis. *J. Cell Biochem.* **119**, 17–27 (2018).
- Wang, D. et al. Sitagliptin ameliorates diabetic nephropathy by blocking TGF-β1/Smad signaling pathway. *Int. J. Mol. Med.* **41**, 2784–2792 (2018).
- Thielitz, A. et al. Inhibitors of dipeptidyl peptidase IV-like activity mediate antifibrotic effects in normal and keloid-derived skin fibroblasts. *J. Invest. Dermatol.* **128**, 855–866 (2008).

58. Guo, Y. et al. Entanglement of GSK-3 β , β -catenin and TGF- β 1 signaling network to regulate myocardial fibrosis. *J. Mol. Cell. Cardiol.* **110**, 109–120 (2017).
59. Vallée, A., Lecarpentier, Y., Guillevin, R. & Vallée, J. N. Interactions between TGF- β 1, canonical WNT/ β -catenin pathway and PPAR γ in radiation-induced fibrosis. *Oncotarget* **8**, 90579–90604 (2017).
60. Butler, A., Hoffman, P., Smibert, P., Papalexi, E. & Satija, R. Integrating single-cell transcriptomic data across different conditions, technologies, and species. *Nat. Biotechnol.* **36**, 411 (2018).
61. Mahmoudi, S. et al. Heterogeneity in old fibroblasts is linked to variability in reprogramming and wound healing. *Nature* **574**, 553–558 (2019).
62. Solé-Boldo, L. et al. Single-cell transcriptomes of the human skin reveal age-related loss of fibroblast priming. *Commun. Biol.* **3**, 188 (2020).
63. Joost, S. et al. The molecular anatomy of mouse skin during hair growth and rest. *Cell Stem Cell* **26**, 441–457.e447 (2020).
64. Ascensión, A. M., Fuertes-Álvarez, S., Ibañez-Solé, O., Izeta, A. & Araújo-Bravo, M. J. Human dermal fibroblast subpopulations are conserved across single-cell RNA sequencing studies. *J. Invest. Dermatol.* **141**, 1735–1744 (2021).
65. Zomer, H. D. & Trentin, A. G. Skin wound healing in humans and mice: challenges in translational research. *J. Dermatol. Sci.* **90**, 3–12 (2018).
66. Chen, L., Mirza, R., Kwon, Y., DiPietro, L. A. & Koh, T. J. The murine excisional wound model: contraction revisited. *Wound Repair Regen.* **23**, 874–877 (2015).
67. Cameron, A. M., Adams, D. H., Greenwood, J. E., Anderson, P. J. & Cowin, A. J. A novel murine model of hypertrophic scarring using subcutaneous infusion of bleomycin. *Plast. Reconstruct. Surg.* **133**, 69–78 (2014).
68. Seo, B. F., Lee, J. Y. & Jung, S. N. Models of abnormal scarring. *BioMed. Res. Int.* **2013**, 423147 (2013).
69. Griffin, D., Colón, S., Gray, D., Overton, B. & Wang, B. *Design and Development of a Novel Sitagliptin-loaded Transdermal Patch for Diabetes Treatment* (2018).
70. Fearmonti, R. M. et al. The modified Patient and Observer Scar Assessment Scale: a novel approach to defining pathologic and nonpathologic scarring. *Plast. Reconstruct. Surg.* **127**, 242–247 (2011).
71. Stuart, T. et al. Comprehensive Integration of Single-Cell. *Data. Cell.* **177**, 1888–1902.e21 (2019).
72. Luecken, M. D. & Theis, F. J. Current best practices in single-cell RNA-seq analysis: a tutorial. *Mol. Syst. Biol.* **15**, e8746 (2019).
73. Rojahn, T. B. et al. Single-cell transcriptomics combined with interstitial fluid proteomics defines cell-type-specific immune regulation in atopic dermatitis. *J. Allergy. Clin. Immunol.* **146**, 1056–1069 (2020).
74. Hammond, T. R. et al. Single-cell RNA sequencing of microglia throughout the mouse lifespan and in the injured brain reveals complex cell-state changes. *Immunity* **50**, 253–271.e256 (2019).
75. Qiu, X. et al. Single-cell mRNA quantification and differential analysis with Census. *Nat. Methods* **14**, 309–315 (2017).
76. Bindea, G. et al. ClueGO: a Cytoscape plug-in to decipher functionally grouped gene ontology and pathway annotation networks. *Bioinformatics* **25**, 1091–1093 (2009).
77. Lotia, S., Montojo, J., Dong, Y., Bader, G. D. & Pico, A. R. Cytoscape app store. *Bioinformatics* **29**, 1350–1351 (2013).
78. Gschwandtner, M. et al. Histamine suppresses epidermal keratinocyte differentiation and impairs skin barrier function in a human skin model. *Allergy* **68**, 37–47 (2013).
79. Rueden, C. T. et al. ImageJ2: ImageJ for the next generation of scientific image data. *BMC Bioinforma.* **18**, 529 (2017).
80. Mildner, M. et al. Knockdown of filaggrin impairs diffusion barrier function and increases UV sensitivity in a human skin model. *J. Investigative Dermatol.* **130**, 2286–2294 (2010).
81. Liu, Y., Keikhosravi, A., Mehta, G. S., Drifka, C. R. & Eliceiri, K. W. Methods for quantifying fibrillar collagen alignment. *Methods Mol. Biol.* **1627**, 429–451 (2017).

Acknowledgements

This research project was financed in part by the FFG Grant “APOSEC” (852748 and 862068; 2015–2019), by the Vienna Business Agency “APOSEC to clinic,” (ID 2343727, 2018–2020), and by the Aposcience AG under group leader HJA. MM was funded by the Sparking Science Program of the Austrian Federal Ministry of Education, Science and Research (SPA06/055). We thank the HPH Haselsteiner and the CRISCAR Familienstiftung for their belief in this private public partnership to augment basic and translational clinical research. We thank Stefan Spalt for his support. The authors acknowledge the core facilities of the Medical University of Vienna, a member of Vienna Life Science Instruments.

Author contributions

M.M., H.J.A., E.T. and V.V. provided study conception and design; W.H. and C.R. provided patient sample material; H.J.A. and M.M. acquired funding; V.V., D.C., K.K., M.D., Y.C. and B.G. conducted experiments and prepared samples; V.V., M.L. and M.M. performed data analysis, visualization and figure design; V.V., M.L., K.K., E.T., K.H. and M.M. participated in data interpretation; V.V., M.L. and M.M. drafted the manuscript. All authors reviewed the manuscript.

Competing interests

The authors declare no competing interests.

Additional information


Supplementary information The online version contains supplementary material available at <https://doi.org/10.1038/s41467-021-26495-2>.

Correspondence and requests for materials should be addressed to Hendrik Jan Ankersmit or Michael Mildner.

Peer review information *Nature Communications* thanks the anonymous reviewer(s) for their contribution to the peer review of this work. Peer reviewer reports are available.

Reprints and permission information is available at <http://www.nature.com/reprints>

Publisher's note Springer Nature remains neutral with regard to jurisdictional claims in published maps and institutional affiliations.

 **Open Access** This article is licensed under a Creative Commons Attribution 4.0 International License, which permits use, sharing, adaptation, distribution and reproduction in any medium or format, as long as you give appropriate credit to the original author(s) and the source, provide a link to the Creative Commons license, and indicate if changes were made. The images or other third party material in this article are included in the article's Creative Commons license, unless indicated otherwise in a credit line to the material. If material is not included in the article's Creative Commons license and your intended use is not permitted by statutory regulation or exceeds the permitted use, you will need to obtain permission directly from the copyright holder. To view a copy of this license, visit <http://creativecommons.org/licenses/by/4.0/>.

© The Author(s) 2021

Supplementary Information

The serine proteases dipeptidyl-peptidase 4 and urokinase are key molecules in human and mouse scar formation

Vera Vorstandlechner^{1,2,3}, Maria Laggner^{1,2}, Dragan Copic^{1,2}, Katharina Klas^{1,2}, Martin Direder^{1,2}, Yiyang Chen^{4,5}, Bahar Golabi⁴, Werner Haslik³, Christine Radtke³, Erwin Tschachler⁴, Konrad Hötzenecker⁶, Hendrik Jan Ankersmit^{1,2*}, Michael Mildner^{4*}

¹Laboratory for Cardiac and Thoracic Diagnosis, Regeneration and Applied Immunology, Department of Thoracic Surgery, Medical University of Vienna

²Aposcience AG (FN 308089y), Dresdner Straße 87/A21, Vienna, Austria.

³Department of Plastic and Reconstructive Surgery, Medical University of Vienna, Vienna, Austria

⁴Department of Dermatology, Medical University of Vienna, Vienna, Austria

⁵University of Applied Sciences FH Campus Wien, Vienna, Austria

⁶Department of Thoracic Surgery, Medical University of Vienna, Vienna, Austria

* contributed equally to this work

corresponding authors:

Michael Mildner, PhD

Department of Dermatology, Medical University of Vienna

Lazarettgasse 14, 1090 Vienna, Austria

e-mail: michael.mildner@meduniwien.ac.at

phone: +43 1-40400-73507

fax: +43-1-40400-73590

	Sex	Ethnicity	Age	Location	Etiology
Skin 1	F	caucasian	30	abdomen	healthy skin
Skin 2	F	caucasian	36	abdomen	healthy skin
Skin 3	F	caucasian	43	abdomen	healthy skin
			Mean 36+/-6,506		
Scar 1	F	caucasian	75	forearm	injury
Scar 2	M	caucasian	24	calf	burn
Scar 3	F	caucasian	54	axilla	surgical scar
			Mean 51±26.6		
			p=0.391		

Table S1: Skin and scar donor demographics. Statistical significance of age was calculated using Student-t-test, p-value > 0.05, not significant.

Target	Supplier	Product Nr.	Host species	Dilution	Application
DPP4	abcam	ab215711	rabbit monoclonal	1:1000	IF (FFPE), WB
PLAU	Novus biologicals	NBP2-20819	rabbit polyclonal	1:100	IF (FFPE), WB
αSMA	abcam	ab7817	mouse monoclonal	1:200	WB
Fibronectin	abcam	ab2413	rabbit polyclonal	1:500	IF (FFPE)
COL3a1	abcam	ab7778	rabbit polyclonal	1:200	IF
GAPDH	abcam	ab8245	mouse monoclonal	1:10000	WB
SMAD 2/3	Cell signaling	Rabbit mAb 8685	rabbit monoclonal	1:500	WB
pSMAD2	Cell signaling	mAb 5339	rabbit polyclonal	1:1000	WB
pSMAD1/5/9	Cell signaling	mAb 13820	rabbit polyclonal	1:1000	WB
ERK 1/2	Cell signaling	Rabbit mAb #	rabbit polyclonal	1:1000	WB
pERK1/2	Cell signaling	mAb 4376	rabbit polyclonal	1:1000	WB
Alexa fluor® 546 anti-mouse IgG (H +	Invitrogen	A-11030	goat polyclonal	1:500	IF, 2nd step
Alexa fluor® 546 anti-rabbit IgG (H + L)	Invitrogen	A-11035	goat polyclonal	1:500	IF, 2nd step
Anti-mouse, HRP-conjugated	GE Healthcare	GENX-A931	goat polyclonal	1:10 000	WB, 2nd step
Anti-rabbit, HRP-conjugated	Bio-Rad	#1706515	goat polyclonal	1:10 000	WB, 2nd step

Table S2: Antibodies used in experiments

Gene	Forward primer	Reverse Primer
<i>B2M</i>	5'-GATGAGTATGCCTGCCGTGTG-3'	5'- CAATCCAAATGCGGCATCT-3'
<i>PLAU</i>	5'-UAAUUCUUCUGGAGGAGAGGGGC-3'	5'-GCCCUCCUCUCCUCCAGAAGAAUUA-3'
<i>DPP4</i>	5'GGAAUGCCAGGAGGAAGGAAUCUUU-3'	5'-AAAGAUUCCUCCUCCUGGCAUUC-3'
<i>COL1A1</i>	5'-GTGCTAAAGGTGCCAATGGT-3'	5'-CTCCTCGCTTTCCTTCTCT-3'
<i>COL3A1</i>	5'-GTCCATGGATGGTGGTTTTTC-3'	5'-CACCTTCATTTGACCCCATC-3'
<i>COL5A1</i>	5'-GTCCATACCCGCTGGAAA-3'	5'-TCCATCAGGCAAGTTGTGAA-3'
<i>FN1</i>	5'-CTGCAGCCACAACCTTCTCTG-3'	5'-AGTTGCCACCAAGTTTGCTT-3'

Table S3: Primers used in PCR analyses

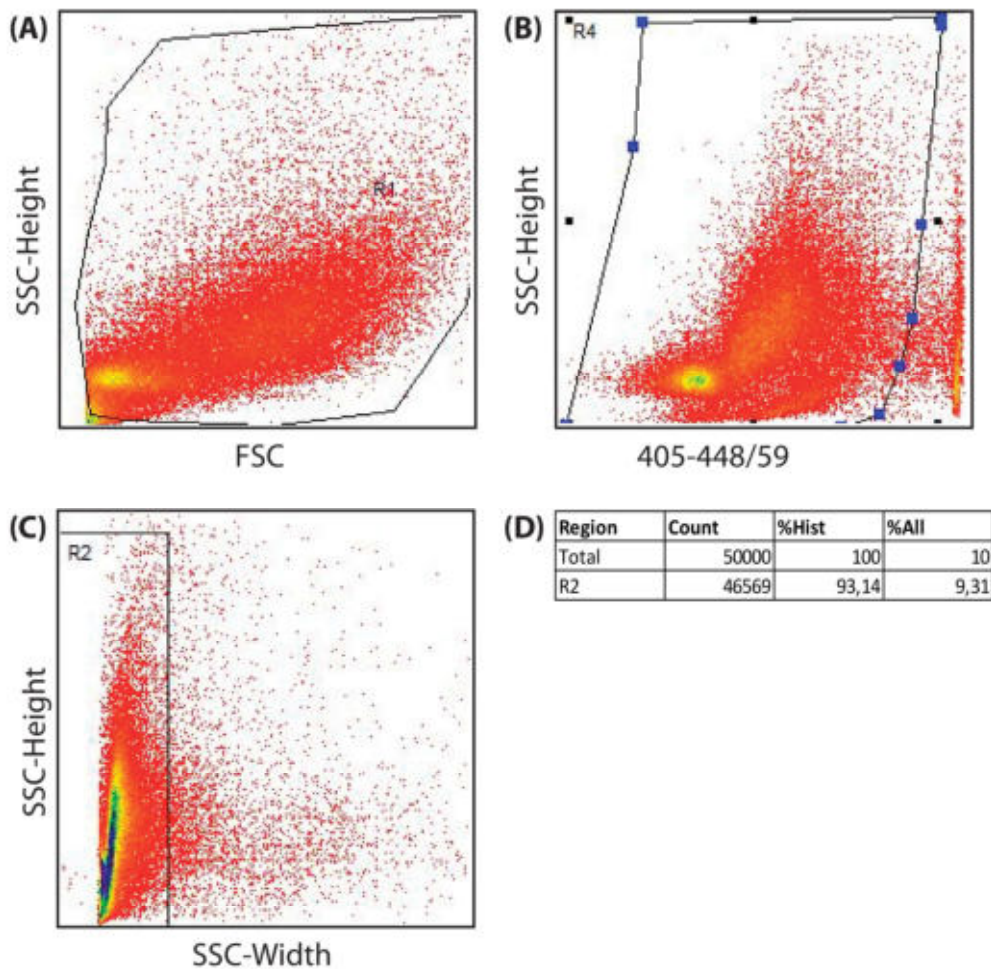


Figure S1: FACS gating strategy for DAPI-negative cell sorting

A) Cells from whole human or mouse skin, gated in side scatter (SSC) and forward scatter (FSC) to include all celltypes. B) Gating to exclude DAPI-positive cells C) Exclusion of cell doublets D) percentage and cell count per gating

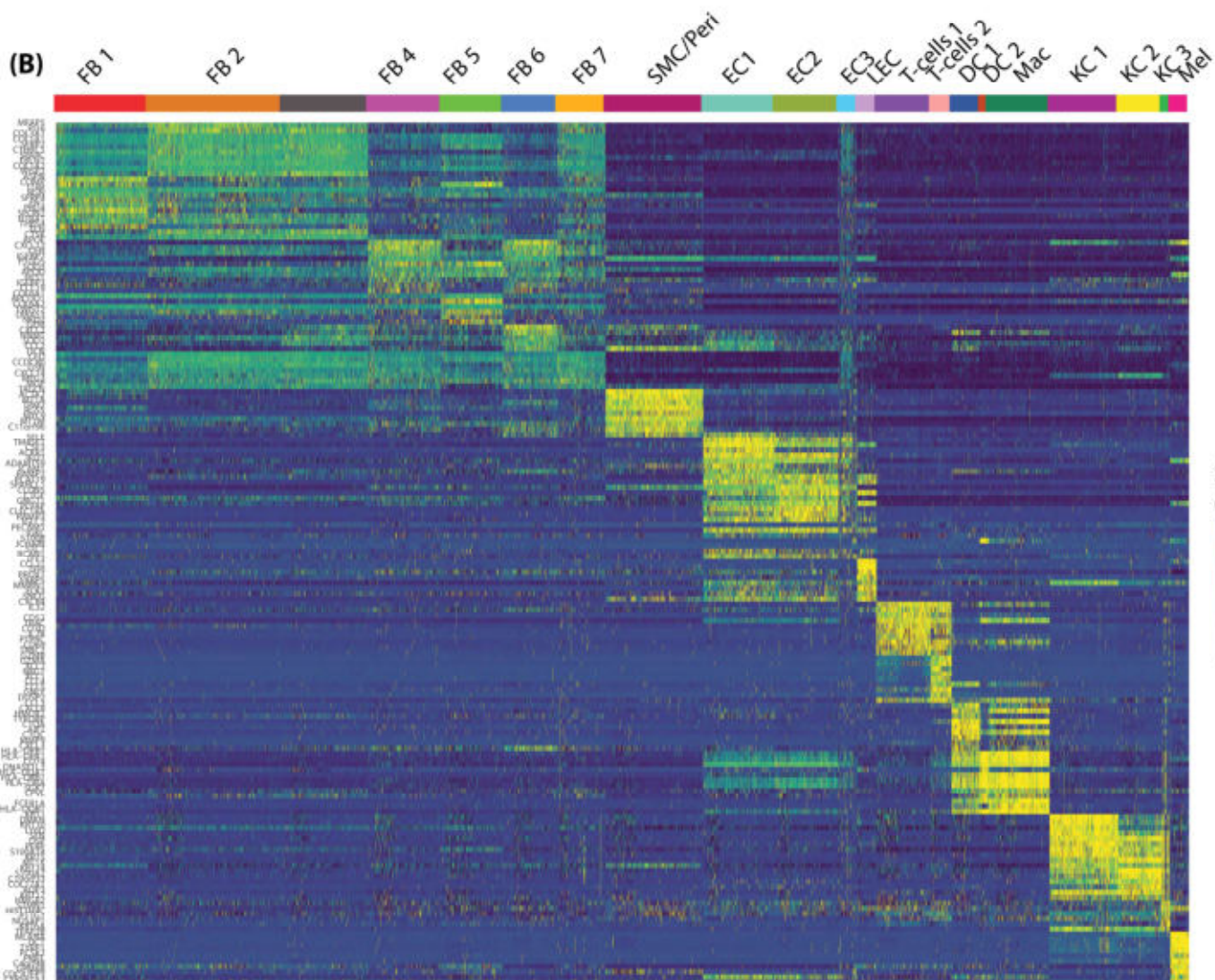
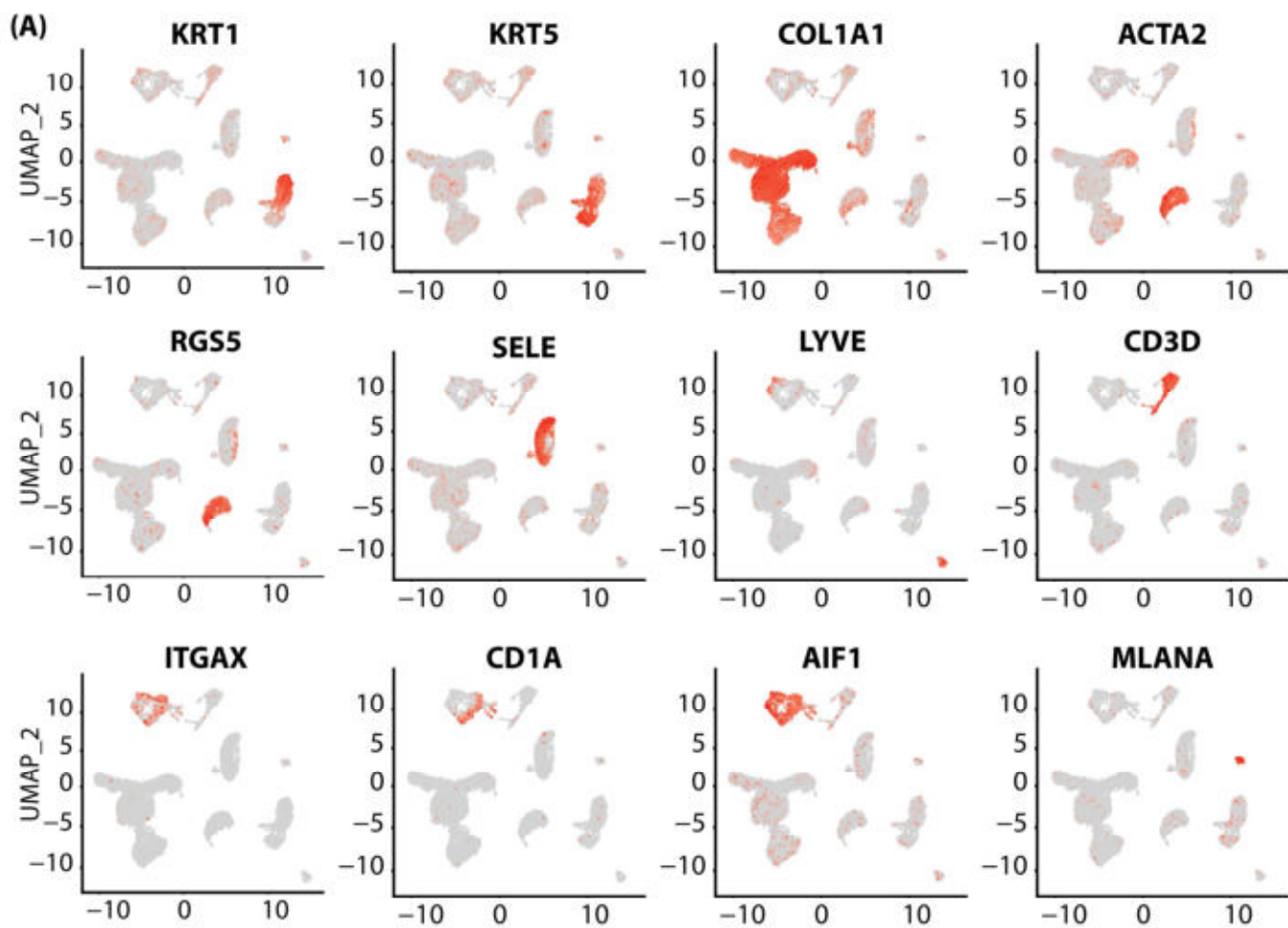
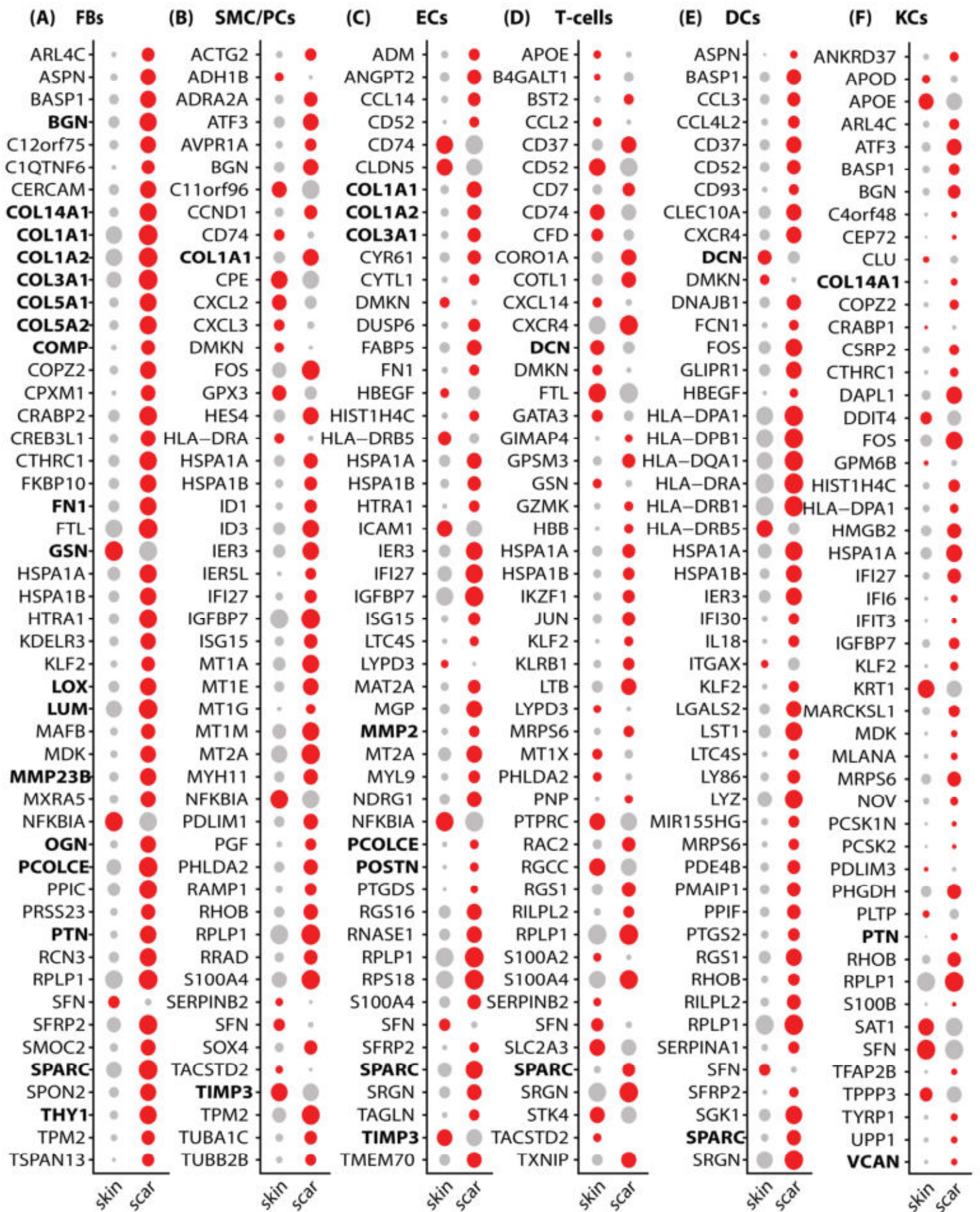


Figure S2: Identification of cell types by marker genes and marker gene expression patterns in human skin and scar.

A) Feature Plots of cluster markers *KRT1* (Keratin1) for spinous and granular keratinocytes (KCs), *KRT5* (Keratin 5) for basal KCs, *COL1A1* (collagen I alpha 1) for fibroblasts (FBs), *ACTA2* (smooth muscle actin) for smooth muscle cells and myofibroblasts, *RGS5* (Regulator Of G Protein Signaling 5) for pericytes, *SELE* (E-selectin) for endothelial cells, *LYVE1* (Lymphatic Vessel Endothelial Hyaluronan Receptor 1) for lymphatic endothelial cells, *CD3D* (cluster of differentiation 3D) for Tcells, *ITGAX* (Integrin Subunit Alpha X, CD11C) and *CD1A* for dendritic cells, *AIF1* (Allograft Inflammatory Factor 1) for macrophages, and *MLANA* (Melan-A) for melanocytes. In feature plots, normalized log expression of the respective gene is mapped onto the UMAP-plot. B) Heatmap of top 10 clustermarker (upregulated genes of each cluster compared to the rest of the dataset). Heatmap shows scaled expression values for genes, rows represent genes, columns represent individual cells. DEGs were calculated per cluster comparing scar versus skin using Wilcoxon rank sum test, including genes with average logarithmic fold change (avglogFC) of > 0.1 or < -0.1 and Bonferroni-adjusted p-value < 0.05 . Feature plot shows projection of nDEG onto the UMAP-plot, color intensity represents nDEG. UMAP, uniform manifold approximation and projection.



Percent Expressed Average Expression



Figure S3: Top 50 regulated genes per cell group in scar compared to skin.

In cell groups, i.e. A) Fibroblasts (FBs), B) smooth muscle cells and pericytes (SMC/PCs), C) endothelial cells (ECs), D) T-cells, E) dendritic cells (DCs), and keratinocytes (KCs), differentially expressed genes (DEGs) were calculated comparing scar versus skin using Wilcoxon rank sum test, including genes with average logarithmic fold change (avglogFC) of > 0.1 or < -0.1 and Bonferroni-adjusted p-value < 0.05 . For each cell group, top 50 DEGs according to lowest adjusted p-value are displayed, split by skin and scar. ECM-related genes are in bold font. Dot size represents percent of cells expressing the respective gene, color correlates with average expression.

Figure S3

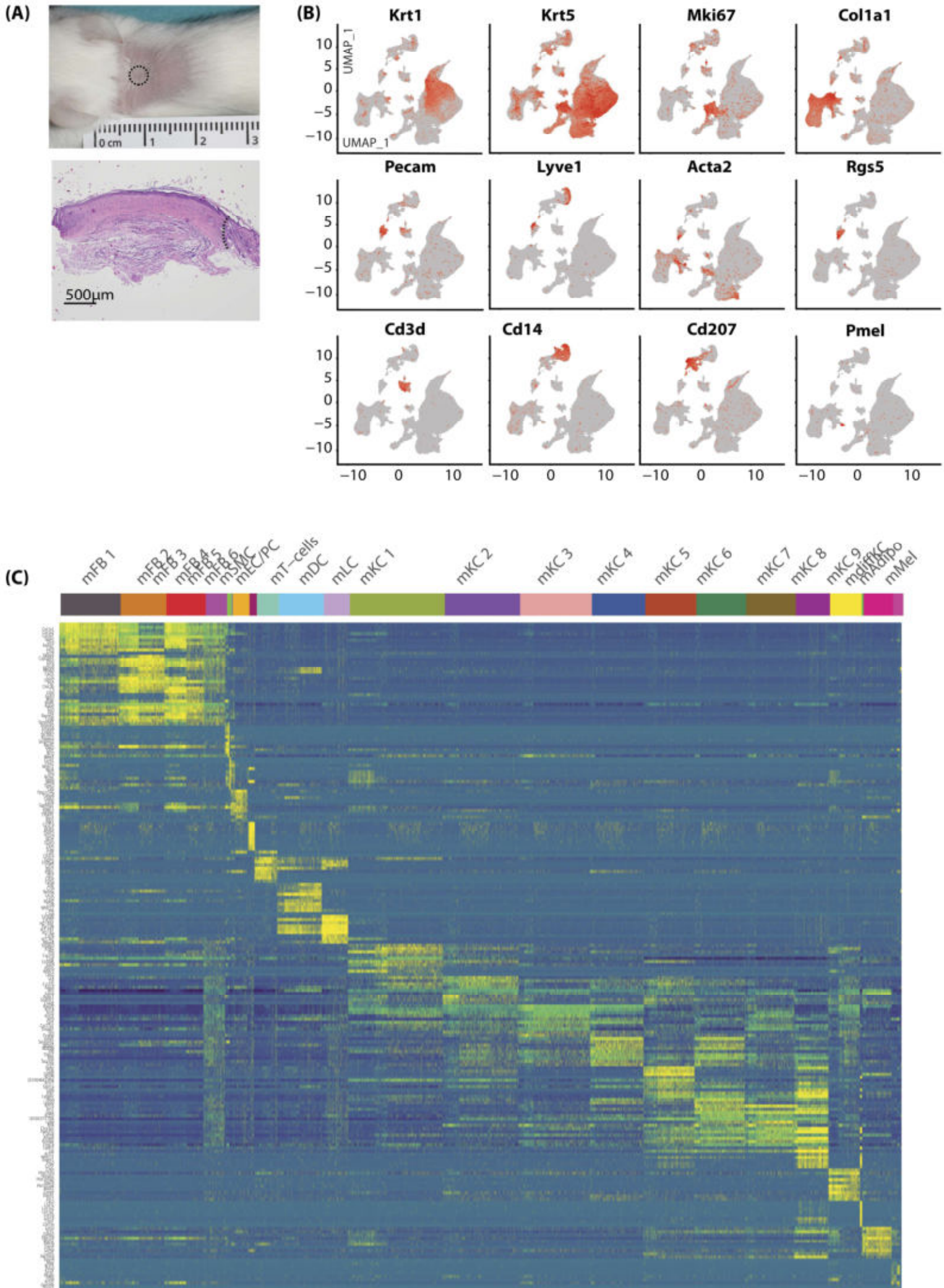


Figure S4: Identification of cell types by marker genes and gene expression patterns in mouse scars.

A) Macroscopic image and 4x microscopic image illustrating scar size relations. Dotted circle and dotted lines indicate scar tissue. B) Feature Plots of cluster markers *Krt1* (Keratin1) for spinous and granular keratinocytes (KCs), *Krt5* (Keratin 5) for basal KCs, *Mki67* (Marker Of Proliferation Ki-67) for proliferating cells, *Col1a1* (collagen I alpha 1) for fibroblasts, *Pecam* (Platelet And Endothelial Cell Adhesion Molecule 1) for endothelial cells, *Lyve1* (Lymphatic Vessel Endothelial Hyaluronan Receptor 1) for lymphatic endothelial cells, *Acta2* (smooth muscle actin) for smooth muscle cells and myofibroblasts, *Rgs5* (Regulator Of G Protein Signaling 5) for pericytes, *Cd3d* (cluster of differentiation 3D) for T-cells, *Cd14* for dendritic cells, *Cd207* (Langerin) for Langerhans cells, and *Pmel* (Premelanosome Protein) for melanocytes. In feature plots, normalized log expression of the respective gene is mapped onto the UMAP-plot. C) heatmap of top 10 upregulated clustermarker (differentially expressed genes of each cluster compared to the rest of the dataset). Heatmap showing scaled expression values for genes, rows represent genes, columns represent individual cells.

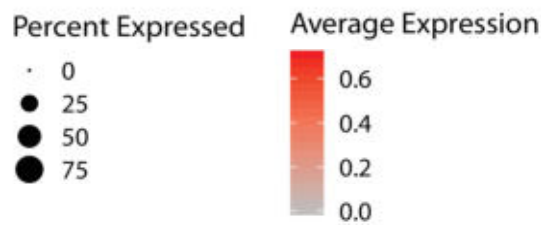


Figure S5: Top 50 regulated genes per cell group in 6 weeks and 8 weeks old murine scars.

In A) Fibroblasts (FBs), B) smooth muscle cells and pericytes (SMC/PCs), C) endothelial cells (ECs), D) T-cells, E) dendritic cells (DCs), and keratinocytes (KCs), differentially expressed genes (DEGs) were calculated comparing 8 weeks versus 6 weeks old mouse scars using Wilcoxon rank sum test, including genes with average logarithmic fold change (avg_logFC) of >0.1 or <-0.1 and Bonferroni-adjusted p-value <0.05 . For each cell group, top 50 DEGs according to lowest adjusted p-value are displayed, split by timepoint. Dot size represents percent of cells expressing the respective gene, color correlates with average expression.

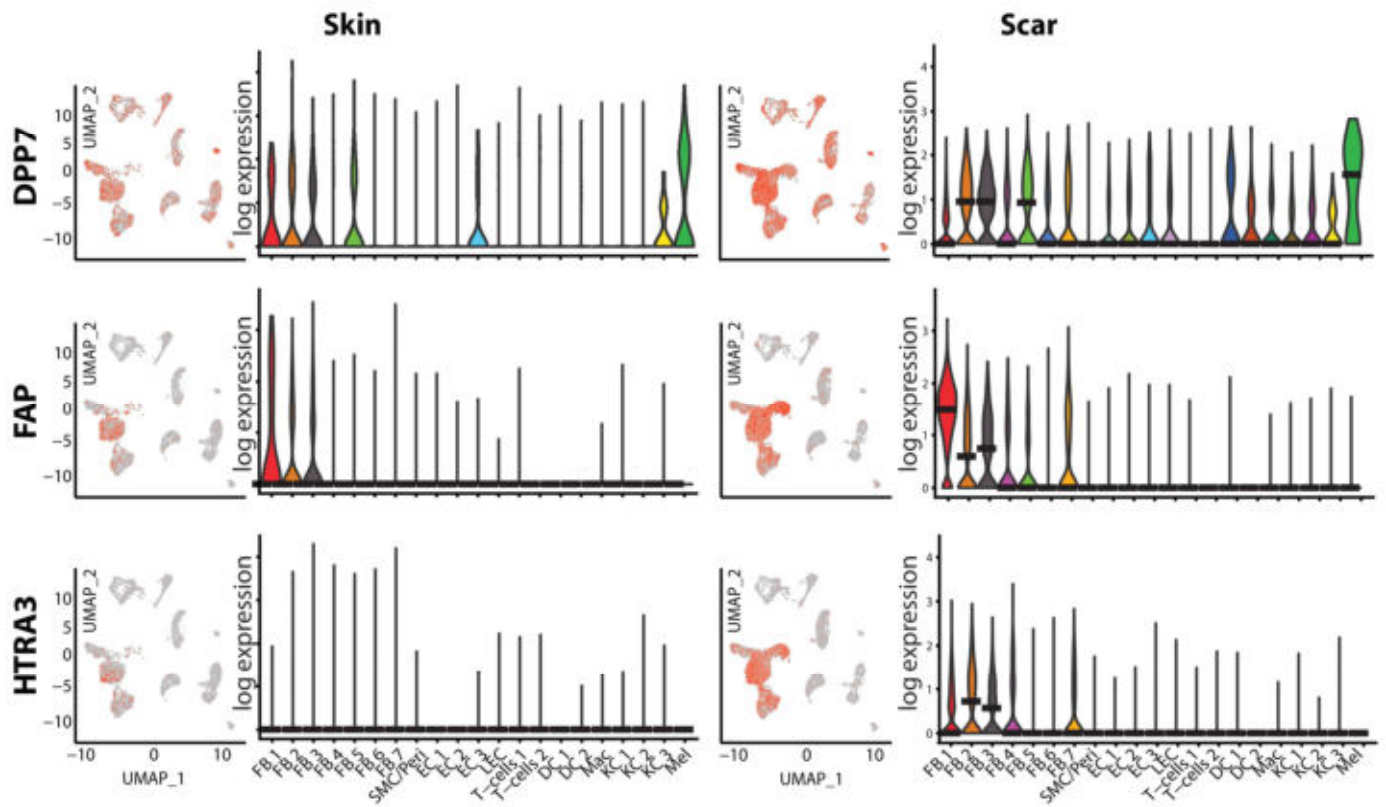


Figure S6: Feature Plots and Violin plots of serine proteases.

A-C) Feature plots and violin plots of serine proteases in human skin and scar. *DPP7* (dipeptidylpeptidase 7), *FAP* (Fibroblast Activation Protein Alpha), *HTRA3* (High-Temperature Requirement A Serine Peptidase 3). In violin plots, dots represent individual cells, y-axis represents log₂ fold change of the normalized genes and log-transformed single cell expression. Vertical lines in violin plots represent maximum expression, shape of each violin represents all results, and width of each violin represents frequency of respective expression level. In feature plots, normalized log expression of the respective gene is mapped onto the UMAP-plot. Color intensity indicates level of gene expressions. UMAP, uniform manifold approximation and projection

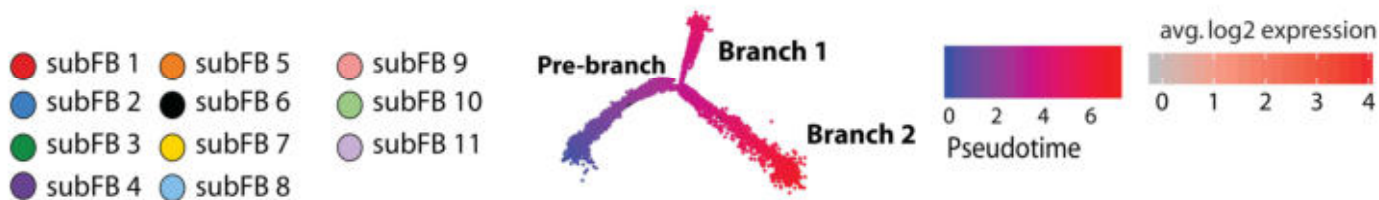
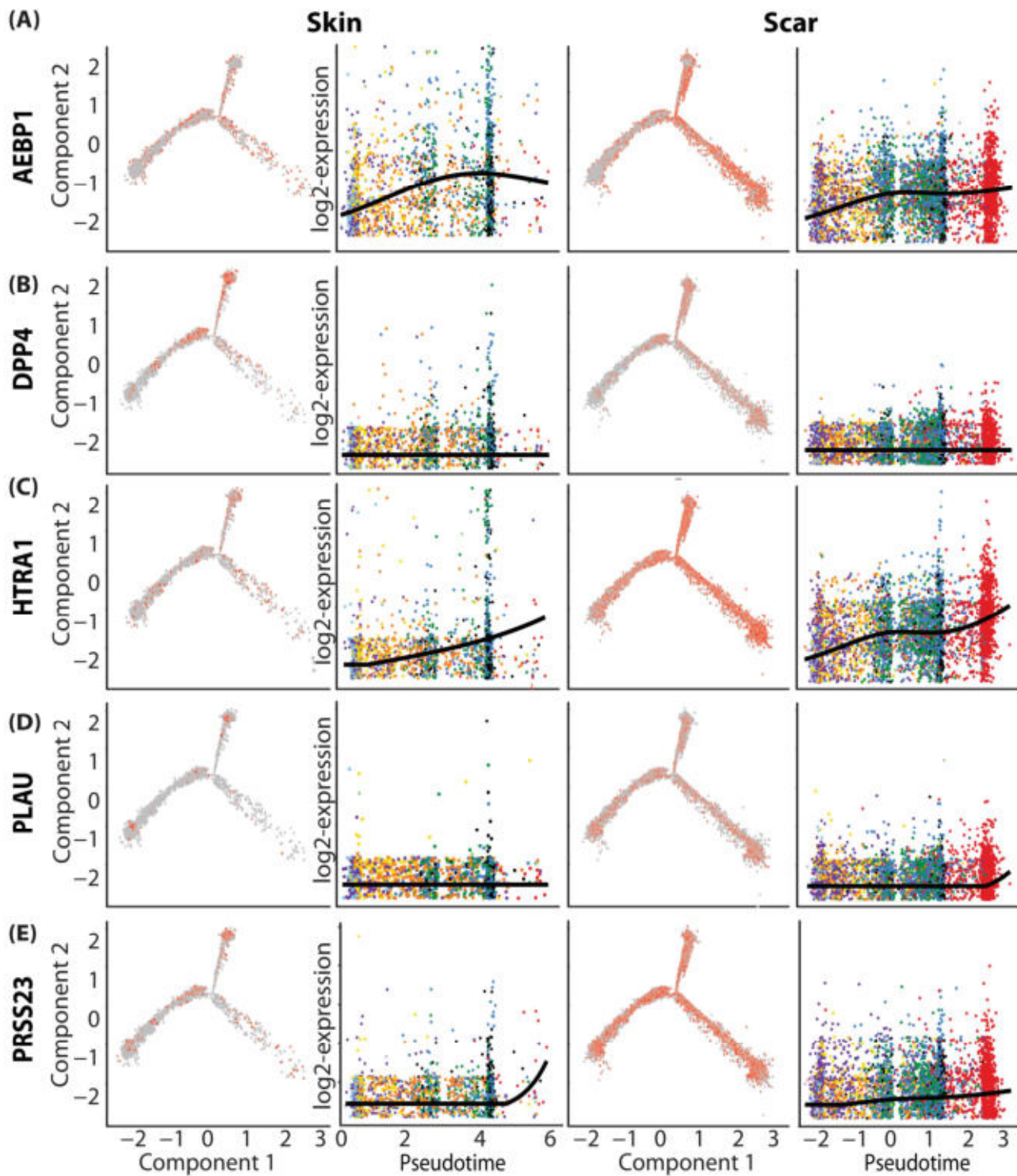


Figure S7: Pseudotime analysis corroborates the putative role of serine proteases as drivers of scar maturation.

A-E) Trajectory plots and pseudotime plots of Serine proteases in skin and scar FBs. *AEBP1* (adipocyte enhancer binding protein 1), *DPP4* (dipeptidyl-peptidase 4), *HTRA1* (High-Temperature Requirement A Serine Peptidase 1), *PLAU* (urokinase), *PRSS23* (Serine protease 23). In trajectory plots, normalized log expressions are plotted on the trajectories, split by skin and scar. In pseudotime plots, normalized log expressions are plotted against the pseudotime axis, and a spline curve represents expression dynamics over pseudotime. Y-axis, normalized log expression of respective gene, x-axis, pseudotime.

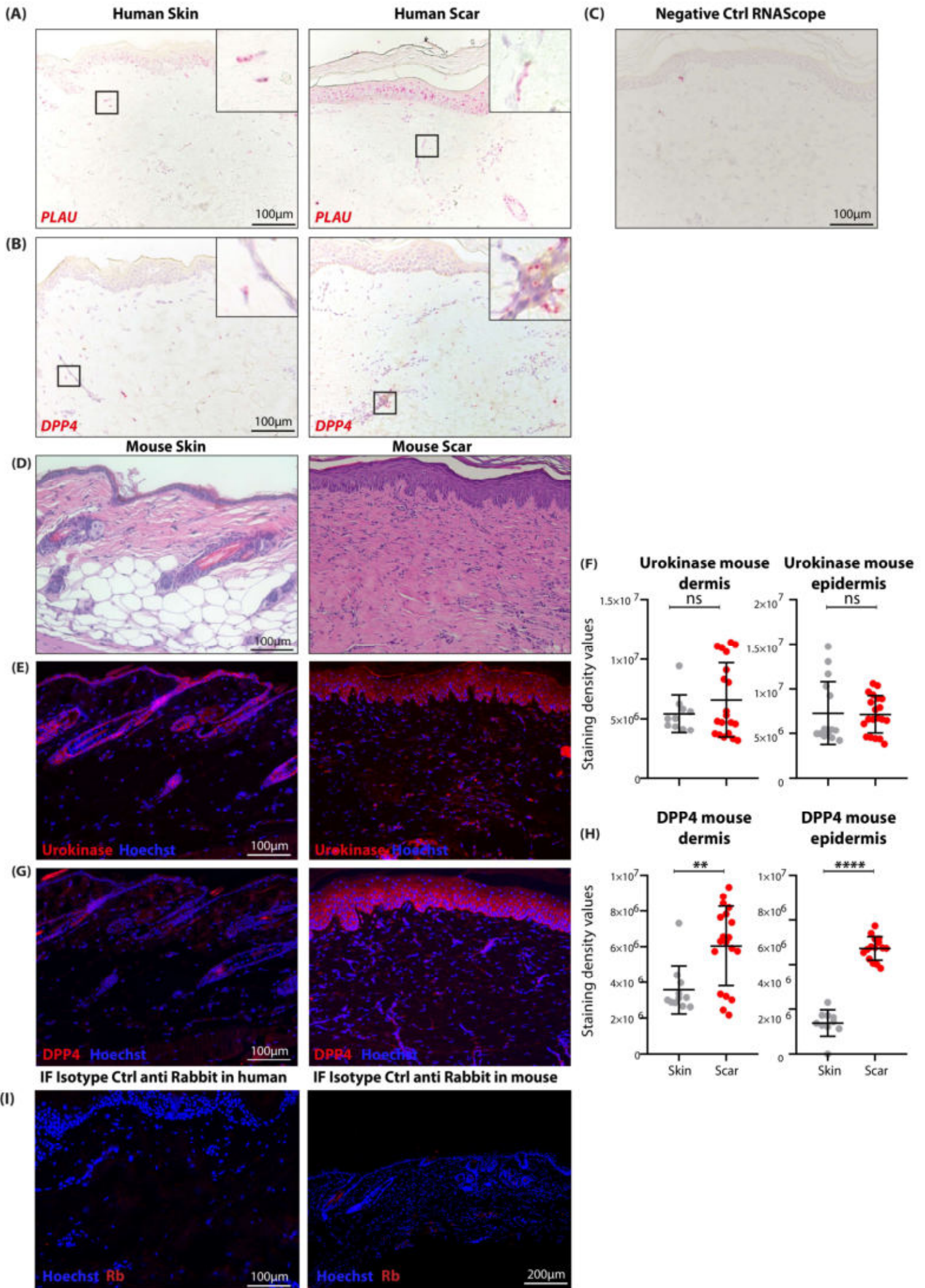


Figure S8: In-situ hybridization of *PLAU* and *DPP4* in human skin and scar.

A, B) RNAScope in-hybridization of skin and scar tissue with *PLAU*- and *DPP4*-probes. Red dots indicate single mRNA molecules. Inserts show high magnification micrographs. C) Negative control image of RNAScope experiments. Universal negative control with probes targeting the *DapB* gene (accession # EF191515) from the *Bacillus subtilis* strain SMY was used. D) H&E images from mouse skin and scar. E, G) Immunofluorescence stainings from E) urokinase and G) *DPP4* in mouse skin and scars. F,H) Quantification of staining intensity from urokinase and *DPP4* in skin and scar, analyzed separately for epidermis and dermis. Urokinase mouse dermis $p=0.2813$; Urokinase mouse epidermis $p=0.8915$; *DPP4* mouse dermis $p=0.0025$; *DPP4* mouse epidermis $p<0.0001$ I) Isotype ctrl images of Rb IgG in human and mouse samples. $n=3$ biologically independent samples of healthy mouse skin and $n=4$ samples of mouse scars were analyzed. Lines and error bars represent mean and standard deviation. From each sample, five regions of interest per sample were quantified. For ELISA, analysis was performed in duplicates for three donors each. Statistical significance was tested using two-tailed unpaired Student t-test. NS $p>0.05$, * $p<0.05$, ** $p<0.01$, *** $p<0.001$.

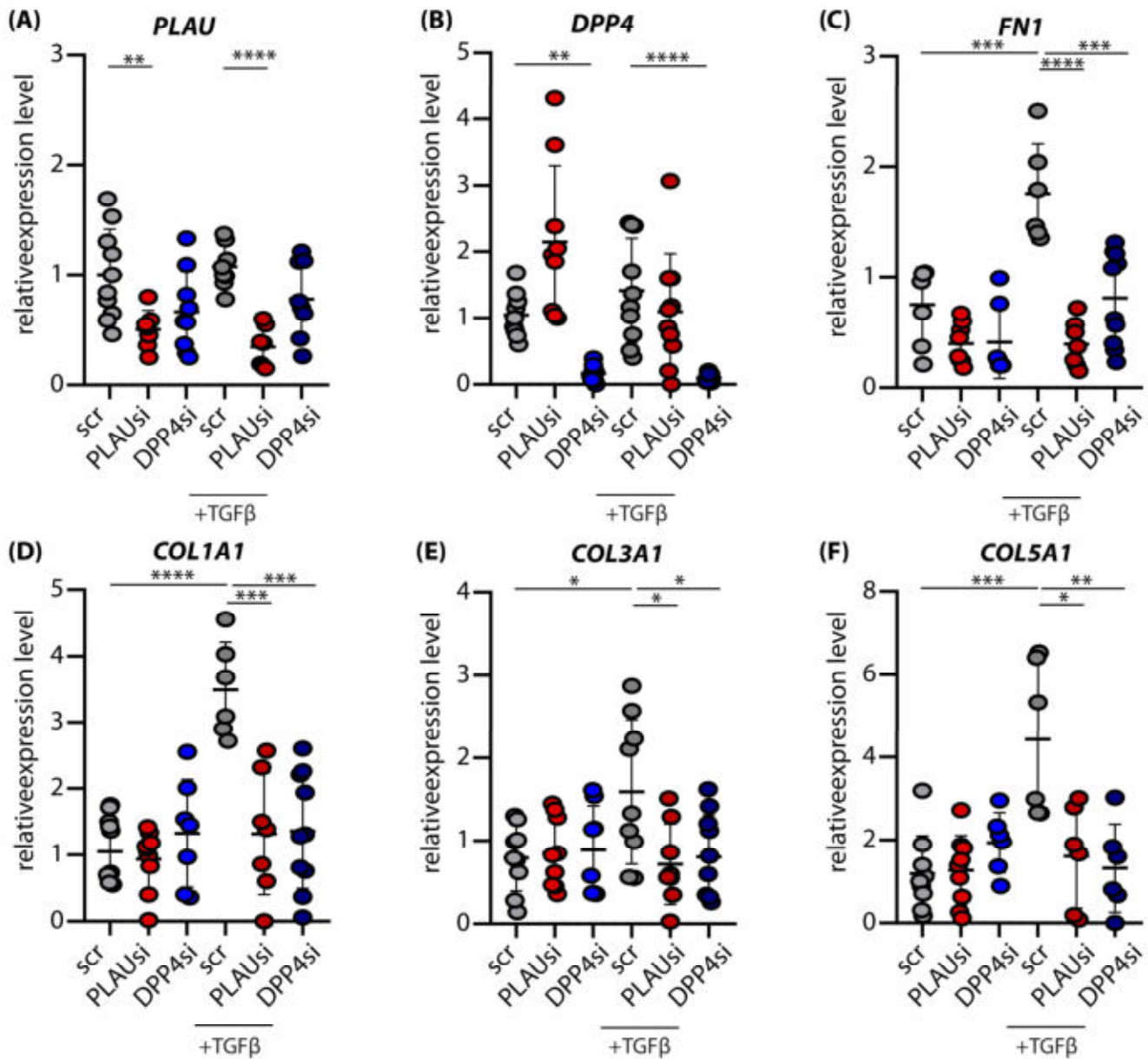
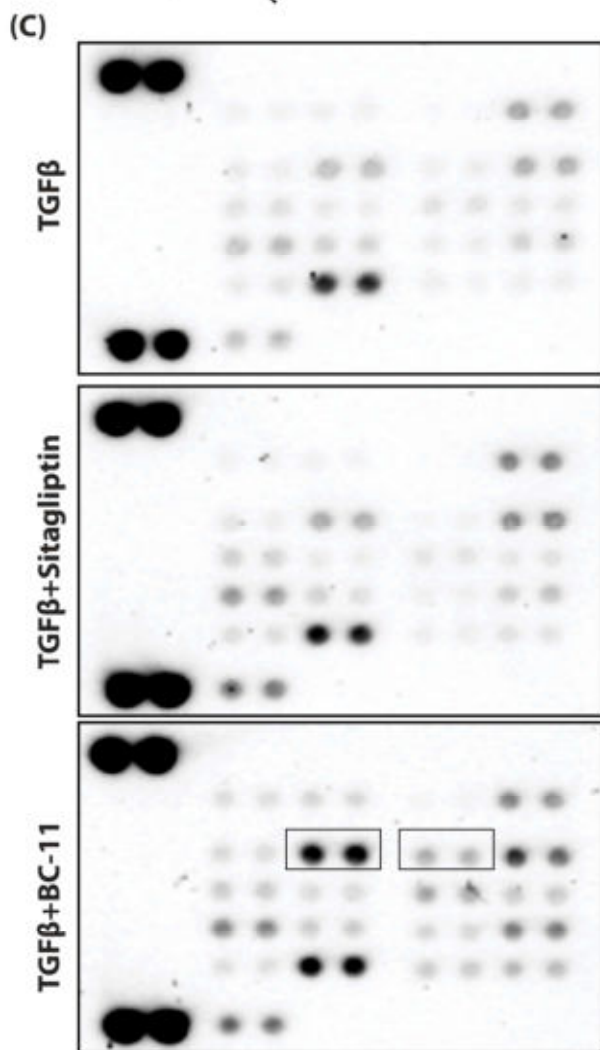
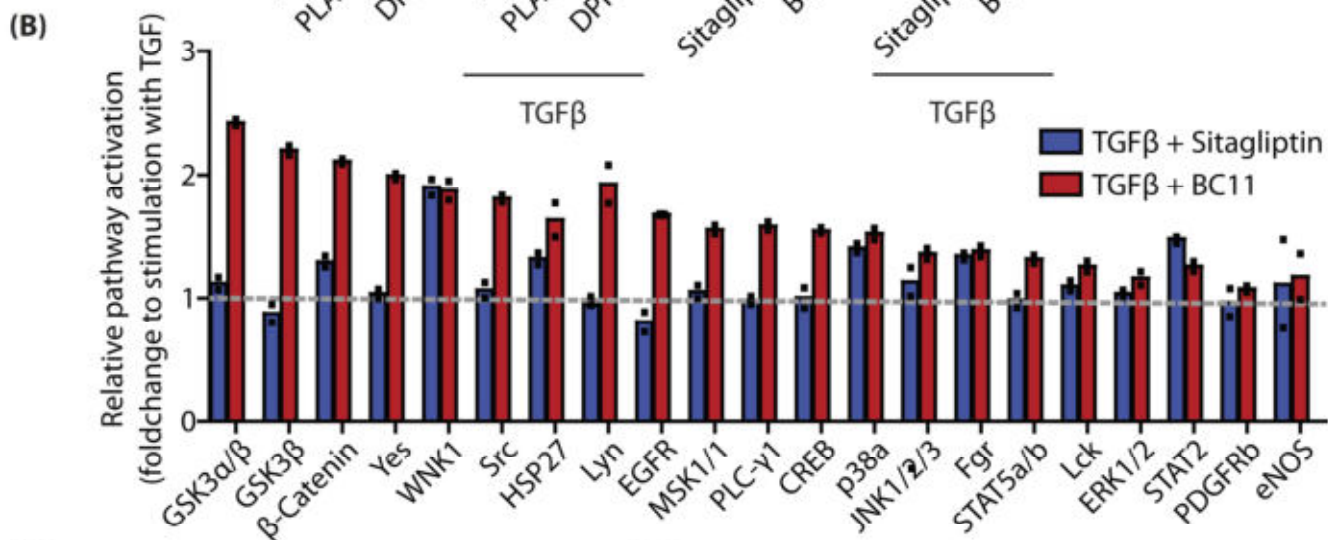
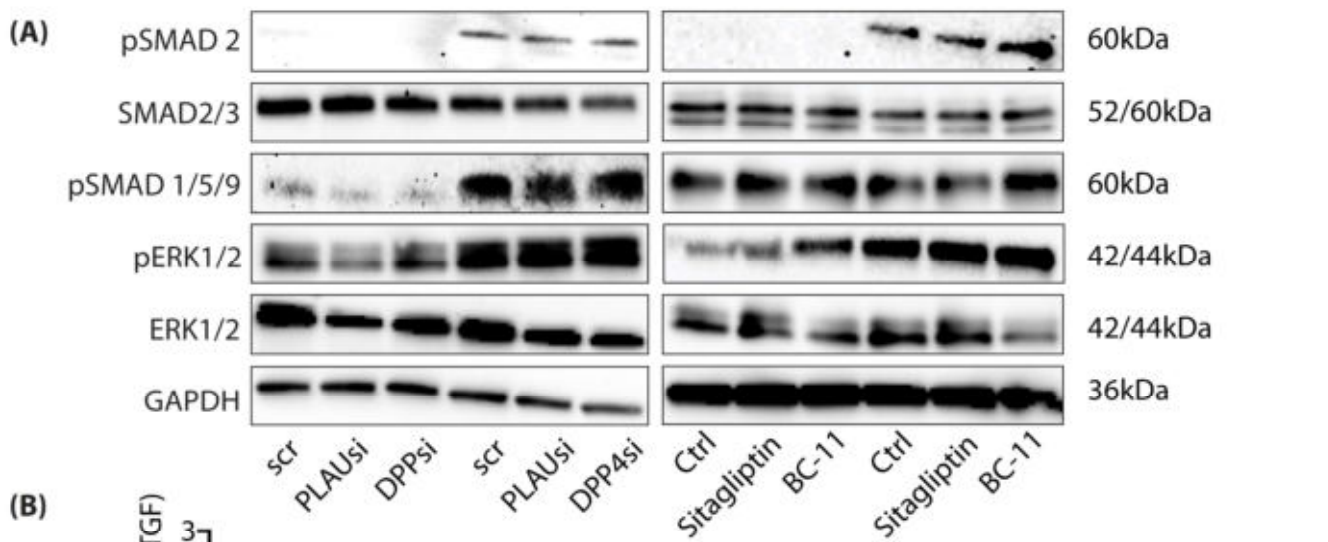


Figure S9: PCR analysis of serine protease and ECM genes after knockdown.

PCR analysis of *PLAU*, *DPP4*, *FN1*, *COL1A1*, *COL3A1* and *COL5A1* expression in primary FBs after stimulation with scrambled (scr) RNA, small interfering (si) RNA targeting *PLAU* or *DPP4*, and upon stimulation with or without TGF₁. Y-axis represents fold expression as calculated in reference to housekeeping gene *B2M*. A) scr vs PLAUsi p=0.0249, scr vs PLAUsi + TGFβ1 p= p>0.001; B) scr + TGFβ1 vs DPP4si p=0.0012, scr + TGFβ1 vs DPP4si + TGFβ1 p= p<0.0001 C) scr vs scr+ TGFβ1 p=0.0008, scr + TGFβ1 vs PLAUsi + TGFβ1 p<0.0001; scr + TGFβ1 vs DPP4si + TGFβ1=0.0008 D) scr vs scr+ TGFβ1 p= 0.0001, scr + TGFβ1 vs PLAUsi + TGFβ1 p= 0.0232; scr+ TGFβ1 vs DPPsi+ TGFβ1 p=0.0039 E) scr vs scr + TGFβ1 p= 0.242, scr vs PLAUsi+ TGFβ1 p=0.010, scr vs DPP4si+ TGFβ1 p=0.0291; F) scr vs scr+ TGFβ1 p= 0.0051, scr + TGFβ1 vs PLAUsi + TGFβ1 p= 0.0144; scr+ TGFβ1 vs DPPsi+ TGFβ1 p=0.040 n=6 biologically independent samples were analyzed in technical duplicates. Lines and error bars represent mean with standard deviation. Statistical significance was tested using one-way ANOVA with Tukey post-test. *p<0.05, **p<0.01, ***p<0.001, ****p<0.0001.



(D)

A1,2	A3,4	A5,6	A7,8	A9,10
Reference spots				
B1,2	B3,4	B5,6	B7,8	B9,10
	CREB	EGFR	eNOS	ERK1/2
C1,2	C3,4	C5,6	C7,8	C9,10
	Fgr	GSK3α/β	GSK3β	HSP27
D1,2	D3,4	D5,6	D7,8	D9,10
	JNK1/2/3	Lck	Lyn	MSK1/2
E1,2	E3,4	E5,6	E7,8	E9,10
	p38a	PDGF β	1 γ C	Src P
F1,2	F3,4	F5,6	F7,8	F9,10
	STAT2	STAT5a/b	WNK1	Yes
G1,2	G3,4	G5,6	G7,8	G9,10
Reference spots				Negative control (PBS)

Figure S10: Signaling pathway activation after TGF β -stimulation and DPP4/PLAU inhibition.

A) Western blot of primary FB lysates stimulated with active TGF β 1 for 1h and analysis of canonical TGF β 1 signaling pathways. B) Analysis of non-canonical TGF β 1 signaling pathways and kinase pathways detected by proteome profiler from lysates of primary FBs after 1h stimulation with TGF β 1 alone, TGF β 1 with sitagliptin, and TGF β 1 with BC-11. Bars represent fold change compared to stimulation with TGF β 1 only, marked by dotted line. Proteome profiler analysis of signaling pathways of primary human skin FBs stimulated with TGF β and inhibitors. Values show technical duplicates of pooled samples from n=3 biologically independent donors. C) TGF β 1, B) TGF β 1 and DPP4-inhibitor Sitagliptin, and TGF β 1 and PLAU-inhibitor BC-11. GSK3 α/β and GSK3 β are marked by squares in the BC-11 treated blot. D) Legend table for proteome profiler data points.

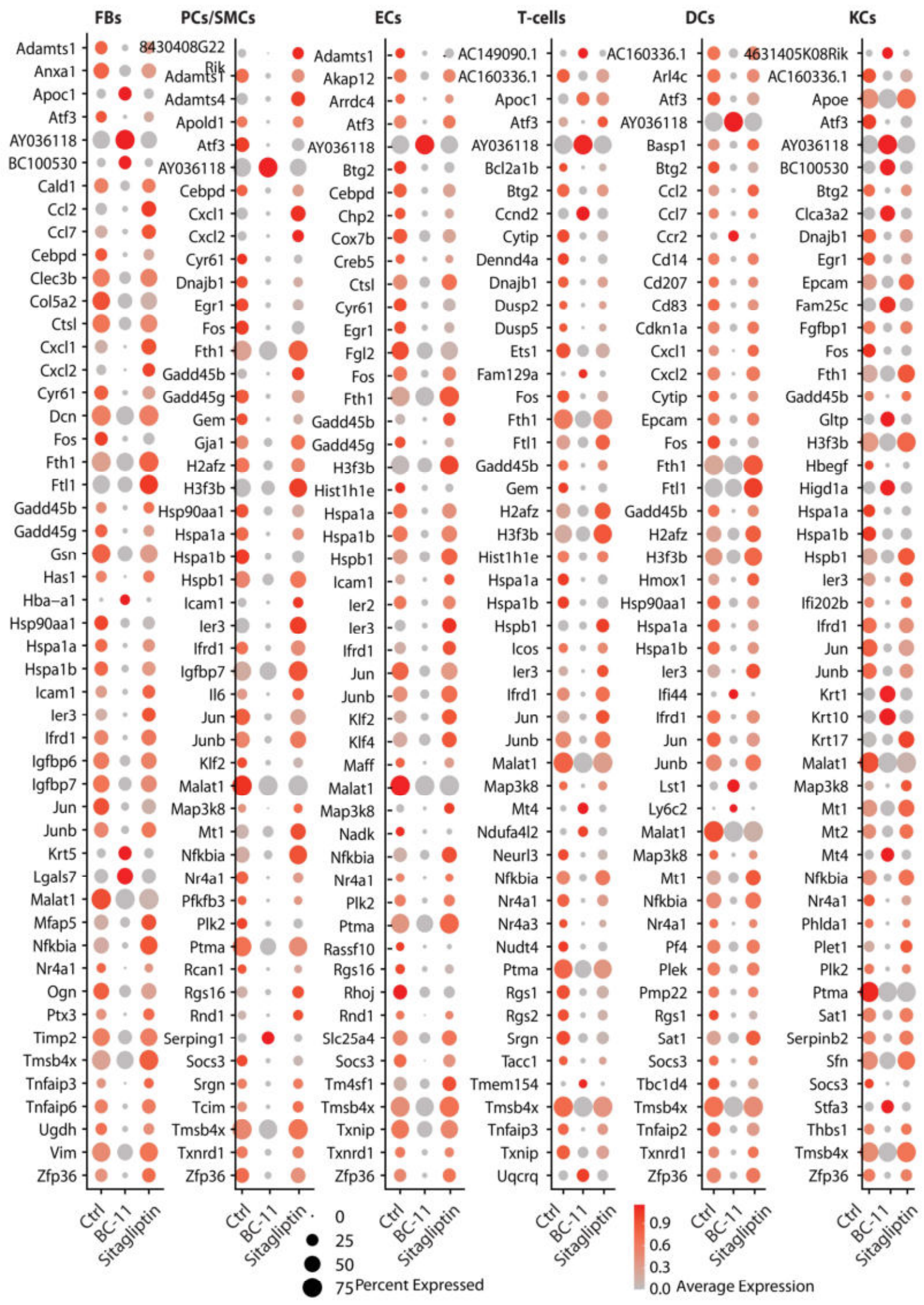


Figure S11: Top 50 regulated genes per cell group in protease-inhibitor stimulated murine scars.

In A) fibroblasts (FBs), B) smooth muscle cells and pericytes (SMC/PCs), C) endothelial cells (ECs), D) T-cells, E) dendritic cells (DCs), and keratinocytes (KCs), differentially expressed genes (DEGs) were calculated comparing BC-11 and Sitagliptin-treated scars with Ctrl scars using Wilcoxon rank sum test, including genes with average logarithmic fold change (avglogFC) of > 0.1 or < -0.1 and Bonferroni-adjusted p-value < 0.05 . For each cell group, top 50 DEGs according to lowest adjusted p-value are displayed, split by timepoint. Dot size represents percent of cells expressing the respective gene, color correlates with average expression.

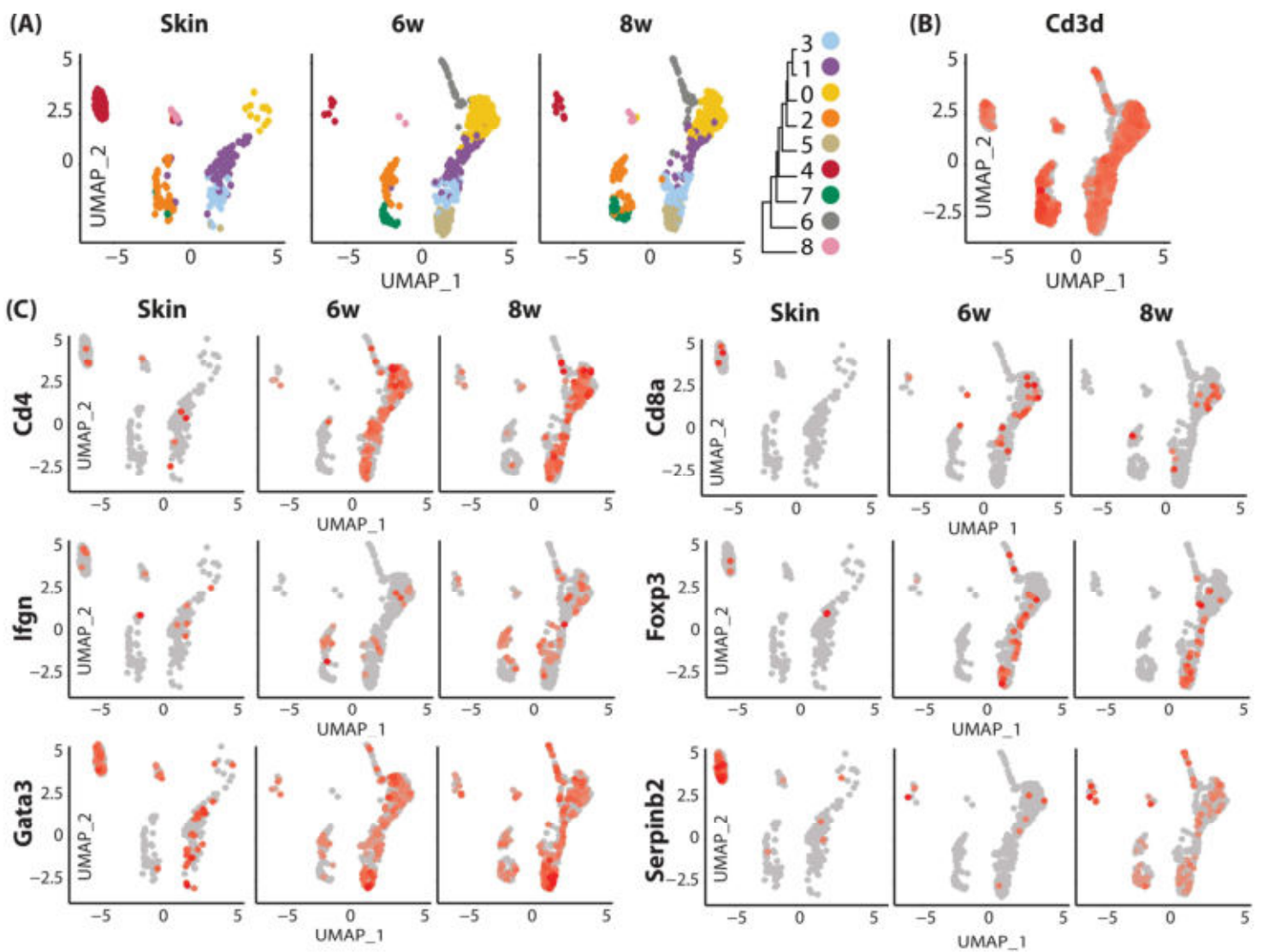


Figure S12: T-cell analysis in mouse scars

A) Subset of t-cells in mouse scar by unsupervised UMAP-clustering, split by timepoint. B) Feature plot of Cd3d in mouse t-cell subset. C) Feature plots of *Cd4* (cluster of differentiation 4), *Cd8a* (cluster of differentiation 4), *Ifgn* (interferon gamma), *Foxp3* (forkhead box P3), *Gata3* (GATA Binding Protein 3) and *Serpinb2* (Serpin Family B Member 2), split by timepoint. In feature plots, normalized log expression of the respective gene is mapped onto the UMAP-plot.

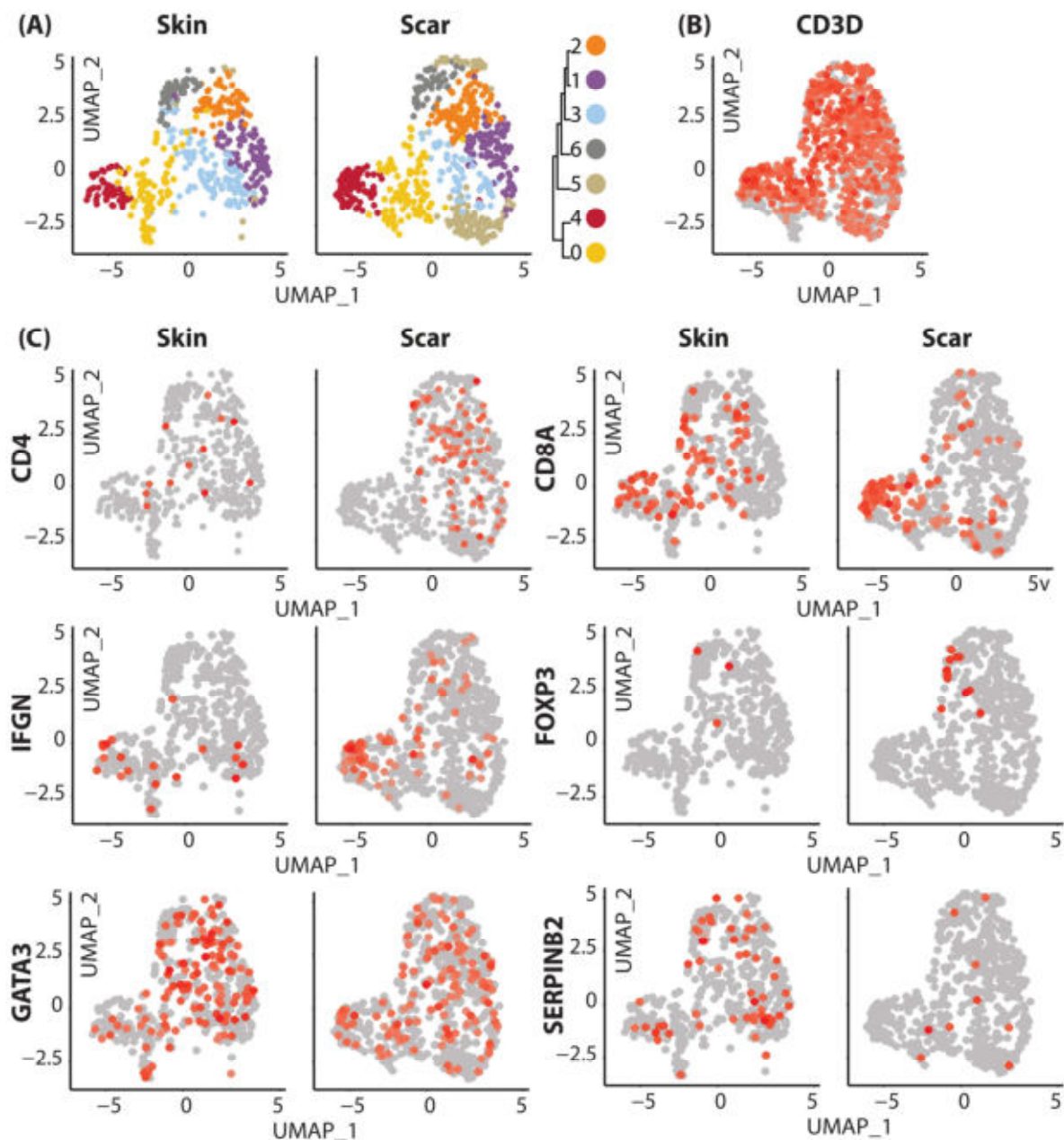


Figure S13: T-cell analysis in human scars.

A) Subset of t-cells in human scar by unsupervised UMAP-clustering, split by tissue. B) Feature plots of *CD3D* in human t-cell subset. C) Feature plots of *CD4* (cluster of differentiation 4), *CD8A* (cluster of differentiation 4), *IFGN* (interferon gamma), *FOXP3* (forkhead box P3), *GATA3* (GATA Binding Protein 3) and *SERPINB2* (Serpin Family B Member 2), split by tissue. In feature plots, normalized log expression of the respective gene is mapped onto the UMAP-plot.

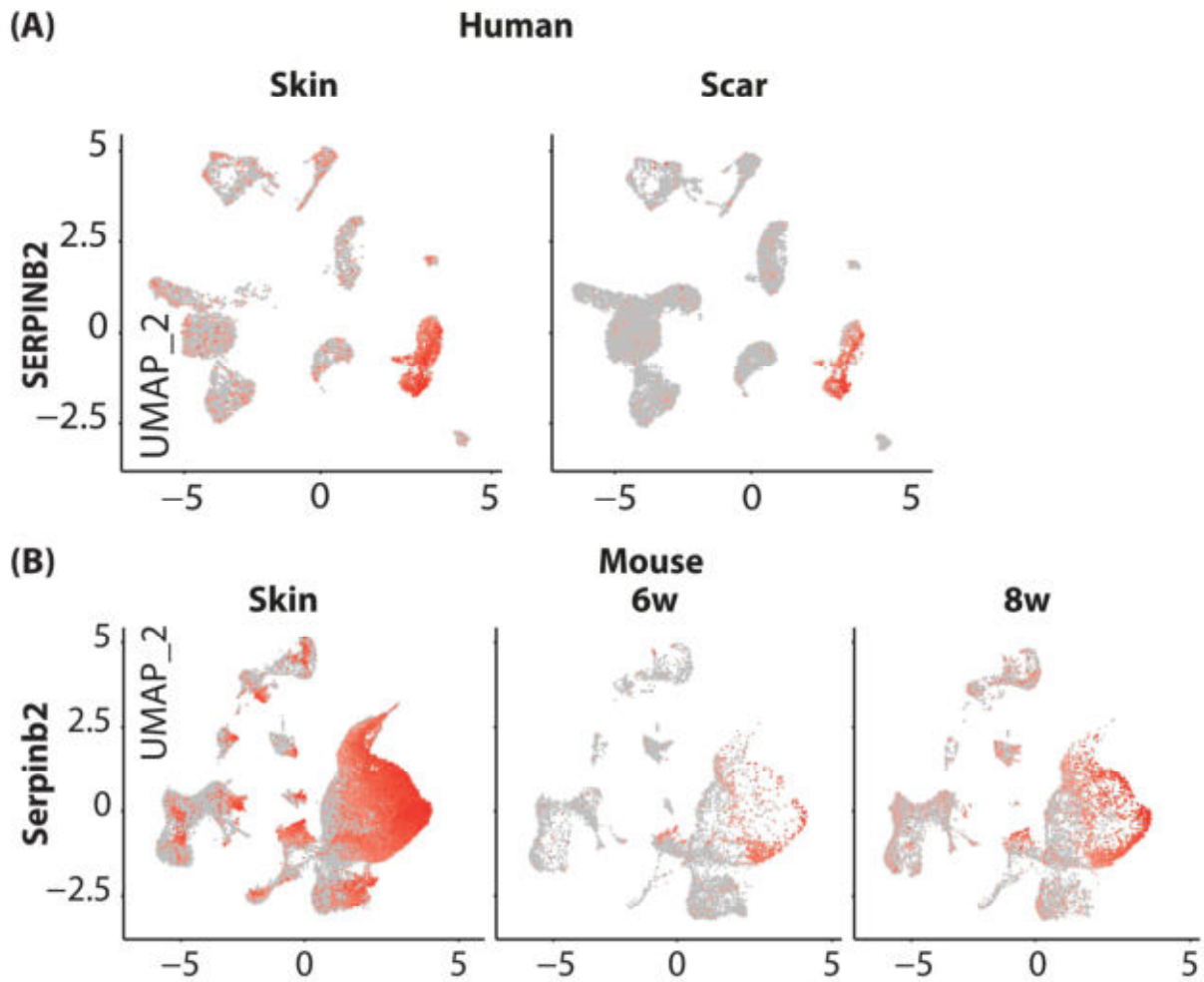


Figure S14: SERPINB2-expression in human and mouse.

Feature plots of *SERPINB2* (Serpin Family B Member 2) in A) human hypertrophic scar and skin and, split by tissue. B) mouse skin, 6 and 8 weeks old scars, split by timepoint. In feature plots, normalized log expression of the respective gene is mapped onto the UMAP-plot.

2.3. Chapter 3: The secretome of irradiated peripheral mononuclear cells attenuates hypertrophic skin scarring

Despite having identified promising targets in our study highlighting the roles of proteases in skin scarring, good treatment options are still scarce. Due to high recurrence rates, poorly known mechanisms of action, and insufficient evidence supporting their safety and efficacy, current therapy alternatives for skin scarring are not satisfying (249). In recent years, stem cells have been proposed as a potential solution, with preclinical studies suggesting effective scar treatment or improvement of scar formation after application of conditioned media derived from different stem cell populations.

However, there are limitations to the applicability of promising preclinical animal research to humans, the costs of the manufacturing of autologous conditioned media costs are high, and scalability for larger quantities are hardly feasible (1). The concept of cell-free paracrine therapy in an allogeneic situation has gained popularity, and peripheral blood mononuclear cells have been suggested as a source of paracrine components.

The secretome of irradiated PBMCs has shown promising results in preclinical studies, with encouraging effects on wound healing, angiogenesis, and antimicrobial activity (1). PBMCsec was found to exert pleiotropic effects, including reducing activation of mast cells and basophils, reducing dendritic cell-mediated T-cell priming, and regenerating infarcted myocardium. Clinically, PBMCsec has been found to be safe and well-tolerated in topical application in a phase I study, and a phase II clinical trial on the efficacy of allogeneic PBMCsec in patients with diabetic foot ulcers is currently ongoing (34, 40).

In this work, we seek to explore possible PBMCsec mechanisms of action on skin scarring using a multi-model murine and human approach at the single-cell level. We hypothesize that the anti-fibrotic effect of PBMCsec both prevents hypertrophic scarring and enhances tissue quality already present scars. Our study provides molecular insights into its anti-fibrotic action, which enables the further investigation of PBMCsec for potential clinical usage as a skin scarring treatment option in the future. By elucidating the cellular mechanisms of PBMCsec, this study builds a basis for the development of novel effective and safe treatments for skin scarring, improving the quality of life of millions of patients worldwide.

Article

The Secretome of Irradiated Peripheral Mononuclear Cells Attenuates Hypertrophic Skin Scarring

Vera Vorstandlechner^{1,2,3}, Dragan Copic^{1,2,4} , Katharina Klas^{1,2}, Martin Direder^{1,2,5}, Bahar Golabi⁶, Christine Radtke³, Hendrik J. Ankersmit^{1,2,†} and Michael Mildner^{6,*,†} 

¹ Laboratory for Cardiac and Thoracic Diagnosis, Regeneration and Applied Immunology, Department of Thoracic Surgery, Medical University of Vienna, 1090 Vienna, Austria

² Aposcience AG, 1200 Vienna, Austria

³ Department of Plastic and Reconstructive Surgery, Medical University of Vienna, 1090 Vienna, Austria

⁴ Department of Medicine III, Division of Nephrology and Dialysis, Medical University of Vienna, 1090 Vienna, Austria

⁵ Department of Orthopedics and Trauma-Surgery, Medical University of Vienna, 1090 Vienna, Austria

⁶ Department of Dermatology, Medical University of Vienna, 1090 Vienna, Austria

* Correspondence: michael.mildner@meduniwien.ac.at

† These authors contributed equally to this work.

Abstract: Hypertrophic scars can cause pain, movement restrictions, and reduction in the quality of life. Despite numerous options to treat hypertrophic scarring, efficient therapies are still scarce, and cellular mechanisms are not well understood. Factors secreted by peripheral blood mononuclear cells (PBMCsec) have been previously described for their beneficial effects on tissue regeneration. In this study, we investigated the effects of PBMCsec on skin scarring in mouse models and human scar explant cultures at single-cell resolution (scRNAseq). Mouse wounds and scars, and human mature scars were treated with PBMCsec intradermally and topically. The topical and intradermal application of PBMCsec regulated the expression of various genes involved in pro-fibrotic processes and tissue remodeling. We identified elastin as a common linchpin of anti-fibrotic action in both mouse and human scars. In vitro, we found that PBMCsec prevents TGF β -mediated myofibroblast differentiation and attenuates abundant elastin expression with non-canonical signaling inhibition. Furthermore, the TGF β -induced breakdown of elastic fibers was strongly inhibited by the addition of PBMCsec. In conclusion, we conducted an extensive study with multiple experimental approaches and ample scRNAseq data demonstrating the anti-fibrotic effect of PBMCsec on cutaneous scars in mouse and human experimental settings. These findings point at PBMCsec as a novel therapeutic option to treat skin scarring.

Keywords: scar; regeneration; peripheral blood mononuclear cell secretome



Citation: Vorstandlechner, V.; Copic, D.; Klas, K.; Direder, M.; Golabi, B.; Radtke, C.; Ankersmit, H.J.; Mildner, M. The Secretome of Irradiated Peripheral Mononuclear Cells Attenuates Hypertrophic Skin Scarring. *Pharmaceutics* **2023**, *15*, 1065. <https://doi.org/10.3390/pharmaceutics15041065>

Academic Editor: Fabiana Quaglia

Received: 14 December 2022

Revised: 15 March 2023

Accepted: 21 March 2023

Published: 25 March 2023



Copyright: © 2023 by the authors. Licensee MDPI, Basel, Switzerland. This article is an open access article distributed under the terms and conditions of the Creative Commons Attribution (CC BY) license (<https://creativecommons.org/licenses/by/4.0/>).

1. Introduction

Skin scarring after surgery, trauma, or burn injury is a major problem affecting 100 million people every year, causing a significant global disease burden [1]. Patients with hypertrophic scars, occurring in 40–90% of cases after injury [2], suffer from pain, pruritus, and reduced quality of life [3,4]. Skin scarring has been extensively studied [5,6], and recently, we were able to elucidate hypertrophic scar formation at the single-cell level [7]. However, many cellular mechanisms remain unclear, and for most conservative therapeutic options, we have low evidence of their efficacy [8]. Wound healing and scar formation are complex, rigidly coordinated processes, with multiple cell types being involved [9]. Wound healing is characterized by an acute inflammatory phase, a proliferative phase, and a remodeling phase [9]. Prolonged inflammation results in increased fibroblast (FB) activity, with enhanced secretion of transforming growth factor beta 1 (TGF β 1), TGF β 2, insulin-like growth factor (IGF1), and other cytokines [10,11]. TGF β 1 induces the differentiation of

FBs into myofibroblasts (myoFBs) [12]. myoFBs show strong contractility and excessively deposit extracellular matrix (ECM) components, eventually leading to (hypertrophic) scar formation. Matured (hypertrophic) scars show dense, parallel ECM and strong tissue contraction [12].

Numerous pharmaceutical attempts to tackle hypertrophic scars have been proposed during recent decades, e.g., intralesional injection of corticosteroids, 5-Fluorouracil (5-FU), or triamcinolone (TAC) [13,14]. Other therapeutic options include compression therapy or topical silicone application. These therapies, however, still lack evidence of efficacy and safety and show high recurrence rates, and the mechanisms of action are not well understood [15,16]. In recent years, numerous pre-clinical studies have shown effective scar treatment or improvement in scar formation after the application of conditioned media derived from different stem cell populations, such as amniotic mesenchymal stem cells (MSCs) [17], fat-derived stem cells [18], bone marrow-induced MSCs [19], and induced pluripotent stem cells [20], amongst others [21]. However, the transferability of promising pre-clinical animal studies to humans was shown to be limited [22]. Furthermore, autologous conditioned media from various stem cell populations have significant disadvantages, as the production of these secretomes is expensive and hardly scalable, due to the limited numbers of available stem cells [23].

Hence, the idea of cell-free paracrine therapies in an allogeneic setting has drawn increasing attention. As different kinds of stem cells still have the same limitations in the allogeneic setting, peripheral blood mononuclear cells (PBMCs) have been proposed as an alternative source of paracrine factors [24].

The secretome of irradiated peripheral blood mononuclear cells (PBMCsec) has been extensively studied in recent years, showing encouraging pre-clinical results. PBMCsec has been found to enhance wound healing [25–27], elicit angiogenic effects [26,28], prevent platelet aggregation and vasodilation [29], exert anti-microbial activity [30], attenuate neurological damage in focal ischemia [31] and spinal cord injury [32], and regenerate infarcted myocardium [33]. Moreover, PBMCsec has been shown to reduce the activation of mast cells and basophils [34] and reduce the maturation and antigen uptake of dendritic cells, as well as dendritic cell-mediated T-cell priming [35]. In a phase I study, PBMCsec was found to be safe and well tolerated in the topical application of autologous PBMCsec on skin wounds [36]. In addition, a phase II clinical trial on the efficacy of allogeneic PBMCsec in patients with diabetic foot ulcers is currently ongoing [37]. It should be noted that the favorable pleiotropic effects of PBMCsec cannot be broken down to a single mode of action [37], as PBMCsec has repeatedly demonstrated its regenerative power with the synergistic action of all components, including proteins, lipids, extracellular vesicles, and nucleic acids [26,28,37].

Therefore, we attempt to provide a multi-model murine and human approach at the single-cell level to identify the potential mechanisms of action of PBMCsec on skin scarring. Due to the plethora of beneficial effects of PBMCsec, we hypothesized that PBMCsec prevents (hypertrophic) scarring or improves tissue quality in already persisting scars. In this study, we demonstrate the anti-fibrotic activity of PBMCsec and provide mechanistic insights into its anti-fibrotic effect. This study facilitates the investigation of PBMCsec for its future clinical use as a treatment option for skin scarring.

2. Materials and Methods

2.1. Ethics Statement

The use of healthy abdominal skin (Vote No. 217/2010) and scar tissue (Vote No. 1533/2017) was approved by the ethics committee of Medical University of Vienna. Animal experiments were approved by the ethics committee of Medical University of Vienna and the Austrian Federal Ministry of Education, Science, and Research (Vote No. BMBWF-66.009/0075-V/3b/2018).

2.2. Patient Material

Resected scar tissue was obtained from three patients who underwent elective scar resection surgery after giving informed consent. Scars were previously classified as hypertrophic, pathological scars according to the Patient and Observer Scar Assessment Scale (POSAS) [38] by a plastic surgeon. All scars were mature scars, i.e., they were at least two years old; had not been operated on; and had not been previously treated with corticosteroids, 5-FU, irradiation, or similar treatments. All scar samples were obtained from male and female patients younger than 45 years old, with no chronic diseases nor chronic medication. Healthy skin was obtained from three healthy female donors between 25 and 45 years of age from surplus abdominal skin removed during elective abdominoplasty.

2.3. Animals

In all mouse experiments, 8–12-week-old female Balb/c mice (Medical University of Vienna Animal Breeding Facility, Himberg, Austria) were used. Mice were housed in a selected pathogen-free environment according to enhanced standard husbandry with a 12/12 h light/dark cycle and ad libitum access to food and water.

2.4. Full-Thickness Wound and Scarring Model in Mice

For the full-thickness skin wound and scarring model, mice were deeply anesthetized with ketamine 80–100 mg/kg and xylazine 10–12.5 mg/kg i.p. They were given postoperative analgesia with the s.c. injection of 0.1 mL/10 mg Buprenorphin and 7.5 mg/mL Piritramid in drinking water. A 9 × 9 mm square area was marked on the back and excised with sharp scissors. The wounds were left to heal uncovered without any further intervention for 4 weeks, and the resulting scar tissue was observed and photographed.

2.5. Production of Irradiated Mononuclear Cell Secretome (PBM_Csec)

The secretome of human PBMCs was produced in compliance with good manufacturing practice (GMP) by the Austrian Red Cross, Blood Transfusion Service for Upper Austria (Linz, Austria), as previously described [26,39] (Figure S1). PBMCs were obtained with Ficoll-Paque PLUS (GE Healthcare, Chicago, IL, USA)-assisted density gradient centrifugation, adjusted to a concentration of 25 × 10⁶ cells/mL (25 U/mL; 1 Unit = secretome of 1 million cells) and exposed to 60 Gy cesium 137 gamma irradiation (IBL 437C; Isotopen Diagnostik CIS GmbH, Dreieich, Germany). Cells were cultured in phenol red-free CellGenix GMP DC medium (CellGenix GmbH, Freiburg, Germany) for 24 ± 2 h. Cells and cellular debris were removed with centrifugation, and supernatants were passed through a 0.2 µm filter. Methylene blue treatment was performed as described [40] for viral clearance. The secretome was lyophilized, terminally sterilized with high-dose gamma irradiation, and stored at −80 °C. All experiments were performed using secretomes of the following batches produced under GMP: A000918399086, A000918399095, A000918399098, A000918399101, A000918399102, and A000918399105. Immediately before performing the experiments, the lyophilizate was reconstituted in 0.9% NaCl to the original concentration of 25 U/mL.

2.6. PBM_Csec Injection into Mouse Scars

Starting on day 29 after skin wounding, mice were injected with 100 µL 0.9% NaCl, medium (phenol red-free CellGenix GMP DC medium), or PBM_Csec, which was prepared as described above, every second day for two weeks. Subsequently, half of the mice from each group (n = 2) were sacrificed and analyzed, while the other half (n = 2) were left for another two weeks without further intervention and then sacrificed.

2.7. PBM_Csec Topical Application on Mouse Scars

Starting on the day of skin wounding (d0), mouse scars were treated with PBM_Csec, medium, or NaCl 0.9%. Ultrasicc/Ultrabas ointment (1:1; Hecht-Pharma, Bremervörde, Germany) was used as a carrier substance for all treatments. Four parts of Ultrasicc/Ultrabas

(50:50) and one part of water were mixed and used as control treatment (i.e., 100 μ L contained 40 μ L of Ultrasicc, 40 μ L of Ultrabas, and 20 μ L of agent or control). Then, 5 U/mL (200 μ L of dissolved lyophilizate) PBMCsec or 200 μ L/mL medium was mixed with ointment. Mice were treated with control or inhibitors by applying 100 μ L of ointment on each wound immediately after wounding.

After application, mice were individually placed in empty cages without litter for 30 min and closely monitored to prevent immediate removal of the treatments and achieve sufficient tissue resorption. Scabs were left intact to prevent wound infections. Mice were treated daily for the first 7 days and thrice a week for 7 weeks. After scar formation, 4 mm biopsies of the scar tissue were taken and cut in half. One half of each scar sample was used for histological analysis, and the other biopsy halves from each treatment group were pooled and analyzed together with scRNAseq as described below.

2.8. Ex Vivo Skin and Scar Stimulation

From human skin and scar tissue, 6 mm punch biopsies were taken; subcutaneous adipose tissue was removed; and biopsies were placed in 12-well plates supplemented with 400 μ L of DMEM (Gibco, Thermo Fisher, Waltham, MA, USA; with 10% fetal bovine serum and 1% penicillin/streptomycin) and 100 μ L of CellGenix medium or 100 μ L of PBMCsec. In addition, 100 μ L of medium or PBMCsec was injected into the upper dermis in the middle of the biopsy. Biopsies were incubated for 24 h and then harvested for scRNAseq analysis. Sample "Skin 1 medium" was lost due to technical difficulties during preparation.

2.9. Skin and Scar PBMCsec Stimulation, Cell Isolation, and Droplet-Based scRNAseq

Mouse scars and stimulated human skin and scar samples were digested using Miltenyi Whole Skin dissociation Kit (Miltenyi Biotec, Bergisch-Gladbach, Germany) for 2.5 h according to the manufacturer's protocol and processed using GentleMACS OctoDissociator (Miltenyi). The cell suspension was filtered through a 100 μ m filter and a 40 μ m filter, centrifuged for 10 min at 1500 rpm, washed twice, and resuspended in 0.04% FBS in phosphate-buffered saline (PBS). DAPI was added at 1 μ L/1 million cells for 30 s; cells were washed twice and sorted for viability using a MoFlo Astrios high-speed cell-sorting device (Beckman-Coulter, Indianapolis, IN, USA). Only distinctly DAPI-negative cells were used for further processing. Immediately after sorting, viable cells were loaded onto a 10X-chromium instrument (Single cell gene expression 3'v 2/3; 10X Genomics, Pleasanton, CA, USA) to generate a gel bead in emulsion (GEM). GEM generation, library preparation, RNA sequencing, demultiplexing, and counting were performed at Biomedical Sequencing Core Facility of Center for Molecular Medicine (CeMM; Vienna, Austria). Sequencing was performed using 2 \times 75 bp, paired-end, with Illumina HiSeq 3000/4000 (Illumina, San Diego, CA, USA).

2.10. Cell–Gene Matrix Preparation and Downstream Analysis

Raw sequencing reads were demultiplexed and aligned to the human (GrChH38) and mouse (mm10) reference genomes using the Cell Ranger mqcfast and count pipelines (v4.0; 10 \times Genomics, Pleasanton, CA, USA) to generate cell–gene matrices. The cell–gene matrices were then loaded into "Seurat" (v4.0; Satija Lab, New York, USA) in an R environment (v4.1.2; R Foundation for Statistical Computing, Vienna, Austria) and processed according to the recommended standard workflow for the integration of several datasets [41,42]. All human skin and scar samples were integrated in a single integration; likewise, all mouse samples were integrated in a single integration. Cells with less than 500 or more than 4000 detected genes, more than 20,000 reads per cell, or a mitochondrial gene count higher than 5% were removed from the dataset to ensure high data quality. After principal component analysis and the identification of significant principal components using the Jackstraw procedure [43], cells were clustered using non-linear dimensional reduction with uniform manifold approximation and projection (UMAP). Differentially expressed genes were calculated in Seurat using the Wilcoxon rank-sum test with Bonferroni correction.

In all datasets, normalized count numbers were used for differential gene expression analysis and for visualization in violin plots, feature plots, and dot plots, as recommended by the guidelines [44]. In all datasets, cell types were identified according to well-established marker gene expression. To avoid the calculation of batch effects, the normalized count numbers of genes present in the integrated dataset were used to identify differentially expressed genes (DEGs). As keratin and collagen genes were previously found to contaminate skin biopsy datasets and potentially provide a false-positive signal [45], these genes (*COL1A1*, *COL1A2*, and *COL3A1*; *KRT1*, *KRT5*, *KRT10*, *KRT14*, and *KRTDAP*) were excluded from DEG calculation in non-fibroblast clusters (collagens) or non-keratinocyte clusters (keratins), respectively. Moreover, genes *Gm42418*, *Gm17056*, and *Gm26917* caused technical background noise and batch effect in mouse scRNAseq, as previously described [46], and were thus excluded from the dataset.

2.11. Gene Ontology (GO) Calculation and Dot Plots

Gene lists of significantly regulated genes (adjusted *p*-value < 0.05; average log fold change (avg_logFC) > 0.1) were inputted into “GO_Biological_Process_2018” in the EnrichR package in R (v3.0; MayanLab, Icahn School of Medicine at Mount Sinai, New York, NY, USA). Dot plots were generated using ggplot2 (H. Wickham. ggplot2: Elegant Graphics for Data Analysis. Springer-Verlag New York, 2016) with color indicating adjusted *p*-value and size showing the odds ratio, sorted by adjusted *p*-value.

2.12. GSEA Matrisome Dot Plots

Curated matrisome gene lists for the terms “NABA_ECM_GLYCOPROTEINS”, “NABA_COLLAGENS”, “NABA_PROTEOGLYCANS”, “NABA_ECM_REGULATORS”, and “REACTOME_ELASTIC_FIBRE_FORMATION” were retrieved from the Gene Set Enrichment Analysis platform <https://www.gsea-msigdb.org/gsea/index.jsp>, accessed on 22 June 2022 [47], and gene names were used to generate dot plots.

2.13. TGFβ Injection Fibrosis Model in Mouse Skin

Mice were anesthetized with 3% isoflurane for three minutes. An intrascapular area of approximately 1 × 1 cm area was marked on the skin with a permanent marker. In total, 800 ng of TGFβ1 dissolved in 100 μL of NaCl 0.9%, medium, or PBMCsec (2.5 U) was injected in the marked area for 5 consecutive days, and mice sacrificed on the 6th day. The marked injection areas were biopsied and prepared for histological analysis.

2.14. Isolation of Primary Skin FBs

Primary skin and scar FBs were isolated as previously described [7]. In brief, skin or scar samples were incubated overnight in Dipase II (Roche, Basel, Switzerland). Subsequently, the epidermis was removed, and the dermis was incubated in Liberase (Merck Millipore, Burlington, MA, USA) for two hours at 37 °C. Afterwards, the tissue was filtered and rinsed with PBS, and the cells were plated in a T175 cell culture flask and cultured until they reached 90% confluency.

2.15. Western Blots

Western blotting was performed as previously described [7]. In brief, after cell lysis in 1 × Laemmli buffer, the lysates were separated on SDS-PAGE gels (Bio-Rad Laboratories, Inc., Hercules, CA, USA), and proteins were transferred to nitrocellulose membranes and blocked with non-fat milk. After overnight incubation at 4 °C with the primary antibody (table of antibodies used reported in Figure S1B), the membranes were incubated with a horseradish peroxidase-conjugated secondary antibody and imaged.

2.16. Immunofluorescence, H&E, and EvG Staining

Immunofluorescence staining on formalin-fixed, paraffin-embedded (FFPE) sections of human and mouse skin and scar tissues was performed according to the protocol provided

by the respective antibody manufacturer (table of antibodies used reported in Figure S1B) as previously described [7]. Hematoxylin and eosin (H&E) staining and Elastica van Gieson (EvG)-staining were performed at Department of Pathology of Medical University of Vienna according to standardized clinical staining protocols.

2.17. TGF β 1-Induced Myofibroblast Differentiation

TGF β 1 stimulation of primary FBs was performed as previously reported [7]. Isolated primary FBs were plated in 6-well plates after the first passage and grown until they reached 100% confluency. FBs were then stimulated with 10 ng/mL TGF β 1 (HEK-293-derived; Peprotech, Rocky Hill, NJ, USA) and with medium or PBMCsec for 24 h. The supernatants were removed, and medium or PBMCsec was resupplied for another 24 h. The supernatants were collected and stored at -80°C , and cells were lysed in $1 \times$ Laemmli buffer (Bio-Rad Laboratories, Inc.) for further analysis.

2.18. Elastase Assay

To measure elastase activity, a commercial kit (EnzChek[®] Elastase Assay Kit; E-12056; Thermo Fisher) was used according to the manufacturer's instructions. Elastase was applied at 250 mU/mL and incubated with NaCl 0.9% ("Ctrl"), medium, or PBMCsec at 1:1 with assay buffer. Fluorescence intensity was measured with a BMG Fluostar Optima plate reader (BMG Labtech, Ortenberg, Germany) at 505/515 nm wavelength (excitation/emission). Raw values were blank-corrected and normalized to the % of the averaged 4 h of the Ctrl samples. Samples were measured 10 min, 1 h, 2 h, 3 h, and 4 h after elastase application. Statistical analysis was performed with a mixed-effects model for the time factor, with Tukey's multiple comparisons test.

2.19. ELISA

The supernatants of TGF β 1-stimulated FBs after treatment with PBMCsec or controls were collected, centrifuged, and stored at -20°C for further use. The protein levels of human elastin (ELISA; LS-F4567; LSBio, Seattle, WA, USA) were measured according to the manufacturer's manual. Absorbance was detected with a FluoStar Optima microplate reader (BMG Labtech).

3. Results

3.1. PBMCsec Improves Scar Formation in Mice after Topical Treatment during Wound Healing and Intradermal Injection of Preformed Scars

As our previous study on wound healing in pig burn wounds revealed a trend towards better tissue elasticity and less stiffness in early pig burn scars [27], we aimed to investigate the effect of PBMCsec on scar formation and on already existing scars in more detail at the single-cell level.

To achieve this, we created full-thickness excision wounds on the back of 6–8-week-old female Balb/c mice and immediately treated with the topical application of PBMCsec for 8 weeks (Figure 1A). In a separate set of experiments, we allowed the scars to develop for 4 weeks after wounding without further intervention and treated the formed scars with intradermal injection for 2 weeks. Scars were either analyzed right after the two weeks of treatment or after two additional weeks without further treatment to determine whether treatment-associated changes were permanent (Figure 1B).

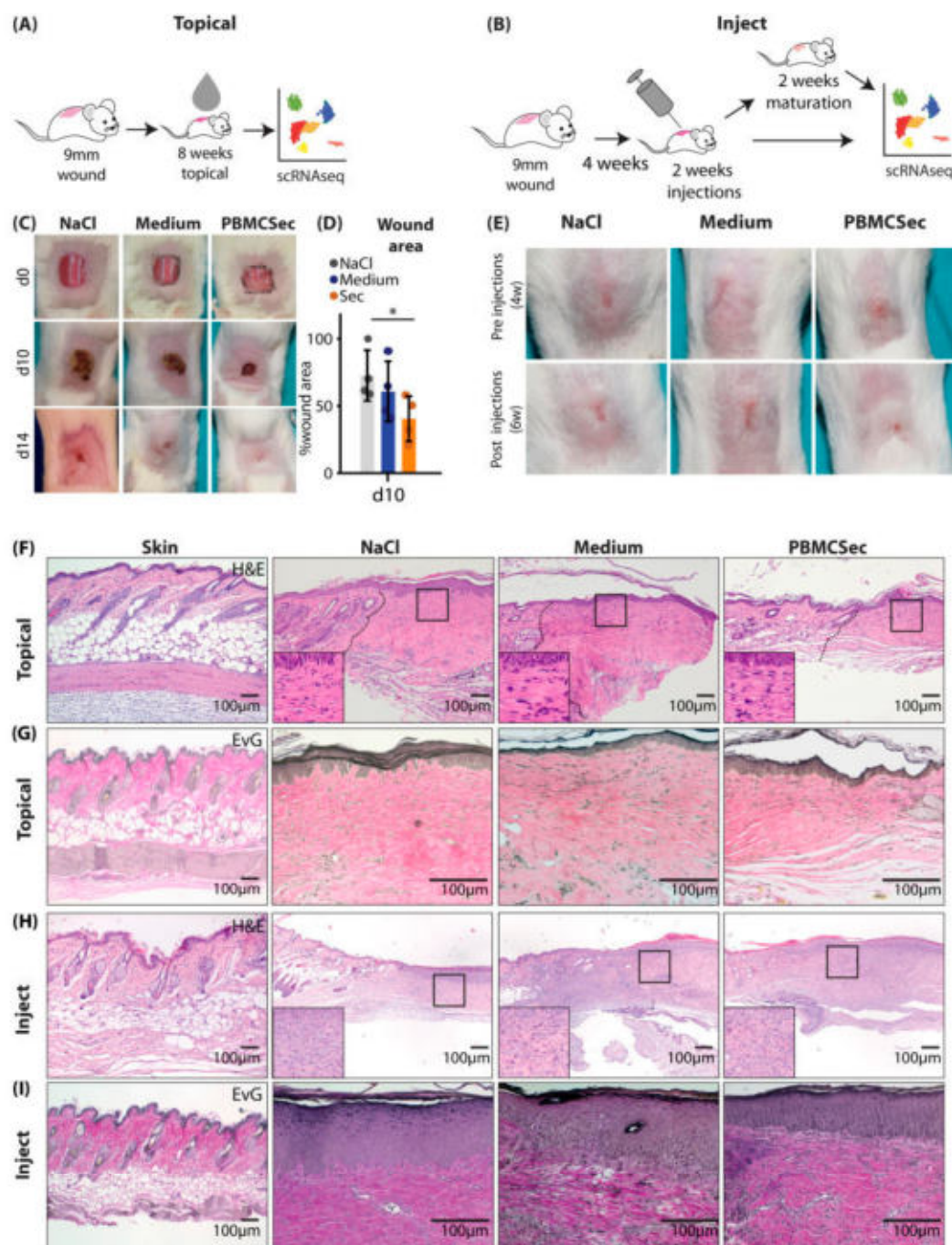


Figure 1. Comparison of PBMCsec-mediated effects on scars after topical or intradermal application. (A,B) Illustration of “topical” or “inject” workflow for mouse scars: (A) square wounds of 9×9 mm were excised on mouse backs ($n = 4$ per group), treated with topical PBMCsec for 8 weeks, and subjected to scRNAseq; (B) square wounds of 9×9 mm were excised on mouse backs ($n = 4$ per group), left to mature for 4 weeks, injected with PBMCsec for 2 weeks, and subjected to scRNAseq, or matured for another 2 weeks and then subjected to scRNAseq. (C) Wound documentation of topically treated scars on post-wounding days 0, 10, and 14. * indicates $p < 0.05$ in one-way ANOVA (D) Wound area measurements normalized to the d0 wound area of each respective wound. (E) Scar documentation of mouse scars before and after injections. (F) Hematoxylin/eosin staining of “topical” mouse wounds. (G) Elastica van Gieson (EvG) staining of “topical” mouse wounds. (H) Hematoxylin/eosin staining of “inject” mouse wounds. (I) Elastica van Gieson (EvG) staining of “inject” mouse wounds.

As previously demonstrated with the secretome of non-irradiated PBMCs [25,26] or PBMCsec in diabetic mice [25,26], we found enhanced wound healing in wild-type mice after the topical application of an emulsion containing PBMCsec (Figure 1C). PBMCsec reduced the wound size significantly more ($40 \pm 14\%$ of the wound size) than NaCl (72 ± 16) and the control medium alone ($60 \pm 19\%$) (Figure 1D). Compared with the intradermal injection of controls, scars appeared softer and reduced in size after the injection of PBMCsec (Figure 1E). Histologically, scars showed a looser structure and reduced fiber density after topical PBMCsec treatment, as evidenced by hematoxylin/eosin (Figure 1F) and Elastica van Gieson (EvG) staining (Figure 1G). Of note, scars treated with intradermal injection exhibited a high number of infiltrating leukocytes (Figure 1H), presumably due to repeated tissue irritation with injections. However, the matrix was looser, and the orientation of collagen fibers showed more vertical structures after the injection of PBMCsec (Figure 1I). These results indicate that PBMCsec not only improves wound healing but also scar formation and the quality of already existing scars in mice.

3.2. PBMCsec Induces Significant Changes in the Transcriptome after Topical and Intradermal Application

Next, we performed scRNAseq on scar tissue from the different experimental settings. After quality control (Figure S2A–C,E–G) we defined clusters based on well-established marker genes [7,48] from scRNAseq of topically treated scars (Figure S2D,H). Clusters were constantly aligned homogeneously under all conditions (Figure 2A,E) and were grouped into fibroblasts (FBs), smooth muscle cells and pericytes (SMCs/PCs), endothelial and lymphatic endothelial cells (ECs), macrophages (Macro), Langerhans cells and dendritic cells (DCs), T cells and B cells (TCs), keratinocytes (KCs), hair follicular cells (HFs), melanocytes (Mel), and adipocytes (Adipo) (Figure 2A). Notably, one fibroblast cluster, FB 4, was expanded after topical treatment with PBMCsec compared with the controls (Figure 2A,B), suggesting an important role in the anti-fibrotic action of PBMCsec. Furthermore, the relative numbers of DCs and TCs were increased with the control medium but slightly reduced with PBMCsec (Figure 2B). We then calculated the differentially expressed genes (DEGs) of all cell populations in PBMCsec-treated scars compared with medium- and NaCl-treated scars. Interestingly, significantly more genes were downregulated than upregulated after the topical application of PBMCsec (Figure 2C), and the highest numbers of regulated genes were found in FBs (red bars), macrophages (pale-green bars), and KCs (yellow bars) (Figure 2C) [35]. To provide an overview of the overall regulation in all cell types, we show the top 50 DEGs per cluster group in Figure S3A–I. The upregulation of numerous genes, previously described to be increased in scar tissue [7,49,50], was significantly inhibited after PBMCsec application.

Next, we analyzed the scRNAseq dataset of scars treated with the intradermal injection of PBMCsec and controls in a similar way. After cluster identification and quality control (Figure S2D–G), clusters aligned homogeneously across samples and conditions (Figure 2D). Although the cellular composition of scars did not change after 6 weeks, the FB and immune cell populations were significantly reduced in 8-week-old scars (Figure 2E). Remarkably, there were again far more downregulated genes than upregulated genes in the injected scars, and transcriptome changes were the highest in FB1 and KC clusters (Figure 2F) after injections. Interestingly, only minor transcriptome changes remained in PBMCsec-treated scars 8 weeks after wounding (Figure 2F). The top 50 DEGs after 6 weeks are shown per cluster group in Figure S4A–I. Numerous genes regulated in the topical dataset and previously found relevant in skin scarring and mouse scar formation [7] were also regulated after PBMCsec injection (Figure S4A–I).

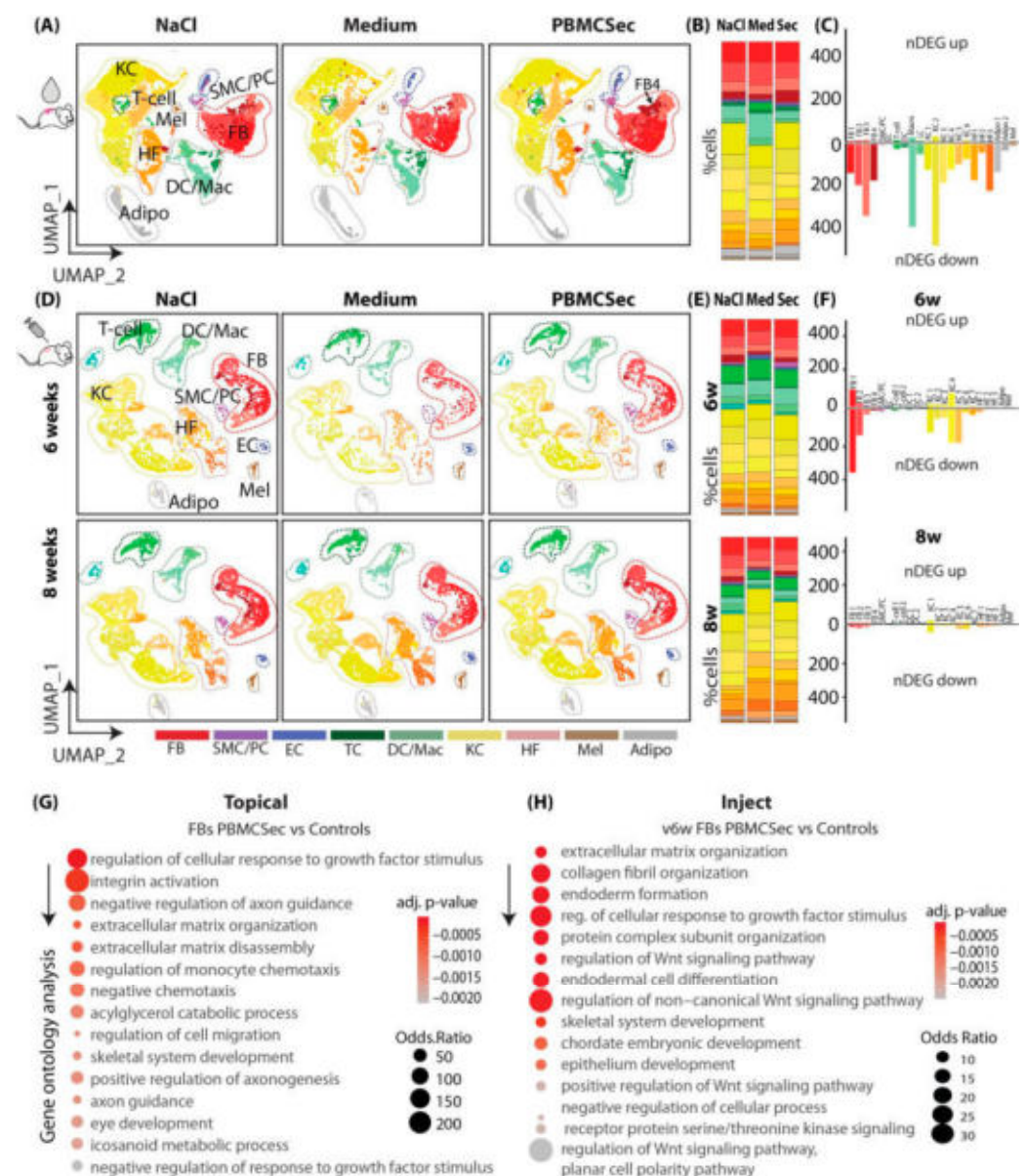


Figure 2. PBMCsec induces significant changes in the transcriptome after topical and intradermal application. (A) UMAP clustering of “topical” mouse wounds (n = 4 per condition, pooled for scRNAseq analysis), split by condition: four fibroblast clusters (FB1-4; red), smooth muscle cells (SMCs) and pericytes (PCs; purple), endothelial cells (ECs; blue), T cells (TCs; dark green), macrophages (Mac) and dendritic cells (DCs; light green), three keratinocyte clusters (KC1-6; yellow), hair follicles (HF 1-3; beige), melanocytes (Mel; brown), and adipocytes (grey). Clusters were grouped as “FB”, “PC”, “TC”, “DC”, “KC”, “HF”, “MEL”, and “Adipo” for readability. (B) Percentages of cells per cluster, split by condition. (C) Number of significantly upregulated (positive y-axis) and downregulated (negative y-axis) genes (“nDEG”) per cluster in “topical” mice. (D) UMAP clustering of “inject” mouse wounds (n = 2 per condition), split by condition, i.e., 6w = mice after two weeks of injections; 8w = mice after injections + 2 weeks of maturation. Clusters FB1-4, SMCs, PCs, ECs, T cells 1+2, DC1+2, KC1-7, HF 1-3, Mel, and Adipo. Clusters were grouped as “FB” (red), “PC” (purple), “EC” (blue), “TC” (dark green), “DC” (light green), “KC” (yellow), “HF” (beige), “MEL” (brown), and

“Adipo” (grey) for readability. (E) Percentages of cells per cluster, split by condition. (F) Number of significantly upregulated (positive y-axis) and downregulated (negative y-axis) genes (“nDEG”) per cluster in “inject” mice, split in 6w and 8w (G) Gene ontology (GO) term calculation of genes downregulated by PBMCsec compared with medium in “topical” FBs. (H) GO term calculation of genes downregulated by PBMCsec vs. medium in 6w “inject” FBs. DEGs were calculated per cluster comparing 8- and 6-week-old scars using a two-sided Wilcoxon-signed rank test, including genes with average logarithmic fold change (avg_logFC) of >0.1 or <-0.1 ; adj. p -value < 0.05 . UMAP, uniform manifold approximation and projection.

As the highest number of regulated genes was observed in FBs and FBs are the main cell type involved in fibrotic processes, we further performed a gene ontology analysis of genes downregulated by PBMCsec application in FBs in both experimental settings (Figure 2G,H).

Our analysis revealed that genes downregulated by PBMCsec mainly showed a strong association with the response to growth factors, integrin activation, monocyte chemotaxis, and extracellular matrix organization, suggesting that the activation of these processes was, at least partially, reduced with topical application (Figure 2G). GO term calculation of downregulated genes in FBs after the injection of PBMCsec revealed changes in ECM and collagen organization, the response to growth factor stimulus, and Wnt signaling (Figure 2H).

Taken together, these bioinformatic data suggest an anti-fibrotic, anti-inflammatory effect of PBMCsec on scar formation, primarily reducing excessive matrix deposition.

3.3. PBMCsec Significantly Alters the Matrisome

Since FBs contributed the most to transcriptome alterations induced by PBMCsec and the GO analysis indicated that genes associated with the ECM were highly affected, we further assessed genes of the matrisome in more detail. Differentially regulated genes in all FBs after topical (Figure 3A–D) and intradermal injection (Figure 3E–H) were analyzed using the curated matrisome gene set enrichment analysis (GSEA) gene lists [51]. For better visualization, the whole matrisome was split into the main components, i.e., collagens, proteoglycans, glycoproteins, and ECM regulators. Interestingly, most of the matrisome-related genes were strongly downregulated by PBMCsec after topical and intradermal application (Figure 3). Similarly, most of the proteoglycans, glycoproteins, and ECM regulators showed reduced expression after PBMCsec treatment. However, some of the glycoproteins and ECM regulators, including *Fn1*, *Igfbp4/5*, *Ecm1*, *Postn*, and *Mfap5*, were even enhanced after PBMCsec treatment (Figure 3C,D), suggesting the targeted regulation of these factors.

Importantly, we also identified a variety of proteases, including *Mmp19* (matrix metalloprotease 19), *Ppcsk5/6* (Subtilisin/Kexin-Like Protease PC5/6), and *Adamts1* (A disintegrin-like and metalloprotease with thrombospondin type 1 motif), regulated by PBMCsec. Furthermore, plasminogen activator/urokinase (*Plau*) and the plasminogen activator/tissue type (*Plat*), as well as serine proteases *Htra1*, *Htra3*, and *Aebp1*, were elevated after the topical application and intradermal injection of PBMCsec. However, a variety of protease inhibitors, including *Timp1* and -3 (Metalloprotease Inhibitor 1 and 3), and *Slpi* (Secretory Leukocyte Protease Inhibitor), and the potent urokinase inhibitors *Serpine1*, *Serpine2*, and *Serpine5* were also increased (Figure 3C,D). These findings confirm our previous work, highlighting the role of proteases and their inhibitors in skin fibrosis [7], and indicate that PBMCsec is able to interfere with the protease system that contributes to scar formation.

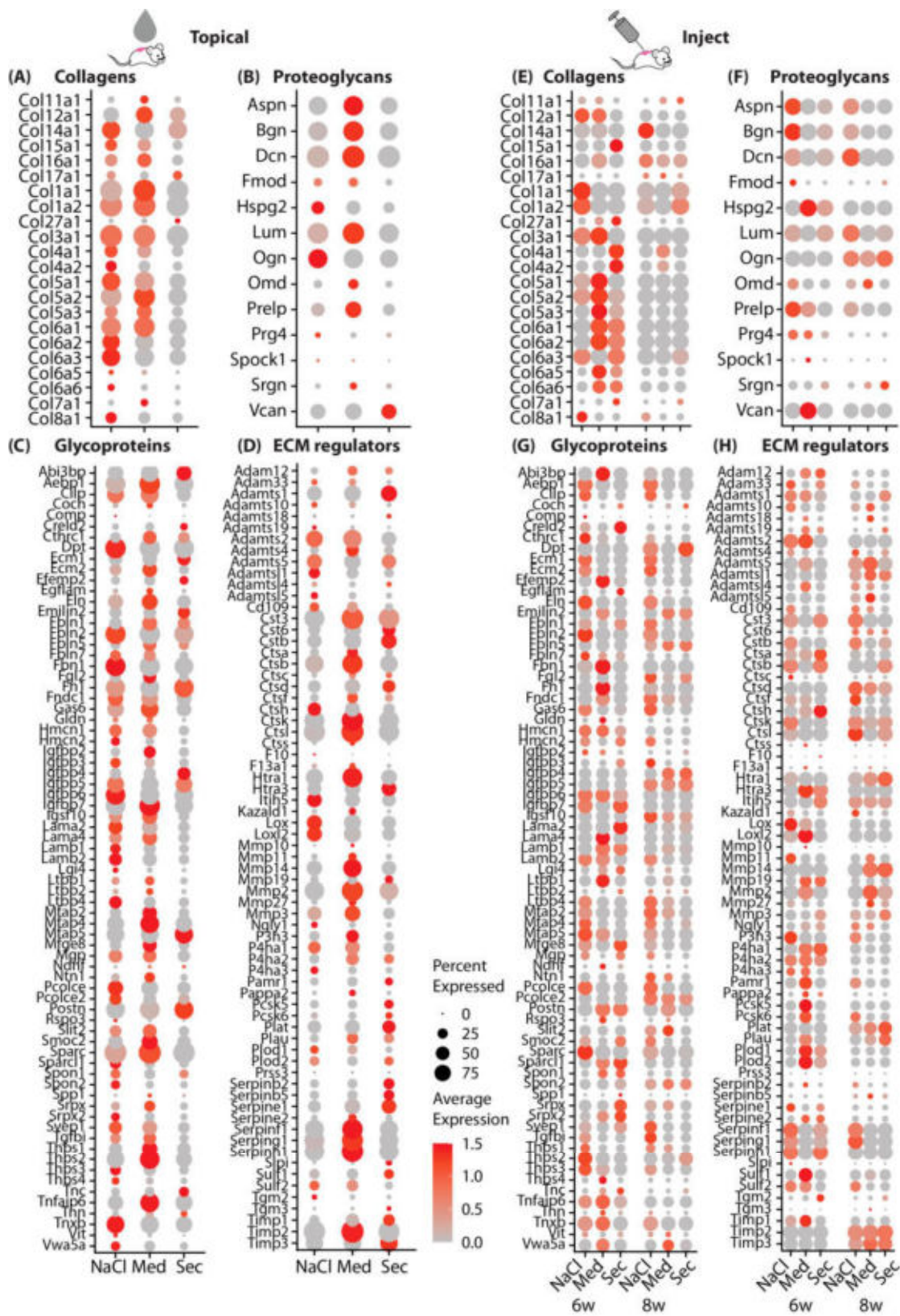


Figure 3. PBMCsec significantly alters the matrisome. Dot plots of gene lists of gene set enrichment of matrisome terms (A,E) “collagens”, (B,F) “proteoglycans”, (C,G) “Glycoproteins”, and (D,H) “ECM regulators” inputted to FBs of the “topical” (A–D) and “inject” (E–H) datasets, split by condition. Circle size correlates with the percent of cells expressing the respective gene, and color (red) correlates with normalized fold change in expression.

3.4. Scars Treated with PBMCsec Ex Vivo Show Strong Similarities to Mouse Models

As we showed an anti-fibrotic effect of PBMCsec during scar formation in mice, we next investigated its effect on human skin and ex vivo cultures of scar tissue. Therefore, we treated biopsies of human skin and human hypertrophic scars with medium or PBMCsec and cultivated them for 24 h (Figure 4A). After quality control and cluster identification (Figure S5A–D), clusters aligned homogeneously across donors and conditions (Figures 4B and S5E). As described in our previous work, the ratio of FBs was increased in scars compared with skin [7], and several FB clusters (here, clusters FB5 and FB7) were specifically found in scars (Figure 4B,C). Remarkably, the percentages of FBs, DCs, and T cells were reduced in scars after PBMCsec treatment (Figure 4C).

Next, we calculated DEGs separately for skin (Figure S6) and scars (Figure S7) and found a much higher number of DEGs in scars than in normal skin, indicating a strong effect of PBMCsec on fibrotic tissue (Figure 4D). In line with our mouse datasets, most regulated genes were found in the FB clusters, and slightly more genes were downregulated than upregulated, particularly in skin tissue (Figure 4D). Numerous genes that we previously described for their regulation in hypertrophic scars [7] were also favorably regulated by PBMCsec (Figures S6 and S7).

Next, we performed the GO term analysis of the DEGs in FBs treated with PBMCsec compared with medium. In line with the mouse data, downregulated terms (Figure 4F) included collagen fibril and ECM organization, cytokine signaling pathway, negative regulation of signal transduction, regulation of extrinsic apoptotic signaling pathway, and type I interferon signaling pathway. Intriguingly, among the upregulated terms (Figure 4E), negative regulation of neuron differentiation and generation of neurons were present. As we previously demonstrated that Schwann cells promote ECM formation in keloids and affect the M2 polarization of macrophages [52], this finding might hint at a mechanism of PBMCsec also affecting this crosstalk.

Next, we assessed the genes of the matrisome in the human dataset (Figure 4H). Similarly to the data obtained for mouse scars, collagens *COL1A1*, *COL3A1*, and *COL6A1/2/3* were also strongly downregulated, more in scars than in skin, and proteases *MMP1/MMP3/10* as well as protease inhibitors *SERPINE1/G1/F1/B2*, *SLPI*, and *TIMP3* were upregulated (Figure 4D). Of note, PBMCsec increased the expression of *PI3*, an elastase-specific protease inhibitor in human scar tissue, indicating a regulatory effect not only on collagens but also on elastic ECM components. Together, our analysis of human ex vivo skin and scars corroborated the findings of the in vivo mouse experiments, indicating an ECM-balancing, anti-fibrotic effect.

3.5. PBMCsec Abolishes Myofibroblast Differentiation In Vitro

After a comprehensive analysis of the effects of PBMCsec in mouse and human models at the single-cell level, we investigated the underlying mechanisms of the observed anti-fibrotic activity in vitro. Using a well-established in vitro fibrosis model [7,53], we stimulated primary human skin FBs with TGF β 1 and investigated the effect of PBMCsec on myofibroblast (myoFB) formation [54]. Upon the stimulation of FBs with TGF β 1, FBs showed robust differentiation to α SMA-expressing myoFBs in all control treatments (NaCl and medium) (Figure 5A). In contrast, the addition of PBMCsec completely abolished myoFB differentiation and α SMA expression (Figure 5A,B). As our scRNAseq revealed that of all major ECM components, *Eln/ELN* was the most consistently downregulated one in the matrisome of both mice and humans, we further assessed the effect of PBMCsec on the expression of elastin in vitro in FBs. Strikingly, elastin protein and mRNA expression were strongly downregulated by PBMCsec (Figure 5A,C), and the secretion of ELN in the supernatant was significantly inhibited (Figure 5D). Next, we investigated whether PBMCsec contains TGF β inhibitors. Therefore, we used an HEK-cell-based reporter assay to assess the activity of canonical TGF β 1 signaling. While PBMCsec showed little-to-no TGF β 1 activity, the addition of PBMCsec to active TGF β 1 did not inhibit canonical TGF β 1 activity (Figure S8A). These data indicate that PBMCsec does not inhibit myoFB differentiation by

inhibiting Smad2/3-mediated TGFβ1 activity, suggesting a more downstream inhibitory or non-canonical action.

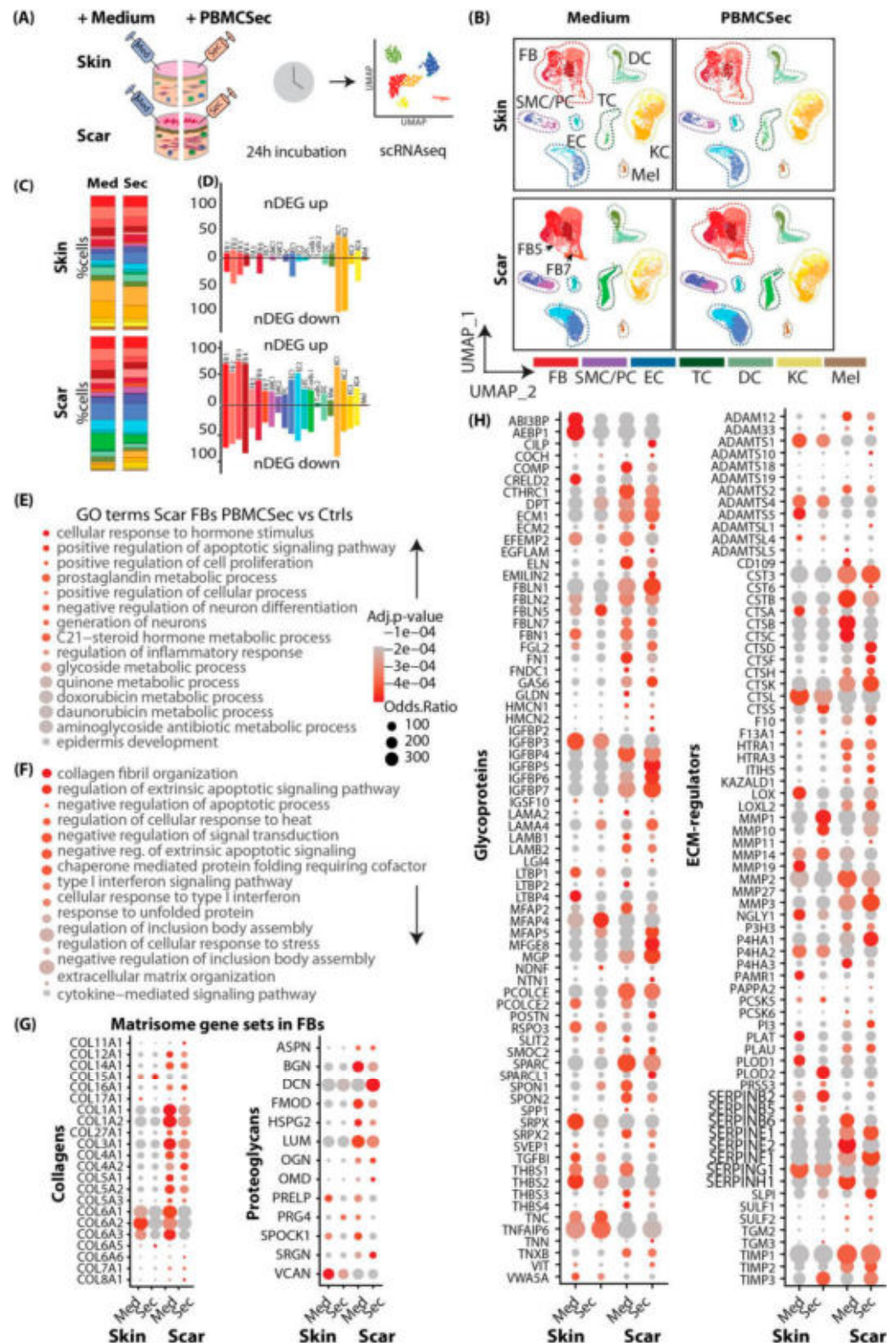


Figure 4. scRNAseq analysis of human skin and scars treated with PBMCsec ex vivo shows strong similarities to mouse models. (A) Illustration of scRNAseq workflow in human skin and scar samples. Skin and scar biopsies were incubated overnight in medium or PBMCsec and subjected to scRNAseq.

(B) UMAP clustering of human skin and scar, split by condition. Seven fibroblast clusters (FB 1–7; red), smooth muscle cells (SMCs) and pericytes (PCs; purple), endothelial cells (ECs; blue), T cells (TCs; dark green), macrophages (Mac) and dendritic cells (DCs; light green), four keratinocyte clusters (KC1–4; yellow), and melanocytes (Mel; brown). Clusters were grouped as “FB”, “PC”, “TC”, “DC”, “KC”, “MEL”, and “HF” for readability. (C) Percentages of cells per cluster, split by condition. (D) Number of significantly upregulated (positive y-axis) and downregulated (negative y-axis) genes (“nDEG”). (E) Gene ontology (GO) term calculation of genes (E) upregulated and (F) downregulated by PBMCsec compared with medium in “topical” FBs. (G) Dot plots of gene lists of gene set enrichment of matrisome terms “collagens” and “proteoglycans”, and (H) “Glycoproteins” and “ECM-regulators” inputted in FBs. DEGs were calculated per cluster by comparing 8- vs. 6-week-old scars using a two-sided Wilcoxon signed-rank test, including genes with average logarithmic fold change (avg_logFC) of >0.1 or <-0.1 ; adj. p -value <0.05 . UMAP, uniform manifold approximation and projection.

To confirm the observed TGF β effects in vivo, we injected TGF β 1 into murine skin (modified after Thielitz et al. [53]) for 5 consecutive days (Figure S8B). Although no morphological changes were visible in hematoxylin–eosin staining (Figure S8C), the immunostaining of Collagen I and III showed patches of increased matrix deposition in all samples (arrows in Figure S8D,E), which were not present in mice also treated with PBMCsec. Remarkably, we also observed accumulations of α SMA-expressing cells in the TGF β 1-injected deep murine dermis (squares), but not in PBMCsec-treated mice (Figure S8F).

Next, we aimed to further investigate changes in ECM composition, particularly elastin, in a human model. Thus, we injected TGF β intradermally in human skin explants with and without NaCl, medium, or PBMCsec (Figure 5E). Morphologically, no changes were observed in H&E staining (Figure 5F); however, when we stained for overall ECM configuration using Elastica van Giesson staining (Figure 5G) and with immunofluorescence for elastin (Figure 5H), we noticed specific subepidermal alterations in elastic fibers. In untreated skin, elastin showed vertical fibers reaching into the dermal papillae with parallel, horizontal fibers in the deeper dermis. These vertical, papillary fibers disappeared after TGF β 1 treatment but were preserved when PBMCsec was added (Figure 5G,H). These data suggest that PBMCsec is able to reduce the breakdown of elastic fibers, which occurs after TGF β stimulation.

3.6. Combined Analysis of Murine and Human scRNAseq Datasets Reveals Elastin and TXNIP as Joint Key Players of Beneficial PBMCsec Effects

To better understand the mutual mechanisms of action of ECM balancing and anti-fibrotic mechanisms of PBMCsec, we performed the subclustering of the FBs of all scRNAseq datasets (Figure S9D) and performed a combined analysis (Figure 6A). As myoFB, i.e., *Acta2*/*ACTA2*-positive FBs, disappear in mature scars [54], these cells were not detected in most of our datasets. Therefore, we were not able to investigate the effects of PBMCsec on myoFB differentiation in our scar models in detail (Figure S9A–C). However, we detected a significant reduction in *ACTA2* in ex vivo PBMCsec-treated human scars (Figure S9C), indicating that even in mature scars, PBMCsec can reduce myoFB content. When overlaying DEGs from FBs from all three experiments, no genes were mutually upregulated (Figure 6B). Interestingly, *Eln*/*ELN* and *Txnip*/*TXNIP* were mutually downregulated in all experimental settings (Figure 6C). Elastin and TXNIP were solidly reduced in all three scRNAseq, at both time points after injection, and in human scars (Figure 6D,E).

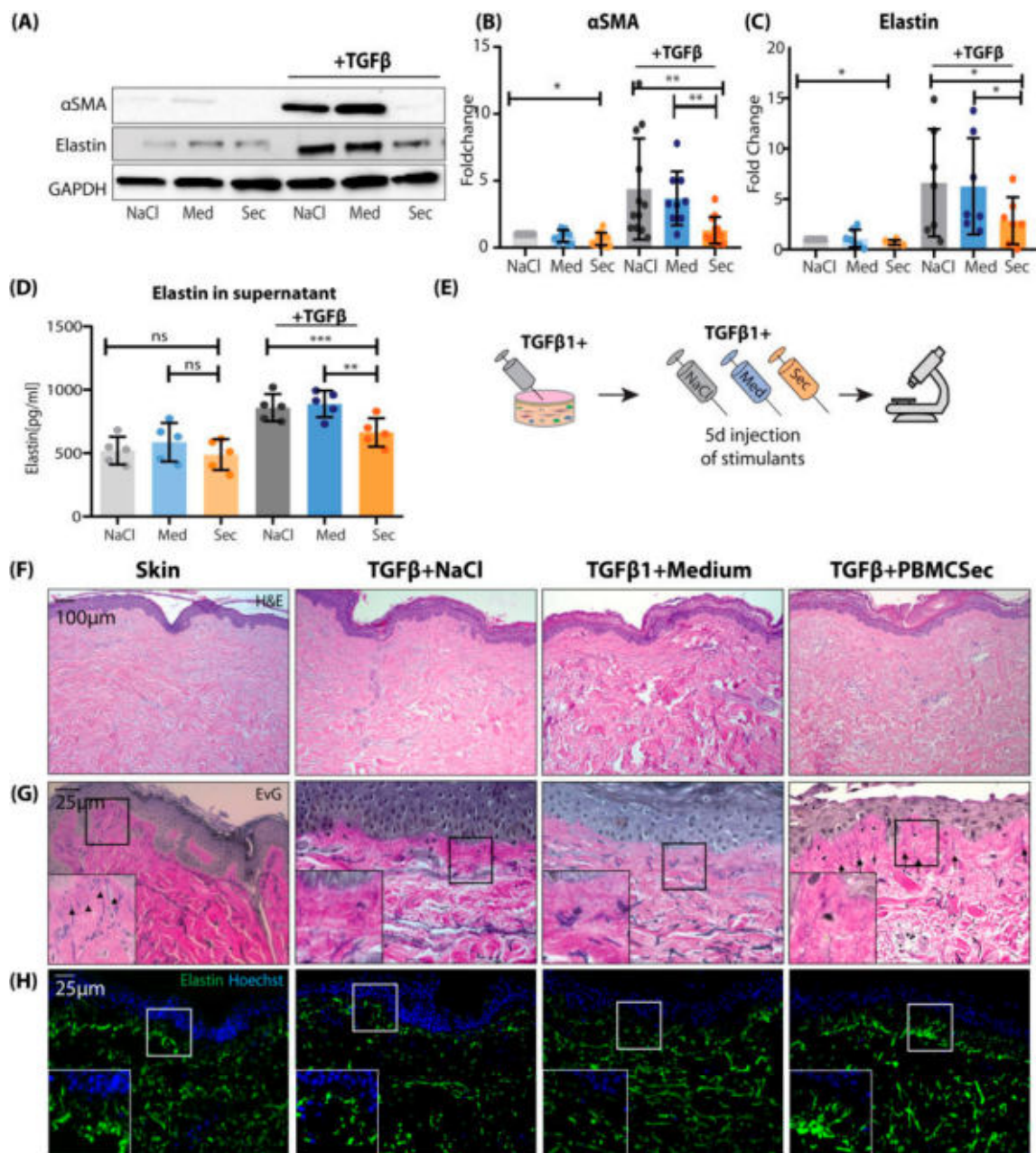


Figure 5. PBMCsec abolishes myofibroblast differentiation in vitro. (A) Western blot stained for alpha Smooth muscle actin (SMA) and elastin, and lysate from human primary FBs stimulated with NaCl, medium, or PBMCsec, without or with TGFβ1, respectively. (B) Quantification of Western blot, normalized to ctrl (n = 6 human donors). (C) Elastin measured with ELISA from primary human FB supernatant, stimulated with NaCl, medium, or PBMCsec, without or with TGFβ1. (D) Workflow illustration of ex vivo human skin TGFβ stimulation experiment, where 5 mm skin biopsies were injected with TGFβ and NaCl, medium, or PBMCsec for 5 consecutive days (E). (E,F,H) Elastica van Gieson. (G) Immunofluorescence staining for elastin in human ex vivo skin samples. Statistical significance was tested using one-sided ANOVA. Lines and error bars indicate means and standard deviation. ns $p > 0.05$, * $p < 0.05$, ** $p < 0.01$, and *** $p < 0.001$.

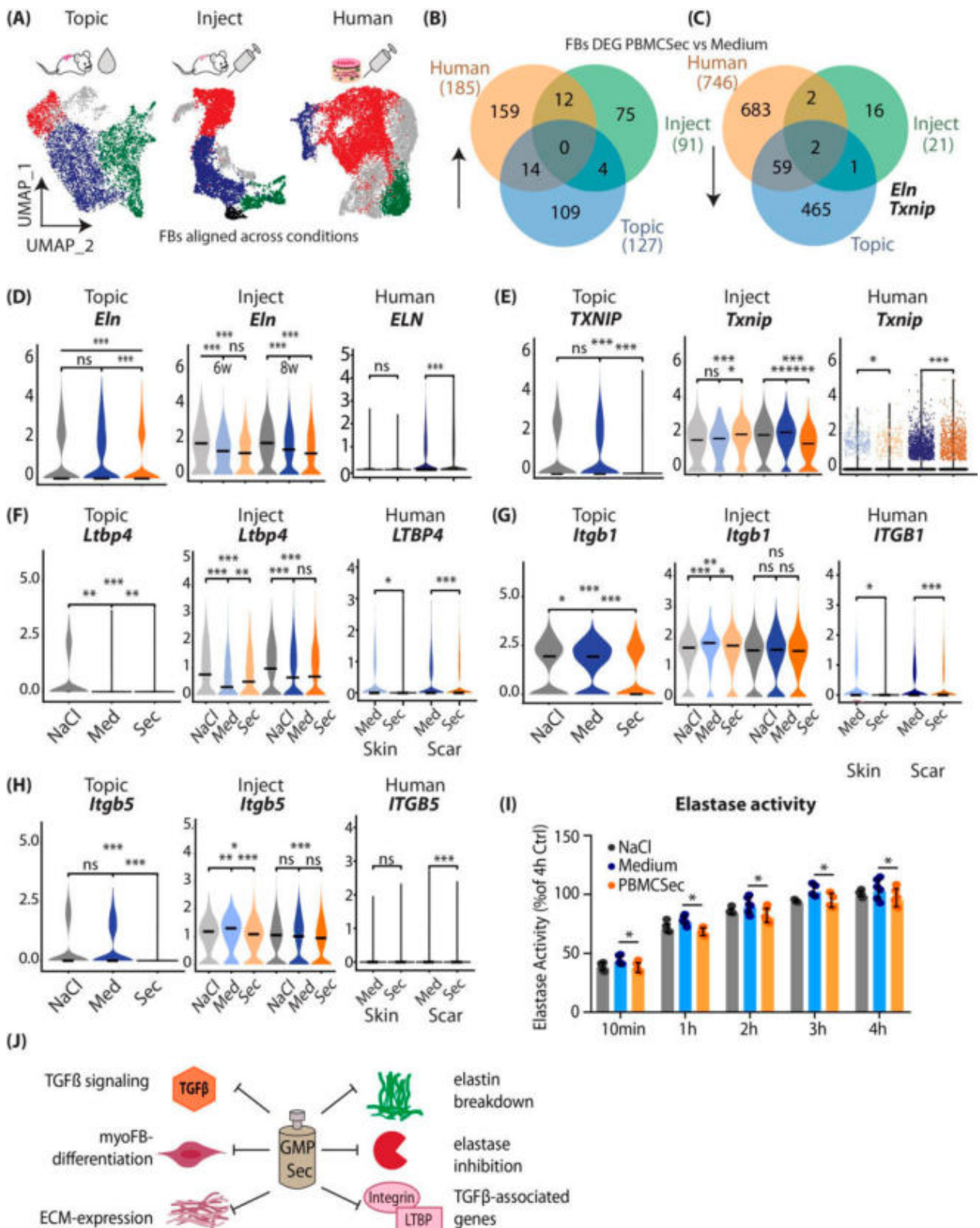


Figure 6. Combined analysis of murine and human scRNAseq datasets reveals elastin as joint key player of beneficial PBMCSec effects. (A) Subclustering of FBs in “mouse topical”, “mouse inject”, and “human” scRNAseq datasets, and FB subcluster alignment. Red, cluster A; blue, cluster B;

green, cluster C; aligned by cluster markers (Figure S9). (B) Venn diagram of overlap of significantly upregulated and (C) downregulated genes in FBs in all three datasets. (D–G) Violin plots of (F) latent TGF β binding protein 4 (*Ltbp4/LTBP4*) and (G,H) Integrin subunit beta 1/5 (*Itgb1/5/ITGB1/5*) in datasets. (I) Elastase assay with fluorescence-marked pig pancreas elastase, with NaCl, medium, or PBMCSec supplementation. Y-axis indicates fluorescence intensity, i.e., elastase activity. Comparison among groups was performed with Student's *t*-test. (J) Illustration of putative mechanisms of PBMCSec in scars. In violin plots, dots represent individual cells; y-axis represents log₂ fold change in normalized genes and log-transformed single-cell expression. Vertical lines in violin plots represent maximum expression; the shape of each violin represents all results; and the width of each violin represents the frequency of cells at the respective expression level. DEGs were calculated in FBs by comparing medium to FBs using a two-sided Wilcoxon signed-rank test, including genes with average logarithmic fold change (*avg_logFC*) of >0.1 or <−0.1 and Bonferroni-adjusted *p*-value < 0.05. For violin plots, a two-sided Wilcoxon signed-rank test was used in R. ns *p* > 0.05, * *p* > 0.05, ** *p* > 0.01, and *** *p* > 0.001.

As we have shown that PBMCSec does not interfere with canonical TGF β 1 activity, we next wanted to know how TGF β signaling is inhibited by PBMCSec. TGF β is one of the most pleiotropic signaling molecules, and its interaction via the regulation of its release and activation by elastin was previously described [55]. TGF β is secreted as inactive and bound to latent TGF β binding proteins (LTBP1–4), together forming the large latent complex (LLC) [56]. The activation of TGF β occurs via a tightly controlled process involving the cleavage of LTBPs or protease-independent activation via integrins [56,57]. We, therefore, wondered whether PBMCSec also regulates molecules indirectly involved in TGF β activation. Surprisingly, we found that *Ltbp4/LTBP4* was decreased by PBMCSec in both mouse and human experimental settings (Figure 6F). *Ltbp4/LTBP4* is involved in both elastogenesis and the regulation of TGF β signaling [57,58], and an increase in *Ltbp4* is associated with fibrosis in scleroderma via TGF- β /SMAD signaling [59]. Additionally, we found that the expression of integrin subunits beta 1 and beta 5 (*Itgb/ITGB 1/5*) was also decreased upon PBMCSec treatment (Figure 6G,H). As both participate in the activation of TGF β [56], these data indicate that their downregulation might indirectly contribute to the reduction in TGF β -mediated fibrotic effects.

Finally, we investigated whether PBMCSec contains endogenous elastase inhibitors that inhibit elastin breakdown and the release of TGF β [60], further enhancing the anti-TGF β feedback loop induced by PBMCSec. However, the elastase activity assay showed only a weak reduction in elastase activity after the addition of PBMCSec (Figure 6H). We, therefore, propose a multi-effect model for the attenuation of fibrosis with PBMCSec (Figure 6): PBMCSec directly inhibits TGF β 1-mediated myoFB differentiation, but not via canonical signaling. PBMCSec attenuates the expression of numerous matrix genes and significantly reduces elastin secretion. PBMCSec prevents elastin breakdown, shows mild elastase inhibition, and interferes with TGF β -induced gene expression (Figure 6J).

4. Discussion

For patients, scars, particularly hypertrophic scars, not only represent an aesthetic problem but often lead to significantly reduced quality of life due to associated limitations of movement, itching, and pain [8]. As the treatment of hypertrophic scars remains difficult, the development of new therapeutic options is of particular interest. Here, we present a multi-model approach to assessing the effects of a secretome-based drug (PBMCSec) on scar formation and treatment in mice and humans. The strong tissue-regenerative activity of PBMCSec has already been demonstrated not only in cutaneous wounds [25–27] but also in various other organs, such as focal brain ischemia [31], spinal cord injury [32], and infarcted myocardium [33]. Interestingly, in all organs mentioned above, PBMCSec significantly reduced the size of the damaged areas and reduced the developing fibrotic tissue, suggesting its potential use in the treatment of cutaneous scars [27,33]. In this study, we compared the effect of PBMCSec on scar formation in mice *in vivo* and in human ex

vivo explant cultures. In mice, we performed the intradermal injection of the secretome into mature scars and applied it topically during wound healing and scar formation. Only a few studies have investigated the effects of paracrine factors on cutaneous scarring using cell secretomes from different stem cell types, including umbilical cord stem cells, adipose tissue-derived stem cells, or mesenchymal stem cells [61–63]. Arjunan et al. and Liu et al. showed that conditioned medium from umbilical cord Wharton’s jelly stem cells or adipose tissue-derived stem cells reduced the activation and growth of keloidal fibroblasts in *in vitro* and *in vivo* keloid models [62]. In addition, Hu et al. suggested a combined treatment of conditioned medium from MSC and botulinum toxin for the treatment of hypertrophic scars [62]. However, in-depth analyses of the underlying mechanisms are still lacking. Thus, our study is the first to use scRNAseq to unravel mechanisms important for improved scar formation after the application of a cell secretome. Generally, scRNAseq generates large datasets with tens of thousands of cells, which helps to smooth out donor and technical variances. Therefore, low donor numbers, as used in our study, are widely acceptable [64–66].

In our mouse experiments, both application routes, topical and intradermal application, showed promising effects on scar formation and treatment. Of note, significantly more genes were regulated after the topical application of PBMCsec, suggesting higher efficacy after wound application than after injection. However, the improved wound healing process per se after PBMCsec application might already be decisive for better scar quality. Therefore, a direct comparison of the two application routes is difficult and requires further experiments where PBMCsec is topically applied to already existing scars. Furthermore, other potential treatment options, such as application after laser treatment [67], microneedling [68,69], or in combination with nanocarriers [68] should be tested in future experiments. Most importantly, and in line with the data on mouse scar formation, we also identified a significant anti-fibrotic effect of PBMCsec on human mature hypertrophic scars in explant cultures. In fact, the treatment of scars with PBMCsec in mice and humans showed high similarities. In both species, we found the strongest transcriptome alterations in FB clusters, specifically in genes of the so-called matrisome, which includes collagens, proteoglycans, glycoproteins, and ECM regulators [22–24]. The matrisome, which was recently defined for large-scale *in silico* analyses, provides a comprehensive overview of the components of the ECM [51,70,71]. Although several characteristics of ECM alterations in (hypertrophic) scars have already been described [72], our study provides the first large dataset analyzing changes in the entire matrisome in mice and humans during wound healing and scar formation. These highly valuable datasets could be the basis for many future studies on the pathophysiology of wound healing and scar formation, as well as on the effects of secretome-based scar treatment.

In the present study, we further focused on elastin, which was similarly downregulated by PBMCsec under all conditions and in all species investigated. Elastin fibril sequences interact with microfibrils and bind to cell surface receptors [73]. Elastin is extremely durable and has a half-life of ~70 years [73,74]. While intact elastin is inert and insoluble, it can be degraded by a plethora of elastases [74], including MMPs, aspartic proteases, serine proteases, and cysteine proteases [74]. In our *ex vivo* assays, we found strong degradation of elastic fibers in human skin induced by TGF β , which was completely inhibited by PBMCsec, suggesting an elastase-inhibiting effect of PBMCsec. Intriguingly, this effect of TGF β on elastic fibers appears to be counterintuitive, and we did not find any other study describing this phenomenon. The interaction of TGF β and elastin is complex. TGF β is generally known to induce elastogenesis [47]), stabilize elastin mRNA [47,48]), and increase elastin secretion (Figure 5), which is most likely due to the post-transcriptional control of elastin [47]. This is in line with our *in vitro* findings, as we could show the strong upregulation of elastin production in fibroblasts treated with TGF β . Interestingly, this upregulation was also significantly inhibited by PBMCsec at the mRNA and protein level. So far, we cannot offer an explanation for this phenomenon. It is tempting to speculate that the proteolytic breakdown of elastin triggers the *de novo* synthesis of elastin. Furthermore,

whether the TGF β -induced overproduction of elastin also leads to the assembly of new functional elastic fibers is still not fully understood. Therefore, the mechanisms by which PBMsec inhibits elastin breakdown need further investigations. Interestingly, our in vitro elastase assay showed only weak anti-elastase activity of PBMsec, suggesting that either the specific enzyme inhibited by PBMsec is not detected by the in vitro assay or PBMsec leads to the induction of endogenous protease inhibitors. In line with the second hypothesis, Copic et al. recently showed that PBMsec is indeed able to induce the production of SERPINB2, a serine protease inhibitor, in human mononuclear cells [75]. Furthermore, with scRNAseq, we showed that some elastase inhibitors, such as *PI3* (peptidase inhibitor 3) and *SLPI* (secretory leukocyte protease inhibitor), were significantly upregulated by PBMsec in FBs in scars (Figure 4H). Despite having been well investigated for their beneficial effects in cystic fibrosis [76], these elastase inhibitors have been hardly assessed for their role in cutaneous scar formation so far. Further, more sophisticated experiments are needed to fully address the role of these enzyme inhibitors in scar formation.

Aside from elastin, the only other gene consistently regulated by PBMsec in all three scRNAseq experimental approaches was *TXNIP* (Thioredoxin interacting protein). *TXNIP* is critically involved in the regulation of reactive oxygen species (ROS) and cellular oxidative stress [77] and was shown to contribute to disturbed wound healing under ischemic conditions [78]. With regard to scar formation, *TXNIP* was shown to be elevated in a murine model of pulmonary fibrosis, and the inhibition of *TXNIP* in this model led to the reduction in ROS and myoFB differentiation [79]. The exact role of *TXNIP* in skin pathologies and in scars, however, has been scarcely investigated [80]. Our finding that the downregulation of *TXNIP* was conserved across all our experimental approaches suggests that PBMsec-induced *TXNIP* downregulation might be an important mechanism contributing to the anti-fibrotic action of PBMsec. However, further studies are needed to fully decipher the mechanism of *TXNIP*-regulation as well as its impact on cutaneous scar formation.

Interestingly, PBMsec also prevented FB activation and myoFB differentiation. In line with our results, previous studies showed that treatment of FBs with conditioned medium of mesenchymal or pluripotent stem cells was able to reduce myoFB differentiation [81,82]. In contrast to these studies, we were not able to identify a direct inhibitory action of PBMsec on canonical TGF β /Smad signaling [82]. However, TGF β has been shown to also induce fibrosis via non-canonical (non-SMAD) signaling pathways [83], and blocking non-canonical signaling prevents pro-fibrotic phenotypes [84]. Possible non-canonical pathways might include glycogen synthase kinase-3 β (GSK-3 β) [85], a pathway we previously found to be regulated upon non-SMAD TGF β -mediated abolishment of myoFB differentiation [7]. Hitherto, only few secreted molecules inhibiting non-canonical TGF-signaling have been described. Del-1 (Developmentally-Regulated Endothelial Cell Locus 1 Protein) was shown to inhibit TGF β and attenuate fibrosis by suppressing the α_v integrin-mediated activation of TGF β [86]. In addition, several proteins, such as fibroblast growth factor (FGF), epidermal growth factor (IGF), interferon gamma, and IL-10, all of which are present in PBMsec, are known to inhibit myoFB differentiation [6]. To identify the exact pathway of TGF β inhibition induced by PBMsec, a detailed proteomic approach and the assessment of multiple pathways will be necessary in the future.

As previously discussed [7], there are some limitations to the current study that need to be considered. There are significant differences between the wound healing mechanisms of mice and humans. While mice mainly rely on the contraction of the subcutaneous panniculus carnosus, human wound healing is characterized by the deposition of extracellular matrix (ECM) followed by re-epithelialization [86,87]. However, recent research has shown that both processes contribute to a similar extent in mice [88]. Therefore, mouse wound models may be considered a valid model for human wound healing. However, it is important to note that the current mouse models of scarring do not fully replicate the pathological fibrotic state observed in human hypertrophic scars. Although mouse models for hypertrophic scars have been developed, such as subcutaneous bleomycin injection [89]

and tight-skin mice [90], the comparability of the transcriptome of these models with human hypertrophic scars is not yet fully understood.

In conclusion, we provide an extensive study with multiple experimental approaches and ample scRNAseq data. Comprehensive analyses suggest a solid anti-fibrotic, ECM reducing, and myoFB-inhibiting effect of PBMCsec. We identified the prevention of elastin breakdown as a putative major underlying mechanism of PBMCsec-mediated scar attenuation. We thus propose future clinical assessment of PBMCsec to attenuate skin scarring during wound healing and to treat already existing mature scars [37].

Supplementary Materials: The following supporting information can be downloaded at: <https://www.mdpi.com/article/10.3390/pharmaceutics15041065/s1>, Figure S1: Methods; Figure S2: Quality control of mouse scRNAseq; Figure S3: Top 50 regulated genes per cell group in 'Topical' mouse scars; Figure S4: Top 50 regulated genes per cell group in 6 weeks 'Inject' mouse scars; Figure S5: Quality control of human scRNAseq; Figure S6: Top 50 regulated genes per cell group in human skin; Figure S7: Top 50 regulated genes per cell group in human scar; Figure S8: The interaction of TGFβ and PBMCsec in vivo; Figure S9: Subcluster analysis of FB populations.

Author Contributions: V.V., H.J.A. and M.M., design of the study; V.V., D.C., K.K., M.D. and B.G., data acquisition; V.V., D.C., K.K., M.D., B.G., H.J.A. and M.M., data analyses and interpretation; C.R., H.J.A. and M.M., resources; V.V., D.C., K.K., M.D. and M.M., access to data and data verification; V.V., H.J.A. and M.M., drafting of original manuscript. All authors have read and agreed to the published version of the manuscript.

Funding: This research project was financed in part by the Austrian Research Promotion Agency grant "APOSEC" (852748 and 862068; 2015–2019), in part by Vienna Business Agency "APOSEC to clinic," (2343727; 2018–2020), and in part by Aposcience AG under group leader H.J.A. M.M. was funded by Sparkling Science Program of the Austrian Federal Ministry of Education, Science, and Research (SPA06/055).

Institutional Review Board Statement: The use of healthy abdominal skin (Vote No. 217/2010) and scar tissue (Vote No. 1533/2017) was approved by the Vienna Medical School ethics committee. Animal experiments were approved by the Medical University of Vienna ethics committee and by the Austrian Federal Ministry of Education, Science, and Research (Vote No. BMBWF-66.009/0075-V/3b/2018).

Informed Consent Statement: Informed consent was obtained from all subjects involved in the study.

Data Availability Statement: The scRNAseq data generated in this study have been deposited in the NCBI GEO database under accession numbers GSE156326 and GSE202544. The raw sequencing data are protected and are not available due to data privacy laws. If raw sequencing data are absolutely necessary for the replication or extension of our research, they will be made available upon request to the corresponding author in a 2-week timeframe. All other relevant data supporting the key findings of this study are available within the article and its Supplementary Information files or from the corresponding author upon reasonable request.

Acknowledgments: We thank H.P. Haselsteiner and Karl Fister, head of the CRISCAR Familiens-tiftung, for their faith in this private public partnership to augment basic and translational clinical research. The authors acknowledge the core facilities of Medical University of Vienna, a member of Vienna Life Science Instruments.

Conflicts of Interest: Medical University of Vienna has claimed financial interest. H.J.A. holds patents related to this work (WO2010079086A1; WO2010070105A1; EP3502692A1; WO2021130305A1; EP4074320A1). M.M. holds a patent related to this work (EP4074320A1). V.V., D.C., K.K., M.D., and H.J.A. are affiliated with the company Aposcience AG, a manufacturer of PBMCsec. All other authors declare no potential conflicts of interest.

References

1. Bayat, A.; McGrouther, D.A.; Ferguson, M.W.J. Skin scarring. *BMJ* **2003**, *326*, 88–92. [[CrossRef](#)]
2. Gauglitz, G.G.; Korting, H.C.; Pavicic, T.; Ruzicka, T.; Jeschke, M.G. Hypertrophic scarring and keloids: Pathomechanisms and current and emerging treatment strategies. *Mol. Med.* **2011**, *17*, 113–125. [[CrossRef](#)]

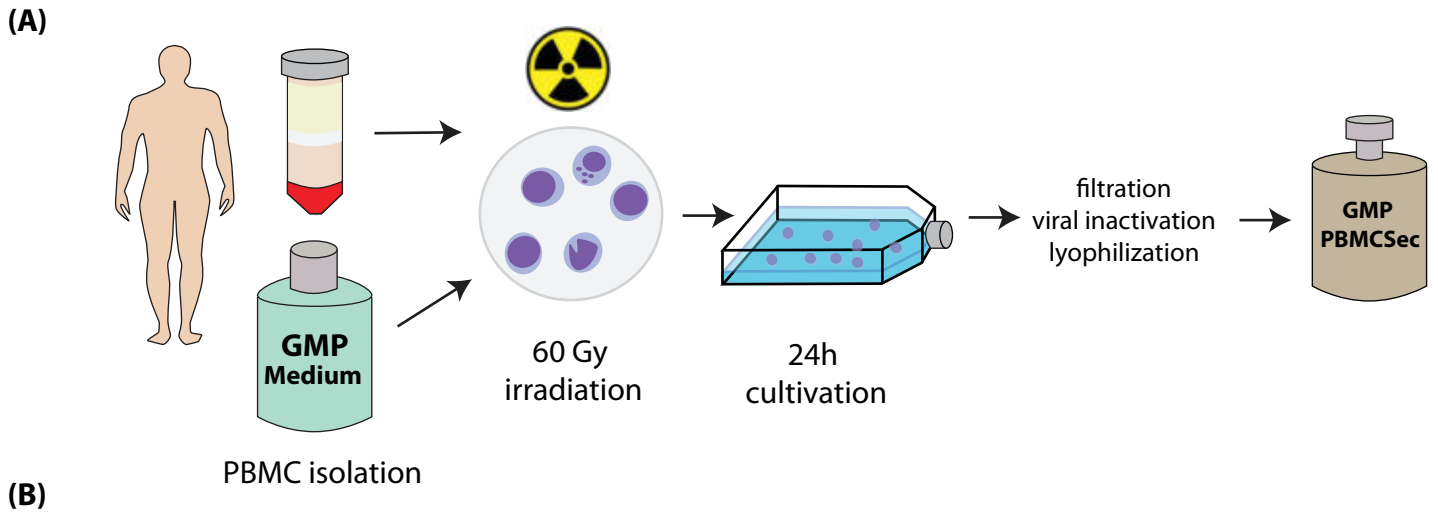
3. Bock, O.; Schmid-Ott, G.; Malewski, P.; Mrowietz, U. Quality of life of patients with keloid and hypertrophic scarring. *Arch. Dermatol. Res.* **2006**, *297*, 433–438. [[CrossRef](#)]
4. Van Loey, N.E.; Bremer, M.; Faber, A.W.; Middelkoop, E.; Nieuwenhuis, M.K. Itching following burns: Epidemiology and predictors. *Br. J. Dermatol.* **2008**, *158*, 95–100. [[CrossRef](#)]
5. Jiang, D.; Rinkevich, Y. Scars or regeneration?-dermal fibroblasts as drivers of diverse skin wound responses. *Int. J. Mol. Sci.* **2020**, *21*, 617. [[CrossRef](#)] [[PubMed](#)]
6. Karppinen, S.M.; Heljasvaara, R.; Gullberg, D.; Tasanen, K.; Pihlajaniemi, T. Toward understanding scarless skin wound healing and pathological scarring. *F1000Research* **2019**, *8*, 787. [[CrossRef](#)] [[PubMed](#)]
7. Vorstandlechner, V.; Laggner, M.; Copic, D.; Klas, K.; Direder, M.; Chen, Y.; Golabi, B.; Haslik, W.; Radtke, C.; Tschachler, E.; et al. The serine proteases dipeptidyl-peptidase 4 and urokinase are key molecules in human and mouse scar formation. *Nat. Commun.* **2021**, *12*, 6242. [[CrossRef](#)] [[PubMed](#)]
8. Sidgwick, G.P.; McGeorge, D.; Bayat, A. A comprehensive evidence-based review on the role of topicals and dressings in the management of skin scarring. *Arch. Dermatol. Res.* **2015**, *307*, 461–477. [[CrossRef](#)]
9. Takeo, M.; Lee, W.; Ito, M. Wound healing and skin regeneration. *Cold Spring Harb. Perspect. Med.* **2015**, *5*, a023267. [[CrossRef](#)]
10. Mack, M. Inflammation and fibrosis. *Matrix Biol.* **2018**, *68–69*, 106–121. [[CrossRef](#)] [[PubMed](#)]
11. Gurtner, G.C.; Werner, S.; Barrandon, Y.; Longaker, M.T. Wound repair and regeneration. *Nature* **2008**, *453*, 314–321. [[CrossRef](#)]
12. Nabai, L.; Pourghadiri, A.; Ghahary, A. Hypertrophic scarring: Current knowledge of predisposing factors, cellular and molecular mechanisms. *J. Burn. Care Res.* **2020**, *41*, 48–56. [[CrossRef](#)]
13. Lee, H.J.; Jang, Y.J. Recent understandings of biology, prophylaxis and treatment strategies for hypertrophic scars and keloids. *Int. J. Mol. Sci.* **2018**, *19*, 711. [[CrossRef](#)] [[PubMed](#)]
14. Anthonissen, M.; Daly, D.; Janssens, T.; Van den Kerckhove, E. The effects of conservative treatments on burn scars: A systematic review. *Burns* **2016**, *42*, 508–518. [[CrossRef](#)]
15. Kafka, M.; Collins, V.; Kamolz, L.P.; Rappl, T.; Branski, L.K.; Wurzer, P. Evidence of invasive and noninvasive treatment modalities for hypertrophic scars: A systematic review. *Wound Repair Regen.* **2017**, *25*, 139–144. [[CrossRef](#)] [[PubMed](#)]
16. Bao, Y.; Xu, S.; Pan, Z.; Deng, J.; Li, X.; Pan, F. Comparative efficacy and safety of common therapies in keloids and hypertrophic scars: A systematic review and meta-analysis. *Aesthetic Plast. Surg.* **2019**, *44*, 207–218. [[CrossRef](#)] [[PubMed](#)]
17. Sato, C.; Yamamoto, Y.; Funayama, E.; Furukawa, H.; Oyama, A.; Murao, N.; Hosono, H.; Kawakubo, K.; Sakamoto, N.; Ohnishi, S. Conditioned medium obtained from amnion-derived mesenchymal stem cell culture prevents activation of keloid fibroblasts. *Plast. Reconstr. Surg.* **2018**, *141*, 390–398. [[CrossRef](#)] [[PubMed](#)]
18. Chen, J.; Li, Z.; Huang, Z.; Liang, L.; Chen, M. Chyle fat-derived stem cells conditioned medium inhibits hypertrophic scar fibroblast activity. *Ann. Plast. Surg.* **2019**, *83*, 271–277. [[CrossRef](#)]
19. Hu, C.H.; Tseng, Y.W.; Chiou, C.Y.; Lan, K.C.; Chou, C.H.; Tai, C.S.; Huang, H.D.; Hu, C.W.; Liao, K.H.; Chuang, S.S.; et al. Bone marrow concentrate-induced mesenchymal stem cell conditioned medium facilitates wound healing and prevents hypertrophic scar formation in a rabbit ear model. *Stem Cell Res. Ther.* **2019**, *10*, 275. [[CrossRef](#)]
20. Ren, Y.; Deng, C.L.; Wan, W.D.; Zheng, J.H.; Mao, G.Y.; Yang, S.L. Suppressive effects of induced pluripotent stem cell-conditioned medium on in vitro hypertrophic scarring fibroblast activation. *Mol. Med. Rep.* **2015**, *11*, 2471–2476. [[CrossRef](#)]
21. Kanji, S.; Das, H. Advances of stem cell therapeutics in cutaneous wound healing and regeneration. *Mediat. Inflamm.* **2017**, *2017*, 5217967. [[CrossRef](#)] [[PubMed](#)]
22. Bojanic, C.; To, K. Mesenchymal stem cell therapy in hypertrophic and keloid scars. *Cell Tissue Res.* **2021**, *383*, 915–930. [[CrossRef](#)] [[PubMed](#)]
23. Beer, L.; Mildner, M.; Ankersmit, H.J. Cell secretome based drug substances in regenerative medicine: When regulatory affairs meet basic science. *Ann. Transl. Med.* **2017**, *5*, 170. [[CrossRef](#)]
24. Korf-Klingebiel, M.; Kempf, T.; Sauer, T.; Brinkmann, E.; Fischer, P.; Meyer, G.P.; Ganser, A.; Drexler, H.; Wollert, K.C. Bone marrow cells are a rich source of growth factors and cytokines: Implications for cell therapy trials after myocardial infarction. *Eur. Heart J.* **2008**, *29*, 2851–2858. [[CrossRef](#)] [[PubMed](#)]
25. Mildner, M.; Hacker, S.; Haider, T.; Gschwandtner, M.; Werba, G.; Barresi, C.; Zimmermann, M.; Golabi, B.; Tschachler, E.; Ankersmit, H.J. Secretome of peripheral blood mononuclear cells enhances wound healing. *PLoS ONE* **2013**, *8*, e60103. [[CrossRef](#)]
26. Wagner, T.; Traxler, D.; Simader, E.; Beer, L.; Narzt, M.-S.; Gruber, F.; Madlener, S.; Laggner, M.; Erb, M.; Vorstandlechner, V.; et al. Different pro-angiogenic potential of γ -irradiated pbmc-derived secretome and its subfractions. *Sci. Rep.* **2018**, *8*, 18016. [[CrossRef](#)]
27. Hacker, S.; Mittermayr, R.; Nickl, S.; Haider, T.; Lebherz-Eichinger, D.; Beer, L.; Mitterbauer, A.; Leiss, H.; Zimmermann, M.; Schweiger, T.; et al. Paracrine factors from irradiated peripheral blood mononuclear cells improve skin regeneration and angiogenesis in a porcine burn model. *Sci. Rep.* **2016**, *6*, 25168. [[CrossRef](#)] [[PubMed](#)]
28. Simader, E.; Beer, L.; Laggner, M.; Vorstandlechner, V.; Gugerell, A.; Erb, M.; Kalinina, P.; Copic, D.; Moser, D.; Spittler, A.; et al. Tissue-regenerative potential of the secretome of gamma-irradiated peripheral blood mononuclear cells is mediated via tnfrsf1b-induced necroptosis. *Cell Death Dis.* **2019**, *10*, 729. [[CrossRef](#)]

29. Hoetzenecker, K.; Assinger, A.; Lichtenauer, M.; Mildner, M.; Schweiger, T.; Starlinger, P.; Jakab, A.; Berényi, E.; Pavo, N.; Zimmermann, M.; et al. Secretome of apoptotic peripheral blood cells (aposec) attenuates microvascular obstruction in a porcine closed chest reperfused acute myocardial infarction model: Role of platelet aggregation and vasodilation. *Basic Res. Cardiol.* **2012**, *107*, 292. [[CrossRef](#)]
30. Kasiri, M.M.; Beer, L.; Nemeč, L.; Gruber, F.; Pietkiewicz, S.; Haider, T.; Simader, E.M.; Traxler, D.; Schweiger, T.; Janik, S.; et al. Dying blood mononuclear cell secretome exerts antimicrobial activity. *Eur. J. Clin. Investig.* **2016**, *46*, 853–863. [[CrossRef](#)]
31. Altmann, P.; Mildner, M.; Haider, T.; Traxler, D.; Beer, L.; Ristl, R.; Golabi, B.; Gabriel, C.; Leutmezer, F.; Ankersmit, H.J. Secretomes of apoptotic mononuclear cells ameliorate neurological damage in rats with focal ischemia. *F1000Research* **2014**, *3*, 131. [[CrossRef](#)] [[PubMed](#)]
32. Haider, T.; Hoftberger, R.; Ruger, B.; Mildner, M.; Blumer, R.; Mitterbauer, A.; Buchacher, T.; Sherif, C.; Altmann, P.; Redl, H.; et al. The secretome of apoptotic human peripheral blood mononuclear cells attenuates secondary damage following spinal cord injury in rats. *Exp. Neurol.* **2015**, *267*, 230–242. [[CrossRef](#)]
33. Ankersmit, H.J.; Hoetzenecker, K.; Dietl, W.; Soleiman, A.; Horvat, R.; Wolfsberger, M.; Gerner, C.; Hacker, S.; Mildner, M.; Moser, B.; et al. Irradiated cultured apoptotic peripheral blood mononuclear cells regenerate infarcted myocardium. *Eur. J. Clin. Investig.* **2009**, *39*, 445–456. [[CrossRef](#)] [[PubMed](#)]
34. Laggner, M.; Acosta, G.S.; Kitzmüller, C.; Copic, D.; Gruber, F.; Altenburger, L.M.; Vorstandlechner, V.; Gugerell, A.; Direder, M.; Klas, K.; et al. The secretome of irradiated peripheral blood mononuclear cells attenuates activation of mast cells and basophils. *EBioMedicine* **2022**, *81*, 104093. [[CrossRef](#)] [[PubMed](#)]
35. Laggner, M.; Copic, D.; Nemeč, L.; Vorstandlechner, V.; Gugerell, A.; Gruber, F.; Peterbauer, A.; Ankersmit, H.J.; Mildner, M. Therapeutic potential of lipids obtained from γ -irradiated pbmcs in dendritic cell-mediated skin inflammation. *EBioMedicine* **2020**, *55*, 102774. [[CrossRef](#)]
36. Simader, E.; Traxler, D. Safety and tolerability of topically administered autologous, apoptotic pbmc secretome (APOSEC) in dermal wounds: A randomized phase 1 trial (MARSYAS I). *Sci. Rep.* **2017**, *7*, 6216. [[CrossRef](#)]
37. Gugerell, A.; Gouya-Lechner, G.; Hofbauer, H.; Laggner, M.; Trautinger, F.; Almer, G.; Peterbauer-Scherb, A.; Seibold, M.; Hoetzenecker, W.; Dreschl, C.; et al. Safety and clinical efficacy of the secretome of stressed peripheral blood mononuclear cells in patients with diabetic foot ulcer—Study protocol of the randomized, placebo-controlled, double-blind, multicenter, international phase ii clinical trial marsyas ii. *Trials* **2021**, *22*, 10.
38. Fearmonti, R.M.; Bond, J.E.; Erdmann, D.; Levin, L.S.; Pizzo, S.V.; Levinson, H. The modified patient and observer scar assessment scale: A novel approach to defining pathologic and nonpathologic scarring. *Plast. Reconstr. Surg.* **2011**, *127*, 242–247. [[CrossRef](#)]
39. Laggner, M.; Gugerell, A.; Bachmann, C.; Hofbauer, H.; Vorstandlechner, V.; Seibold, M.; Gouya Lechner, G.; Peterbauer, A.; Madlener, S.; Demyanets, S.; et al. Reproducibility of gmp-compliant production of therapeutic stressed peripheral blood mononuclear cell-derived secretomes, a novel class of biological medicinal products. *Stem Cell Res. Ther.* **2020**, *11*, 9. [[CrossRef](#)]
40. Gugerell, A.; Sorgenfrey, D.; Laggner, M.; Raimann, J.; Peterbauer, A.; Bormann, D.; Suessner, S.; Gabriel, C.; Moser, B.; Ostler, T.; et al. Viral safety of aposec. *Blood Transfus.* **2019**, *18*, 30–39.
41. Stuart, T.; Butler, A.; Hoffman, P.; Hafemeister, C.; Papalexi, E.; Mauck, W.M., 3rd; Hao, Y.; Stoeckius, M.; Smibert, P.; Satija, R. Comprehensive integration of single-cell data. *Cell* **2019**, *177*, 1888–1902.e1821. [[CrossRef](#)]
42. Butler, A.; Hoffman, P.; Smibert, P.; Papalexi, E.; Satija, R. Integrating single-cell transcriptomic data across different conditions, technologies, and species. *Nat. Biotechnol.* **2018**, *36*, 411. [[CrossRef](#)] [[PubMed](#)]
43. Macosko, E.Z.; Basu, A.; Satija, R.; Nemeš, J.; Shekhar, K.; Goldman, M.; Tirosh, I.; Bialas, A.R.; Kamitaki, N.; Martersteck, E.M.; et al. Highly parallel genome-wide expression profiling of individual cells using nanoliter droplets. *Cell* **2015**, *161*, 1202–1214. [[CrossRef](#)]
44. Luecken, M.D.; Theis, F.J. Current best practices in single-cell rna-seq analysis: A tutorial. *Mol. Syst. Biol.* **2019**, *15*, e8746. [[CrossRef](#)]
45. Rojahn, T.B.; Vorstandlechner, V.; Krausgruber, T.; Bauer, W.M.; Alkon, N.; Bangert, C.; Thaler, F.M.; Sadeghyar, F.; Fortelny, N.; Gernedl, V.; et al. Single-cell transcriptomics combined with interstitial fluid proteomics defines cell type-specific immune regulation in atopic dermatitis. *J. Allergy Clin. Immunol.* **2020**, *146*, 1056–1069. [[CrossRef](#)]
46. Hammond, T.R.; Dufort, C.; Dissing-Olesen, L.; Giera, S.; Young, A.; Wysoker, A.; Walker, A.J.; Gergits, F.; Segel, M.; Nemeš, J.; et al. Single-cell rna sequencing of microglia throughout the mouse lifespan and in the injured brain reveals complex cell-state changes. *Immunity* **2019**, *50*, 253–271.e256. [[CrossRef](#)]
47. Subramanian, A.; Tamayo, P.; Mootha, V.K.; Mukherjee, S.; Ebert, B.L.; Gillette, M.A.; Paulovich, A.; Pomeroy, S.L.; Golub, T.R.; Lander, E.S.; et al. Gene set enrichment analysis: A knowledge-based approach for interpreting genome-wide expression profiles. *Proc. Natl. Acad. Sci. USA* **2005**, *102*, 15545–15550. [[CrossRef](#)] [[PubMed](#)]
48. Tabib, T.; Morse, C.; Wang, T.; Chen, W.; Lafyatis, R. Sfrp2/dpp4 and fmo1/lsp1 define major fibroblast populations in human skin. *J. Invest. Dermatol.* **2017**, *138*, 802–810. [[CrossRef](#)]
49. Zhang, S.; Zhang, Y.; Min, P. Single-cell and bulk transcriptome data integration reveals dysfunctional cell types and aberrantly expressed genes in hypertrophic scar. *Front. Genet.* **2021**, *12*, 806740. [[CrossRef](#)]
50. Ma, L.; Gan, C.; Huang, Y.; Wang, Y.; Luo, G.; Wu, J. Comparative proteomic analysis of extracellular matrix proteins secreted by hypertrophic scar with normal skin fibroblasts. *Burn. Trauma* **2014**, *2*, 76–83.

51. Naba, A.; Clauser, K.R.; Ding, H.; Whittaker, C.A.; Carr, S.A.; Hynes, R.O. The extracellular matrix: Tools and insights for the “omics” era. *Matrix Biol.* **2016**, *49*, 10–24. [[CrossRef](#)] [[PubMed](#)]
52. Direder, M.; Weiss, T.; Copic, D.; Vorstandlechner, V.; Laggner, M.; Pfisterer, K.; Mildner, C.S.; Klas, K.; Bormann, D.; Haslik, W.; et al. Schwann cells contribute to keloid formation. *Matrix Biol.* **2022**, *108*, 55–76. [[CrossRef](#)] [[PubMed](#)]
53. Thielitz, A.; Vetter, R.W.; Schultze, B.; Wrenger, S.; Simeoni, L.; Ansorge, S.; Neubert, K.; Faust, J.; Lindenlaub, P.; Gollnick, H.P.; et al. Inhibitors of dipeptidyl peptidase iv-like activity mediate antifibrotic effects in normal and keloid-derived skin fibroblasts. *J. Investig. Dermatol.* **2008**, *128*, 855–866. [[CrossRef](#)]
54. Hinz, B. Myofibroblasts. *Exp. Eye Res.* **2016**, *142*, 56–70. [[CrossRef](#)] [[PubMed](#)]
55. Zhang, X.; Alanazi, Y.F. Elastic fibre proteins in elastogenesis and wound healing. *Int. J. Mol. Sci.* **2022**, *23*, 4087. [[CrossRef](#)]
56. Khan, Z.; Marshall, J.F. The role of integrins in $\text{tgf}\beta$ activation in the tumour stroma. *Cell Tissue Res.* **2016**, *365*, 657–673. [[CrossRef](#)] [[PubMed](#)]
57. Su, C.T.; Urban, Z. *Ltp4* in health and disease. *Genes* **2021**, *12*, 795. [[CrossRef](#)] [[PubMed](#)]
58. Godwin, A.R.F.; Singh, M.; Lockhart-Cairns, M.P.; Alanazi, Y.F.; Cain, S.A.; Baldock, C. The role of fibrillin and microfibril binding proteins in elastin and elastic fibre assembly. *Matrix Biol.* **2019**, *84*, 17–30. [[CrossRef](#)]
59. Lu, J.; Liu, Q.; Wang, L.; Tu, W.; Chu, H.; Ding, W.; Jiang, S.; Ma, Y.; Shi, X.; Pu, W.; et al. Increased expression of latent $\text{tgf}\beta$ -binding protein 4 affects the fibrotic process in scleroderma by $\text{tgf}\beta$ /smad signaling. *Lab. Investig.* **2017**, *97*, 591–601. [[CrossRef](#)]
60. Buczek-Thomas, J.A.; Lucey, E.C.; Stone, P.J.; Chu, C.L.; Rich, C.B.; Carreras, I.; Goldstein, R.H.; Foster, J.A.; Nugent, M.A. Elastase mediates the release of growth factors from lung in vivo. *Am. J. Respir. Cell Mol. Biol.* **2004**, *31*, 344–350. [[CrossRef](#)]
61. Arjunan, S.; Gan, S.U.; Choolani, M.; Raj, V.; Lim, J.; Biswas, A.; Bongso, A.; Fong, C.Y. Inhibition of growth of asian keloid cells with human umbilical cord wharton’s jelly stem cell-conditioned medium. *Stem Cell Res. Ther.* **2020**, *11*, 78. [[CrossRef](#)]
62. Hu, C.H.; Tseng, Y.W.; Lee, C.W.; Chiou, C.Y.; Chuang, S.S.; Yang, J.Y.; Lee, O.K. Combination of mesenchymal stem cell-conditioned medium and botulinum toxin type a for treating human hypertrophic scars. *J. Plast. Reconstr. Aesthetic Surg.* **2020**, *73*, 516–527. [[CrossRef](#)] [[PubMed](#)]
63. Liu, J.; Ren, J.; Su, L.; Cheng, S.; Zhou, J.; Ye, X.; Dong, Y.; Sun, S.; Qi, F.; Liu, Z.; et al. Human adipose tissue-derived stem cells inhibit the activity of keloid fibroblasts and fibrosis in a keloid model by paracrine signaling. *Burns* **2018**, *44*, 370–385. [[CrossRef](#)] [[PubMed](#)]
64. Mahmoudi, S.; Mancini, E.; Xu, L.; Moore, A.; Jahanbani, F.; Hebestreit, K.; Srinivasan, R.; Li, X.; Devarajan, K.; Prélôt, L.; et al. Heterogeneity in old fibroblasts is linked to variability in reprogramming and wound healing. *Nature* **2019**, *574*, 553–558. [[CrossRef](#)]
65. Solé-Boldo, L.; Raddatz, G.; Schütz, S.; Mallm, J.-P.; Rippe, K.; Lonsdorf, A.S.; Rodríguez-Paredes, M.; Lyko, F. Single-cell transcriptomes of the human skin reveal age-related loss of fibroblast priming. *Commun. Biol.* **2020**, *3*, 188. [[CrossRef](#)]
66. Joost, S.; Annusver, K.; Jacob, T.; Sun, X.; Dalessandri, T.; Sivan, U.; Sequeira, I.; Sandberg, R.; Kasper, M. The molecular anatomy of mouse skin during hair growth and rest. *Cell Stem Cell* **2020**, *26*, 441–457. [[CrossRef](#)]
67. Hsiao, C.Y.; Yang, S.C.; Alalaiwe, A.; Fang, J.Y. Laser ablation and topical drug delivery: A review of recent advances. *Expert Opin. Drug Deliv.* **2019**, *16*, 937–952. [[CrossRef](#)] [[PubMed](#)]
68. Aich, K.; Singh, T.; Dang, S. Advances in microneedle-based transdermal delivery for drugs and peptides. *Drug Deliv. Transl. Res.* **2022**, *12*, 1556–1568. [[CrossRef](#)]
69. Qu, F.; Geng, R.; Liu, Y.; Zhu, J. Advanced nanocarrier- and microneedle-based transdermal drug delivery strategies for skin diseases treatment. *Theranostics* **2022**, *12*, 3372–3406. [[CrossRef](#)]
70. Naba, A.; Clauser, K.R.; Hoersch, S.; Liu, H.; Carr, S.A.; Hynes, R.O. The matrisome: In silico definition and in vivo characterization by proteomics of normal and tumor extracellular matrices. *Mol. Cell. Proteom.* **2012**, *11*, M111.014647. [[CrossRef](#)]
71. Tellman, T.V.; Dede, M.; Aggarwal, V.A.; Salmon, D.; Naba, A.; Farach-Carson, M.C. Systematic analysis of actively transcribed core matrisome genes across tissues and cell phenotypes. *Matrix Biol.* **2022**, *111*, 95–107. [[CrossRef](#)]
72. The biology of extracellular matrix proteins in hypertrophic scarring. *Adv. Wound Care* **2022**, *11*, 234–254. [[CrossRef](#)] [[PubMed](#)]
73. Mithieux, S.M.; Weiss, A.S. Elastin. *Adv. Protein Chem.* **2005**, *70*, 437–461. [[PubMed](#)]
74. Heinz, A. Elastases and elastokines: Elastin degradation and its significance in health and disease. *Crit. Rev. Biochem. Mol. Biol.* **2020**, *55*, 252–273. [[CrossRef](#)]
75. Copic, D.; Direder, M.; Schossleitner, K.; Laggner, M.; Klas, K.; Bormann, D.; Ankersmit, H.J.; Mildner, M. Paracrine factors of stressed peripheral blood mononuclear cells activate proangiogenic and anti-proteolytic processes in whole blood cells and protect the endothelial barrier. *Pharmaceutics* **2022**, *14*, 1600. [[CrossRef](#)] [[PubMed](#)]
76. Zani, M.L.; Tanga, A.; Saidi, A.; Serrano, H.; Dallet-Choisy, S.; Baranger, K.; Moreau, T. Slpi and trappin-2 as therapeutic agents to target airway serine proteases in inflammatory lung diseases: Current and future directions. *Biochem. Soc. Trans.* **2011**, *39*, 1441–1446. [[CrossRef](#)]
77. Zhou, J.; Chng, W.J. Roles of thioredoxin binding protein (TXNIP) in oxidative stress, apoptosis and cancer. *Mitochondrion* **2013**, *13*, 163–169. [[CrossRef](#)]
78. Saad, I.; Fournier, C.T.; Wilson, R.L.; Lakshmanan, R.; Selvaraju, V.; Thirunavukkarasu, M.; Alexander Palesty, J.; McFadden, D.W.; Maulik, N. Thioredoxin-1 augments wound healing and promote angiogenesis in a murine ischemic full-thickness wound model. *Surgery* **2018**, *164*, 1077–1086. [[CrossRef](#)]

79. Han, Y.Y.; Gu, X.; Yang, C.Y.; Ji, H.M.; Lan, Y.J.; Bi, Y.Q.; Si, R.; Qu, J.; Cheng, M.H.; Gao, J. Protective effect of dimethyl itaconate against fibroblast-myofibroblast differentiation during pulmonary fibrosis by inhibiting TXNIP. *J. Cell. Physiol.* **2021**, *236*, 7734–7744. [[CrossRef](#)]
80. Hsiao, P.F.; Huang, Y.T.; Lu, P.H.; Chiu, L.Y.; Weng, T.H.; Hung, C.F.; Wu, N.L. Thioredoxin-interacting protein regulates keratinocyte differentiation: Implication of its role in psoriasis. *FASEB J.* **2022**, *36*, e22313. [[CrossRef](#)]
81. Popova, A.P.; Bozyk, P.D.; Goldsmith, A.M.; Linn, M.J.; Lei, J.; Bentley, J.K.; Hershenson, M.B. Autocrine production of tgf-beta1 promotes myofibroblastic differentiation of neonatal lung mesenchymal stem cells. *Am. J. Physiol. Lung Cell. Mol. Physiol.* **2010**, *298*, L735–L743. [[CrossRef](#)]
82. Zhou, Y.; Zhang, Q.; Gao, Y.; Tan, M.; Zheng, R.; Zhao, L.; Zhang, X. Induced pluripotent stem cell-conditioned medium suppresses pulmonary fibroblast-to-myofibroblast differentiation via the inhibition of tgf-β1/smad pathway. *Int. J. Mol. Med.* **2018**, *41*, 473–484. [[CrossRef](#)] [[PubMed](#)]
83. Meng, X.M.; Nikolic-Paterson, D.J.; Lan, H.Y. Tgf-β: The master regulator of fibrosis. *Nat. Rev. Nephrol.* **2016**, *12*, 325–338. [[CrossRef](#)] [[PubMed](#)]
84. Akboua, H.; Eghbalzadeh, K.; Keser, U.; Wahlers, T.; Paunel-Görgülü, A. Impaired non-canonical transforming growth factor-β signalling prevents profibrotic phenotypes in cultured peptidylarginine deiminase 4-deficient murine cardiac fibroblasts. *J. Cell. Mol. Med.* **2021**, *25*, 9674–9684. [[CrossRef](#)]
85. Kim, D.-Y.; Lee, S.-H.; Fu, Y.; Jing, F.; Kim, W.-Y.; Hong, S.-B.; Song, J.-A.; Choe, H.; Ryu, H.J.; Kim, M.; et al. Del-1, an endogenous inhibitor of tgf-β activation, attenuates fibrosis. *Front. Immunol.* **2020**, *11*, 68. [[CrossRef](#)] [[PubMed](#)]
86. Zomer, H.D.; Trentin, A.G. Skin wound healing in humans and mice: Challenges in translational research. *J. Dermatol. Sci.* **2018**, *90*, 3–12. [[CrossRef](#)]
87. Eming, S.A.; Martin, P.; Tomic-Canic, M. Wound repair and regeneration: Mechanisms, signaling, and translation. *Sci. Transl. Med.* **2014**, *6*, 265sr6. [[CrossRef](#)]
88. Chen, L.; Mirza, R.; Kwon, Y.; DiPietro, L.A.; Koh, T.J. The murine excisional wound model: Contraction revisited. *Wound Repair Regen.* **2015**, *23*, 874–877. [[CrossRef](#)]
89. Cameron, A.M.; Adams, D.H.; Greenwood, J.E.; Anderson, P.J.; Cowin, A.J. A novel murine model of hypertrophic scarring using subcutaneous infusion of bleomycin. *Plast. Reconstr. Surg.* **2014**, *133*, 69–78. [[CrossRef](#)]
90. Seo, B.F.; Lee, J.Y.; Jung, S.N. Models of abnormal scarring. *BioMed Res. Int.* **2013**, *2013*, 423147. [[CrossRef](#)]

Disclaimer/Publisher’s Note: The statements, opinions and data contained in all publications are solely those of the individual author(s) and contributor(s) and not of MDPI and/or the editor(s). MDPI and/or the editor(s) disclaim responsibility for any injury to people or property resulting from any ideas, methods, instructions or products referred to in the content.



Target	Supplier	Product Nr.	Host species	Dilution	Application
GAPDH	abcam	ab8245	mouse monoclonal	1:10000	WB
Collagen I	abcam	ab34710	rabbit polyclonal	1:200	IF
Collagen III	abcam	ab7778	rabbit polyclonal	1:200	IF
Elastin	Merck	Mab2503	mouse monoclonal	1:100	IF, WB
Alexa fluor® 546 anti-mouse IgG (H + L)	Invitrogen	A-11030	goat polyclonal	1:500	IF, 2nd step
Alexa fluor® 546 anti-rabbit IgG (H + L)	Invitrogen	A-11035	goat polyclonal	1:500	IF, 2nd step
Anti-mouse, HRP-conjugated	GE Healthcar	GENX-A931	goat polyclonal	1:10 000	WB, 2nd step
Anti-rabbit, HRP-conjugated	Bio-Rad	#1706511	goat polyclonal	1:10 000	WB, 2nd step

Figure S1: Methods

A) Workflow of GMP-PBMCsec-production: leukocyte cones are obtained as blood-donation by-product, PBMCs are isolated by Ficoll-centrifugation, cells are irradiated with 60Gy and incubated for 24h. Superantatants are filtrated and lyophilized, and off-the-shelf PBMCsec is stored at -20° until use.

B) Table of antibodies used. IF = immunofluorescence, WB = western blot

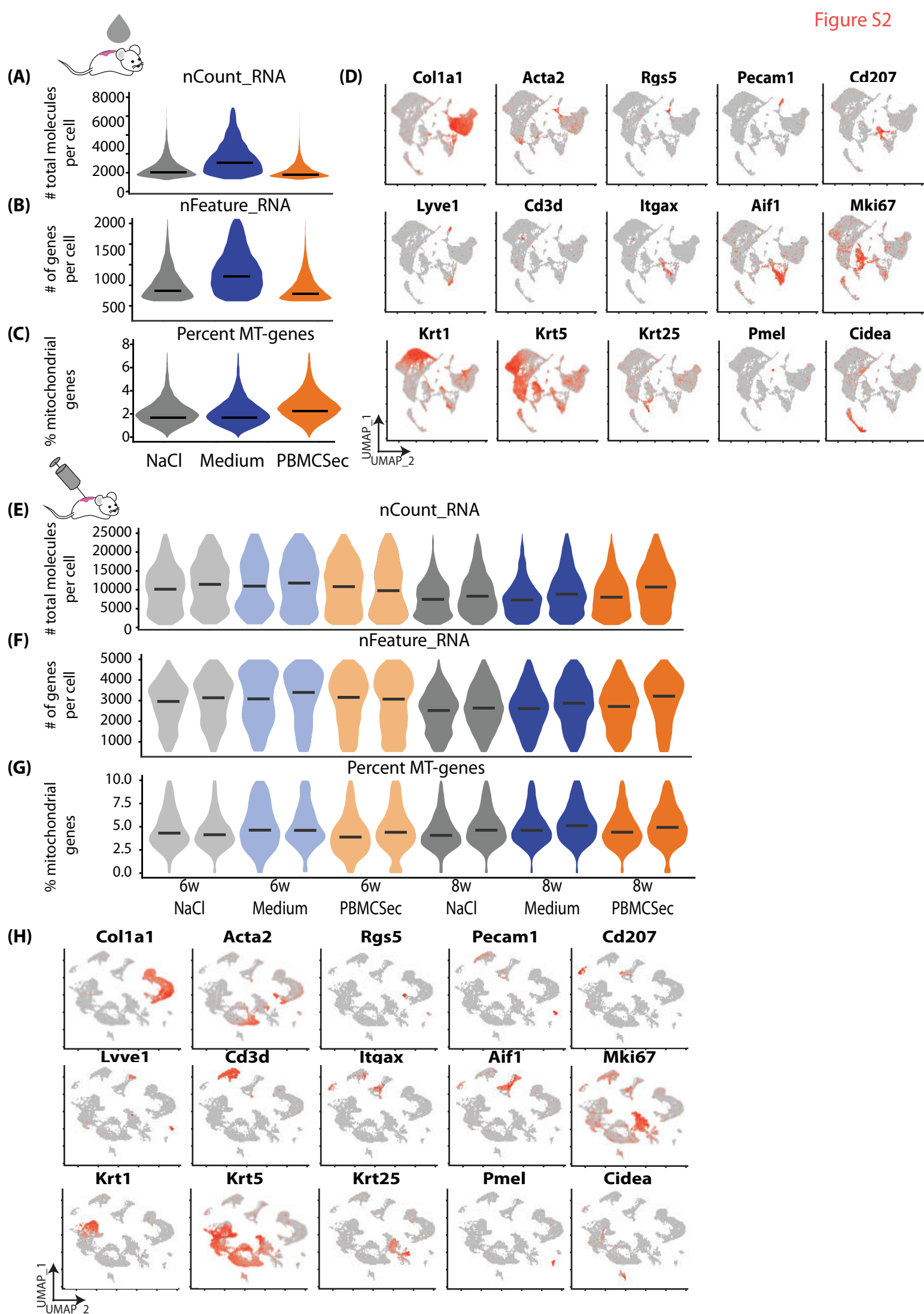


Figure S2: Quality control of mouse scRNAseq

A-C, E-G) Violin plots of quality control parameters of the 'topical' and 'inject' dataset. A, E) total molecules per cell B, F) (gene count per cell and C, G) mitochondrial gene content. D, H) Feature Plots of cluster markers for cluster identification in the 'topical' and 'inject' dataset: *Col1a1* (collagen I alpha 1) for fibroblasts, *Acta2* (smooth muscle actin) for smooth muscle cells and myofibroblasts, *Rgs5* (Regulator Of G Protein Signaling 5) for pericytes, *Pecam* (Platelet And Endothelial Cell Adhesion Molecule 1) for endothelial cells, *Lyve1* (Lymphatic Vessel Endothelial Hyaluronan Receptor 1) for lymphatic endothelial cells, *Cd207* (Langerin) for Langerhans cells, *Cd3d* (cluster of differentiation 3D) for T-cells, *Itgax* for dendritic cells, *Aif1* (allograft inflammatory factor 1) for macrophages, *Mki67* (Marker Of Proliferation Ki-67) for proliferating cells, *Krt1* (Keratin1) for spinous and granular keratinocytes (KCs), *Krt5* (Keratin 5) for basal KCs, *Krt25* (Keratin 25) for hair follicles, *Pmel* (Premelanosome Protein) for melanocytes, *Cidea* (Cell Death Inducing DFFA Like Effector A) for adipocytes. Vertical lines in violin plots represent maximum expression, shape of each violin represents all results, and width of each violin represents frequency of cells at the respective expression level. In feature plots, normalized log expression of the respective gene is mapped onto the UMAP-plot. Color intensity indicates level of gene expressions. UMAP, uniform manifold approximation and projection.

Figure S3: Top 50 regulated genes per cell group in 'Topical' mouse scars

In A) fibroblasts (FBs, red circles), B) smooth muscle cells and pericytes (SMC/PCs, purple), C) endothelial cells (ECs, blue), D) T-cells (dark green), E) dendritic cells and macrophages (DCs, light green), and keratinocytes (KCs, yellow), hair follicles (HF, beige), melanocytes (Mel, brown), adipocytes (Adipo, grey); differentially expressed genes (DEGs) were calculated comparing 'PBMCsec' mouse scars to 'NaCl'-mouse scars, using Wilcoxon rank sum test, including genes with average logarithmic fold change (avglogFC) of > 0.1 or < -0.1 and Bonferroni-adjusted p-value < 0.05 . For each cellgroup, top 50 DEGs according to lowest adjusted p-value are displayed, split by treatment. Dot size represents percent of cells expressing the respective gene, color correlates with average expression.

Figure S4: Top 50 regulated genes per cell group in 6 weeks 'Inject' mouse scars

In A) fibroblasts (FBs, red circles), B) smooth muscle cells and pericytes (SMC/PCs, purple), C) endothelial cells (ECs, blue), D) T-cells (dark green), E) dendritic cells and macrophages (DCs, light green), and keratinocytes (KCs, yellow), hair follicles (HF, beige), melanocytes (Mel, brown), adipocytes (Adipo, grey); differentially expressed genes (DEGs) were calculated comparing 'PBMCsec' mouse scars to 'NaCl'-mouse scars, using Wilcoxon rank sum test, including genes with average logarithmic fold change (avglogFC) of > 0.1 or < -0.1 and Bonferroni-adjusted p-value < 0.05 . For each cellgroup, top 50 DEGs according to lowest adjusted p-value are displayed, split by treatment and timepoint. Dot size represents percent of cells expressing the respective gene, color correlates with average expression.

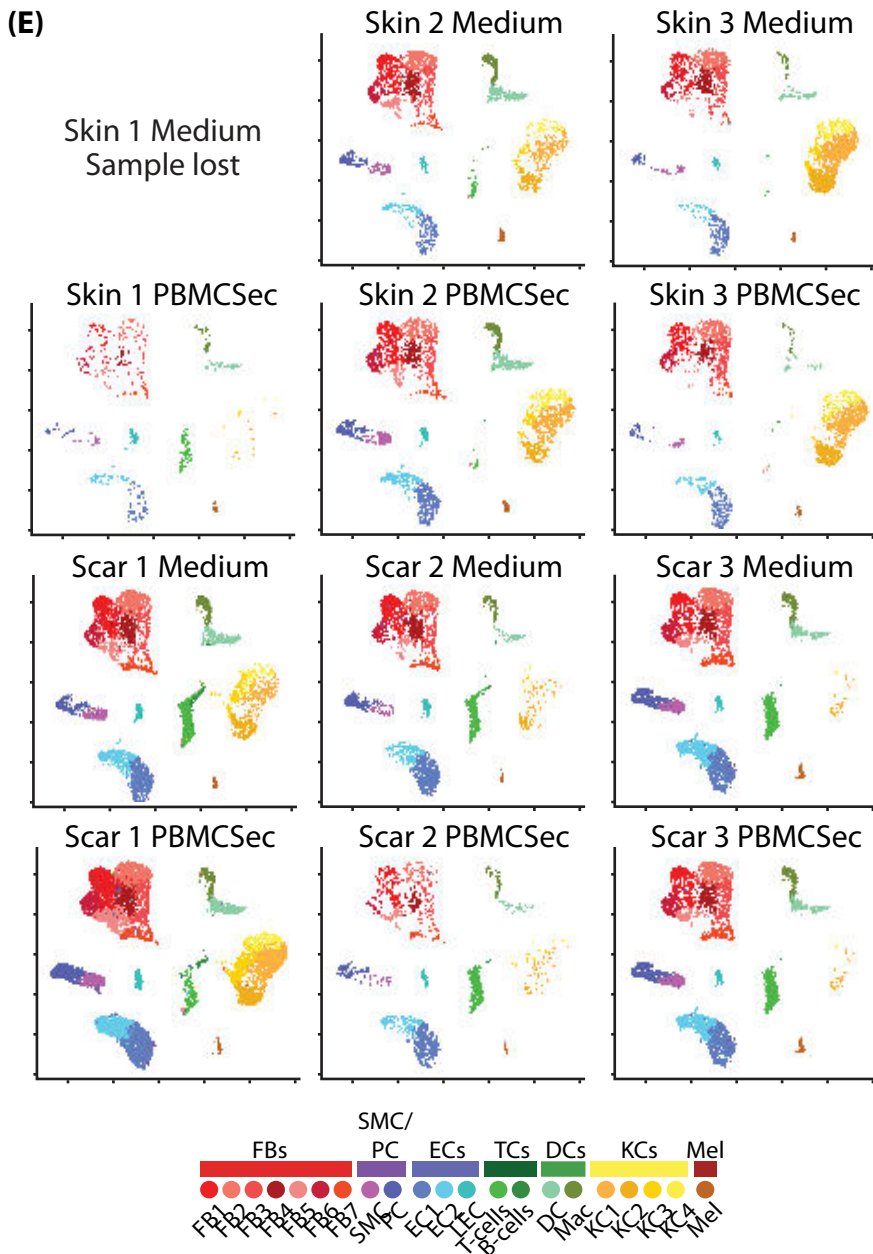
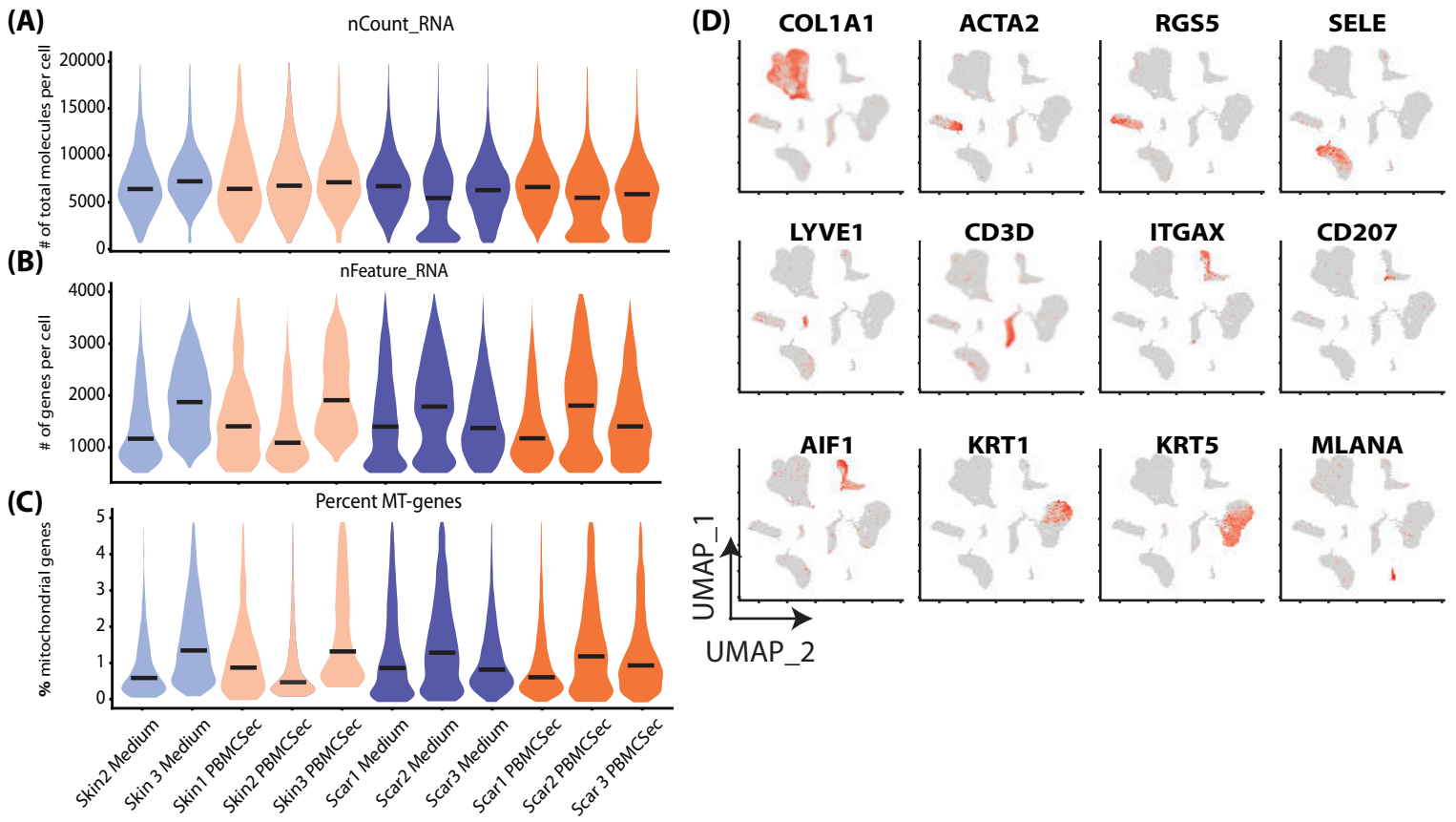


Figure S5: Quality control of human scRNAseq

A-C) Violin plots of quality control parameters of the 'human' dataset. A) total molecules per cell B) (gene count per cell and C) mitochondrial gene content. D) Feature Plots of cluster markers for cluster identification in the 'topical' and 'inject' dataset: *COL1A1* (collagen I alpha 1) for fibroblasts, *ACTA2* (smooth muscle actin) for smooth muscle cells and myofibroblasts, *RGS5* (Regulator Of G Protein Signaling 5) for pericytes, *SELE* (Selectin E) for endothelial cells, *LYVE1* (Lymphatic Vessel Endothelial Hyaluronan Receptor 1) for lymphatic endothelial cells, *Cd3d* (cluster of differentiation 3D) for T-cells, *ITGAX* for dendritic cells, *CD207* (Langerin) for Langerhans cells, *AIF1* (allograft inflammatory factor 1) for macrophages, *KRT1* (Keratin1) for spinous and granular keratinocytes (KCs), *KRT5* (Keratin 5) for basal KCs, *MLANA* (Melan-A) for melanocytes. E) UMAP-clustering in the 'human' dataset, split by samples. Sample "Skin 1 medium" was lost due to technical difficulties during preparation. Vertical lines in violin plots represent maximum expression, shape of each violin represents all results, and width of each violin represents frequency of cells at the respective expression level. In feature plots, normalized log expression of the respective gene is mapped onto the UMAP-plot. Color intensity indicates level of gene expressions. UMAP, uniform manifold approximation and projection

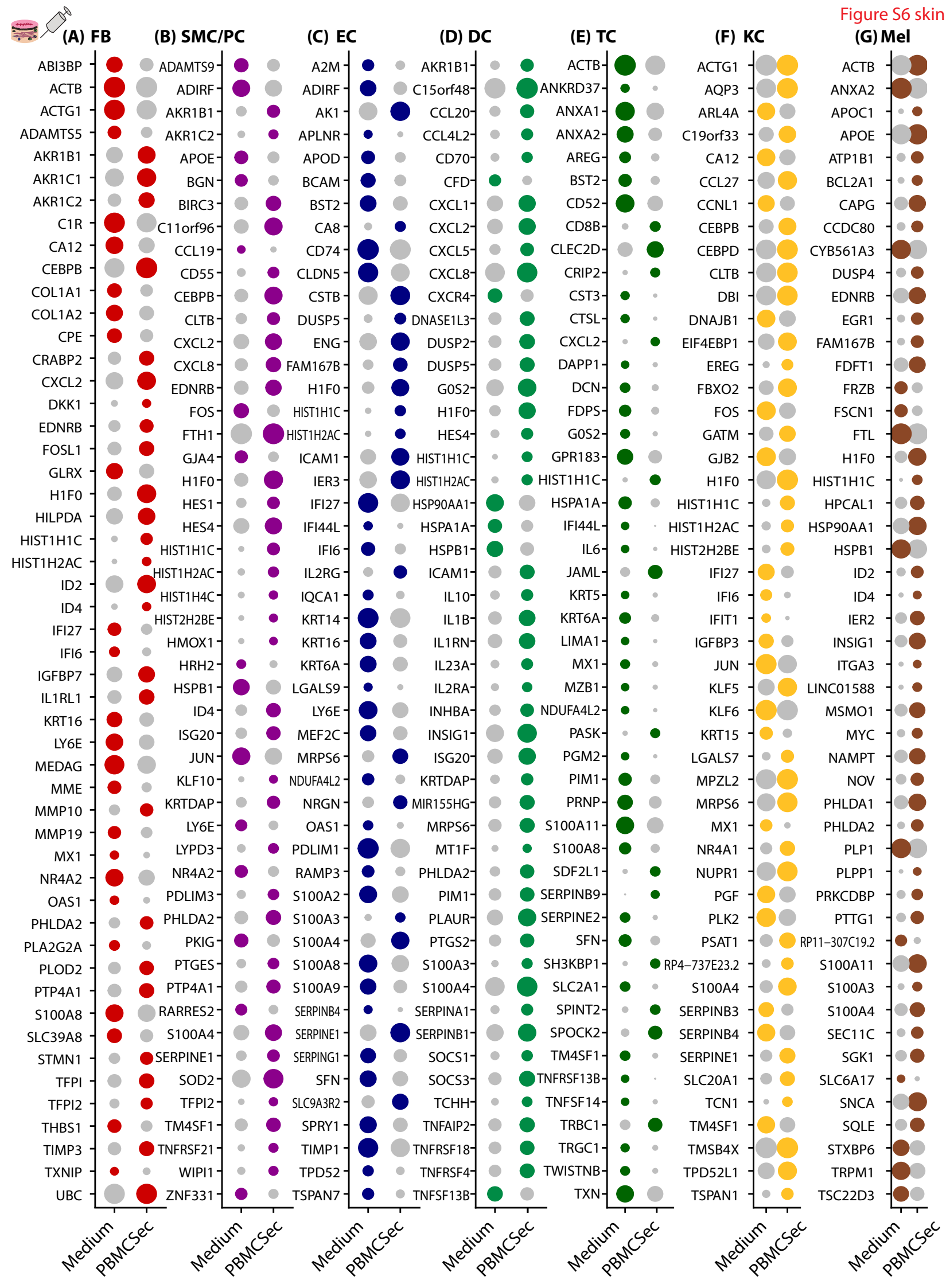


Figure S6: Top 50 regulated genes per cell group in human skin

In A) fibroblasts (FBs, red circles), B) smooth muscle cells and pericytes (SMC/PCs, purple), C) endothelial cells (ECs, blue), D) T-cells (dark green), E) dendritic cells and macrophages (DCs, light green), and keratinocytes (KCs, yellow), melanocytes (Mel, brown); differentially expressed genes (DEGs) were calculated comparing 'PBMsec' skin biopsies to 'Medium' skin biopsies, using Wilcoxon rank sum test, including genes with average logarithmic fold change (avglogFC) of > 0.1 or < -0.1 and Bonferroni-adjusted p-value < 0.05 . For each cellgroup, top 50 DEGs according to lowest adjusted p-value are displayed, split by treatment. Dot size represents percent of cells expressing the respective gene, color correlates with average expression.

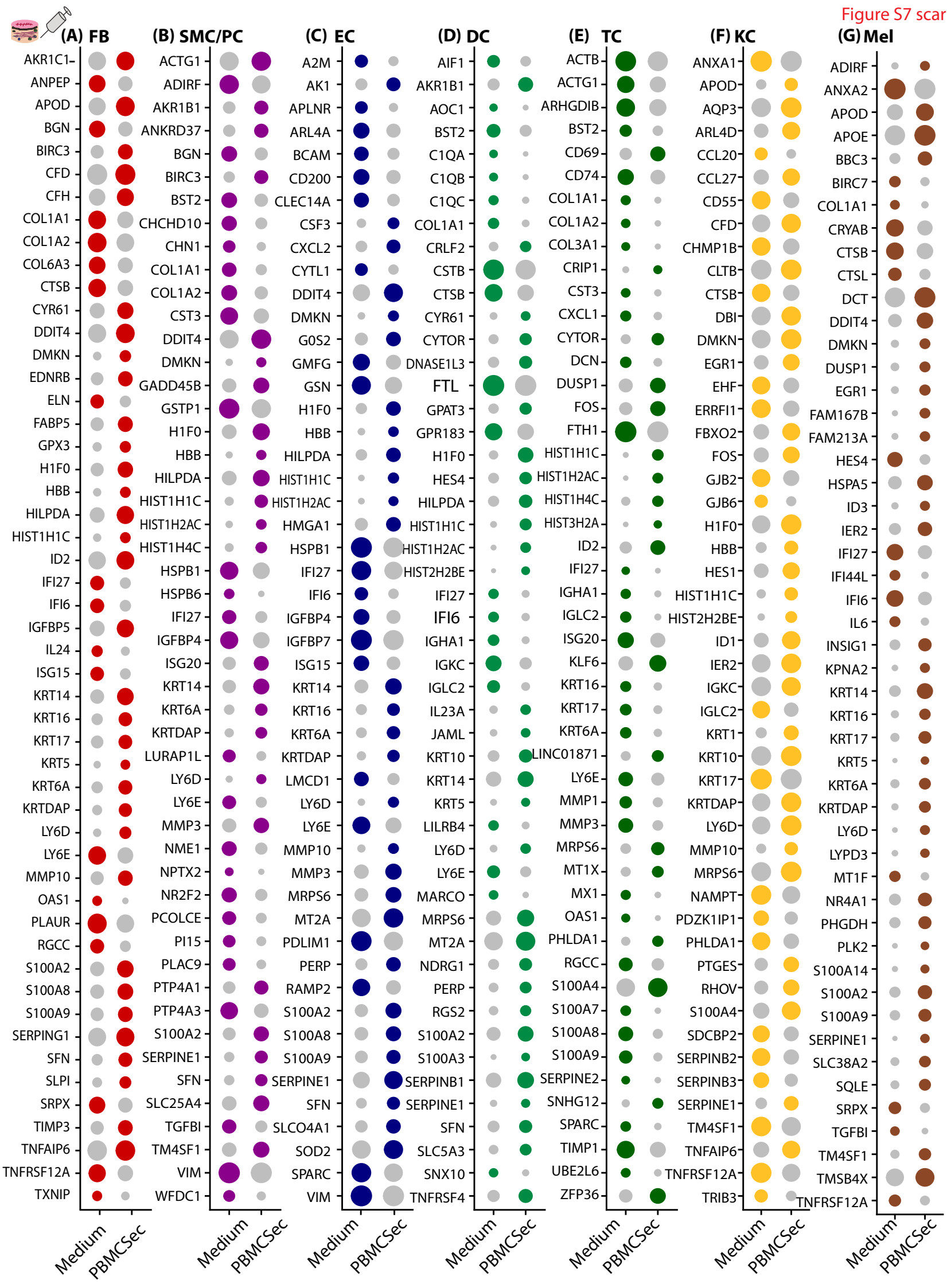


Figure S7: Top 50 regulated genes per cell group in human scar

In A) fibroblasts (FBs, red circles), B) smooth muscle cells and pericytes (SMC/PCs, purple), C) endothelial cells (ECs, blue), D) T-cells (dark green), E) dendritic cells and macrophages (DCs, light green), and keratinocytes (KCs, yellow), melanocytes (Mel, brown); differentially expressed genes (DEGs) were calculated comparing 'PBMsec' scar biopsies to 'Medium' scar biopsies, using Wilcoxon rank sum test, including genes with average logarithmic fold change (avglogFC) of > 0.1 or < -0.1 and Bonferroni-adjusted p-value < 0.05 . For each cellgroup, top 50 DEGs according to lowest adjusted p-value are displayed, split by treatment. Dot size represents percent of cells expressing the respective gene, color correlates with average expression.

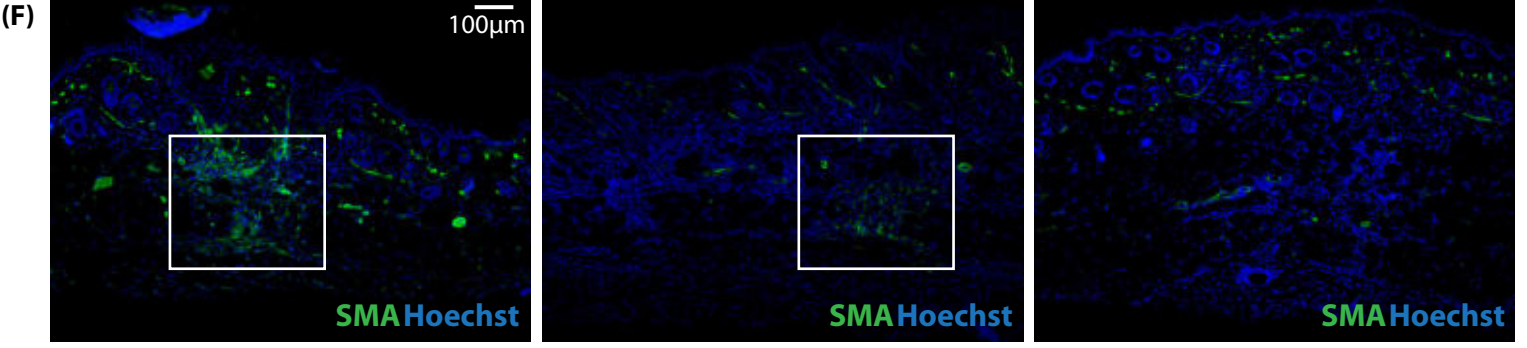
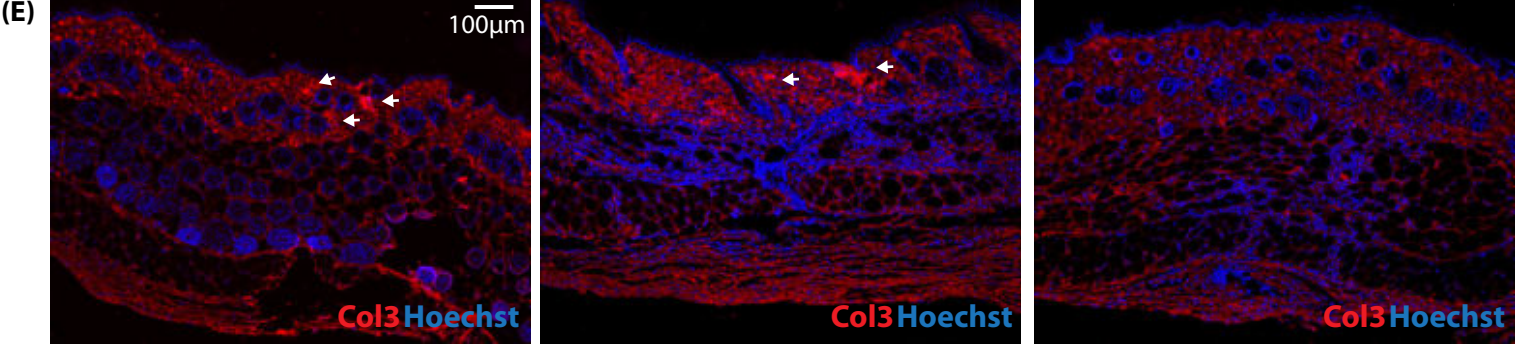
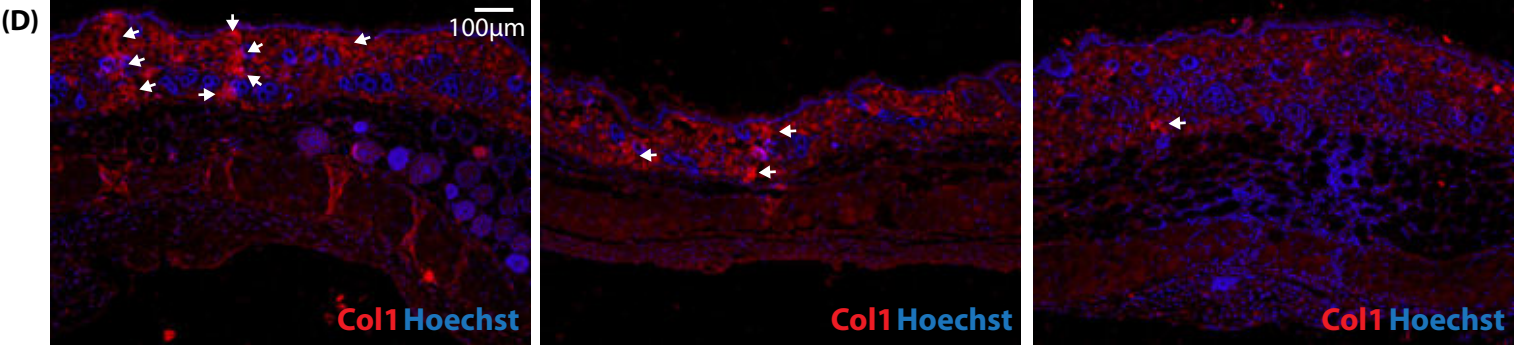
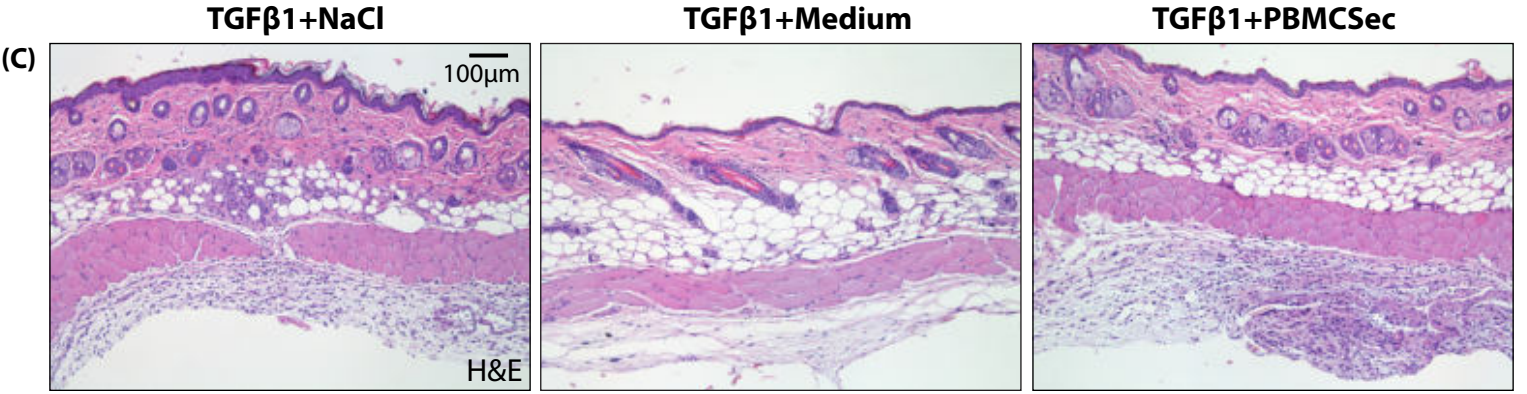
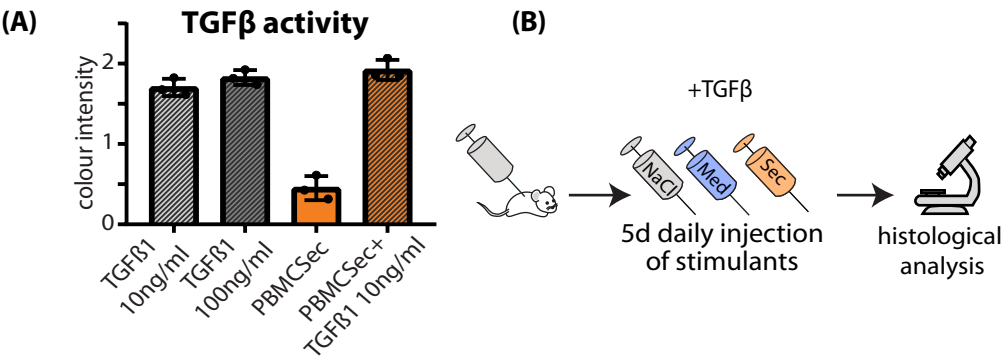


Figure S8: The interaction of TGF β and PBMCsec *in vivo*

A) In vitro TGF β -activity assay. HEK-cells colorimetrically detecting SMAD2/3 TGF β -activity were incubated with recombinant TGF β 1, with PBMCsec alone, and with TGF β 1 and PBMCsec combined. Color intensity correlates with TGF β 1-signaling activity. B) Workflow of mice intradermally injected with TGF β 1 and treatments. Mice were intradermally injected with 800ng TGF β 1 dissolved 100 μ l in NaCl 0,9%, Medium or PBMCsec on five consecutive days and sacrificed on the 6th day. C) H&E staining of resulting "scars" of the injected area. Immunofluorescence stainings of D) collagen 1, E) collagen 3, F) smooth muscle actin in TGF β 1-injected mouse skin. Arrows indicate areas of dense matrix deposition.

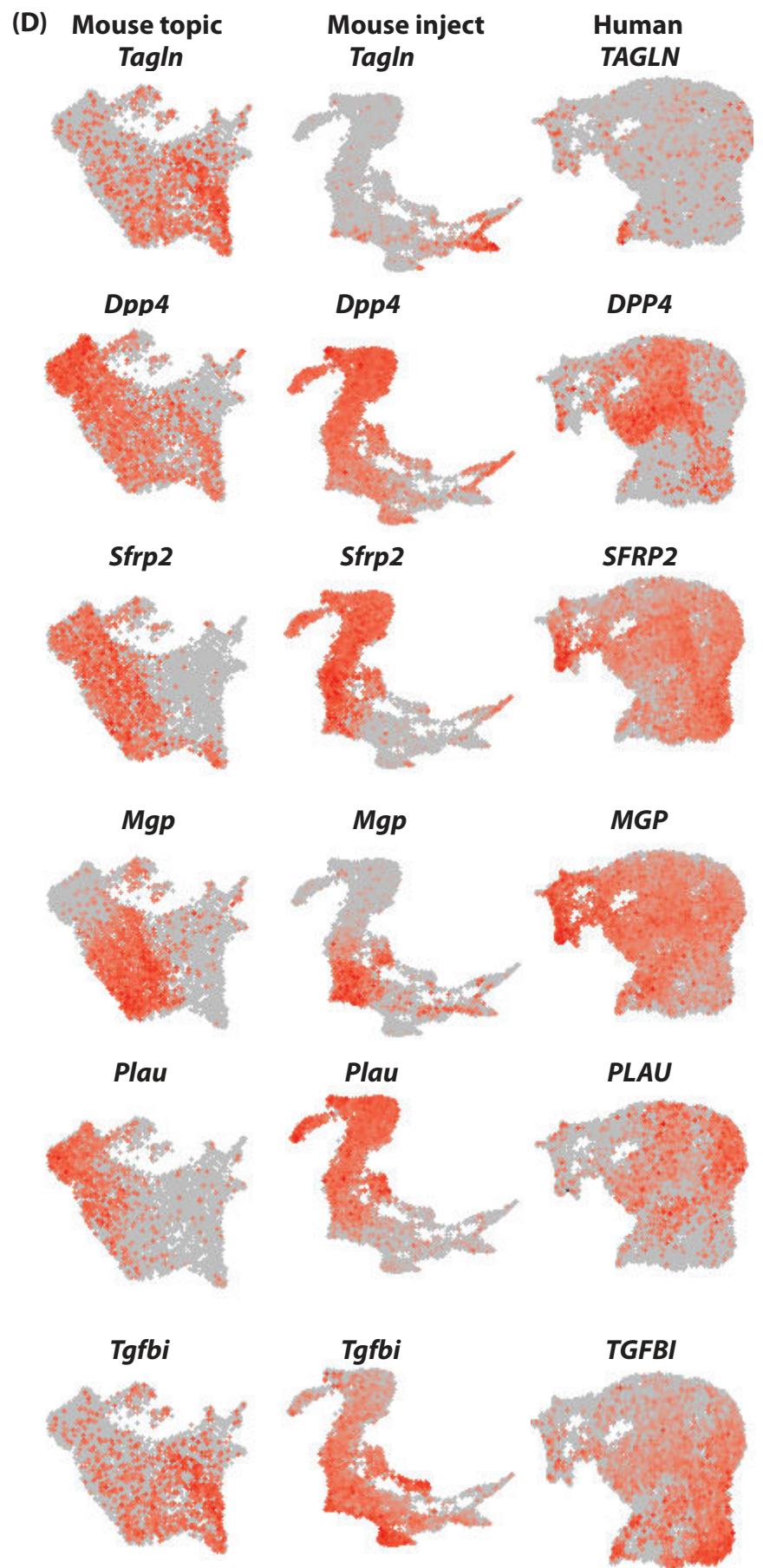
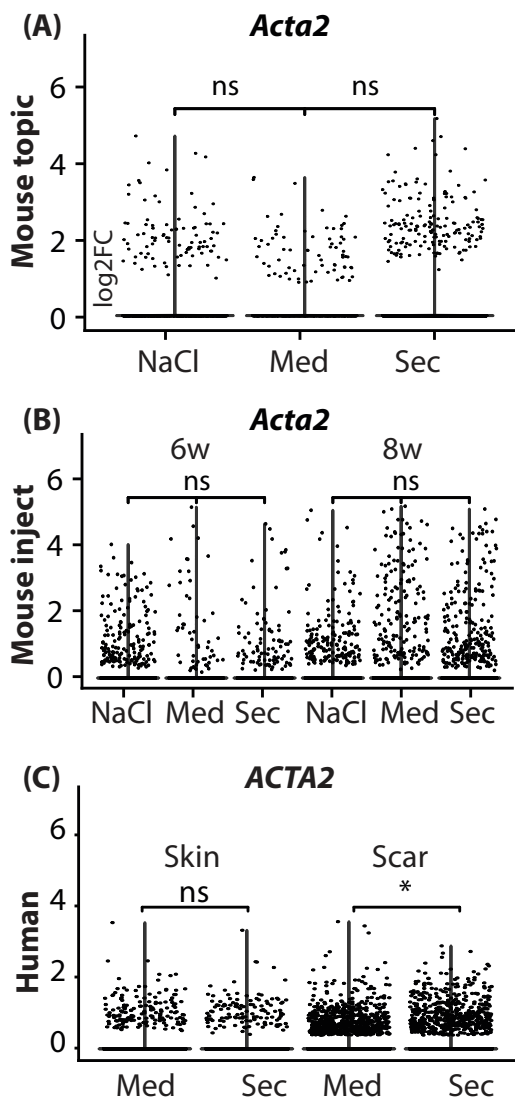


Figure S9: Subcluster analysis of FB populations

A-C) Violin plots of *Acta2/ACTA2* in mouse and human datasets, split by treatments. D) Feature plots of FB subcluster markers in FB subclusters of mouse and human datasets. *Tagln/TAGLN*, Transgelin; *Dpp4/DPP4*, dipeptidyl-peptidase 4; *Sfrp2/SFRP2*, Secreted Frizzled Related Protein 2; *Mgp/MGP*, Matrix Gla Protein; *Plau/PLAU*, urokinase; *Tgfbi/TGFBI*, Transforming Growth Factor Beta Induced. In violin plots, dots represent individual cells, y-axis represents log₂ fold change of the normalized genes and log-transformed single-cell expression. Vertical lines in violin plots represent maximum expression, shape of each violin represents all results, and width of each violin represents frequency of cells at the respective expression level. In feature plots, normalized log expression of the respective gene is mapped onto the UMAP-plot. Color intensity indicates level of gene expressions. UMAP, uniform manifold approximation and projection. A two-sided Wilcoxon-signed rank test was used in R. NS $p > 0.05$, * $p < 0.05$, ** $p < 0.01$, *** $p < 0.001$.

3. Discussion

3.1. General discussion

The initial question of this dissertation project was to elucidate the effects of PBMCsec on skin and scar. However, many cellular processes in (hypertrophic) scarring were not well understood, and transcriptomes of skin and hypertrophic scars were not studied on single cell level before. Therefore, a basis characterizing the cellular characteristics of skin and scars on a hitherto unmet resolution needed to be established. Thus, the project was structured into three main research questions: We aimed 1) to thoroughly investigate the transcriptome landscape of healthy human skin, with particular focus on FB populations, 2) to elucidate the transcriptome alterations of human (hypertrophic) scars compared to skin, and to identify and functionally characterize potential new drug targets for treatments of hypertrophic scars and 3) to describe the effects of PBMCsec on human skin and scar, and decipher the mechanisms of action that lead to its potentially beneficial effects in fibrosis and skin scarring.

Several recurring themes running through our research like common threads became apparent in all three studies. Foremost, we identified FBs as the linchpins of action, common agents, and targets of interest in this comprehensive work. We initially attempted to thoroughly characterize all cell types present in human healthy skin on a single cell transcriptome level (103). However, we found that the diversity and functional characteristics of FBs was the most prominent feature of our human skin single-cell dataset in our first study (Figure 5). Others described before that skin FBs displayed distinct clusters marked by, among others, DPP4 (102), and that DPP4+ FB are a specific FB lineage responsible for secretion of ECM in mice (153). However, we were the first to demonstrate a specific DPP4+ FB cluster in human skin that was identified as the main source of ECM (103). Additionally, the identification of several markers that specifically mark only FBs (e.g. *SDC2*, *PLPP3*, *MXRA8*) further contributes to this field by aiding in purifying FB populations from cell cultures, or by removing FBs from other cell cultures of interest (250, 251). At the time of the preparation of this dissertation, the study has been cited by more than 70 other works, highlighting that the characterization of FBs, the diversity of FBs in human skin and the role of a DPP4+ FB cluster is of particular interest to the dermatological research (103).

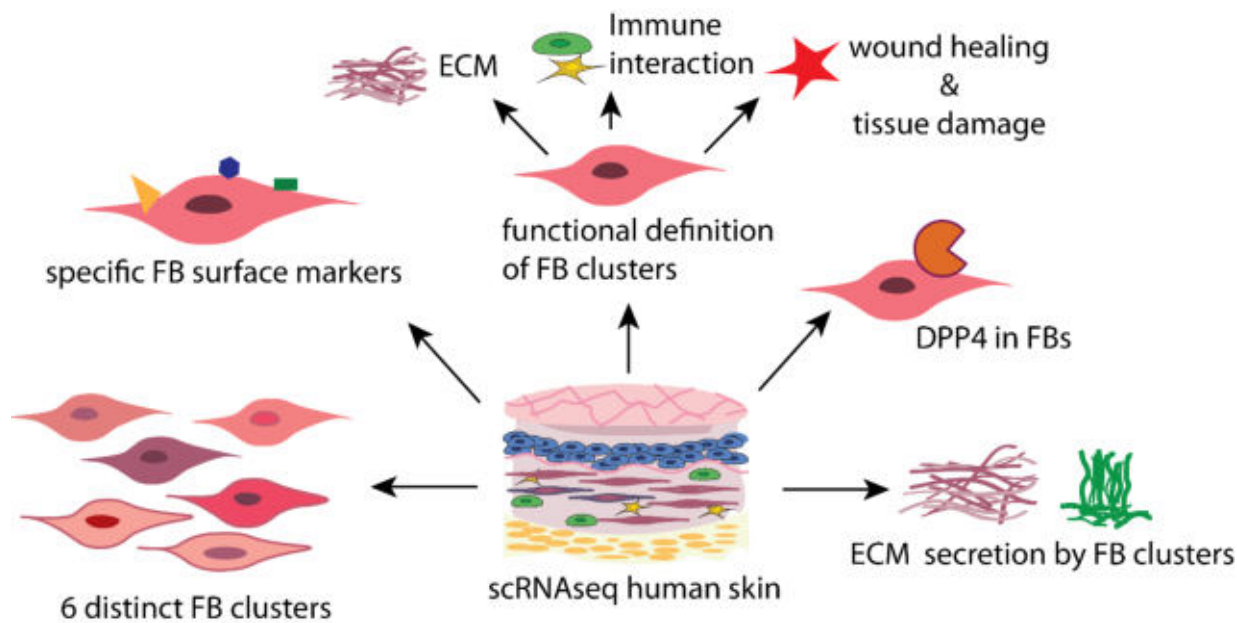


Figure 5 Graphic summary: The characterization of functional heterogeneity of human skin fibroblasts. Human FB clusters were defined using scRNAseq, six distinct FB clusters were found, new surface markers were identified. A specific DPP4-positive FB cluster was characterized, which was primarily responsible for the secretion of ECM (103).

Subsequently, when analyzing hypertrophic scar FBs compared to healthy human skin (252), we again found a specific DPP4-expressing FB cluster in human scars. This FB cluster was significantly expanded in FBs, and strikingly, was also responsible for the abundance of ECM-secretion in scars (252). Another work assessing FBs in keloids compared to skin confirmed our findings and found a similar transcriptome signature (253). The authors also identified specific mesenchymal FB cluster, comparable to our cluster FB1 in scars, that was also exclusively expanded in keloids, but hardly present in healthy skin (253).

Lastly, FBs were also the main mediators of beneficial effects after treatment of scars with PBMCsec, and scar-specific FB clusters were also present in this dataset (44). In FB clusters, the highest number of genes was regulated by PBMCsec, and the most regulated genes were associated with ECM and remodeling (44). Therefore, we closely explored the matrisome alterations in FBs after PBMCsec-treatment, i.e., in collagens, proteoglycans, glycoproteins, and ECM regulators. The characteristic of several ECM alterations in (hypertrophic) scars are well investigated (254). However, the ‘matrisome’ for large-scale in silico analyses was defined and further investigated only recently (206, 255, 256). The

comprehensive matrisome was characterized in human skin and keloids (257), but no studies hitherto used scRNAseq and matrisome analysis to elucidate the effect of conditioned medium or secretome in scarring or wound models. Taken together, this thesis comprises an entirely new view on FBs in human skin and in scarring, their interaction with PBMCsec, and the secretion of ECM and matrisome components.

When considering FBs in the context of scars, their differentiation into activated FBs or myoFBs are key mechanisms in all fibrotic processes (95, 106, 107). Thus, we established a model for testing potential inhibitors of myoFB-differentiation by stimulating primary human skin FBs with TGF β , inducing the activated FB phenotype. Pleasantly, we found that the FBs were prevented from differentiating into myoFB by inhibiting DPP4 using the specific inhibitor Sitagliptin, or the urokinase-inhibitor BC-11 (Figure 6) (252). Abolishment of myoFB-differentiation by inhibition of DPP4 was described before (168). However, we were the first to use the clinically approved pharmaceutical Sitagliptin, and BC-11 to prevent myoFB-differentiation (252).

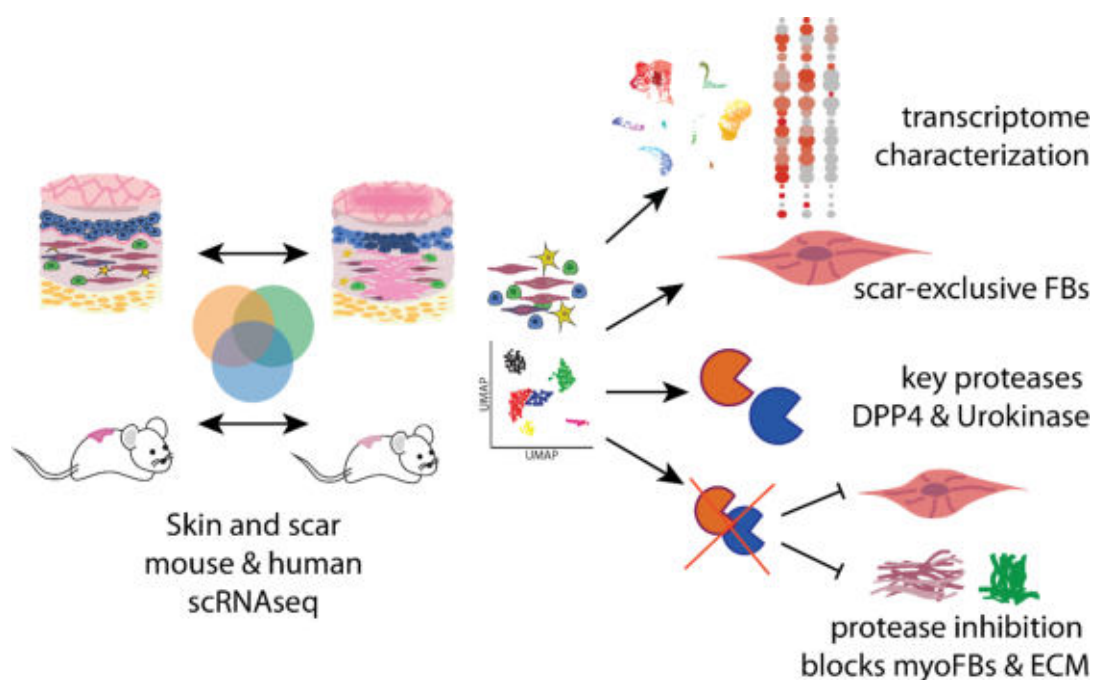


Figure 6 Graphic summary: The serine proteases dipeptidyl-peptidase 4 and urokinase are key molecules in human and mouse scar formation. Human and mouse skin and scar transcriptomes were characterized and compared. Scar-exclusive FB clusters were found, and serine proteases DPP4 and urokinase were identified as key regulators. Blockage of proteases abolished myoFB differentiation and inhibited excessive ECM deposition (252).

DPP4⁺ FBs were shown to mediate fibrotic pathologies in various other organs in animal studies, and pharmacological inhibition of DPP4 using gliptins attenuated renal (163), heart (159, 160), lung (162), and liver fibrosis (161). Further studies (258) are required to investigate whether such a FB subset with comparable contribution to fibrotic processes indeed exists in other organs in humans.

Surprisingly, PBMCsec also entirely prevented TGF β -mediated myoFB-differentiation (44), indicating its high anti-fibrotic potential. According to earlier studies that corroborated our findings, mesenchymal or pluripotent stem cell conditioned media treatment of FBs suppressed myoFB-differentiation (259, 260). Connecting the findings from the second study with the investigation of PBMCsec in scars, we initially hypothesized that endogenous DPP4 or urokinase inhibitors might be present in PBMCsec, however, none could be identified. The myoFB-preventing effect was only present when the full secretome was used, but not upon stimulation with its components (lipids, proteins, extracellular vesicles), suggesting a synergistic effect (44).

In our experimental approach, DPP4- and urokinase-inhibition, as well as treatment with PBMCsec, all consistently prevented TGF β -induced myoFB-differentiation. However, to our surprise, none of them interfered with the canonical TGF β -signaling pathway. In earlier studies, it has been shown that DPP4 inhibition blocks both TGF β -mediated myoFB differentiation by inhibiting ERK signaling and classical TGF β signaling via Smad2 in renal fibrosis (261, (168)). We could not confirm this mechanism in our approach. Moreover, we also did not find any interference of BC-11 with the canonical TGF β 1 signaling pathway. While BC-11 showed a significant activation of GSK3 α/β in TGF β 1-stimulated FBs, we did not find this effect upon stimulation with Sitagliptin. Prior research (262, 263) revealed that GSK3 interacts with WNT/-catenin signaling, and deletion of GSK3 β resulted in a pro-fibrotic myoFB phenotype in isolated mouse cardiac FBs.(259). We thus suppose that activating GSK3 α/β functions as a counter-regulatory mechanism for TGF1-signaling and that BC-11, at least in part, exhibits its anti-fibrotic activity through activating GSK3 α/β (259).

PBMCsec-application also did not affect the canonical TGF β -signaling. While others found direct inhibition of the canonical TGF β /Smad signaling through conditioned media (260), we found no inhibition of this pathway. However, we assume that PBMCsec again hardly acts via a single mechanism but

contains various compounds and endogenous TGF β inhibitors that prevent the myoFB-induction. Only few secreted endogenous non-canonical TGF β -signaling inhibitors are described; e.g. Del-1 (Developmentally-Regulated Endothelial Cell Locus 1 Protein, *EDIL3*), extracellularly secreted also by leukocytes, was found to tackle TGF β -signaling and prevent fibrosis via suppressing α_v integrin-mediated activation of TGF β (261)

As TGF β can also initiate fibrosis via non-canonical (non-SMAD) signaling pathways (262), and impaired non-canonical signaling prevented profibrotic phenotypes (263), we suppose that the inhibition of myoFB-induction occurs thereby. To pinpoint the precise mechanism of the TGF β -inhibition by Sitagliptin, BC-11 and PBMCSec, a thorough proteomic approach and evaluation of several pathways will be the focus of our future work.

The common property of DPP4 and urokinase is their activity as serine proteases, and several components of PBMCSec include (serine) protease inhibitors. Thirteen clans and forty families make up the broad, diversified group of proteases known as serine proteases/peptidases (264). Proteases involved in critical processes such blood coagulation, fibrinolysis, apoptosis, and immunology constitute the trypsin family (265). This family includes the enzymes urokinase (*PLAU*), *HTRA1/3* (high temperature requirement A1/3 peptidase), a number of coagulation factors and complement elements, PRSS-like serine proteases, granzymes, and cathepsin G (264). Human in vitro studies and mice trials with urokinase inhibitors have demonstrated that they can inhibit the fibrotic processes that lead to heart and pulmonary fibrosis (157, 266). Thus, they have recently been the focus of therapeutic research for fibrotic disorders (226, 266, 267).

In the context of fibrosis, the literature on urokinase inhibitors is inconsistent. Urokinase was found before to critically regulate fibrinolysis and ECM-turnover, explaining its to anti-fibrotic action (226). Therefore, inhibition of urokinase to mitigate tissue fibrosis may seem counterintuitive. The most extensively studied endogenous urokinase inhibitor, plasminogen activator inhibitor-1 (PAI-1, *SERPINE1*), has been discovered to significantly increase matrix accumulation upon injury (266). Previous studies, confirming our pertinent results, found that inhibition of urokinase by PAI-1 abolishes profibrotic effects in FBs from fibrotic lungs and prevents cardiac fibrosis in mice (156). PBMCSec most likely also contains plethora of

various endogenous serine protease inhibitors. Serine protease inhibitors, Serpins, are potent endogenous protease inhibitors, and dysregulation of serpin activity is involved in fibrotic pathologies (156, 266). We hypothesize that a combination of serpins in PBMCsec contributes to the elastase inhibition and also to the positive effects observed in wound healing. For example, *SERPINA1* (Alpha 1-antichymotrypsin) is a specific inhibitor of leukocyte-derived chymotrypsin-like proteases, which improved wound healing and scar formation in mice (268, 269), and was upregulated upon PBMCsec-stimulation.

Aside from DPP4, urokinase and PBMCsec components, another substrate of specific proteases, elastin (*ELN*), became a focus of this work. We did not closer address elastin, and did not find substantial regulation when first comparing skin and scar transcriptomes (252). However, elastin expression was significantly reduced upon stimulation with PBMCsec, and was found acting as a hinge of the mechanistic explanation of PBMCsec effects (44).

In contrast to the well described effect of elastin stabilization and overexpression through TGF β (183), we observed the opposite in our *ex vivo* model. Upon *ex vivo* stimulation with TGF β , papillary elastin fibers were truncated in the skin, and were preserved upon addition of PBMCsec. This appears counterintuitive to the literature, and we did not find any studies that described this phenomenon before. The interaction of TGF β and elastin is complex: TGF β is well described to enhance the expression of elastin (187) and stabilize elastin mRNA, promoting elastin secretion (187). Elastic fiber degradation can release elastin fragments named elastokines, exerting cytokine-like signaling properties, that mediate cell signaling via integrin and syndecan receptors (190). Moreover, microfibrils store TGF β family growth factors for later release, which is critical for homeostasis and remodeling (190).

In our *ex vivo* biopsies, elastin was truncated by TGF β and preserved by PBMCsec. Serine proteases, and also metalloproteases play a crucial role in TGF-*elastin*-interaction (270). Both are able to activate TGF β via direct cleavage of latent TGF β , or interaction with integrin mediated TGF β activation pathways (270). Moreover, neutrophil elastase can also induce TGF β secretion (271), and release latent TGF β from the ECM (272). TGF β was demonstrated to establish complex autocrine enhancing and inhibiting feedback signaling loops (273, 274). We thus suppose that in our *ex vivo* biopsies, the inhibition of

proteases by PBMCsec prevented the cleavage of elastin, abolishing the release of further TGF β from the matrix, on the one hand, averting the positive feedback loop (Figure 7). In contrast, PBMCsec directly downregulated the expression of genes associated with TGF β activation, integrins and latent TGF β proteins (44).

Interestingly, elastin-cleaving elastases *ELANE* and *CELA1* are also both serine proteases like DPP4 and urokinase (41), further emphasizing the role of serine proteases in hypertrophic scar formation. Even though we did not find *ELANE* and thus no regulation of it in mouse or human skin or scar cells, PBMCsec did exert an endogenous elastase inhibiting effect (Figure 7). Potent elastase inhibitors possibly present in PBMCsec might be Elafin (PI3, skin-derived antileukoprotease) and *SLPI* (secretory leukocyte protease inhibitor, Antileukoproteinase). Both were also directly upregulated in FBs by PBMCsec in scar. They are scarcely evaluated for their involvement in skin and scar formation despite being highly researched for their positive benefits in cystic fibrosis (275), but we suggest they merit additional research (44).

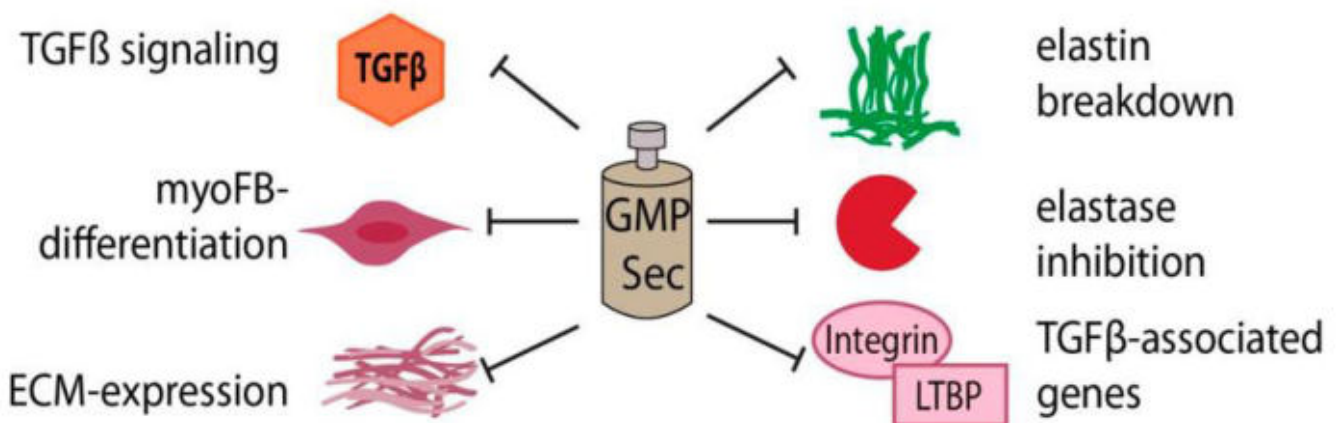


Figure 7 Graphic summary: The anti-fibrotic mechanisms of PBMCsec in scars. PBMCsec prevents TGF β 1-mediated myoFB differentiation, attenuates the expression of ECM genes and significantly reduces elastin secretion. PBMCsec abolishes elastin breakdown, inhibits elastase, and inhibits with TGF β -induced gene expression (44). Use of graphic permitted according to CC BY 4.0 license.

In a rat model of acute myocardial infarction, we previously found that injection of apoptotic PBMCs (an earlier version of PBMCsec) increased elastin content after AMI in the myocardial scar (18), and apoptotic PBMCs increased elastin expression in primary human FBs (18). While *ex vivo*, PBMCsec preserved elastin fibers, we observed the opposite effect *in vitro*: TGF β induced elastin secretion (187, 188), and PBMCsec abolished the abundant secretion. Taken together, we propose that PBMCsec interacts with elastases (i.e., serine proteases), stabilizes elastin, prevents breakdown under the influence of TGF β -mediated fibrotic remodeling, and reduces the excess expression through TGF β -signaling (Figure 7).

Aside from our main targets of interest DPP4, PLAU and PBMCsec, our transcriptome studies revealed numerous further genes regulated in scar compared to skin, or upon treatment with PBMCsec, that merit further investigation. Many of them have hardly been investigated in the context of scarring and fibrosis. For example, Superoxide dismutase 2/3 (*SOD2/3*), an important antioxidant enzyme that controls the release of reactive oxygen species (ROS) (276), discovered to be significantly downregulated in scar-forming FBs (277). The failure of ROS scavenging has been previously linked to hypertrophic scar formation. In line with that discovery, all three scRNAseq experimental techniques showed consistent regulation of TXNIP (Thioredoxin interacting protein) expression by PBMCsec. Additionally, *TXNIP* is essential for controlling ROS and cellular oxidative stress (75), and has been implicated in impaired wound healing under ischemic conditions (76). Despite its potential involvement in skin pathologies and scar formation being hardly investigated (78), our discovery that PBMCsec downregulates *TXNIP* in all experimental settings raises the possibility that PBMCsec-induced TXNIP downregulation functions as a significant mechanism underlying its anti-fibrotic effects.

Furthermore, several cytokines and ECM-regulators, such as periostin (*POSTN*), pleiotrophin (*PTN*) and midkine (*MDK*), both involved in cell growth, migration, and angiogenesis, were found to be consistently upregulated in scar-forming fibroblasts. Some genes, including *POSTN*, were even enhanced after PBMCsec treatment, suggesting a targeted regulation of these factors. Stratifin (*SFN*), a potent collagenase-stimulating factor in FBs (278), was also considerably downregulated in scars, suggesting a role for matrix preservation in the maintenance and/or development of the fibrotic phenotype. Interestingly, *SFN* was upregulated in several cell types in human scar upon PBMCsec-stimulation.

These findings suggest that the interaction of many more genes hitherto unknown contributes to skin scarring, and that PBMCsec mitigates through a great variety of processes.

All of the three studies presented here certainly do have some limitations. Wound healing and scarring physiology in rodents significantly differ from human (279). While human skin predominantly heals via re-epithelialization, mouse wounds exhibit stronger contraction through the subcutaneous panniculus carnosus (88, 280). To accurately mimic hypertrophic skin scarring, tight-skin mice (279) and subcutaneous bleomycin injection (281, 282) have been proposed. However, it has not been examined whether their transcriptome can be compared to human hypertrophic scars. Nonetheless, studies looking at the contributions of contraction and epithelialization in mice found that each accounted for 40–60%, and animal wound models can therefore be considered a good model for human wound healing (280). Thus, and as our main conclusions drawn from the mouse models are also consistent in the human analyses, we presume that the mouse model provides valid insights.

An important aspect that should be considered in our studies is the potential presence of a sex bias. As the majority of patients undergoing aesthetic body-contouring surgery are women, and because female mice are much less aggressive in frequent handling, almost all samples in our studies are thus derived from females. The influence of estrogen was found to inhibit the pro-fibrotic effects of TGF β (283). The study found that in dermal FBs, 17- β -estradiol treatment significantly reduced the stimulatory effects of TGF- β on collagen synthesis and myofibroblast differentiation (283). Moreover, it also significantly reduced the activation of canonical TGF β signaling and significantly reduced the expression of TGF β target genes (283). Estrogen was also found to influence psoriasis-like skin inflammation (284), and the response to photodamage in skin (285). Additionally, a sex-specific difference of drug distribution in skin was observed in mice, showing higher accumulation of nanoparticles in female hair follicles than in male mice (286). These studies implicate that the sex of trial participants and experimental animal might influence our results. We thus propose that future studies evaluating potential therapies in scar formation and the application of PBMCsec should include both male and female samples.

One main drawback of the mouse model is the significantly different structure of elastin in the upper dermis making comparison of our findings of elastin breakdown difficult in mouse skin. In a pig burn scar

model, mesenchymal stem cells were applied; elastin fibers exhibited regeneration, and elastin fibers could be assessed using EvG-staining (280). Although we have previously evaluated PBMCsec in burn pig wounds (21), the main objective of this study was to examine wound healing rather than scarring.

In our experimental models assessing DPP4, BC-11 and PBMCsec, scar tissue and open wounds were treated topically with creams containing protease inhibitors. It is still unknown if the active ingredients may penetrate wound scabs and/or scar tissue or if the initial care given to open wounds is sufficient to reduce the need for scarring. However, a recent study (287) looking at Sitagliptin transdermal resorption shows adequate skin penetration. As BC-11 has hitherto not been used in humans, future investigation is required to assess its pharmacodynamic and pharmacokinetic characteristics.

For PBMCsec-application, our scRNAseq identified many more differently expressed genes in topical PBMCsec than after injection, i.e., stronger transcriptome alterations, thus we suppose higher efficacy of topical application in wounds than after injections. PBMCsec contains a great variety of active components, including extracellular vesicles, proteins, and lipids (27). Our previous works coherently found that PBMCsec only unfolds its full regenerative potential when all its components are applied, and only when secretome of all cell types of PBMCs are included (27, 34). Future assessment of the permeability of PBMCsec components into the skin is necessary, however, we suppose that large molecules such as proteins and extracellular vesicles are not able to permeate the stratum corneum of the skin. Thus, other galenics to apply PBMCsec are needed, and future investigations might apply laser treatment (288), micro needling (289), or nanocarriers (290) to deliver all PBMCsec components into the skin.

Having characterized the antifibrotic properties of DPP4- and urokinase inhibitors and PBMCsec, a clinical translation for their application in patients would be desirable. Specific DPP4-inhibitors, gliptins, among them the here used Sitagliptin, are in wide clinical use for treatment of diabetes mellitus (158). It would be worthwhile to further evaluate gliptins in their efficacy on scar formation and scar quality in diabetic patients compared to other drugs that inhibit serine proteases. To fully understand effectiveness of gliptins in treating skin scarring, it would be encouraging to investigate their off-label topical administration in non-diabetic patients given that they are already approved for clinical usage.

Encouraging results for hypertrophic scar formation have already been observed in diabetic Japanese patients who are treated with gliptins (291). As mentioned above, inhibition of DPP4 activity by gliptins reduced fibrotic processes in the kidney (163), heart (159, 160), lung (162), and liver (161). Thus, of the therapeutic strategies assessed here, DPP4- inhibitor Sitagliptin would be closest to a potential clinical application in scarring.

Hardly any literature was found for the previous use of BC-11, only an *in vitro* study exists, assessing its cytotoxicity in breast cancer cells (292). We did not directly investigate the safety and tolerability of BC-11 in our *in vitro* and *in vivo* experiments; nonetheless, we also did not observe any toxic effects. As we have shown substantial variations in collagen contraction between the particular knock-down of *PLAU* and *DPP4* and their respective inhibitors, it is possible that both exhibit side effects that must be thoroughly addressed in subsequent research. Extensive further *in vitro* and *in vivo* testing is necessary to facilitate further clinical application for BC-11. In contrast to BC-11, PBMCsec has already undergone clinical phase I-testing, and is currently under investigation in a phase II trial for topical application in diabetic foot ulcers (33). The preparation and approval for clinical testing of PBMCsec has been challenging (293), as every single step and every component used in its preparation has to follow good-manufacturing-practice guidelines. Having mastered this extensive process, approval of topical application for skin scarring will be a much smaller challenge.

3.2. Conclusions and future prospects

This dissertation presents a comprehensive trilogy of studies that investigate the transcriptome of healthy skin, the genetic landscape of skin scarring, and the use of PBMCsec in (hypertrophic) scars. Novel fibroblast clusters were defined, specific proteases were identified as key players in fibrosis, and the mechanisms of action of PBMCsec in skin scarring were characterized. However, several key points warrant further investigation in future studies. For instance, clinical investigations of DPP4 and urokinase inhibitors and their role in preventing or treating scars would be of great interest. Moreover, BC-11 has received little attention so far, and our study is the first to investigate its *in vivo* effects. Therefore, safety and efficacy studies should be conducted before further clinical investigations. Sitagliptin, a DPP4

inhibitor that is clinically established for the treatment of diabetes mellitus, might be a promising topical treatment for skin scarring in the near future.

PBMCsec (APOSEC®) is currently undergoing Phase II investigation for topical application in wound healing of diabetic foot ulcers (33). Once topical application in wound healing is approved by Austrian and European authorities, clinical studies for the prevention of (hypertrophic) scarring, particularly in burn patients, are likely to follow soon. In the future, phase I and II studies could be conducted to evaluate the intracutaneous injection of PBMCsec in already existing hypertrophic scars, which could be a promising approach.

Taken together, this dissertation builds a solid base for new treatment options of hypertrophic skin scarring. Moreover, this thesis provides a solid foundation for the development of new treatment options for hypertrophic skin scarring. The studies presented in this work shed light on the underlying mechanisms of skin scarring and highlight potential new therapeutic targets. The findings pave the way for future investigations that could lead to the development of effective treatments for this common and often debilitating condition.

4. Materials and Methods

Materials and methods were applied as stated in the papers comprised in this thesis. Specific methods used in all three studies are summarized here.

4.1. Skin and scar samples

Healthy normal skin samples for single-cell RNA sequencing (scRNAseq) analysis were taken from three healthy female donors, 30, 36, and 43 years old, from surplus trunk skin removed during abdominoplasty. From patients who underwent elective scar resection or other surgery that comprised scar tissue, resected scar tissue ($n = 3$) was collected. A plastic surgeon characterized the scars using the POSAS classification system as hypertrophic, pathological scars. For all studies, only adult scars that had not previously undergone treatment and had been present for more than two years were utilized. None of the donors had any known chronic illnesses or were taking any long-term medications. Histological examination was used to evaluate the scar tissue; in none of the scar sample's neighboring normal skin was observed macroscopically (44, 252).

4.2. Mouse scar models

Female Balb/c mice were procured from the animal facility of the Medical University of Vienna (Himberg, Austria) and were reared under specific-pathogen-free conditions at a room temperature of 22 ± 2 °C and a humidity of $55 \pm 10\%$ as described before (44, 252). Female mice were preferred over male mice due to their superior experimental compliance and easier handling, which was essential for frequent handling and administration of treatment. To induce full-thickness skin wounds, mice were subjected to intraperitoneal anesthesia with 100 mg/kg Xylazine and 5 mg/kg Ketamine (both procured from Sigma-Aldrich, St. Louis, MO, USA). Post-operative analgesia was provided through subcutaneous administration of 0.1 mg/kg Buprenorphine (Temgesic®, Indivior Inc., North Chesterfield, VA, USA) and by adding 0.125 mg/ml Piritramide (Janssen-Cilag Pharma, Vienna, Austria) to drinking water. A 9×9 mm² area was marked on the shaved backs of the mice, and the skin was excised using sharp scissors. The excised areas were left uncovered to heal naturally and received no further care. The mice were euthanized 6- or 8-weeks post-wounding, and scar tissue was isolated. Biopsies with four-millimeter diameter were excised from the scar tissue and used separately for scRNAseq. Histological analysis was

used to evaluate the quality of scar tissue, and samples were chosen for further examination with a maximum of 20% normal surrounding skin (44, 252).

4.3. Mouse wound and scar treatments

Full-thickness skin wounds were created in mice as described above. For all interventions, Ultrasicc/Ultrabas ointment (1:1; Hecht-Pharma, Bremervörde, Germany) was utilized as carrier substance. A control treatment was prepared by mixing four parts Ultrasicc/Ultrabas and one part water. Protein inhibitors, Sitagliptin (final concentration 1 mM) or BC-11 (final concentration 5 mM), were combined with the ointment after being dissolved in water. For PBMsec experiments, four parts Ultrasicc/Ultrabas and one part water were blended as a control treatment. PBMsec (5U/ml, 200 μ l dissolved lyophilizate) or 200 μ l/ml medium was mixed with ointment. Immediately following wounding, mice were given either a control or inhibitor treatment by having 100 μ l of ointment applied to each wound. The mice were then kept under close observation for 30 min in litter-free, empty cages to avoid the treatments from being removed too soon and to give enough time for tissue resorption. To prevent wound infections, scabs were kept intact. Mice received treatment every day for the first seven days and three times per week for the following seven weeks. Following the development of scars, 4 mm samples of the scar tissue were extracted and divided in two. The other biopsy halves from each therapy group were combined and examined with scRNAseq in addition to the one half of each scar sample used for histological analysis. In the "injection" scar model, mice were injected every other day for two weeks starting on day 29 after skin injury with 100 μ l 0,9% NaCl, medium (CellGenix GMP DC Medium phenol red-free), or PBMsec. In each group, half the mice (n=2) were slaughtered and examined, and the other half (n=2) were allowed to age for a further two weeks before sacrifice (44, 252).

4.4. Cell isolation and generation of single-cell suspension for single-cell RNA sequencing

Skin, scar, and mouse samples were enzymatically digested using GentleMACS Human Whole Skin dissociation kit (Miltenyi Biotech, Bergisch-Gladbach, Germany) for 2.5 hours according to the manufacturer's protocol and processed on a GentleMACS OctoDissociator (Miltenyi). Cell suspensions were filtered through 70- and 40- μ m filters and stained with DAPI-dye for 10 seconds. Cells were resuspended in phosphate-buffered saline (PBS) containing 0.04% bovine serum albumin and washed

twice. Cells were sorted for viability using an AriaFusion (BD Biosciences, San Jose, CA, USA) or on a MoFlo Astrios high-speed cell sorting device (Beckman-Coulter, Brea, CA, USA)(103). For scRNAseq, only DAPI-negative cells representing live cells were employed. (44, 252).

4.5. Generation of single-cell gel-bead in emulsions (GEMs) and library preparation

After sorting, viable cells were immediately put onto a 10X-chromium device (single-cell gene expression 3'v2/3, 10X Genomics, Pleasanton, CA, USA) to create GEMs. The Biomedical Sequencing Core Facility of the Center for Molecular Medicine (CeMM) carried out RNA-sequencing, demultiplexing, and counting (CeMM, Vienna, Austria). Illumina's HiSeq 3000/4000 (Illumina, San Diego, CA, USA) was used for the sequencing process. with 3 samples per lane, 2 × 75 bp, and paired-end sequencing (44, 252).

4.6. Cell–gene matrix preparation and downstream analysis

The Cellranger pipelines were used to process the raw sequencing files (v3/4, 10X Genomics), demultiplexed the files and aligned them to the human or mouse reference genome (GrCh38/mm10). The Cellranger Count pipeline was then used to count the cell barcodes and unique molecular identifiers (UMIs), which generated a gene-barcode matrix. The “Skin” samples were aggregated in the Cellranger Aggregate pipeline to create a single gene-barcode matrix for all cells, which served as the basis for secondary analysis (44, 252).

The R-package “Seurat” (v2/3/4, Satija Lab, NYU, New York, USA) was applied for all secondary analyses running with R-Studio software in R (The R Foundation, Vienna, Austria). Cells with low or high UMI counts or high percentages of mitochondrial genes were removed from the dataset to eliminate unwanted variations. The data scaling and principal component analysis, statistically significant principal components PCs were extracted using the JackStraw Procedure. The Louvain algorithm was applied for clustering, and t-stochastic neighbor embedding (tSNE) or UMAP was used for visualization (44, 252)).

Cells with very high or low UMI counts (>3000 and <200) were removed to filter out inappropriate variations and low-quality cells. The cells from the healthy skin, or scar samples respectively, were integrated separately to prevent clusters forming according to donors instead for conditions, and to correct for batch-specific variations. Subsequently, the data was double-integrated into a single dataset using the suggested workflow by Butler et al. and Stuart et al. For differential gene expression analysis

and visualization in violin plots, feature plots, dot plots, and heatmaps across all datasets, normalized count were employed. By analyzing the expression of established marker genes, cell types were determined To avoid calculating batch effects, differentially expressed genes (DEGs) were calculated using normalized count values, which included genes present in the integrated dataset. In non-fibroblast clusters (collagens) or non-keratinocyte clusters (keratins), contaminating genes such as keratin and collagen genes (COL1A1, COL1A2, COL3A1, KRT1, KRT5, KRT10, KRT14, and KRTDAP) were omitted from DEG computation. Additionally, genes (Gm42418, Gm17056, and Gm26917) that caused batch effects and technical background noise in mouse scRNAseq were removed from the dataset (44, 252))(252).

References

1. Beer L, Mildner M, Gyöngyösi M, Ankersmit HJ. Peripheral blood mononuclear cell secretome for tissue repair. *Apoptosis : an international journal on programmed cell death*. 2016;21(12):1336-53.
2. Scorsin M, Hagège A, Vilquin JT, Fiszman M, Marotte F, Samuel JL, et al. Comparison of the effects of fetal cardiomyocyte and skeletal myoblast transplantation on postinfarction left ventricular function. *The Journal of thoracic and cardiovascular surgery*. 2000;119(6):1169-75.
3. Kocher AA, Schuster MD, Szabolcs MJ, Takuma S, Burkhoff D, Wang J, et al. Neovascularization of ischemic myocardium by human bone-marrow-derived angioblasts prevents cardiomyocyte apoptosis, reduces remodeling and improves cardiac function. *Nat Med*. 2001;7(4):430-6.
4. Orlic D, Kajstura J, Chimenti S, Bodine DM, Leri A, Anversa P. Transplanted adult bone marrow cells repair myocardial infarcts in mice. *Annals of the New York Academy of Sciences*. 2001;938:221-9; discussion 9-30.
5. Orlic D, Kajstura J, Chimenti S, Jakoniuk I, Anderson SM, Li B, et al. Bone marrow cells regenerate infarcted myocardium. *Nature*. 2001;410(6829):701-5.
6. Oshima H, Inoue H, Matsuzaki K, Tanabe M, Kumagai N. Permanent restoration of human skin treated with cultured epithelium grafting--wound healing by stem cell based tissue engineering. *Human cell*. 2002;15(3):118-28.
7. Strauer BE, Brehm M, Zeus T, Gattermann N, Hernandez A, Sorg RV, et al. [Intracoronary, human autologous stem cell transplantation for myocardial regeneration following myocardial infarction]. *Deutsche medizinische Wochenschrift (1946)*. 2001;126(34-35):932-8.
8. Bartsch T, Brehm M, Zeus T, Kögler G, Wernet P, Strauer BE. Transplantation of autologous mononuclear bone marrow stem cells in patients with peripheral arterial disease (the TAM-PAD study). *Clinical research in cardiology : official journal of the German Cardiac Society*. 2007;96(12):891-9.
9. Orlic D, Hill JM, Arai AE. Stem cells for myocardial regeneration. *Circ Res*. 2002;91(12):1092-102.
10. Assmus B, Schächinger V, Teupe C, Britten M, Lehmann R, Döbert N, et al. Transplantation of Progenitor Cells and Regeneration Enhancement in Acute Myocardial Infarction (TOPCARE-AMI). *Circulation*. 2002;106(24):3009-17.
11. Hatzistergos KE, Quevedo H, Oskouei BN, Hu Q, Feigenbaum GS, Margitich IS, et al. Bone marrow mesenchymal stem cells stimulate cardiac stem cell proliferation and differentiation. *Circ Res*. 2010;107(7):913-22.
12. Premer C, Blum A, Bellio MA, Schulman IH, Hurwitz BE, Parker M, et al. Allogeneic Mesenchymal Stem Cells Restore Endothelial Function in Heart Failure by Stimulating Endothelial Progenitor Cells. *EBioMedicine*. 2015;2(5):467-75.
13. Nguyen PK, Lan F, Wang Y, Wu JC. Imaging: guiding the clinical translation of cardiac stem cell therapy. *Circ Res*. 2011;109(8):962-79.
14. Wollert KC, Drexler H. Mesenchymal stem cells for myocardial infarction: promises and pitfalls. *Circulation*. 2005;112(2):151-3.
15. Gneocchi M, He H, Liang OD, Melo LG, Morello F, Mu H, et al. Paracrine action accounts for marked protection of ischemic heart by Akt-modified mesenchymal stem cells. *Nature Medicine*. 2005;11(4):367-8.
16. Holzinger C, Zuckermann A, Kopp C, Schöllhammer A, Imhof M, Zwölfer W, et al. Treatment of non-healing skin ulcers with autologous activated mononuclear cells. *European journal of vascular surgery*. 1994;8(3):351-6.
17. Ankersmit HJ, Hoetzenecker K, Dietl W, Soleiman A, Horvat R, Wolfsberger M, et al. Irradiated cultured apoptotic peripheral blood mononuclear cells regenerate infarcted myocardium. *European journal of clinical investigation*. 2009;39(6):445-56.
18. Lichtenauer M, Mildner M, Baumgartner A, Hasun M, Werba G, Beer L, et al. Intravenous and intramyocardial injection of apoptotic white blood cell suspensions prevents ventricular remodelling by increasing elastin expression in cardiac scar tissue after myocardial infarction. *Basic research in cardiology*. 2011;106(4):645-55.
19. Lichtenauer M, Mildner M, Hoetzenecker K, Zimmermann M, Podesser BK, Sipos W, et al. Secretome of apoptotic peripheral blood cells (APOSEC) confers cytoprotection to cardiomyocytes and

- inhibits tissue remodelling after acute myocardial infarction: a preclinical study. *Basic research in cardiology*. 2011;106(6):1283-97.
20. Mildner M, Hacker S, Haider T, Gschwandtner M, Werba G, Barresi C, et al. Secretome of peripheral blood mononuclear cells enhances wound healing. *PLoS one*. 2013;8(3):e60103.
 21. Hacker S, Mittermayr R, Nickl S, Haider T, Leberherz-Eichinger D, Beer L, et al. Paracrine Factors from Irradiated Peripheral Blood Mononuclear Cells Improve Skin Regeneration and Angiogenesis in a Porcine Burn Model. *Scientific reports*. 2016;6:25168.
 22. Pavo N, Zimmermann M, Pils D, Mildner M, Petrás Z, Petneházy Ö, et al. Long-acting beneficial effect of percutaneously intramyocardially delivered secretome of apoptotic peripheral blood cells on porcine chronic ischemic left ventricular dysfunction. *Biomaterials*. 2014;35(11):3541-50.
 23. Altmann P, Mildner M, Haider T, Traxler D, Beer L, Ristl R, et al. Secretomes of apoptotic mononuclear cells ameliorate neurological damage in rats with focal ischemia. *F1000Res*. 2014;3:131.
 24. Haider T, Hoftberger R, Ruger B, Mildner M, Blumer R, Mitterbauer A, et al. The secretome of apoptotic human peripheral blood mononuclear cells attenuates secondary damage following spinal cord injury in rats. *Experimental neurology*. 2015;267:230-42.
 25. Beer L, Zimmermann M, Mitterbauer A, Ellinger A, Gruber F, Narzt MS, et al. Analysis of the Secretome of Apoptotic Peripheral Blood Mononuclear Cells: Impact of Released Proteins and Exosomes for Tissue Regeneration. *Scientific reports*. 2015;5:16662.
 26. Kasiri MM, Beer L, Nemeč L, Gruber F, Pietkiewicz S, Haider T, et al. Dying blood mononuclear cell secretome exerts antimicrobial activity. *European journal of clinical investigation*. 2016;46(10):853-63.
 27. Wagner T, Traxler D, Simader E, Beer L, Narzt M-S, Gruber F, et al. Different pro-angiogenic potential of γ -irradiated PBMC-derived secretome and its subfractions. *Scientific reports*. 2018;8(1):18016.
 28. Simader E, Beer L, Laggner M, Vorstandlechner V, Gugerell A, Erb M, et al. Tissue-regenerative potential of the secretome of γ -irradiated peripheral blood mononuclear cells is mediated via TNFRSF1B-induced necroptosis. *Cell death & disease*. 2019;10(10):729.
 29. Beer L, Mildner M, Ankersmit HJ. Cell secretome based drug substances in regenerative medicine: when regulatory affairs meet basic science. *Annals of translational medicine*. 2017;5(7):170.
 30. Gugerell A, Gouya-Lechner G, Hofbauer H, Laggner M, Trautinger F, Almer G, et al. Safety and clinical efficacy of the secretome of stressed peripheral blood mononuclear cells in patients with diabetic foot ulcer—study protocol of the randomized, placebo-controlled, double-blind, multicenter, international phase II clinical trial MARSYAS II. *Trials*. 2021;22(1):10.
 31. Laggner M, Gugerell A, Bachmann C, Hofbauer H, Vorstandlechner V, Seibold M, et al. Reproducibility of GMP-compliant production of therapeutic stressed peripheral blood mononuclear cell-derived secretomes, a novel class of biological medicinal products. *Stem cell research & therapy*. 2020;11(1):9.
 32. Wuschko S, Gugerell A, Chabicovsky M, Hofbauer H, Laggner M, Erb M, et al. Toxicological testing of allogeneic secretome derived from peripheral mononuclear cells (APOSEC): a novel cell-free therapeutic agent in skin disease. 2019;9(1):5598.
 33. Gugerell A, Gouya-Lechner G, Hofbauer H, Laggner M, Trautinger F, Almer G, et al. Safety and clinical efficacy of the secretome of stressed peripheral blood mononuclear cells in patients with diabetic foot ulcer—study protocol of the randomized, placebo-controlled, double-blind, multicenter, international phase II clinical trial MARSYAS II. *Trials*. 2021;22(1):10.
 34. Simader E, Traxler D. Safety and tolerability of topically administered autologous, apoptotic PBMC secretome (APOSEC) in dermal wounds: a randomized Phase 1 trial (MARSYAS I). 2017;7(1):6216.
 35. Hacker S, Mittermayr R, Traxler D, Keibl C, Resch A, Salminger S, et al. The secretome of stressed peripheral blood mononuclear cells increases tissue survival in a rodent epigastric flap model. *Bioengineering & translational medicine*. 2021;6(1):e10186.
 36. Laggner M, Acosta GS, Kitzmüller C, Copic D, Gruber F, Altenburger LM, et al. The secretome of irradiated peripheral blood mononuclear cells attenuates activation of mast cells and basophils. *EBioMedicine*. 2022;81:104093.
 37. Klas K, Ondracek AS, Hofbauer TM, Mangold A, Pfisterer K, Laggner M, et al. The Effect of Paracrine Factors Released by Irradiated Peripheral Blood Mononuclear Cells on Neutrophil Extracellular Trap Formation. *Antioxidants*. 2022;11(8):1559.

38. Copic D, Direder M, Schossleitner K, Laggner M, Klas K, Bormann D, et al. Paracrine Factors of Stressed Peripheral Blood Mononuclear Cells Activate Proangiogenic and Anti-Proteolytic Processes in Whole Blood Cells and Protect the Endothelial Barrier. *Pharmaceutics*. 2022;14(8):1600.
39. Ankersmit HJ, Hoetzenecker K, Dietl W, Soleiman A, Horvat R, Wolfsberger M, et al. Irradiated cultured apoptotic peripheral blood mononuclear cells regenerate infarcted myocardium. *European journal of clinical investigation*. 2009;39(6):445-56.
40. Hoetzenecker K, Assinger A, Lichtenauer M, Mildner M, Schweiger T, Starlinger P, et al. Secretome of apoptotic peripheral blood cells (APOSEC) attenuates microvascular obstruction in a porcine closed chest reperfused acute myocardial infarction model: role of platelet aggregation and vasodilation. *Basic research in cardiology*. 2012;107(5):292.
41. Hoetzenecker K, Zimmermann M, Hoetzenecker W, Schweiger T, Kollmann D, Mildner M, et al. Mononuclear cell secretome protects from experimental autoimmune myocarditis. *European heart journal*. 2013;36(11):676-85.
42. Pavo N, Zimmermann M, Pils D, Mildner M, Petrás Z, Petneházy Ö, et al. Long-acting beneficial effect of percutaneously intramyocardially delivered secretome of apoptotic peripheral blood cells on porcine chronic ischemic left ventricular dysfunction. *Biomaterials*. 2014;35(11):3541-50.
43. Laggner M, Copic D, Nemeč L, Vorstandlechner V, Gugerell A, Gruber F, et al. Therapeutic potential of lipids obtained from γ -irradiated PBMCs in dendritic cell-mediated skin inflammation. *EBioMedicine*. 2020;55:102774.
44. Vorstandlechner V, Copic D, Klas K, Direder M, Golabi B, Radtke C, et al. The Secretome of Irradiated Peripheral Mononuclear Cells Attenuates Hypertrophic Skin Scarring. *Pharmaceutics*. 2023;15(4).
45. Panahipour L, Kochergina E, Laggner M, Zimmermann M, Mildner M, Ankersmit HJ, et al. Role for Lipids Secreted by Irradiated Peripheral Blood Mononuclear Cells in Inflammatory Resolution in Vitro. *International journal of molecular sciences*. 2020;21(13):4694.
46. Hacker S, Mittermayr R, Nickl S, Haider T, Leberz-Eichinger D, Beer L, et al. Paracrine Factors from Irradiated Peripheral Blood Mononuclear Cells Improve Skin Regeneration and Angiogenesis in a Porcine Burn Model. *Scientific reports*. 2016;6:25168.
47. Simader E, Beer L, Laggner M, Vorstandlechner V, Gugerell A, Erb M, et al. Tissue-regenerative potential of the secretome of gamma-irradiated peripheral blood mononuclear cells is mediated via TNFRSF1B-induced necroptosis. *Cell death & disease*. 2019;10(10):729.
48. Mildner CS, Copic D, Zimmermann M, Lichtenauer M, Direder M, Klas K, et al. Secretome of Stressed Peripheral Blood Mononuclear Cells Alters Transcriptome Signature in Heart, Liver, and Spleen after an Experimental Acute Myocardial Infarction: An In Silico Analysis. *Biology*. 2022;11(1):116.
49. Bormann D, Gugerell A, Ankersmit HJ, Mildner M. Therapeutic Application of Cell Secretomes in Cutaneous Wound Healing. *Journal of Investigative Dermatology*. 2023;143(6):893-912.
50. Bayat A, McGrouther DA, Ferguson MWJ. Skin scarring. *BMJ : British Medical Journal*. 2003;326(7380):88-92.
51. Leavitt T, Hu MS, Marshall CD, Barnes LA, Lorenz HP, Longaker MT. Scarless wound healing: finding the right cells and signals. *Cell and tissue research*. 2016;365(3):483-93.
52. Sen CK, Gordillo GM, Roy S, Kirsner R, Lambert L, Hunt TK, et al. Human skin wounds: a major and snowballing threat to public health and the economy. *Wound repair and regeneration : official publication of the Wound Healing Society [and] the European Tissue Repair Society*. 2009;17(6):763-71.
53. Bock O, Schmid-Ott G, Malewski P, Mrowietz U. Quality of life of patients with keloid and hypertrophic scarring. *Archives of dermatological research*. 2006;297(10):433-8.
54. Van Loey NE, Bremer M, Faber AW, Middelkoop E, Nieuwenhuis MK. Itching following burns: epidemiology and predictors. *The British journal of dermatology*. 2008;158(1):95-100.
55. Bloemen MC, van der Veer WM, Ulrich MM, van Zuijlen PP, Niessen FB, Middelkoop E. Prevention and curative management of hypertrophic scar formation. *Burns : journal of the International Society for Burn Injuries*. 2009;35(4):463-75.
56. Anthonissen M, Daly D, Janssens T, Van den Kerckhove E. The effects of conservative treatments on burn scars: A systematic review. *Burns : journal of the International Society for Burn Injuries*. 2016;42(3):508-18.
57. Kafka M, Collins V, Kamolz LP, Rappl T, Branski LK, Wurzer P. Evidence of invasive and noninvasive treatment modalities for hypertrophic scars: A systematic review. *Wound repair and*

- regeneration : official publication of the Wound Healing Society [and] the European Tissue Repair Society. 2017;25(1):139-44.
58. Bao Y, Xu S, Pan Z, Deng J, Li X, Pan F. Comparative Efficacy and Safety of Common Therapies in Keloids and Hypertrophic Scars: A Systematic Review and Meta-analysis. *Aesthetic plastic surgery*. 2019.
 59. Sontheimer RD. Skin Is Not the Largest Organ. *Journal of Investigative Dermatology*. 2014;134(2):581-2.
 60. Takeo M, Lee W, Ito M. Wound Healing and Skin Regeneration. *Cold Spring Harbor Perspectives in Medicine*. 2015;5(1):a023267.
 61. Belokhvostova D, Berzanskyte I, Cujba AM, Jowett G, Marshall L, Prueller J, et al. Homeostasis, regeneration and tumour formation in the mammalian epidermis. *The International journal of developmental biology*. 2018;62(6-7-8):571-82.
 62. Proksch E, Brandner JM, Jensen J-M. The skin: an indispensable barrier. *Experimental dermatology*. 2008;17(12):1063-72.
 63. Homberg M, Magin TM. Beyond expectations: novel insights into epidermal keratin function and regulation. *International review of cell and molecular biology*. 2014;311:265-306.
 64. Ojeh N, Pastar I, Tomic-Canic M, Stojadinovic O. Stem Cells in Skin Regeneration, Wound Healing, and Their Clinical Applications. *International journal of molecular sciences*. 2015;16(10):25476-501.
 65. Werner S, Krieg T, Smola H. Keratinocyte-fibroblast interactions in wound healing. *The Journal of investigative dermatology*. 2007;127(5):998-1008.
 66. Deckers J, Hammad H, Hoste E. Langerhans Cells: Sensing the Environment in Health and Disease. *Frontiers in immunology*. 2018;9:93-.
 67. Wong R, Geyer S, Weninger W, Guimberteau JC, Wong JK. The dynamic anatomy and patterning of skin. *Experimental dermatology*. 2016;25(2):92-8.
 68. Nguyen AV, Soulika AM. The Dynamics of the Skin's Immune System. *International journal of molecular sciences*. 2019;20(8).
 69. Zimmerman A, Bai L, Ginty DD. The gentle touch receptors of mammalian skin. *Science (New York, NY)*. 2014;346(6212):950-4.
 70. Rippa AL, Kalabusheva EP, Vorotelyak EA. Regeneration of Dermis: Scarring and Cells Involved. 2019;8(6).
 71. Janson DG, Saintigny G, van Adrichem A, Mahé C, El Ghalbzouri A. Different Gene Expression Patterns in Human Papillary and Reticular Fibroblasts. *Journal of Investigative Dermatology*. 2012;132(11):2565-72.
 72. Janson D, Saintigny G, Mahe C, El Ghalbzouri A. Papillary fibroblasts differentiate into reticular fibroblasts after prolonged in vitro culture. *Experimental dermatology*. 2013;22(1):48-53.
 73. Canty EG, Kadler KE. Procollagen trafficking, processing and fibrillogenesis. *Journal of cell science*. 2005;118(Pt 7):1341-53.
 74. Weihermann AC, Lorencini M, Brohem CA, de Carvalho CM. Elastin structure and its involvement in skin photoageing. *International journal of cosmetic science*. 2017;39(3):241-7.
 75. Halper J, Kjaer M. Basic components of connective tissues and extracellular matrix: elastin, fibrillin, fibulins, fibrinogen, fibronectin, laminin, tenascins and thrombospondins. *Advances in experimental medicine and biology*. 2014;802:31-47.
 76. Bodnar RJ, Satish L, Yates CC, Wells A. Pericytes: A newly recognized player in wound healing. *Wound repair and regeneration : official publication of the Wound Healing Society [and] the European Tissue Repair Society*. 2016;24(2):204-14.
 77. Guerrero-Juarez CF, Plikus MV. Emerging nonmetabolic functions of skin fat. *Nature reviews Endocrinology*. 2018;14(3):163-73.
 78. Gurtner GC, Werner S, Barrandon Y, Longaker MT. Wound repair and regeneration. *Nature*. 2008;453(7193):314-21.
 79. Eming SA, Martin P, Tomic-Canic M. Wound repair and regeneration: mechanisms, signaling, and translation. *Science translational medicine*. 2014;6(265):265sr6.
 80. Gebhard F, Huber-Lang M. Polytrauma—pathophysiology and management principles. *Langenbeck's Archives of Surgery*. 2008;393(6):825-31.
 81. Denning NL, Aziz M, Gurien SD, Wang P. DAMPs and NETs in Sepsis. *Frontiers in immunology*. 2019;10:2536.

82. Hettiaratchy S, Dziewulski P. ABC of burns: pathophysiology and types of burns. *BMJ (Clinical research ed)*. 2004;328(7453):1427-9.
83. Mack M. Inflammation and fibrosis. *Matrix biology : journal of the International Society for Matrix Biology*. 2018;68-69:106-21.
84. Rock KL, Latz E, Ontiveros F, Kono H. The Sterile Inflammatory Response. *Annual Review of Immunology*. 2010;28(1):321-42.
85. Driskell RR, Lichtenberger BM, Hoste E, Kretzschmar K, Simons BD, Charalambous M, et al. Distinct fibroblast lineages determine dermal architecture in skin development and repair. *Nature*. 2013;504:277.
86. Lovvorn HN, 3rd, Cheung DT, Nimni ME, Perelman N, Estes JM, Adzick NS. Relative distribution and crosslinking of collagen distinguish fetal from adult sheep wound repair. *Journal of pediatric surgery*. 1999;34(1):218-23.
87. Gushiken LFS, Beserra FP, Bastos JK, Jackson CJ, Pellizzon CH. Cutaneous Wound Healing: An Update from Physiopathology to Current Therapies. *Life*. 2021;11(7):665.
88. Zomer HD, Trentin AG. Skin wound healing in humans and mice: Challenges in translational research. *Journal of dermatological science*. 2018;90(1):3-12.
89. Lindblad WJ. Considerations for selecting the correct animal model for dermal wound-healing studies. *Journal of Biomaterials Science, Polymer Edition*. 2008;19(8):1087-96.
90. Wong VW, Sorkin M, Glotzbach JP, Longaker MT, Gurtner GC. Surgical approaches to create murine models of human wound healing. *Journal of biomedicine & biotechnology*. 2011;2011:969618.
91. Ferguson MW, O'Kane S. Scar-free healing: from embryonic mechanisms to adult therapeutic intervention. *Philosophical transactions of the Royal Society of London Series B, Biological sciences*. 2004;359(1445):839-50.
92. Pakshir P, Hinz B. The big five in fibrosis: Macrophages, myofibroblasts, matrix, mechanics, and miscommunication. *Matrix biology : journal of the International Society for Matrix Biology*. 2018;68-69:81-93.
93. Walthall J, Anand P, Rehman UH. Dupuytren's Contracture. StatPearls. Treasure Island (FL): StatPearls Publishing
StatPearls Publishing LLC.; 2020.
94. Schmieder SJ, Ferrer-Bruker SJ. Hypertrophic Scarring. StatPearls. Treasure Island (FL): StatPearls Publishing
StatPearls Publishing LLC.; 2020.
95. Hinz B. Myofibroblasts. *Experimental eye research*. 2016;142:56-70.
96. Walraven M, Hinz B. Therapeutic approaches to control tissue repair and fibrosis: Extracellular matrix as a game changer. *Matrix biology : journal of the International Society for Matrix Biology*. 2018;71-72:205-24.
97. LeBleu VS, Neilson EG. Origin and functional heterogeneity of fibroblasts. *FASEB journal : official publication of the Federation of American Societies for Experimental Biology*. 2020;34(3):3519-36.
98. Sorrell JM, Caplan AI. Fibroblasts-a diverse population at the center of it all. *International review of cell and molecular biology*. 2009;276:161-214.
99. Korosec A, Frech S, Gesslbauer B, Vierhapper M, Radtke C, Petzelbauer P, et al. Lineage Identity and Location within the Dermis Determine the Function of Papillary and Reticular Fibroblasts in Human Skin. *The Journal of investigative dermatology*. 2019;139(2):342-51.
100. Hu MS, Moore AL, Longaker MT. A Fibroblast Is Not a Fibroblast Is Not a Fibroblast. *The Journal of investigative dermatology*. 2018;138(4):729-30.
101. Larson BJ, Longaker MT, Lorenz HP. Scarless Fetal Wound Healing: A Basic Science Review. *Plastic and reconstructive surgery*. 2010;126(4):1172-80.
102. Tabib T, Morse C, Wang T, Chen W, Lafyatis R. SFRP2/DPP4 and FMO1/LSP1 Define Major Fibroblast Populations in Human Skin. *The Journal of investigative dermatology*. 2017.
103. Vorstandlechner V, Laggner M, Kalinina P, Haslik W, Radtke C, Shaw L, et al. Deciphering the functional heterogeneity of skin fibroblasts using single-cell RNA sequencing. *FASEB journal : official publication of the Federation of American Societies for Experimental Biology*. 2020.

104. Ascensión AM, Fuertes-Álvarez S, Ibañez-Solé O, Izeta A, Araúzo-Bravo MJ. Human Dermal Fibroblast Subpopulations Are Conserved across Single-Cell RNA Sequencing Studies. *The Journal of investigative dermatology*. 2020.
105. Walmsley GG, Rinkevich Y, Hu MS, Montoro DT, Lo DD, McArdle A, et al. Live fibroblast harvest reveals surface marker shift in vitro. *Tissue engineering Part C, Methods*. 2015;21(3):314-21.
106. Hinz B, Celetta G, Tomasek JJ, Gabbiani G, Chaponnier C. Alpha-Smooth Muscle Actin Expression Upregulates Fibroblast Contractile Activity. *Molecular Biology of the Cell*. 2001;12(9):2730-41.
107. Kisseleva T, Cong M, Paik Y, Scholten D, Jiang C, Benner C, et al. Myofibroblasts revert to an inactive phenotype during regression of liver fibrosis. *Proceedings of the National Academy of Sciences*. 2012;109(24):9448-53.
108. Carthy JM. TGFbeta signaling and the control of myofibroblast differentiation: Implications for chronic inflammatory disorders. *Journal of cellular physiology*. 2018;233(1):98-106.
109. Zeisberg EM, Tarnavski O, Zeisberg M, Dorfman AL, McMullen JR, Gustafsson E, et al. Endothelial-to-mesenchymal transition contributes to cardiac fibrosis. *Nature Medicine*. 2007;13(8):952-61.
110. Lin S-L, Kisseleva T, Brenner DA, Duffield JS. Pericytes and Perivascular Fibroblasts Are the Primary Source of Collagen-Producing Cells in Obstructive Fibrosis of the Kidney. *The American journal of pathology*. 2008;173(6):1617-27.
111. Bucala R, Spiegel LA, Chesney J, Hogan M, Cerami A. Circulating Fibrocytes Define a New Leukocyte Subpopulation That Mediates Tissue Repair. *Molecular Medicine*. 1994;1(1):71-81.
112. Mori L, Bellini A, Stacey MA, Schmidt M, Mattoli S. Fibrocytes contribute to the myofibroblast population in wounded skin and originate from the bone marrow. *Experimental Cell Research*. 2005;304(1):81-90.
113. Shi-Wen X, Leask A, Abraham D. Regulation and function of connective tissue growth factor/CCN2 in tissue repair, scarring and fibrosis. *Cytokine & Growth Factor Reviews*. 2008;19(2):133-44.
114. Brigstock DR. Connective tissue growth factor (CCN2, CTGF) and organ fibrosis: lessons from transgenic animals. *Journal of Cell Communication and Signaling*. 2010;4(1):1-4.
115. Heldin C-H. Targeting the PDGF signaling pathway in tumor treatment. *Cell Communication and Signaling*. 2013;11(1):97.
116. Siani A, Tirelli N. Myofibroblast differentiation: main features, biomedical relevance, and the role of reactive oxygen species. *Antioxidants & redox signaling*. 2014;21(5):768-85.
117. Liu CJ, Wang YK, Kuo FC, Hsu WH, Yu FJ, Hsieh S, et al. Helicobacter pylori Infection-Induced Hepatoma-Derived Growth Factor Regulates the Differentiation of Human Mesenchymal Stem Cells to Myofibroblast-Like Cells. *Cancers*. 2018;10(12).
118. Hinz B, McCulloch CA, Coelho NM. Mechanical regulation of myofibroblast phenoconversion and collagen contraction. *Exp Cell Res*. 2019;379(1):119-28.
119. Castella LF, Buscemi L, Godbout C, Meister JJ, Hinz B. A new lock-step mechanism of matrix remodelling based on subcellular contractile events. *Journal of cell science*. 2010;123(Pt 10):1751-60.
120. Russo FP, Alison MR, Bigger BW, Amofah E, Florou A, Amin F, et al. The bone marrow functionally contributes to liver fibrosis. *Gastroenterology*. 2006;130(6):1807-21.
121. Varcoe RL, Mikhail M, Guiffre AK, Pennings G, Vicaretti M, Hawthorne WJ, et al. The role of the fibrocyte in intimal hyperplasia. *Journal of thrombosis and haemostasis : JTH*. 2006;4(5):1125-33.
122. Pilling D, Vakil V, Cox N, Gomer RH. TNF-alpha-stimulated fibroblasts secrete lumican to promote fibrocyte differentiation. *Proceedings of the National Academy of Sciences of the United States of America*. 2015;112(38):11929-34.
123. Quan TE, Cowper SE, Bucala R. The role of circulating fibrocytes in fibrosis. *Current Rheumatology Reports*. 2006;8(2):145-50.
124. Abe R, Donnelly SC, Peng T, Bucala R, Metz CN. Peripheral Blood Fibrocytes: Differentiation Pathway and Migration to Wound Sites. *The Journal of Immunology*. 2001;166(12):7556-62.
125. Yang L, Scott PG, Giuffre J, Shankowsky HA, Ghahary A, Tredget EE. Peripheral blood fibrocytes from burn patients: identification and quantification of fibrocytes in adherent cells cultured from peripheral blood mononuclear cells. *Laboratory investigation; a journal of technical methods and pathology*. 2002;82(9):1183-92.

126. Wada T, Sakai N, Matsushima K, Kaneko S. Fibrocytes: A new insight into kidney fibrosis. *Kidney International*. 2007;72(3):269-73.
127. Borthwick LA, Wynn TA, Fisher AJ. Cytokine mediated tissue fibrosis. *Biochimica et Biophysica Acta (BBA) - Molecular Basis of Disease*. 2013;1832(7):1049-60.
128. Bergers G, Song S. The role of pericytes in blood-vessel formation and maintenance. *Neuro-Oncology*. 2005;7(4):452-64.
129. Rock JR, Barkauskas CE, Cronce MJ, Xue Y, Harris JR, Liang J, et al. Multiple stromal populations contribute to pulmonary fibrosis without evidence for epithelial to mesenchymal transition. *Proceedings of the National Academy of Sciences*. 2011;108(52):E1475-E83.
130. Murphy MM, Lawson JA, Mathew SJ, Hutcheson DA, Kardon G. Satellite cells, connective tissue fibroblasts and their interactions are crucial for muscle regeneration. *Development (Cambridge, England)*. 2011;138(17):3625-37.
131. Papayannopoulos V. Neutrophil extracellular traps in immunity and disease. *Nature Reviews Immunology*. 2018;18(2):134-47.
132. Martinod K, Witsch T. Peptidylarginine deiminase 4 promotes age-related organ fibrosis. 2017;214(2):439-58.
133. Smigiel KS, Parks WC. Macrophages, Wound Healing, and Fibrosis: Recent Insights. *Curr Rheumatol Rep*. 2018;20(4):17.
134. Wynn TA, Vannella KM. Macrophages in Tissue Repair, Regeneration, and Fibrosis. *Immunity*. 2016;44(3):450-62.
135. Lucas T, Waisman A, Ranjan R, Roes J, Krieg T, Müller W, et al. Differential Roles of Macrophages in Diverse Phases of Skin Repair. *The Journal of Immunology*. 2010;184(7):3964-77.
136. Tredget EE LY, Megan Delehanty, Heather Shankowsky, and Paul G. Scott. Polarized Th2 Cytokine Production in Patients with Hypertrophic Scar Following Thermal Injury. *Journal of Interferon & Cytokine Research*. 2006;26(3):179-89.
137. Gieseck RL, 3rd, Wilson MS, Wynn TA. Type 2 immunity in tissue repair and fibrosis. *Nature reviews Immunology*. 2018;18(1):62-76.
138. Stone RC, Pastar I, Ojeh N, Chen V, Liu S, Garzon KI, et al. Epithelial-mesenchymal transition in tissue repair and fibrosis. *Cell and tissue research*. 2016;365(3):495-506.
139. Ghahary A, Ghaffari A. Role of keratinocyte-fibroblast cross-talk in development of hypertrophic scar. *Wound repair and regeneration : official publication of the Wound Healing Society [and] the European Tissue Repair Society*. 2007;15 Suppl 1:S46-53.
140. Kiritsi D, Nystrom A. The role of TGFbeta in wound healing pathologies. *Mechanisms of ageing and development*. 2017.
141. Lodyga M, Hinz B. TGF-beta1 - A truly transforming growth factor in fibrosis and immunity. *Seminars in cell & developmental biology*. 2019.
142. Miyazawa K, Miyazono K. Regulation of TGF-β Family Signaling by Inhibitory Smads. *Cold Spring Harbor perspectives in biology*. 2017;9(3).
143. Transforming Growth Factor Beta Signaling in Cutaneous Wound Healing: Lessons Learned from Animal Studies. *Advances in wound care*. 2013;2(5):225-37.
144. Barrientos S, Stojadinovic O, Golinko MS, Brem H, Tomic-Canic M. Growth factors and cytokines in wound healing. *Wound repair and regeneration : official publication of the Wound Healing Society [and] the European Tissue Repair Society*. 2008;16(5):585-601.
145. Wilgus TA. Vascular Endothelial Growth Factor and Cutaneous Scarring. *Advances in wound care*. 2019;8(12):671-8.
146. Lian N, Li T. Growth factor pathways in hypertrophic scars: Molecular pathogenesis and therapeutic implications. *Biomedicine & Pharmacotherapy*. 2016;84:42-50.
147. Dvorak HF. VPF/VEGF and the angiogenic response. *Seminars in Perinatology*. 2000;24(1):75-8.
148. DiPietro LA. Angiogenesis and scar formation in healing wounds. *Current opinion in rheumatology*. 2013;25(1):87-91.
149. Tonnesen MG, Feng X, Clark RA. Angiogenesis in wound healing. *The journal of investigative dermatology Symposium proceedings*. 2000;5(1):40-6.
150. Guo Y, Xiao L, Sun L, Liu F. Wnt/beta-catenin signaling: a promising new target for fibrosis diseases. *Physiological research*. 2012;61(4):337-46.

151. Katoh M. Multilayered prevention and treatment of chronic inflammation, organ fibrosis and cancer associated with canonical WNT/betacatenin signaling activation (Review). *International journal of molecular medicine*. 2018;42(2):713-25.
152. Cruciat C-M, Niehrs C. Secreted and transmembrane wnt inhibitors and activators. *Cold Spring Harbor perspectives in biology*. 2013;5(3):a015081-a.
153. Rinkevich Y, Walmsley GG, Hu MS, Maan ZN, Newman AM, Drukker M, et al. Skin fibrosis. Identification and isolation of a dermal lineage with intrinsic fibrogenic potential. *Science (New York, NY)*. 2015;348(6232):aaa2151.
154. Zhang K-W, Liu S-Y, Jia Y, Zou M-L, Teng Y-Y, Chen Z-H, et al. Insight into the role of DPP-4 in fibrotic wound healing. *Biomedicine & Pharmacotherapy*. 2022;151:113143.
155. Klemann C, Wagner L, Stephan M, von Horsten S. Cut to the chase: a review of CD26/dipeptidyl peptidase-4's (DPP4) entanglement in the immune system. *Clinical and experimental immunology*. 2016;185(1):1-21.
156. Gupta KK, Donahue DL. Plasminogen Activator Inhibitor-1 Protects Mice Against Cardiac Fibrosis by Inhibiting Urokinase-type Plasminogen Activator-mediated Plasminogen Activation. 2017;7(1):365.
157. Schuliga M, Jaffar J, Harris T, Knight DA, Westall G, Stewart AG. The fibrogenic actions of lung fibroblast-derived urokinase: a potential drug target in IPF. *Scientific reports*. 2017;7:41770.
158. Makrilakis K. The Role of DPP-4 Inhibitors in the Treatment Algorithm of Type 2 Diabetes Mellitus: When to Select, What to Expect. *International journal of environmental research and public health*. 2019;16(15).
159. Aroor AR, Habibi J, Kandikattu HK, Garro-Kacher M, Barron B, Chen D, et al. Dipeptidyl peptidase-4 (DPP-4) inhibition with linagliptin reduces western diet-induced myocardial TRAF3IP2 expression, inflammation and fibrosis in female mice. *Cardiovascular diabetology*. 2017;16(1):61.
160. Hong SK, Choo EH, Ihm SH, Chang K, Seung KB. Dipeptidyl peptidase 4 inhibitor attenuates obesity-induced myocardial fibrosis by inhibiting transforming growth factor-beta1 and Smad2/3 pathways in high-fat diet-induced obesity rat model. *Metabolism: clinical and experimental*. 2017;76:42-55.
161. Kaji K, Yoshiji H, Ikenaka Y, Noguchi R, Aihara Y, Douhara A, et al. Dipeptidyl peptidase-4 inhibitor attenuates hepatic fibrosis via suppression of activated hepatic stellate cell in rats. *Journal of gastroenterology*. 2014;49(3):481-91.
162. Suzuki T, Tada Y, Gladson S, Nishimura R, Shimomura I, Karasawa S, et al. Vildagliptin ameliorates pulmonary fibrosis in lipopolysaccharide-induced lung injury by inhibiting endothelial-to-mesenchymal transition. *Respiratory research*. 2017;18(1):177.
163. Uchida T, Oda T, Matsubara H, Watanabe A, Takechi H, Oshima N, et al. Renoprotective effects of a dipeptidyl peptidase 4 inhibitor in a mouse model of progressive renal fibrosis. *Renal failure*. 2017;39(1):340-9.
164. Schuliga M, Grainge C, Westall G, Knight D. The fibrogenic actions of the coagulant and plasminogen activation systems in pulmonary fibrosis. *Int J Biochem Cell Biol*. 2018;97:108-17.
165. Lay AJ, Zhang HE, McCaughan GW, Gorrell MD. Fibroblast activation protein in liver fibrosis. *Frontiers in bioscience (Landmark edition)*. 2019;24:1-17.
166. Shi S, Koya D, Kanasaki K. Dipeptidyl peptidase-4 and kidney fibrosis in diabetes. *Fibrogenesis & tissue repair*. 2016;9:1.
167. Hu MS, Longaker MT. Dipeptidyl Peptidase-4, Wound Healing, Scarring, and Fibrosis. *Plastic and reconstructive surgery*. 2016;138(5):1026-31.
168. Thielitz A, Vetter RW, Schultze B, Wrenger S, Simeoni L, Ansorge S, et al. Inhibitors of dipeptidyl peptidase IV-like activity mediate antifibrotic effects in normal and keloid-derived skin fibroblasts. *The Journal of investigative dermatology*. 2008;128(4):855-66.
169. Thielitz A, Ansorge S, Bank U, Tager M, Wrenger S, Gollnick H, et al. The ectopeptidases dipeptidyl peptidase IV (DP IV) and aminopeptidase N (APN) and their related enzymes as possible targets in the treatment of skin diseases. *Frontiers in bioscience : a journal and virtual library*. 2008;13:2364-75.
170. van Lingen RG, van de Kerkhof PC, Seyger MM, de Jong EM, van Rens DW, Poll MK, et al. CD26/dipeptidyl-peptidase IV in psoriatic skin: upregulation and topographical changes. *The British journal of dermatology*. 2008;158(6):1264-72.
171. Pantano S, Dubost V, Darribat K, Couttet P, Grenet O, Busch S, et al. Differential expression of dipeptidyl peptidase IV in human versus cynomolgus monkey skin eccrine sweat glands. *Journal of molecular histology*. 2013;44(6):733-47.

172. Philippeos C, Telerman SB, Oules B, Pisco AO, Shaw TJ, Elgueta R, et al. Spatial and Single-Cell Transcriptional Profiling Identifies Functionally Distinct Human Dermal Fibroblast Subpopulations. *The Journal of investigative dermatology*. 2018;138(4):811-25.
173. Van den Oord JJ. Expression of CD26/dipeptidyl-peptidase IV in benign and malignant pigment-cell lesions of the skin. *The British journal of dermatology*. 1998;138(4):615-21.
174. Novelli M, Savoia P, Fierro MT, Verrone A, Quaglino P, Bernengo MG. Keratinocytes express dipeptidyl-peptidase IV (CD26) in benign and malignant skin diseases. *The British journal of dermatology*. 1996;134(6):1052-6.
175. Driskell RR, Lichtenberger BM, Hoste E, Kretzschmar K, Simons BD, Charalambous M, et al. Distinct fibroblast lineages determine dermal architecture in skin development and repair. *Nature*. 2013;504(7479):277-81.
176. Driskell RR, Watt FM. Understanding fibroblast heterogeneity in the skin. *Trends in Cell Biology*. 2015;25(2):92-9.
177. Sun Y, Zhu D, Chen F, Qian M, Wei H, Chen W, et al. SFRP2 augments WNT16B signaling to promote therapeutic resistance in the damaged tumor microenvironment. *Oncogene*. 2016;35(33):4321-34.
178. Heinosaalo T, Gabriel M, Kallio L, Adhikari P, Huhtinen K, Laajala TD, et al. Secreted frizzled-related protein 2 (SFRP2) expression promotes lesion proliferation via canonical WNT signaling and indicates lesion borders in extraovarian endometriosis. *Human reproduction (Oxford, England)*. 2018;33(5):817-31.
179. Di Lullo GA, Sweeney SM, Korkko J, Ala-Kokko L, San Antonio JD. Mapping the ligand-binding sites and disease-associated mutations on the most abundant protein in the human, type I collagen. *The Journal of biological chemistry*. 2002;277(6):4223-31.
180. Wu M CK, Crane JS. *Biochemistry, . Collagen Synthesis. . StatPearls Publishing*. 2021.
181. Canty EG, Kadler KE. Procollagen trafficking, processing and fibrillogenesis. *Journal of cell science*. 2005;118(7):1341-53.
182. Eremenko E, Ding J, Kwan P, Tredget EE. The Biology of Extracellular Matrix Proteins in Hypertrophic Scarring. *Advances in wound care*. 2022;11(5):234-54.
183. Mithieux SM, Weiss AS. Elastin. *Advances in protein chemistry*. 2005;70:437-61.
184. Reichheld SE, Muiznieks LD, Lu R, Sharpe S, Keeley FW. Sequence variants of human tropoelastin affecting assembly, structural characteristics and functional properties of polymeric elastin in health and disease. *Matrix biology : journal of the International Society for Matrix Biology*. 2019;84:68-80.
185. Almine JF, Wise SG, Weiss AS. Elastin signaling in wound repair. *Birth defects research Part C, Embryo today : reviews*. 2012;96(3):248-57.
186. Schultz GS, Wysocki A. Interactions between extracellular matrix and growth factors in wound healing. *Wound Repair and Regeneration*. 2009;17(2):153-62.
187. Davidson JM, Zang MC, Zoia O, Giro MG. Regulation of elastin synthesis in pathological states. *Ciba Foundation symposium*. 1995;192:81-94; discussion -9.
188. Kähäri VM, Olsen DR, Rhudy RW, Carrillo P, Chen YQ, Uitto J. Transforming growth factor-beta up-regulates elastin gene expression in human skin fibroblasts. Evidence for post-transcriptional modulation. *Laboratory investigation; a journal of technical methods and pathology*. 1992;66(5):580-8.
189. Daamen WF, Quaglino D. Signaling pathways in elastic tissues. *Cellular signalling*. 2019;63:109364.
190. Godwin ARF, Singh M, Lockhart-Cairns MP, Alanazi YF, Cain SA, Baldock C. The role of fibrillin and microfibril binding proteins in elastin and elastic fibre assembly. *Matrix biology : journal of the International Society for Matrix Biology*. 2019;84:17-30.
191. Pankov R, Yamada KM. Fibronectin at a glance. *Journal of cell science*. 2002;115(Pt 20):3861-3.
192. Lenselink EA. Role of fibronectin in normal wound healing. *International wound journal*. 2015;12(3):313-6.
193. Moretti L, Stalfort J, Barker TH, Abeyayehu D. The interplay of fibroblasts, the extracellular matrix, and inflammation in scar formation. *The Journal of biological chemistry*. 2022;298(2):101530.
194. Iozzo RV. MATRIX PROTEOGLYCANS: From Molecular Design to Cellular Function. *Annual Review of Biochemistry*. 1998;67(1):609-52.

195. Iozzo RV, Schaefer L. Proteoglycan form and function: A comprehensive nomenclature of proteoglycans. *Matrix Biology*. 2015;42:11-55.
196. Pang X, Dong N, Zheng Z. Small Leucine-Rich Proteoglycans in Skin Wound Healing. *Frontiers in pharmacology*. 2019;10:1649.
197. Halper J. Proteoglycans and diseases of soft tissues. *Advances in experimental medicine and biology*. 2014;802:49-58.
198. Honardoust D, Varkey M, Hori K, Ding J, Shankowsky HA, Tredget EE. Small leucine-rich proteoglycans, decorin and fibromodulin, are reduced in postburn hypertrophic scar. *Wound repair and regeneration* : official publication of the Wound Healing Society [and] the European Tissue Repair Society. 2011;19(3):368-78.
199. Velasco J, Li J, DiPietro L, Stepp MA, Sandy JD, Plaas A. Adamts5 deletion blocks murine dermal repair through CD44-mediated aggrecan accumulation and modulation of transforming growth factor β 1 (TGF β 1) signaling. *The Journal of biological chemistry*. 2011;286(29):26016-27.
200. Lalonde M-E, Durocher Y. Therapeutic glycoprotein production in mammalian cells. *Journal of Biotechnology*. 2017;251:128-40.
201. Brik A, Ficht S, Yang Y-Y, Wong C-H. Sugar-Assisted Ligation of N-Linked Glycopeptides with Broad Sequence Tolerance at the Ligation Junction. *Journal of the American Chemical Society*. 2006;128(46):15026-33.
202. Adams JC, Lawler J. The thrombospondins. *Cold Spring Harbor perspectives in biology*. 2011;3(10):a009712.
203. Bach LA. Insulin-Like Growth Factor Binding Proteins--an Update. *Pediatric endocrinology reviews* : PER. 2015;13(2):521-30.
204. Malinda KM, Kleinman HK. The laminins. *Int J Biochem Cell Biol*. 1996;28(9):957-9.
205. Chiquet-Ehrismann R. Tenascins. *Int J Biochem Cell Biol*. 2004;36(6):986-90.
206. Naba A, Clauser KR, Hoersch S, Liu H, Carr SA, Hynes RO. The matrisome: in silico definition and in vivo characterization by proteomics of normal and tumor extracellular matrices. *Molecular & cellular proteomics* : MCP. 2012;11(4):M111.014647.
207. Aumailley M. The laminin family. *Cell adhesion & migration*. 2013;7(1):48-55.
208. Trebault A, Chan EK, Midwood KS. Regulation of fibroblast migration by tenascin-C. *Biochemical Society transactions*. 2007;35(Pt 4):695-7.
209. de Vega S, Iwamoto T, Yamada Y. Fibulins: multiple roles in matrix structures and tissue functions. *Cellular and molecular life sciences* : CMLS. 2009;66(11-12):1890-902.
210. Timpl R, Sasaki T, Kostka G, Chu M-L. Fibulins: a versatile family of extracellular matrix proteins. *Nature Reviews Molecular Cell Biology*. 2003;4(6):479-89.
211. Murphy-Ullrich JE, Sage EH. Revisiting the matricellular concept. *Matrix biology* : journal of the International Society for Matrix Biology. 2014;37:1-14.
212. Kyriakides TR, Bornstein P. Matricellular proteins as modulators of wound healing and the foreign body response. *Thrombosis and haemostasis*. 2003;90(6):986-92.
213. Wong GS, Rustgi AK. Matricellular proteins: priming the tumour microenvironment for cancer development and metastasis. *British Journal of Cancer*. 2013;108(4):755-61.
214. Gerarduzzi C, Hartmann U, Leask A, Drobetsky E. The Matrix Revolution: Matricellular Proteins and Restructuring of the Cancer Microenvironment. *Cancer Research*. 2020;80(13):2705-17.
215. Takada Y, Ye X, Simon S. The integrins. *Genome Biol*. 2007;8(5):215.
216. Labat-Robert J. Cell-Matrix interactions, the role of fibronectin and integrins. A survey. *Pathologie Biologie*. 2012;60(1):15-9.
217. Khan Z, Marshall JF. The role of integrins in TGF β activation in the tumour stroma. *Cell and tissue research*. 2016;365(3):657-73.
218. Asano Y, Ihn H, Jinnin M, Mimura Y, Tamaki K. Involvement of α 5 β 1 integrin in the establishment of autocrine TGF- β signaling in dermal fibroblasts derived from localized scleroderma. *The Journal of investigative dermatology*. 2006;126(8):1761-9.
219. Verma RP, Hansch C. Matrix metalloproteinases (MMPs): chemical-biological functions and (Q)SARs. *Bioorganic & medicinal chemistry*. 2007;15(6):2223-68.
220. Visse R, Nagase H. Matrix Metalloproteinases and Tissue Inhibitors of Metalloproteinases. *Circulation Research*. 2003;92(8):827-39.
221. Bode W, Maskos K. Structural basis of the matrix metalloproteinases and their physiological inhibitors, the tissue inhibitors of metalloproteinases. *Biological chemistry*. 2003;384(6):863-72.

222. Nagase H, Visse R, Murphy G. Structure and function of matrix metalloproteinases and TIMPs. *Cardiovascular research*. 2006;69(3):562-73.
223. Lambert E, Dassé E, Haye B, Petitfrère E. TIMPs as multifacial proteins. *Critical reviews in oncology/hematology*. 2004;49(3):187-98.
224. Arpino V, Brock M, Gill SE. The role of TIMPs in regulation of extracellular matrix proteolysis. *Matrix biology : journal of the International Society for Matrix Biology*. 2015;44-46:247-54.
225. Hedstrom L. Serine protease mechanism and specificity. *Chemical reviews*. 2002;102(12):4501-24.
226. Ghosh AK, Vaughan DE. PAI-1 in tissue fibrosis. *Journal of cellular physiology*. 2012;227(2):493-507.
227. Heinz A. Elastases and elastokines: elastin degradation and its significance in health and disease. *Critical reviews in biochemistry and molecular biology*. 2020;55(3):252-73.
228. Voynow JA, Shinbashi M. Neutrophil Elastase and Chronic Lung Disease. *Biomolecules*. 2021;11(8).
229. Greene AG, Eivers SB, Dervan EWJ, O'Brien CJ, Wallace DM. Lysyl Oxidase Like 1: Biological roles and regulation. *Experimental eye research*. 2020;193:107975.
230. Ma L, Zeng Y, Wei J, Yang D, Ding G, Liu J, et al. Knockdown of LOXL1 inhibits TGF- β 1-induced proliferation and fibrogenesis of hepatic stellate cells by inhibition of Smad2/3 phosphorylation. *Biomedicine & Pharmacotherapy*. 2018;107:1728-35.
231. Fu X, Liu G, Halim A, Ju Y, Luo Q, Song AG. Mesenchymal Stem Cell Migration and Tissue Repair. *Cells*. 2019;8(8).
232. Falanga V, Iwamoto S, Chartier M, Yufit T, Butmarc J, Kouttab N, et al. Autologous bone marrow-derived cultured mesenchymal stem cells delivered in a fibrin spray accelerate healing in murine and human cutaneous wounds. *Tissue engineering*. 2007;13(6):1299-312.
233. Ojeh N, Pastar I, Tomic-Canic M, Stojadinovic O. Stem Cells in Skin Regeneration, Wound Healing, and Their Clinical Applications. *International journal of molecular sciences*. 2015;16(10):25476-501.
234. Cai Y, Li J, Jia C, He Y, Deng C. Therapeutic applications of adipose cell-free derivatives: a review. 2020;11(1):312.
235. Jo H, Brito S, Kwak BM. Applications of Mesenchymal Stem Cells in Skin Regeneration and Rejuvenation. 2021;22(5).
236. Borovikova AA, Ziegler ME, Banyard DA, Wirth GA, Paydar KZ, Evans GRD, et al. Adipose-Derived Tissue in the Treatment of Dermal Fibrosis: Antifibrotic Effects of Adipose-Derived Stem Cells. *Annals of plastic surgery*. 2018;80(3):297-307.
237. Xie F, Teng L, Xu J, Lu J, Zhang C, Yang L, et al. Adipose-derived mesenchymal stem cells inhibit cell proliferation and migration and suppress extracellular matrix synthesis in hypertrophic-scar and keloid fibroblasts. *Experimental and therapeutic medicine*. 2021;21(2):139.
238. Eming SA, Martin P, Tomic-Canic M. Wound repair and regeneration: Mechanisms, signaling, and translation. *Science translational medicine*. 2014;6(265):265sr6.
239. Montero-Vilchez T, Sierra-Sánchez Á, Sanchez-Diaz M, Quiñones-Vico MI, Sanabria-de-la-Torre R, Martinez-Lopez A, et al. Mesenchymal Stromal Cell-Conditioned Medium for Skin Diseases: A Systematic Review. *Frontiers in cell and developmental biology*. 2021;9:654210.
240. Fang F, Huang R-L, Zheng Y, Liu M, Huo R. Bone marrow derived mesenchymal stem cells inhibit the proliferative and profibrotic phenotype of hypertrophic scar fibroblasts and keloid fibroblasts through paracrine signaling. *Journal of dermatological science*. 2016;83(2):95-105.
241. Templin C, Grote K, Schledzewski K, Ghadri J-R, Schnabel S, Napp LC, et al. Ex vivo expanded haematopoietic progenitor cells improve dermal wound healing by paracrine mechanisms. *Experimental dermatology*. 2009;18(5):445-53.
242. Deng C, He Y, Feng J, Dong Z, Yao Y, Mok H, et al. Extracellular matrix/stromal vascular fraction gel conditioned medium accelerates wound healing in a murine model. *Wound Repair and Regeneration*. 2017;25(6):923-32.
243. Zhou H, Li X, Yin Y, He X-T, An Y, Tian B-M, et al. The proangiogenic effects of extracellular vesicles secreted by dental pulp stem cells derived from periodontally compromised teeth. *Stem cell research & therapy*. 2020;11(1):110.

244. Cho JW, Kang MC, Lee KS. TGF- β 1-treated ADSCs-CM promotes expression of type I collagen and MMP-1, migration of human skin fibroblasts, and wound healing in vitro and in vivo. *International journal of molecular medicine*. 2010;26(6):901-6.
245. Arjunan S, Gan SU, Choolani M, Raj V, Lim J, Biswas A, et al. Inhibition of growth of Asian keloid cells with human umbilical cord Wharton's jelly stem cell-conditioned medium. 2020;11(1):78.
246. Hu CH, Tseng YW, Lee CW, Chiou CY, Chuang SS, Yang JY, et al. Combination of mesenchymal stem cell-conditioned medium and botulinum toxin type A for treating human hypertrophic scars. *Journal of plastic, reconstructive & aesthetic surgery : JPRAS*. 2020;73(3):516-27.
247. Liu J, Ren J, Su L, Cheng S, Zhou J, Ye X, et al. Human adipose tissue-derived stem cells inhibit the activity of keloid fibroblasts and fibrosis in a keloid model by paracrine signaling. *Burns : journal of the International Society for Burn Injuries*. 2018;44(2):370-85.
248. Lee MJ, Kim J, Lee KI, Shin JM, Chae JI, Chung HM. Enhancement of wound healing by secretory factors of endothelial precursor cells derived from human embryonic stem cells. *Cytotherapy*. 2011;13(2):165-78.
249. Lee HJ, Jang YJ. Recent Understandings of Biology, Prophylaxis and Treatment Strategies for Hypertrophic Scars and Keloids. *International journal of molecular sciences*. 2018;19(3).
250. Xiao L, McCann JV, Dudley AC. Isolation and Culture Expansion of Tumor-specific Endothelial Cells. *Journal of visualized experiments : JoVE*. 2015(105):e53072.
251. Halfon S, Abramov N, Grinblat B, Ginis I. Markers distinguishing mesenchymal stem cells from fibroblasts are downregulated with passaging. *Stem cells and development*. 2011;20(1):53-66.
252. Vorstandlechner V, Laggner M, Copic D, Klas K, Direder M, Chen Y, et al. The serine proteases dipeptidyl-peptidase 4 and urokinase are key molecules in human and mouse scar formation. *Nature Communications*. 2021;12(1):6242.
253. Deng C-C, Hu Y-F, Zhu D-H, Cheng Q, Gu J-J, Feng Q-L, et al. Single-cell RNA-seq reveals fibroblast heterogeneity and increased mesenchymal fibroblasts in human fibrotic skin diseases. *Nature Communications*. 2021;12(1):3709.
254. Ma L, Gan C, Huang Y, Wang Y, Luo G, Wu J. Comparative proteomic analysis of extracellular matrix proteins secreted by hypertrophic scar with normal skin fibroblasts. *Burns & trauma*. 2014;2(2):76-83.
255. Liu B, Zhang S, Wang W, Yun Z, Lv L, Chai M, et al. Matrisome Provides a Supportive Microenvironment for Skin Functions of Diverse Species. 2020;6(10):5720-33.
256. Tellman TV, Dede M, Aggarwal VA, Salmon D, Naba A, Farach-Carson MC. Systematic Analysis of Actively Transcribed Core Matrisome Genes Across Tissues and Cell Phenotypes. *Matrix biology : journal of the International Society for Matrix Biology*. 2022.
257. Zhang S, Liu B, Wang W, Lv L, Gao D, Chai M, et al. The "Matrisome" reveals the characterization of skin keloid microenvironment. 2021;35(4):e21237.
258. Zheng Q, Zhang X, Bao P. Understanding Mammalian Hair Follicle Ecosystems by Single-Cell RNA Sequencing. 2022;12(18).
259. Lal H, Ahmad F, Zhou J, Yu JE, Vagnozzi RJ, Guo Y, et al. Cardiac fibroblast glycogen synthase kinase-3 β regulates ventricular remodeling and dysfunction in ischemic heart. *Circulation*. 2014;130(5):419-30.
260. Zhou Y, Zhang Q, Gao Y, Tan M, Zheng R, Zhao L, et al. Induced pluripotent stem cell-conditioned medium suppresses pulmonary fibroblast-to-myofibroblast differentiation via the inhibition of TGF- β 1/Smad pathway. *International journal of molecular medicine*. 2018;41(1):473-84.
261. Kim D-Y, Lee S-H, Fu Y, Jing F, Kim W-Y, Hong S-B, et al. Del-1, an Endogenous Inhibitor of TGF- β Activation, Attenuates Fibrosis. *Frontiers in immunology*. 2020;11.
262. Meng XM, Nikolic-Paterson DJ, Lan HY. TGF- β : the master regulator of fibrosis. *Nature reviews Nephrology*. 2016;12(6):325-38.
263. Akboua H, Eghbalzadeh K, Keser U, Wahlers T, Paunel-Görgülü A. Impaired non-canonical transforming growth factor- β signalling prevents profibrotic phenotypes in cultured peptidylarginine deiminase 4-deficient murine cardiac fibroblasts. 2021;25(20):9674-84.
264. Page MJ, Di Cera E. Serine peptidases: classification, structure and function. *Cellular and molecular life sciences : CMLS*. 2008;65(7-8):1220-36.
265. Di Cera E. Serine proteases. *IUBMB life*. 2009;61(5):510-5.
266. Rabieian R, Boshtam M, Zareei M, Kouhpayeh S, Masoudifar A, Mirzaei H. Plasminogen Activator Inhibitor Type-1 as a Regulator of Fibrosis. 2018;119(1):17-27.

267. Horowitz JC, Tschumperlin DJ, Kim KK, Osterholzer JJ, Subbotina N, Ajayi IO, et al. Urokinase Plasminogen Activator Overexpression Reverses Established Lung Fibrosis. *Thrombosis and haemostasis*. 2019;119(12):1968-80.
268. Hoffmann DC, Textoris C, Oehme F, Klaassen T, Goppelt A, Römer A, et al. Pivotal role for alpha1-antichymotrypsin in skin repair. *The Journal of biological chemistry*. 2011;286(33):28889-901.
269. Zhang L, Yaron JR, Tafoya AM, Wallace SE, Kilbourne J, Haydel S, et al. A Virus-Derived Immune Modulating Serpin Accelerates Wound Closure with Improved Collagen Remodeling. *Journal of clinical medicine*. 2019;8(10).
270. Jenkins G. The role of proteases in transforming growth factor-beta activation. *Int J Biochem Cell Biol*. 2008;40(6-7):1068-78.
271. Lee KY, Ho SC, Lin HC, Lin SM, Liu CY, Huang CD, et al. Neutrophil-derived elastase induces TGF-beta1 secretion in human airway smooth muscle via NF-kappaB pathway. *American journal of respiratory cell and molecular biology*. 2006;35(4):407-14.
272. Taipale J, Lohi J, Saarinen J, Kovanen PT, Keski-Oja J. Human mast cell chymase and leukocyte elastase release latent transforming growth factor-beta 1 from the extracellular matrix of cultured human epithelial and endothelial cells. *The Journal of biological chemistry*. 1995;270(9):4689-96.
273. Ungefroren H. Autocrine TGF- β in Cancer: Review of the Literature and Caveats in Experimental Analysis. *International journal of molecular sciences*. 2021;22(2).
274. Hu H-H, Chen D-Q, Wang Y-N, Feng Y-L, Cao G, Vaziri ND, et al. New insights into TGF- β /Smad signaling in tissue fibrosis. *Chemico-Biological Interactions*. 2018;292:76-83.
275. Zani ML, Tanga A, Saidi A, Serrano H, Dallet-Choisy S, Baranger K, et al. SLPI and trappin-2 as therapeutic agents to target airway serine proteases in inflammatory lung diseases: current and future directions. *Biochemical Society transactions*. 2011;39(5):1441-6.
276. Miao L, St Clair DK. Regulation of superoxide dismutase genes: implications in disease. *Free radical biology & medicine*. 2009;47(4):344-56.
277. Carney BC, Chen JH, Kent RA, Rummani M, Alkhalil A, Moffatt LT, et al. Reactive Oxygen Species Scavenging Potential Contributes to Hypertrophic Scar Formation. *The Journal of surgical research*. 2019;244:312-23.
278. Ghahary A, Karimi-Busheri F, Marcoux Y, Li Y, Tredget EE, Taghi Kilani R, et al. Keratinocyte-releasable stratifin functions as a potent collagenase-stimulating factor in fibroblasts. *The Journal of investigative dermatology*. 2004;122(5):1188-97.
279. Seo BF, Lee JY, Jung SN. Models of abnormal scarring. *BioMed research international*. 2013;2013:423147.
280. Chen L, Mirza R, Kwon Y, DiPietro LA, Koh TJ. The murine excisional wound model: Contraction revisited. *Wound repair and regeneration : official publication of the Wound Healing Society [and] the European Tissue Repair Society*. 2015;23(6):874-7.
281. Yamamoto T, Takagawa S, Katayama I, Yamazaki K, Hamazaki Y, Shinkai H, et al. Animal model of sclerotic skin. I: Local injections of bleomycin induce sclerotic skin mimicking scleroderma. *The Journal of investigative dermatology*. 1999;112(4):456-62.
282. Cameron AM, Adams DH, Greenwood JE, Anderson PJ, Cowin AJ. A novel murine model of hypertrophic scarring using subcutaneous infusion of bleomycin. *Plastic and reconstructive surgery*. 2014;133(1):69-78.
283. Avouac J, Pezet S, Gonzalez V, Baudoin L, Cauvet A, Ruiz B, et al. Estrogens Counteract the Profibrotic Effects of TGF- β and their Inhibition Exacerbates Experimental Dermal Fibrosis. *Journal of Investigative Dermatology*. 2020;140(3):593-601.e7.
284. Wu H, Zeng L, Ou J, Wang T, Chen Y, Nandakumar KS. Estrogen Acts Through Estrogen Receptor- β to Promote Mannan-Induced Psoriasis-Like Skin Inflammation. *Frontiers in immunology*. 2022;13:818173.
285. Tongkao-On W, Yang C, McCarthy BY, De Silva WGM, Rybchyn MS. Sex Differences in Photoprotective Responses to 1,25-Dihydroxyvitamin D3 in Mice Are Modulated by the Estrogen Receptor- β . 2021;22(4).
286. Mahdiah Z, Postma B, Herritt LA, Hamilton RF, Harkema JR, Holian A. Hyperspectral microscopy of subcutaneously released silver nanoparticles reveals sex differences in drug distribution. *Micron*. 2022;153:103193.
287. Griffin D, Colón S, Gray D, Overton B, Wang B, editors. *Design and Development of a Novel Sitagliptin-Loaded Transdermal Patch for Diabetes Treatment* 2018.

288. Hsiao CY, Yang SC, Alalaiwe A, Fang JY. Laser ablation and topical drug delivery: a review of recent advances. *Expert opinion on drug delivery*. 2019;16(9):937-52.
289. Aich K, Singh T, Dang S. Advances in microneedle-based transdermal delivery for drugs and peptides. 2022;12(7):1556-68.
290. Qu F, Geng R, Liu Y, Zhu J. Advanced nanocarrier- and microneedle-based transdermal drug delivery strategies for skin diseases treatment. *Theranostics*. 2022;12(7):3372-406.
291. Suwanai H, Watanabe R, Sato M, Odawara M, Matsumura H. Dipeptidyl Peptidase-4 Inhibitor Reduces the Risk of Developing Hypertrophic Scars and Keloids following Median Sternotomy in Diabetic Patients: A Nationwide Retrospective Cohort Study Using the National Database of Health Insurance Claims of Japan. *Plastic and reconstructive surgery*. 2020;146(1):83-9.
292. Longo A, Librizzi M, Chuckowree IS, Baltus CB, Spencer J, Luparello C. Cytotoxicity of the Urokinase-Plasminogen Activator Inhibitor Carbamimidiothioic Acid (4-Boronophenyl) Methyl Ester Hydrobromide (BC-11) on Triple-Negative MDA-MB231 Breast Cancer Cells. *Molecules*. 2015;20(6):9879-89.
293. Beer L, Mildner M, Ankersmit HJ. Cell secretome based drug substances in regenerative medicine: when regulatory affairs meet basic science. *Annals of translational medicine*. 2017;5(7):170.